Diss. ETH No. 27494

Stochastic Investment and Dispatch Optimization of Distributed Energy Resources in a Market Environment

A thesis submitted to attain the degree of
Doctor of Sciences of ETH Zurich
(Dr. sc. ETH Zurich)

presented by

Xuejiao Han

M.Sc., Technical University of Munich
B.Eng., Southeast University
born on November 18, 1991
citizen of China

accepted on the recommendation of
Prof. Dr. Gabriela Hug, examiner
Prof. Dr. Jalal Kazempour, co-examiner
Dr. Christian Schaffner, co-examiner

2021

ETH Zurich
EEH - Power Systems Laboratory
ETL G22
Physikstrasse 3
8092 Zurich, Switzerland

DOI: 10.3929/ethz-b-000488764
ISBN: 978-3-907234-49-5

Printed in Switzerland by the ETH Druckzentrum

To my family.

Preface

This thesis summarizes the work I have done during my PhD study at the Power Systems Laboratory of ETH Zurich. With this section, I would like to express my thankfulness to all the people that support me during this process.

First and foremost, I would like to express my sincere gratitude to my advisor Prof. Gabriela Hug for offering me this opportunity to pursue my PhD at Power Systems Laboratory (PSL). I really appreciate the guidance, the support, the belief and the freedom she has been providing all the time, especially during the hard times of my PhD. To me, she is not only the role model from the career perspective but also the role model in maintaining the work-life balance.

Special thanks should go to Prof. Jalal Kazempour for accepting to be the co-examiner of my thesis and for taking time to review the thesis. Jalal's excellent work and our communications at different conferences have been inspiring me since the beginning of my PhD. I am so thankful for the guidance he provided during my attendance of the DTU summer school in 2017 and I really appreciate the detailed feedback and suggestions he provided on the project and on my PhD studies.

Special thanks should also go to Dr. Christian Schaffner, both for accepting to be my co-examiner and for all the supports and guidance he has been providing within the frame of the Nexus-e project. It has been a pleasure to work with Christian and I am really grateful for the fruitful discussions, the helpful feedback and suggestions as well as his frequent sharing of interesting articles, the recent changes in industries and governmental policies, which all contribute to the great improvement of the work in terms of both the quality and the practicality.

I would like to extend my thanks to all members of the Nexus-e project, both research and industry partners. In particular, I would like to thank the Bun-

desamt für Energie (BFE) for financing this project and for the lots of fruitful discussions and valuable feedback. Further, I want to thank all the principle investigators Prof. Dr. Gabriela Hug, Dr. Christian Schaffner, Dr. Turhan Hilmi Demiray, Prof. Dr. Giovanni Sansavini, Prof. Dr. Sebastian Rausch and Prof. Dr. Massimo Filippini for their guidance. Special thanks should go to Dr. Evaggelos Kardakos for his importance not only as the teammate on the Nexus-e project, but also as a mentor and a friend. I would like to thank Dr. Jared Garrison for the countless brainstorming sessions. I also want to thank Dr. Schwarz Marius for his support as the project manager as well as for providing lots of valuable feedback on the abstract and for helping with the translation. Of course I would like to extend the thanks to all my teammates in Nexus-e, to Blazhe, Florian, Elena, Xuqian, Renger, Phillip and Pedro.

I would like to thank all the students that chose to work with me on the semester and the master theses. Special thanks should go to Filippo Ferrando, Heider Anya, Katamay Smith Tara, Jeizinger Annik, Zhang Shuang, Frei Aurelio, Gimple Henning Jan, Dai Ling and Szybiak Maciej. It has been fortunate to supervise these projects and I really appreciate the trust and the contributions they provided. Thanks should also go to the academic and industry partners that co-supervise these projects.

It has been, as always, a pleasure and an honor to be part of the PSL family. I always feel grateful for being in such a pleasant atmosphere. I would like to thank all the family members for making this possible and for all the moments and experiences we shared together. Special thanks go to Nadezhda for the lots of girl talk about life and work during the breaks and during the trips, to Thierry with whom I shared the same office for the longest time and shared a lot of stories and happy moments, to Conor, Aleksandar, Uros, Eleni, Johanna, Conleigh, Ashwin, Ognjen, Emmanouil, Yi, Shuo, Chenye, Jack, Andrew, Adrian, Stavros, Petros, Stefanos, Deep, Anya, Michael H., Michael F., Evangelos V., Tomas, Gustavo, Spyros, Line and Olivier for the many discussions, exchanges, the valuable suggestions and the time we have spent together during workshops, conferences, ski trips, excursions etc. I would also like to thank Judith for taking care of all the administrative things, for always being willing to help as well as for the lots of talks and story sharing about life.

Last but not the least, I would like to thank my family especially my mom and dad for giving me the freedom to study abroad and to pursue my dreams. In particular, I would like to thank my dear half Boxiao for the patience, the support, the love and for always being there for me. Thanks for not giving up on me even when I gave up on myself during the darkest times.

Xuejiao Han
Zürich, March 2021

P.S. This thesis was written at the time when the world is suffering from the COVID-19 pandemic and I would also like to express my deepest gratefulness to all the doctors, nurses and medical workers. Hope everything will be back to normal soon!

Abstract

Across the world, electric power systems are experiencing drastic changes mainly attributable to the technical improvements and cost reductions of technologies such as wind, solar, and batteries, along with ambitious climate and energy targets (e.g., net-zero greenhouse gas emission, coal, and nuclear/coal phase-out). These trends lead to the proliferation of distributed energy resources and contribute to transforming the traditional centralized power system into a more decentralized system. However, both the intermittency nature of the variable generation and the gradual phase-out of favorable policies pose significant challenges to the operations and the investments of distributed energy resources. To better exploit the economic value of distributed energy resources, an aggregator is considered to enable their market participation and integrate the characteristics of diverse resources into a single entity. The research question of what would be the optimal dispatch and the optimal mix of distributed energy resources in a market environment is addressed.

The first part of the thesis focuses on developing the optimal dispatch and bidding strategies for an aggregator of distributed energy resources' mix in a market environment. We first assume that the aggregator is a price-taker. To assess the benefits of participating in sequential markets, we derive the optimal bidding strategy for each market using a rolling-horizon approach. This approach allows the aggregator to modify the dispatch schedules and market biddings based on the updated information (e.g., more accurate generation forecast of wind and PV) when getting closer to real-time. The value of aggregating and combining different energy resources is also quantified. Second, we assume that the aggregator is a price-maker and model the aggregator's market power using a bi-level structure. We investigate the impacts of market share, price elasticity of the demand curve, the import electricity price, and the generation mix on the incentives of exerting the market power. We further explore the influence of the variable generation output uncertainty on the

optimal bidding and dispatch strategies using a distributionally robust optimization model. This model enables us to describe the uncertainties using a family of possible distributions without requiring the full knowledge of the uncertainty distribution. Based on the out-of-sample analysis, the distributionally robust optimization model is shown to achieve a good balance between the expected performance and performance in extreme cases, with acceptable computational effort. Additionally, the performance of the model can be further improved using an auto-regressive moving average model.

In the second part, we aim to optimize the investment decisions of an aggregator in a market environment by considering the detailed hourly operational decisions and thus accounting for the fluctuations in electricity demand and supply. We investigate the impacts of market participation, the flexibility of the reserve products, demand response potentials, policy targets, and forecast errors on the investment and operational decisions. Results show that both participating in the reserve market and increasing the flexibility of reserve products encourage investments in flexible units (e.g., dispatchable generation units and storage units). However, the investment profitability is highly sensitive to the forecast accuracy of the variable generation output. To model the short-term forecast errors of the variable generation output in a proper way, we propose a model that jointly optimizes the investment and operational decisions based on distributionally robust optimization. Further, we analyze the impacts of including different statistical information of the uncertainty distribution in distributionally robust optimization.

Finally, the third part presents a techno-economic optimization model to analyze the economic viability of PV-battery systems for different customer groups in Switzerland. The customer groups are clustered based on their annual electricity consumption values, rooftop sizes, annual irradiation levels, and geographical locations. For each customer group, the investment decisions to be optimized include the investment capacity of the PV unit, the investment energy capacity, and the power capacity of the battery unit. The investment decisions are optimized by maximizing the net present value over a 30-year horizon. The considered cash inflows and outflows comprise the investment costs and subsidies, the distribution system injection tariffs or the profits from selling the generation surplus to the market, tax rebates, savings

from self-consumption, degradation costs, operational costs, and the reinvestment costs. To investigate how the investment decisions change over time, we conduct simulations for the years 2020-2050 with a five-year step while accounting for the long-term developments of the parameters. Driven by the projected cost decrease, results show that the optimal PV and battery sizes increase over the years, and in 2050 the PV investment is limited mainly by the rooftop size. The payback periods of the investment fluctuate between 2020 and 2035 as a result of the mixed effects of policy changes, electricity price, and cost developments. By analyzing the economic viability of the PV-battery system across different customer groups, it is found that the investments are most likely to favor the customer groups with higher annual irradiation levels and electricity consumption values. Furthermore, the conducted sensitivity analyses illustrate the impacts of parameters such as payback periods, costs, load profiles, electricity prices, and tariffs. Finally, we analyze the dynamics of residual load profiles caused by the seasonal and diurnal patterns of the solar generation output and identify the need for flexibilities in the electricity system considering the increasing penetration of solar power.

Kurzfassung

Weltweit untergehen Energiesysteme drastischen Veränderungen, hauptsächlich aufgrund technischer Verbesserungen und sinkenden Kosten von Technologien wie Wind, Solar und Batterien, sowie ambitionierten Klima- und Energiezielen. Diese Veränderungen führen zur Verbreitung dezentraler Energieressourcen und tragen dazu bei, dass sich traditionelle zentralisierte Energiesysteme in vermehrt dezentralisierte Systeme verwandeln. Allerdings stellen sowohl die fluktuierende Stromerzeugung als auch auslaufende Subventionen große Herausforderungen für den Betrieb und die Investitionen von dezentraler Energieressourcen dar. Um die Wirtschaftlichkeit dezentraler Energieressourcen zu steigern, können Aggregator deren Marktteilnahme ermöglichen und die Eigenschaften der verschiedenen Ressourcen in einer einzigen Einheit integriert. Die Forschungsfrage, wie der optimale Einsatz (Dispatch) und Mix von dezentralen Energieressourcen in einer Marktumgebung wäre, wird behandelt.

Der erste Teil der Arbeit konzentriert sich auf die Entwicklung der optimalen Dispatch- und Gebotsstrategien für einen Aggregator mit einem Mix aus dezentralen Energieressourcen in einer Marktumgebung. Erstens, nehmen wir an, dass der Aggregator ein Preisnehmer ist. Um die Vorteile der Teilnahme an sequenziellen Märkten zu bewerten, wird die Gebotsstrategie für jeden Markt unter einer rollierenden Planung optimiert. Dieser Ansatz ermöglicht es dem Aggregator, die Einsatzpläne und Marktgebote auf der Grundlage der aktualisierten Informationen (z. B. genauere Erzeugungsprognosen für Wind und PV) zu ändern, wenn er sich der Echtzeit nähert. Der Wert der Aggregation und Kombination verschiedener Energieressourcen wird ebenfalls quantifiziert. Zweitens nehmen wir an, dass der Aggregator ein Preissetzer ist und modellieren die Marktmacht des Aggregators unter Verwendung einer zweistufigen Struktur. Wir untersuchen die Auswirkungen des Marktanteils, der Preiselastizität der Nachfragekurve, des Importstrompreises und

des Erzeugungsmixes auf die Anreize zur Ausübung der Marktmacht. Des Weiteren untersuchen wir den Einfluss der Unsicherheit der variablen Erzeugungsleistung auf die optimalen Gebots- und Dispatch-Strategien mit Hilfe eines verteilungsrobusten Optimierungsmodells. Dieses Modell ermöglicht es uns, die Unsicherheiten mit Hilfe einer Familie von möglichen Verteilungen zu beschreiben, ohne dass die vollständige Kenntnis der Unsicherheitsverteilung erforderlich ist. Basierend auf der Out-of-Sample-Analyse wird gezeigt, dass das verteilungsrobuste Optimierungsmodell ein gutes Gleichgewicht zwischen der erwarteten Leistung und der Leistung in Extremfällen bei akzeptablem Rechenaufwand erreicht. Zusätzlich kann die Leistung des Modells durch ein autoregressives gleitendes Mittelwertmodell weiter verbessert werden.

Im zweiten Teil zielen wir darauf ab, die Investitionsentscheidungen eines Aggregators in einer Marktumgebung zu optimieren, indem wir die detaillierten stündlichen Betriebsentscheidungen berücksichtigen und somit die Schwankungen der Stromnachfrage und des Angebots berücksichtigen. Wir untersuchen die Auswirkungen der Marktteilnahme, der Flexibilität der Reserveprodukte, der Demand-Response-Potenziale, der politischen Ziele und der Prognosefehler auf die Investitions- und Betriebsentscheidungen. Die Ergebnisse zeigen, dass sowohl die Teilnahme am Reservemarkt als auch die Erhöhung der Flexibilität der Reserveprodukte Investitionen in flexible Einheiten (z.B. steuerbare Erzeugungseinheiten und Speichereinheiten) fördern. Die Rentabilität der Investitionen ist jedoch stark abhängig von der Prognosegenauigkeit der variablen Erzeugungsleistung. Um die Prognosefehler der kurzfristigen variablen Erzeugungsleistung in geeigneter Weise zu modellieren, schlagen wir ein Modell vor, das die Investitions- und Betriebsentscheidungen gemeinsam auf Basis einer verteilungsrobusten Optimierung optimiert. Weiterhin analysieren wir die Auswirkungen der Einbeziehung verschiedener statistischer Informationen der Unsicherheitsverteilung in die verteilungsrobuste Optimierung.

Schließlich wird im dritten Teil ein techno-ökonomisches Optimierungsmodell vorgestellt, um die Wirtschaftlichkeit von PV-Batterie-Systemen für verschiedene Kundengruppen in der Schweiz zu analysieren, die anhand ihrer jährlichen Stromverbrauchswerte, Dachgrößen, jährlichen Einstrahlungsniveaus und der geografischen Standorte gruppiert werden. Für

jede Kundengruppe umfassen die zu optimierenden Investitionsentscheidungen die Kapazität der PV-Anlage sowie die Energie- und Leistungskapazität der Batterieeinheit. Die Investitionsentscheidungen werden durch Maximierung des Kapitalwerts über einen 30-Jahres-Horizont optimiert. Die betrachteten Einnahmen und Kosten umfassen die Investitionskosten und Subventionen, die Einspeisetarife des Verteilnetzes (Gewinne aus dem Verkauf des Erzeugungsüberschusses an den Markt), Steuerrückerstattungen, Einsparungen aus dem Eigenverbrauch, Degradationskosten, Betriebskosten und die Reinvestitionskosten. Um zu untersuchen, wie sich die Investitionsentscheidungen im Laufe der Zeit verändern, werden Simulationen für die Jahre 2020-2050 (jedes fünfte Jahr) durchgeführt, wobei die langfristigen Entwicklungen der Parameter berücksichtigt werden. Vor allem aufgrund des prognostizierten Kostenrückgangs zeigen die Ergebnisse, dass die optimalen PV- und Batteriegrößen mit der Zeit zunehmen und im Jahr 2050 die PV-Investition hauptsächlich durch die Dachgröße begrenzt wird. Die Amortisationszeiten der Investition schwanken zwischen 2020 und 2035 als Ergebnis der gemischten Effekte von politischen Änderungen, Strompreis- und Kostenentwicklungen. Durch die Analyse der Wirtschaftlichkeit des PV-Batterie-Systems über verschiedene Kundengruppen hinweg wird festgestellt, dass die Investitionen am ehesten die Kundengruppen mit höheren jährlichen Einstrahlungswerten und Stromverbrauchswerten begünstigen. Darüber hinaus veranschaulichen die durchgeführten Sensitivitätsanalysen die Auswirkungen von Parametern wie Amortisationszeiten, Kosten, Lastprofilen, Strompreisen und -tarifen, etc. Schließlich analysieren wir die Dynamik der Restlastprofile, die durch die saisonalen und tageszeitlichen Muster der solaren Erzeugungsleistung verursacht werden, und identifizieren den Bedarf an Flexibilitäten im Elektrizitätssystem unter Berücksichtigung der zunehmenden Durchdringung mit Solarstrom.

Contents

List of Acronyms **xxvii**

List of Figures **xxxv**

List of Tables **xxxix**

1 Introduction **1**

1.1 Background and Motivation 1

1.2 Contributions 3

1.3 Thesis Organization 6

1.4 List of Publications 9

I Stochastic Dispatch Optimization in a Market Environment **11**

2 Dispatch Optimization of the Aggregator as a Price-taker **13**

2.1 Introduction 14

2.1.1 Motivation and Related Work 14

2.1.2 Chapter Organization 16

2.2 Problem Descriptions and Model Assumptions 16

2.2.1 Structure of the Aggregator 17

2.2.2 Sequential Market Environment 17

2.3 Multi-stage Stochastic Programming 19

2.4 Mathematical Formulation 22

2.4.1 Aggregator Modeling 22

2.4.2 Formulation of the Electricity Markets 26
2.4.3 Formulation of Risk Constraints 28
2.4.4 Formulation of the Optimization Problem 29
2.5 Wind Scenario Generation 30
2.6 Case Study 33
2.6.1 Input Data 33
2.6.2 Results: Analysis of the Day-ahead Market Behavior 35
2.6.3 Results: Impacts of the Intraday Market 39
2.6.4 Results: Effects of the Intraday Market Trading Limit . . . 43
2.7 Limitations and Future Work 43
2.8 Summary and Conclusions 45

3 Dispatch Optimization of the Aggregator as a Price-maker 47
3.1 Introduction 48
3.1.1 Motivation and Related Work 48
3.1.2 Chapter Organization 50
3.2 Problem Descriptions and Model Assumptions 50
3.2.1 Multi-market Environment 50
3.2.2 Uncertainty Characterization 51
3.2.3 Stochastic Bi-level Model 52
3.2.4 Model Assumptions 52
3.3 Mathematical Formulation 53
3.3.1 Upper Level Formulation 54
3.3.2 Lower Level Formulation 55
3.3.3 Bi-level Formulation with Two Lower Levels 56
3.3.4 Mathematical Program with Equilibrium Constraints (MPEC) Formulation 57
3.3.5 Mixed-integer Linear Programming (MILP) Formulation . 57
3.3.6 Modeling Variable Generation Output Uncertainties Using Probabilistic Constraints 60
3.3.7 Modeling Market Uncertainties using Scenarios 62

3.4 Case Study - Test System . . . 63
3.5 Case Study - Results . . . 67
3.5.1 Strategic offering vs. Non-strategic offering . . . 68
3.5.2 Impacts of the Market Share . . . 71
3.5.3 Impacts of the Import Electricity Price . . . 75
3.5.4 Impacts of the Price Elasticity of Demand . . . 76
3.5.5 Impacts of the Generation Mix of the Aggregator . . . 77
3.5.6 Impacts of the Forecast Uncertainty . . . 78
3.6 Limitations and Future Work . . . 81
3.7 Summary and Conclusions . . . 82

4 Modeling Uncertainty using Distributionally Robust Optimization 85
4.1 Introduction . . . 86
4.1.1 Motivation and Related Work . . . 86
4.1.2 Chapter Organization . . . 89
4.2 Model Assumptions . . . 90
4.3 Formulation of the Optimization Problem . . . 90
4.3.1 Bi-level Bidding Model . . . 91
4.3.2 Linearization of the Bidding Model . . . 94
4.3.3 Modelling of Wind Uncertainty . . . 96
4.4 Case Study . . . 105
4.4.1 Input Data . . . 105
4.4.2 Results . . . 106
4.5 Limitations and Future Work . . . 117
4.6 Summary and Conclusions . . . 118

5 The Integration of Storage Units 121
5.1 Introduction . . . 122
5.1.1 Motivation and Related Work . . . 122
5.1.2 Chapter Organization . . . 124
5.2 Model Assumptions . . . 124

5.3 Mathematical Formulation . . . 125
5.3.1 Bi-level Bidding Model . . . 125
5.3.2 Modelling of Uncertainty . . . 128
5.4 Case Study . . . 133
5.4.1 Input Data . . . 133
5.4.2 Results . . . 135
5.5 Limitations and Future Work . . . 146
5.6 Summary and Conclusions . . . 147

II Stochastic Investment Optimization in a Market Environment 149

6 Investment Optimization considering Joint Reserve and Energy Market Participation 151
6.1 Introduction . . . 152
6.1.1 Motivation and Related Work . . . 152
6.1.2 Chapter Organization . . . 153
6.2 Problem Description and Model Assumptions . . . 154
6.3 Mathematical Formulation . . . 155
6.4 Case Study . . . 162
6.4.1 Input Data . . . 162
6.4.2 Results . . . 163
6.5 Limitations and Future Work . . . 181
6.6 Summary and Conclusions . . . 182

7 Investment Optimization Focusing on the Forecast Uncertainty Modeling 185
7.1 Introduction . . . 186
7.1.1 Motivation and Related Work . . . 186
7.1.2 Chapter Organization . . . 187
7.2 Mathematical Formulation . . . 187
7.2.1 General Stochastic Formulations . . . 188

7.2.2 Uncertainty modeling . . . 188
7.3 Case Study . . . 191
7.3.1 Results: Comparison of Different Optimization Models . . 195
7.3.2 Results: Effects of Statistical Constraints in the Ambiguity Set . . . 204
7.3.3 Results: Impacts of the Imbalance Price . . . 207
7.4 Limitations and Future Work . . . 208
7.5 Summary and Conclusions . . . 208

III Techno-economic Analysis of PV-battery Systems 211

8 Case study: Techno-economic Analysis of PV-battery Systems in Switzerland 213
8.1 Introduction . . . 215
8.1.1 Motivation . . . 215
8.1.2 Literature review . . . 215
8.1.3 Status of PV and Battery in Switzerland . . . 219
8.2 Data . . . 220
8.2.1 General Assumptions . . . 220
8.2.2 Rooftop Potential and Data Clustering . . . 220
8.2.3 Parameters of the PV-battery System . . . 222
8.2.4 Load and Generation Profiles . . . 225
8.2.5 Policies and Regulations . . . 226
8.2.6 Scenarios . . . 227
8.3 Method . . . 231
8.3.1 Investment Constraints . . . 232
8.3.2 Operational Constraints . . . 233
8.3.3 Power Balance Constraints . . . 234
8.3.4 Formulation of the Optimization Problem . . . 235
8.3.5 Technical and Economic Indicators . . . 237
8.4 Case Study Results . . . 238

8.4.1 Results for One Representative Customer Group 239
8.4.2 Results for All Customer Groups within Canton Zurich . . 245
8.4.3 Results for Switzerland 249
8.5 Discussions 257
8.5.1 From Investors' Perspective 257
8.5.2 From Retailers' Perspective 258
8.5.3 From System Operators' Perspective 259
8.5.4 From Policy-makers' Perspective 259
8.6 Limitations and Future Work 260
8.7 Conclusions 261

9 Conclusions and Outlook **263**
9.1 Summary 263
9.2 Conclusions 264
9.3 Outlook 266

Bibliography **269**

Curriculum Vitae **293**

Appendices **295**

List of Acronyms

ANN	Artificial Neural Network
ARMA	Auto-regressive Moving Average
ARIMA	Auto-regressive Integrated Moving Average
BM	Balancing Market
BESS	Battery Energy Storage Systems
BFE	Bundesamt für Energie
CAISO	California Independent System Operator
CHP	Combined Heat and Power
CLP	Continuous Linear Programming
CVaR	Conditional Value at Risk
DA	Day-ahead
DAM	Day-ahead Market
DER	Distributed Energy Resource
DO	Deterministic Optimization
DOD	Depth of Discharge
DR	Demand Response
DRP	Demand Response Program
DRO	Ditributionally Robust Optimization
DSM	Demand-side Management
DSO	Distribution System Operator

EPEX European Power Exchange
EPEC Equilibrium Problem with Equilibrium Constraints
EV Electric Vehicles

GARCH Generalized Autoregressive Conditional Heteroskedastic

ID Intraday
IDA Intraday Auction
IDM Intraday Market
IRENA International Renewable Energy Agency

KKT Karush-Kuhn-Tucker

LDR Linear Decision Rule
LL Lower-Level

MAD Mean Absolute Deviation
MCP Market Clearing Price
MILP Mixed-Integer Linear Programming
MPEC Mathematical Program with Equilibrium Constraints

NPV Net Present Value

PBP Payback Period
PDF Probability Distribution Function
PSL Power Systems Laboratory
PV Photovoltaic
PVB Photovoltaic-battery

RES Renewable Energy Source

RM	Reserve Market
RO	Robust Optimization
RT	Real-time
SCR	Self-consumption Rate
SD	Standard Deviation
SO	Stochastic Optimization
SOC	State of Charge
SOCP	Second-order Cone Program
SS	Self-suffiency
SSR	Self-suffiency Rate
UL	Upper-Level
VRE	Variable Renewable Energy
VPP	Virtual Power Plant
WACC	Weighted Average Cost of Capital
WPP	Wind Power Plant

List of Figures

2.1 Structure for the aggregator of distributed energy resources' mix. 17
2.2 Structure of the day-ahead market and the intraday market with multiple intraday auctions. 18
2.3 Example probabilistic forecasts generated using the method from [1] with the 13-hour to 36-hour ahead lead time along with the day-ahead point forecast and the real-time measurement data for the simulation day. 30
2.4 Example day-ahead wind forecast scenarios generated using the method from [1] along with the day-ahead point forecast data from Nord Pool for the same time period as Fig. 2.3. 31
2.5 Updated wind generation scenarios over different bidding stages along with the realized wind output at real-time. From top to down the figures correspond to the real-time wind output scenarios S^{w1}, S^{w2}, S^{w3} and S^{w4}. 32
2.6 Scenarios for day-ahead, intraday and balancing market prices. . 34
2.7 Single scenario analysis for the aggregator participating only in the day-ahead and the balancing markets: market trading behaviors are shown in the top figure; deviations of the wind generation of the considered scenario from the expected wind generation of all scenarios named as "Delta-Wind" are shown in the bottom figure. 35
2.8 Single scenario analysis for the aggregator participating only in the day-ahead and the balancing markets: optimal real-time dispatch of different units within the aggregator as well as the aggregator's market biddings and the rescheduled hourly load named as "Load-New". 36

2.9 Day-ahead bidding curves of the aggregator under $\beta = 0$ and $\beta = 0.8$ for example hours 9, 10 and 11. 39

2.10 Impacts of risk aversion on the expected imbalance quantities (i.e., left figure) and the aggregator profits (i.e., right figure). . . . 39

2.11 Realized imbalance quantity and cost developments at real-time considering different numbers of intraday auctions. 41

2.12 Re-dispatch of the units and the adjustment of the market biddings under an example day-ahead market price scenario, as a reaction to the updated wind forecasts considering four intraday auctions compared to the case considering only one intraday auction. 42

3.1 Structure of the sequential spot electricity markets. 51

3.2 Structure of the bi-level model. 52

3.3 Average aggregated hourly day-ahead offering curve of rival producers and an inelastic demand curve with the demand quantity equaling to the average hourly day-ahead market demand quantity. 66

3.4 Average aggregated hourly intraday offering curves of rival producers under different intraday market offering price scenarios and an intraday market inelastic demand curve with the demand quantity equaling to the hourly average of the intraday market demand quantity. 67

3.5 The hourly average positive and negative imbalance prices, as well as the day-ahead and intraday market prices over all intraday price scenarios considering only the offering of the non-strategic rivals for the four representative weeks corresponding to four seasons (from left to right: winter, spring, summer, autumn). 68

3.6 Hourly capacity factors of wind and PV units for four weeks corresponding to four seasons (from left to right: winter, spring, summer, autumn). 68

3.7 Day-ahead offering quantities and the resulting market clearing prices for strategic and non-strategic offerings in the Baseline scenario for four selected days from four seasons. 69

3.8 Average intraday offering quantities and the resulting market clearing prices for strategic and non-strategic offerings in the Baseline scenario for four selected days from four seasons. 72

3.9 Average hourly day-ahead and intraday market offering quantities and the resulting market clearing prices for strategic and non-strategic offerings over the four representative weeks under two extreme generation mix cases: 100% wind and 100% PV. 79

3.10 Impacts of forecast uncertainty on the aggregator profits: results under the strategic offering are shown in the top figure; results under the non-strategic offering are shown in the bottom figure. 80

4.1 Approximation of the optimal second-stage decisions, i.e. positive and negative imbalances, using the enhanced linear decision rule applied by the distributionally robust optimization model. . 107

4.2 Approximation of the optimal second-stage decisions, i.e. positive and negative imbalances, using the results of stochastic optimization. 108

4.3 Resulting day-ahead offers of the deterministic, stochastic and the distributionally robust optimization models assuming the aggregator market share as 5%, 10%, 15% and 20%. 110

4.4 Aggregator's day-ahead offering quantities and the resulting day-ahead market prices with 10% market share and forecast errors generated under Gaussian distributions with mean zero and standard deviations ranging from 0.05 to 0.3. 111

4.5 Distribution of forecast errors included in the training set 1 and in the out-of-sample test set 2 with mean zero and standard deviations ranging from 0.05 to 0.2 with a step of 0.05. 113

4.6 Distributions for the resulting imbalance quantities of distributionally robust optimization, stochastic optimization and robust optimization models assuming that the forecast errors are subject to Gaussian, beta and uniform distributions with standard deviations set as 0.05 and 0.2. 116

5.1 Comparison of the original market offering/bidding curves and the approximated offering/bidding curves for an example hour. . 133

5.2 Comparison of the original and the approximated market clearing prices and quantities for the simulation year 2018. 134

5.3 Comparison of the offering quantities (i.e., top figure) and the resulting market clearing prices of PT2 and PM2 (i.e., bottom figure) for four selected weeks in 2018 corresponding to four seasons. All weeks start from a Monday. 138

5.4 The top figure shows the storage operations in the case of PM2 for the four selected weeks; the bottom figure illustrates the original market clearing prices and the market clearing prices of PT2 and PM2 for the four selected weeks. All weeks start from a Monday. . 140

5.5 The real-time battery operations along with the day-ahead market price and the day-ahead wind forecast error of the DRO case over an example week. The battery operations are influenced by both the day-ahead market prices and the day-ahead wind forecast errors. 145

6.1 Comparison of the annual generation and the installed capacity by technology type for years 2020, 2030, 2040 and 2050 under the Baseline scenario. 165

6.2 The hourly generation by technology type over an example winter and summer week for 2020 under the Baseline scenario. . . . 166

6.3 The hourly generation by technology type over an example winter and summer week for 2050 under the Baseline scenario. . . . 167

6.4 Day-ahead dispatch of battery and demand response programs over an example winter and summer week for 2050 along with the day-ahead market prices for the same period under the Baseline scenario. 169

6.5 Day-ahead and real-time battery operations, reserve capacity biddings as well as the reserve activations over an example winter and summer week for years 2050 under the Baseline scenario. . . 171

6.6 Impacts of coordinated bidding on the investments decisions. . . 172

6.7 Comparison of the total generation and costs for 2020 and 2050 under different renewable targets. Data shown are from simulations of applying the renewable target from 0% to 100% while keeping the remaining parameters equal to the Baseline scenario value. 176

6.8 Comparison of the total generation and costs for 2020 and 2050 under different self-sufficiency targets. Data shown are from simulation of applying the self-sufficiency target from 0% to 100% while keeping the remaining parameters equal to the Baseline scenario values. 177

6.9 Comparison of the investment and cost results for 2020 and 2050 under different forecast error assumption. 180

7.1 Nominal PV and wind power output forecast as well as demand values over four weeks corresponding to four seasons (from left to right: winter, spring, summer, autumn). 192

7.2 Whisker plot on nominal PV and wind forecast errors categorized according to the hours of the day and seasons of the year (from left to right: winter, spring, summer, autumn). 193

7.3 Comparison of the resulting investment decisions of the robust optimization (i.e., top figure), the distributionally robust optimization (i.e., middle figure) and the stochastic optimization models (i.e., bottom figure) with and without considering the reserve market participation. 196

7.4 Historical PV and wind forecast errors and the corresponding Gaussian distribution fitting assumed by stochastic optimization for an example hour. 199

7.5 Comparison of the day-ahead bidding strategies of the robust optimization and the distributionally robust optimization models for 2020 without considering the reserve market. 200

7.6 The relative difference between the imbalance price and the day-ahead market price over the four representative weeks (top figure); the day-ahead biddings of the stochastic optimization model over the four representative weeks for 2020 without considering the reserve market (bottom figure). 201
7.7 Hourly mean absolute deviation of the day-ahead PV output forecast errors (i.e., top plot) and wind output forecast errors (i.e., bottom plot) simulated for distributionally robust optimization and calculated for the Gaussian distributed scenarios with the same mean and absolute deviation. 206
7.8 Demand cost and the imbalance cost developments by running the distributionally robust optimization model under different values of positive and negative imbalance price parameters a_1 and a_2. 207
8.1 Structure and power flows of the modeled PV-battery system. . . 222
8.2 Normalized aggregated load profile for canton Zurich and synthetic individual load profiles for consumption categories L1-L11. 229
8.3 Dispatch of the PV-battery system for the representative rooftop of the example customer group in 2030 and 2050. 241
8.4 Cumulative PV investments in different size categories for the canton of Zurich, years 2020-2050. 246
8.5 Optimal investments against payback periods of the Baseline scenario of 2020-2050 for the canton of Zurich. 248
8.6 Investment changes in the example of the canton of Zurich under different scenarios. 249
8.7 Optimal yearly investment under different payback periods. . . . 251
8.8 Optimal regional investment of a fast and a moderately fast recoverable investment cases under the Baseline scenario in 2020 and 2050. 252
8.9 Distribution of the fast recoverable investment of the Baseline scenario in 2050. 253
8.10 Monthly load and residual-load of different years under a fast and a moderately fast recoverable investment case. 254

8.11 Hourly original Swiss load and residual-load of a winter and a summer week under a fast and a moderately fast recoverable investment case. 256
9.1 Battery operations over an example winter and summer week for years 2030 to 2050 under the Baseline scenario. 297
9.2 Day-ahead dispatch of battery and demand response programs over an example winter and summer week for 2020 to 2040. . . . 298

List of Tables

2.1 Parameters of units within the aggregator. 33

2.2 Impacts of coordinations on the profit obtained by each unit within the aggregator and the total aggregator profit. 37

2.3 Impacts of including different numbers of intraday auctions. . . 40

2.4 Effects of the intraday market trading limit. 43

3.1 Parameters of the units simulated for the modified Swiss system. 63

3.2 Capacity factors for different types of hydro power plants. 64

3.3 Modeled input parameters in the Baseline and the sensitivity scenarios. 70

3.4 Impact of the aggregator's market share on day-ahead market prices and the aggregator profit. 73

3.5 Impact of the aggregator's market share on market revenues and costs. 74

3.6 Impact of the import electricity price. 75

3.7 Impact of the price elasticity of demand. 76

3.8 Impact of the aggregator's generation mix. 77

4.1 Market profits resulted by the distributionally robust optimization model under different aggregator market shares 111

4.2 Comparison of aggregator's expected simulation profits, the expected and the worst-case out-of-sample profits with standard deviations ranging from 0.05 to 0.2 resulted by deterministic, robust, distributionally robust and stochastic optimization models. 114

4.3 Problem size and the average computational time for solving the optimization problem of one time step using different methods. 117

5.1 Parameters of the wind-storage aggregator . . . 133
5.2 Impacts of market power. . . . 137
5.3 Effects of output-based subsidies. . . . 139
5.4 Effects of the aggregation level. . . . 141
5.5 Day-ahead forecast improvements using the ARMA model. . . . 143
5.6 Impact of the forecast error. . . . 144
5.7 Comparison of the aggregator's profits in cases with and without storage units along with the resulting maximum acceptable investment cost of the storage unit. . . . 146
6.1 Parameters of candidate units. . . . 163
6.2 Input parameters and market prices for modeling. . . . 164
6.3 Comparison of the results with and without coordinated bidding considering the same investment decisions. . . . 173
6.4 Impacts of different reserve products on investments and costs. . . 174
6.5 Impact of demand response on the results for years 2020 to 2050. 178
7.1 Annualized investment cost, total annual simulation cost and demand cost of different optimization methods for 2020 to 2050. . . 198
7.2 The expected, worst-case and the standard deviation of the out-of-sample imbalance and total costs of different optimization methods for 2020 to 2050 with and without considering the reserve market. . . . 202
7.3 Problem size and the computational time of different optimization methods. . . . 204
7.4 Impact of considering different statistical data in the ambiguity set. . . . 205
8.1 Overview of the existing techno-economic studies of the PV-battery system. . . . 216
8.2 Parameters of the PV-battery system. . . . 223
8.3 Overview of lithium-ion battery system costs. . . . 224
8.4 Input parameters for modeled policies and regulations. . . . 227
8.5 Parameters of price scenarios SP1-SP9. . . . 230
8.6 Summary of the sensitivity scenarios. . . . 231

8.7 Baseline analysis for the representative rooftop of the example customer group. 240
8.8 Sensitivity analysis for the representative rooftop of the example customer group in 2050. 243
8.9 Baseline results analysis for canton Zurich, years 2020-2050. . . . 245
8.10 Baseline self-consumption results analysis for the fast / moderately fast recoverable investments, years 2020-2050. 257
9.1 Estimation of the total load and the flexible load. 295
9.2 Battery (2-hour) cost for 2020-2050 [2]. 296
9.3 PV cost for 2020-2050 [2]. 296
9.4 Wind cost for 2020-2050 [2]. 296
9.5 CHP cost for 2020-2050 [3]. 296
9.6 A Baseline, a high and a low PV cost scenario for 2020-2050. . . . 304
9.7 A Baseline, a high and a low battery cost scenario for 2020-2050. . 305
9.8 The DSO injection tariff in cent/kWh for PV estimated for each Swiss Canton for years 2020 to 2050 [4]. 306
9.9 The base retail electricity tariff in cent/kWh estimated for consumption categories L1-L11 of each Swiss Canton in 2020 [5]. . . 307
9.10 Information of electricity consumption categories [5]. 308

Chapter 1

Introduction

1.1 Background and Motivation

Motivated by the ambitious energy and climate goals, the favorable government policies that help achieve the goals, and the technological improvements and cost declines, the electric power systems worldwide have been undergoing a transition from a traditional centralized energy system towards a more decarbonized and more decentralized system. Distributed Energy Resources (DERs), which are mainly small-scale renewable energy sources (e.g., distributed solar, wind and storage units) connected to the distribution system, play a significant role in this transition. According to the report published by Navigant Research [6], the annual installation capacity of DERs, including the distributed generation, distributed energy storage, electric vehicles, demand response, and energy efficiency, is expected to exceed 200 GW by 2025. This is nearly twice as much as the annual investment capacity in 2019. Furthermore, the annual global DER capacity addition is foreseen to surpass the annual investments in centralized generation units in the near future [6].

Despite the proliferation of renewables and DERs, to align with the global climate goals to limit global warming to well below 2 degree Celsius above the pre-industrial levels by the end of this century, the annual investments in renewables are required to be almost tripled from the current level of around 300 billion US dollars to 800 billion US dollars by 2050 [7]. Moreover, new generation investments are needed to fill the energy demand gap introduced

by the policies such as nuclear and coal phase-out. However, after a continuous growth for over a decade, according to the data published by International Renewable Energy Agency (IRENA) in March 2020 [8], the global power capacity expansion of renewables has seen a slowdown in 2019, which was the first time since 2001. This is likely to be attributed to the gradual phase-out of favorable policies such as investment subsidies, feed-in tariffs, and tax rebates worldwide. The COVID-19 pandemic further worsens the situation by having a widespread negative impact on the world economy, including the power industry.

To enable a smooth transition from a subsidy-based to a market-based scheme and to realize the sustainable growth in renewables and DERs, it is essential to develop the optimal investment and dispatch strategies when depending entirely on markets instead of government supports or incentives. Additionally, the issues caused by the intermittency and the uncertainty of variable generation units, which pose significant challenges to the power plant operators and the electric power system operators, need to be addressed.

This thesis focuses on the investment and dispatch optimization of DERs in a market environment. An aggregator is considered to integrate the characteristics of diverse DERs into a single entity and to enable the DERs to behave similarly to a conventional unit. Note that the proposed methods (especially the modeling of uncertainty and the market bidding strategies) in general could also be applied to large-scale renewable sources. Consequently, we aim to address the following questions with this thesis:

- What is the optimal bidding[1] strategy for a DER aggregator in a sequential market environment, and how does the market environment influence the bidding strategies?
- What are the benefits of aggregating and coordinating different types of energy resources?
- How does the bidding strategy of the aggregator impact the market results? What are the influences of the aggregator's market share, the output-based subsidies, the price elasticity of demand, the potential market price cap, and the generation mix of the aggregator on the market power of the aggregator?

[1] In this context, bidding refers to both the offers made by the market participant to sell the electricity to the market and to purchase the electricity from the market.

- How can the effects brought by output uncertainties of variable generation units (e.g., wind and Photovoltaic (PV)) be mitigated?
- Given the policy targets and the demand profile, what is the optimal mix of DER technologies in terms of the cost in a market environment? How are the investment decisions influenced by market participation and different levels of uncertainties?
- When optimizing the investments in PV-battery systems from an individual household's perspective, how are the decisions affected by the customer heterogeneity, and how does the optimal decision change over time?
- How sensitive is the economic viability of the PV-battery system to uncertainties related to parameters such as investment and operational costs, load profiles, electricity prices and tariffs? Which are the driving factors?
- Considering the potential investments of PV-battery systems in the coming years, what are the potential challenges and opportunities for investors, retailers, electricity system operators, and policy-makers?

1.2 Contributions

The main contributions of this thesis are divided into three parts following the structure of the thesis.

Stochastic Dispatch Optimization

We derive a stochastic optimization model to determine the optimal bidding strategies for an aggregator that acts as either a price-taker or a price-maker in a market environment.

- We assess the impacts of participating in sequential markets and including different numbers of intraday auctions using a rolling-horizon optimization approach, which enables the aggregator to modify the real-time dispatch and bidding decisions for each market using the updated information closer to the real-time delivery. To account for the development of forecast errors over time, we use a probabilistic forecasting method to generate scenarios for variable generation outputs. In this way, the model manages to reflect

the motivation of variable generation units to participate in sequential markets (especially the intraday market) better by integrating a reduced level of variable generation output uncertainties when trading in markets that are cleared closer to real-time.

- We incorporate the risk control into the modeling to characterize the risk associated with profit variability, which stems from different levels of uncertainties (e.g., uncertainties of market prices and variable generation outputs).
- To consider the potential influence of the biddings on the market results, we develop a stochastic bi-level model to derive the strategic biddings for a hybrid wind-solar aggregator that acts as a price-maker in sequential electricity markets. A probabilistic chance-constrained formulation is utilized to model the uncertainty regarding wind and PV productions.
- The benefits of strategic bidding are verified by comparing its results against the non-strategic bidding case. Moreover, we conduct comprehensive sensitivity analyses to investigate the influences of the aggregator's market share, the import electricity prices, the price elasticity of the system demand curve, and the generation mix of the aggregator on the incentives to exercise market power.
- We then extend the stochastic bi-level model by modeling the uncertainty using Ditributionally Robust Optimization (DRO). Out-of-sample analyses are carried out to compare the performance of the DRO model to the models applying two popular alternative methods, namely Stochastic Optimization (SO) and Robust Optimization (RO). Results show that DRO outperforms RO in the expected out-of-sample performance with comparable computational efforts, and it achieves similar expected results as SO but better worst-case performance than SO with much less computational time.
- To further improve the uncertainty modeling, we propose to use the Autoregressive Moving Average (ARMA) model to learn the auto-correlations and the cross-correlations of uncertainties using the historical data and to generate the scenarios for the future path in a rolling manner. The effectiveness of the method is validated by comparing with two benchmark cases, i.e., the perfect information case and the deterministic case, using one year's worth of data.

Stochastic Investment Optimization

We formulate a multi-stage stochastic optimization model to derive the optimal investment decisions of a DER aggregator, which consists of storage units, variable and dispatchable generation units, and Demand Response (DR), considering its participation in the reserve, energy, and balancing markets.

- We first propose a model to optimize the investments considering the operational decisions over 8760 hours of the examined year to account for the seasonal, daily, and hourly variations from both the demand and the supply side. Uncertainties of the variable generation outputs are modeled using robust optimization. With this model, we investigate the impacts of market participation, the flexibility of the reserve products, demand response potentials, policy targets and forecast errors on the investment, and operational decisions.
- We then improve the modeling of short-term variable generation output uncertainty using distributionally robust optimization. As the distributionally robust optimization model is shown to achieve a good balance between the expected performance and the performance in extreme cases with acceptable computational effort, we further investigate the influence of including different statistical information into the ambiguity set for DRO.

Techno-economic Analysis of PV-battery Systems

We propose a techno-economic optimization model to analyze the economic viability of the Photovoltaic-battery (PVB) systems using the Net Present Value (NPV) over a 30-year horizon. A case study is conducted for a variety of customer groups in Switzerland. The revenue streams considered comprise the subsidies, Distribution System Operator (DSO) injection tariffs, potential profits from selling generation surplus to the market, tax rebates, savings from self-consumption, operational costs, degradation costs, and investment costs, which include the reinvestment cost of the battery as it has a shorter lifetime than the simulation horizon.

- By simulating the investment years from 2020 through 2050 with a five-year step while accounting for the potential developments of parameters such as the investment costs, electricity prices, tariffs, and subsidies in future years,

we show how the economic viability of the PVB system changes over time. The results are illustrated at three levels, i.e., the single customer group's level, the regional and the national levels.
- We investigate the influence of customer group heterogeneity on the economic viability of the investments by clustering the customers using different rooftop sizes, annual irradiation levels, electricity consumption values, individual load profiles, and geographical regions.
- We conduct a comprehensive sensitivity analysis to investigate the impacts of costs, load profiles, electricity prices, and tariffs on the optimal investment decisions, including the optimal C-rate of the battery units.
- We analyze the potential grid impacts caused by the seasonal and diurnal patterns of the solar generation and identify the needs for system flexibility.
- We identify the potential challenges and opportunities for the investors, retailers, electricity system operators, and policy-makers in the coming decades considering the proliferation of solar power.

1.3 Thesis Organization

The remainder of the dissertation is divided into three parts. The first part focuses on dispatch optimization of DERs in a market environment, whereas the second part focuses on joint investment and dispatch optimization. The third part focuses on the techno-economic analysis of investments in PVB systems.

PART I: Stochastic Dispatch Optimization in a Market Environment

Chapter 2 focuses on deriving optimal dispatch and bidding strategies for an aggregator who participates in sequential markets, including a day-ahead market, an intraday market with several intraday auctions, and a balancing market. The considered aggregator consists of storage devices, loads, dispatchable and variable generation units. The optimization problem is solved using multi-stage stochastic programming, which is subject to different levels of uncertainties such as variable generation outputs, day-ahead and intraday market prices. Risk management is conducted to investigate the effect of risk exposure on the

total profits of the aggregator. We use a rolling-horizon optimization approach to optimize the bidding strategy for each market bidding session using the updated information and quantify the benefits of sequential market participation.

Chapter 3 investigates the impact of considering market power on a hybrid wind-solar aggregator's optimal dispatch and trading strategies. A stochastic bi-level model is presented to derive optimal offering strategies for the aggregator, who participates as a price-maker in both the day-ahead and intraday markets, and a deviator in the balancing market. The problem considered is stochastic and subject to different levels of uncertainties. Uncertainties concerning intraday rival producers' offers are modeled using scenarios, while the uncertainty of the variable generation output is taken into consideration by formulating probabilistic constraints (i.e., chance constraints).

Chapter 4 improves the uncertainty modeling in the previously introduced models by applying distributionally robust optimization. A two-stage distributionally robust optimization model is proposed to derive optimal bidding strategies for an aggregated wind power plant that participates as a price-maker in the day-ahead market and a deviator in the balancing market. Following the principle of distributionally robust optimization, the uncertainty in wind generation output is characterized by an ambiguity set that defines a family of distributions, and the optimal decision is robust to the expectation over the worst-case uncertainty distribution.

Chapter 5 extends the works in Chapter 3 and Chapter 4 by integrating storage units into the aggregator. Hence, distributionally robust optimal bidding strategies for a price-maker wind-storage aggregator that participates in the day-ahead market and the balancing market are derived. To further improve the method's performance, an ARMA model is used to learn the auto-correlations and the cross-correlations of historical forecast errors and then generate the future paths of day-ahead forecast errors in a rolling manner.

PART II: Stochastic Investment Optimization in a Market Environment

Chapter 6 presents an optimization model to jointly optimize the generation mix and the operations for an aggregator of distributed energy resources' mix to satisfy the demand and policy targets while minimizing the total costs. The components considered include the distributed storage units, demand response programs, variable and dispatchable generation units. To better exploit the economic value of the distributed energy resources, distributed energy resources are assumed to have access to reserve and energy markets. Comprehensive sensitivity analyses are carried out to investigate the impacts of market participation, demand response potentials, policy targets, and forecast errors.

Chapter 7 extends the work in Chapter 6 by modeling the uncertainties in wind and PV generation forecasts using distributionally robust optimization. A case study demonstrates the effectiveness of the proposed distributionally robust optimization model. Out-of-sample analyses are conducted to compare its performance to two benchmark models, i.e., a robust optimization model and a stochastic optimization model. Furthermore, the impacts of considering different statistical constraints in the ambiguity set and the imbalance prices are investigated.

PART III: Techno-economic Analysis of PV-battery Systems

Chapter 8 presents a techno-economic optimization model to analyze the economic viability of a PVB system for different customer groups in Switzerland clustered based on their annual electricity consumption values, rooftop sizes, annual irradiation levels, and geographical locations. The simulations for a static investment model are carried out for the years 2020-2050. A comprehensive sensitivity analysis is conducted to investigate the impacts of individual parameters such as costs, load profiles, electricity prices, and tariffs.

Chapter 9 summarizes the thesis, concludes, and provides the potential future work.

1.4 List of Publications

The work presented in this thesis has been reported in the following publications:

Journal Publications

1. **X. Han**, E.G. Kardakos, and G. Hug, "A distributionally robust bidding strategy for a wind power plant", *Electric Power Systems Research*, vol. 177, pp. 105986, 2019.
2. **X. Han** and G. Hug, "A distributionally robust bidding strategy for a wind-storage aggregator", *Electric Power Systems Research*, vol. 189, pp. 106745, 2020.
3. **X. Han**, J. Garisson, and G. Hug, "Techno-economic analysis of PV-battery systems in Switzerland", *arXiv preprint arXiv:2103.16298*, 2021.

Conference Publications

1. **X. Han**, E.G. Kardakos, and G. Hug, "Trading strategy for decentralized energy resources in sequential electricity markets: A Swiss case study", *Innovative Smart Grid Technologies Conference Asia*, Auckland, NZ, pp. 1–7, December 2017.
2. **X. Han**, E.G. Kardakos, and G. Hug, "Offering strategy of a price-maker PV power plant: Multi-stage stochastic programming with probabilistic constraints", *Power Systems Computation Conference*, Dublin, Ireland, pp. 1–7, June 2018.
3. **X. Han** and G. Hug, "Distributionally robust generation expansion planning model considering RES integrations", *Innovative Smart Grid Technologies Conference Asia*, Chengdu, China, pp. 1716-1721, May 2019.
4. **X. Han** and G. Hug, "Joint investment and operation optimization of a distribution system in a market environment", *PowerTech Conference*, Milan, Italy, pp. 1–6, June 2019.

The following papers have been completed in the course of the PhD studies, but their content is not included in the thesis:

Journal Publications

1. Gjorgiev et al., "A platform of interfaced high-resolution models for energy-economic assessments of future electricity systems", submitted to *Applied Energy*.

Conference Publications

1. E. Raycheva, **X. Han**, and G. Hug, "Coordinated Generation Expansion Planning for Transmission and Distribution Systems", *PowerTech Conference*, Madrid, Spain, pp. 1–6, June 2021.

Other Publications and Reports

1. NEXUS-e Project, "DistIv Module Documentation", https://nexus-e.org/documentation, June 2020.
2. NEXUS-e Project, "Simulation Framework and Interfaces", https://nexus-e.org/documentation, June 2020.
3. NEXUS-e Project, "Scenario Results Report", https://nexus-e.org/documentation, June 2020.
4. NEXUS-e Project, "Validation and Calibration of Modules", https://nexus-e.org/documentation, June 2020.

Part I

Stochastic Dispatch Optimization in a Market Environment

Chapter 2

Dispatch Optimization of the Aggregator as a Price-taker

In this chapter, optimal dispatch and bidding strategies are derived for an aggregator of distributed energy resources' mix. The aggregator participates in sequential electricity markets, including a day-ahead market, an intraday market with several intraday auctions, and a balancing market. The considered aggregator consists of storage devices, loads, dispatchable and variable generation units. The optimization problem is solved using multi-stage stochastic programming, subject to different levels of uncertainties such as variable generation outputs, day-ahead, and intraday market prices. Risk management is conducted to investigate the effect of risk exposure on the aggregator profit. A rolling-horizon optimization approach is used to derive the optimal bidding strategy for each market using the updated information and quantify the benefits of participating in sequential markets. Results show that the coordination of different units within the aggregator realizes higher flexibility provisions and more profits for the aggregator. Furthermore, the presented rolling-horizon optimization method enables the aggregator to modify the dispatch schedules and market biddings based on the updated information when getting closer to the real-time delivery. Integration of more intraday auctions increases the total aggregator profits while guaranteeing lower imbalance quantities. This chapter is based on [9].

2.1 Introduction

2.1.1 Motivation and Related Work

Favorable governmental policies along with decreasing costs have been driving the growth in the penetration of Distributed Energy Resources (DERs), which are dominated by wind and Photovoltaic (PV) and are steadily replacing existing conventional units. As DER industries mature, more and more governments have announced cuts to subsidies. As a consequence, DERs urgently need to develop optimal strategies to make a profit when depending entirely on markets instead of government supports or incentives. However, DERs' participation in the market is still challenging due to the restrictions imposed by market regulations and the lack of communications with the system operators. These factors thus limit DERs' contributions to system operations and could lead to low overall energy efficiency. In order to fully utilize the value of flexibility potentials of different DERs, coordinated dispatch of diverse technologies such as combining the variable generation units with storage or dispatchable generation units is of great interest. The study presented in [10] shows that combining variable generation units with the dispatchable generation unit (e.g. Combined Heat and Power (CHP) unit) could reduce the imbalance error due to the forecast error of variable generations (up to 90% depending on the season and the strategy) by rescheduling the operations of dispatchable units at real-time. Depending on the scale of the resources, the principle of Virtual Power Plant (VPP) and hybrid project have been proposed and a number of related projects have been initiated or are under development. According to the study [11] published in 2020, there have been in total 4.6 GW of wind, gas, oil and PV power plants co-located with batteries in the US, while another 14.7 GW are in the immediate development pipeline. In the following context, we will refer to the operators of such hybrid systems as (hybrid) aggregators.

Despite the proliferation of DERs, their intermittent and uncertain nature poses great challenges to both the power plant operators and the electricity system operators. The work in [12] proposes a method to assess the impact of wind prediction errors on the incomes of the wind power plant and concludes that the error prediction costs can reach as much as 10% of its annual incomes in the electricity market. Based on the fact that the forecast error is

highly related to the forecast lead time[2], the intraday trading is more interesting to DERs as it is cleared closer to real-time and thus provides opportunities to adjust schedules and to trade with lower uncertainty levels. Actually, the reduction of imbalance costs is one of the main drivers for trading in the intraday market [13]. Therefore, besides the coordination and the aggregation of different types of DERs, considering a complete market structure is also important for increasing the profits of DER operations.

A lot of work has been done in the field of designing optimal trading strategies in sequential short-term markets. For example, the works in [14, 15, 16, 17] focus on designing optimal trading strategies for large-scale wind power plants, while references [18, 19, 20, 21] present strategies either for wind producers coordinated with energy storage technologies or a mixed renewable portfolio. In addition, different market structures are considered in different works, for instance, [14] and [16] focus on the bidding of wind energy in the Intraday Market (IDM), while [22] considers the additional participation in the Day-ahead Market (DAM). The method presented in [18] incorporates the participation in both the DAM and the Balancing Market (BM), and a more complete market structure that consists of the DAM, the IDM and the BM is considered in [15].

In this chapter, we assume that a mix of distributed storage devices, loads, variable and dispatchable generation units can participate in an electricity market including different trading floors through an aggregator. The aggregator establishes an interface between the individual unit and the system operators, following the principle of VPP[3]. While most of the existing research on bidding strategies of VPPs focuses on one specific market [14, 16, 23] or neglect the details of the market [24, 25], this work aims to provide optimal trading strategies for an aggregator considering its participation in multiple trading floors, namely a DAM, an IDM with multiple intraday auctions and a BM. Similar to the method applied in [26], a rolling-horizon approach is used to optimize the bidding decisions for each trading floor and to modify the real-time dispatch decisions with the reduced forecast uncertainties closer to real-time. Details of the rolling-horizon method will be described in Section 2.6.

[2] Forecast lead time is defined as the length of time between making the forecast and the actual realization of the value (e.g. generation, demand, price etc.) that is predicted.

[3] VPPs provide an alternative way to enable the bidding of different types of distributed energy resources in power markets, by aggregation and provision of an overall operating profile.

Consequently, the contributions of this chapter are as follows:

1. Derive a stochastic optimization model to determine the optimal trading strategies for an aggregator, which consists of storage units, loads, dispatchable and variable generation units, in a multi-market environment.
2. Use a rolling-horizon optimization method to enable the aggregator to use the updated information and to modify the real-time dispatch and the market bidding decisions in a rolling manner. To do so, the model incorporates a reduced level of variable generation output uncertainties when trading in markets that are cleared closer to the real-time delivery.
3. Model an intraday market with multiple intraday auctions and assess the impacts of including different numbers of intraday auctions.
4. Incorporate the risk control into the modeling to characterize the risk associated with profit variability, which stems from the uncertainties of market prices and variable generation outputs.

Note that wind is the only type of variable generation units considered in this work, however, it is straightforward to apply the presented approach to other variable generation units such as PV power plants.

2.1.2 Chapter Organization

The remainder of the chapter is organized as follows: the problem description and the main modeling assumptions are presented in Section 2.2, and Section 2.3 focuses on the multi-stage stochastic programming method. The mathematical formulations and the proposed optimization model are presented in Section 2.4. The method applied to generate wind scenarios considering the lead time is described in Section 2.5. Section 2.6 provides an analysis for a case study. Finally, limitations and the future work are provided in Section 2.7, and conclusions are drawn in Section 2.8.

2.2 Problem Descriptions and Model Assumptions

In this chapter, questions concerning the design of optimal trading strategies for the aggregator are addressed, enabling its participation in multiple electricity markets. The aggregator is assumed as a price-taker, i.e. its bidding

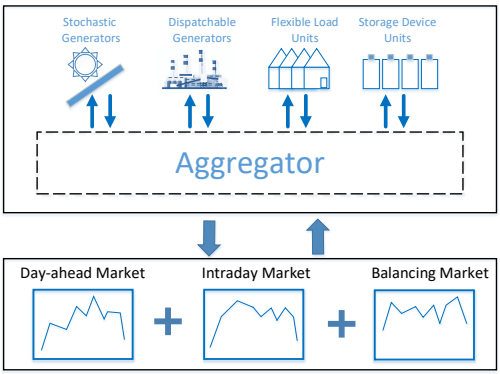

Figure 2.1: Structure for the aggregator of distributed energy resources' mix.

decisions have little impact on markets and all its offerings and biddings can be accepted by the considered electricity markets.

2.2.1 Structure of the Aggregator

The aggregator is modeled as a cluster of storage devices, loads, dispatchable and variable generators (i.e., wind generator). It integrates the characteristics of diverse units into a single entity and generates a single dispatch portfolio. Aggregation is required to take the advantage of different technologies and simultaneously enable their participation in power markets, in order to mitigate uncertainty problems and contribute to the provision of flexibility. The structure of the aggregator is shown in Fig. 2.1. All units within the aggregator are assumed to be sited in the same location, i.e. no transmission limits of the power flows between the units are considered.

2.2.2 Sequential Market Environment

The aggregator is assumed to participate in an electricity market that is organized around three trading floors: the day-ahead, the intraday and the balancing market, with multiple intraday auctions considered for the IDM. As shown in Fig. 2.2, similar to the regulations of European Power Exchange (EPEX), the DAM is assumed to be cleared the day before (i.e. day $d-1$) at 11:00 offering the hourly product in a uniform auction for the following day (i.e. day d).

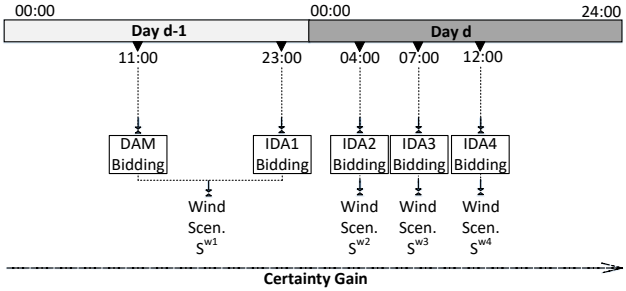

Figure 2.2: Structure of the day-ahead market and the intraday market with multiple intraday auctions.

There are mainly two forms of intraday tradings in Europe: continuous intraday trading that uses the pay-as-bid pricing scheme and the auction-based intraday trading that is based on the uniform pricing. Although the intraday markets in most of the European countries are in the form of continuous trading or a mix of continuous and auction-based tradings (e.g. Switzerland), the auction-based intraday trading is proved to have higher allocative efficiency and price transparency than the continuous one [13]. A study in [27] demonstrates that both the liquidity and the market depth increase while the price volatility decreases when introducing auctions to the existing continuous intraday trading, which is consistent with the observations that liquidity in Central Western European power markets based on the continuous intraday trading is lower than in Italy and Spain where auction based intraday tradings are implemented [28]. Thus, to increase the flexibility of the market framework and to provide more opportunities for market participants to modify their schedules, multiple Intraday Auctions (IDAs) are considered in this work.

Inspired by the structure of the auction based intraday bidding sessions in Spain, four IDAs named as **IDA1**-**IDA4**, which are cleared one hour before the start of each corresponding delivery period, are considered. As illustrated in Fig. 2.2, IDA1 to IDA4 are cleared at 23:00 on the day before the delivery day (i.e. day $d-1$), 4:00, 7:00 and 12:00 on the delivery day (i.e. day d), respectively. The considered power delivery periods in sequence for IDA1 to IDA4 are assumed to be 00:00-24:00, 5:00-24:00, 8:00-24:00 and 13:00-24:00 for day d. When bidding closer to real-time, the wind forecast scenarios are updated (from S^{w1} to

S^{w4}) using the newly arrived information, leading to a reduced level of forecast uncertainty, which will be referred to as the certainty gain effect in the following context.

In addition, in order to focus on the certainty gain effect brought by the reduced forecast uncertainty closer to the delivery time, we assume that the aggregator participates in multiple IDAs only for the purpose to reduce the imbalance costs. This is equivalent to reducing imbalance quantities, since the imbalance prices are modeled in a way to be always unfavorable to the corresponding DAM and IDM prices. To better quantify the impacts of including multiple IDAs on imbalance costs, we exclude the possibility of arbitrage between different IDAs by assuming the same market prices for all IDAs. Details of the bidding process and the generation of wind forecast scenarios will be explained in Section 2.3 and Section 2.5, respectively.

Finally, the balancing market is designed to compensate the differences between the scheduled and the measured energy and it is cleared after the realizations of supply and demand [29]. In this context, it is assumed that all imbalances can be corrected through the balancing market.

2.3 Multi-stage Stochastic Programming

As the aforementioned problem is subject to different levels of uncertainties such as market prices and wind generation outputs, the stochastic programming framework is used. Since the most straightforward way to model a stochastic process is to use scenarios, in this work, a set of scenarios characterizing different sources of uncertainties is developed based on the following structure [30]:

1. Generate N^{da} scenarios for DAM prices.
2. For each DAM price scenario, generate N^{id} scenarios for IDM prices.
3. For each IDM price scenario, generate N^{w} scenarios for real-time wind output.

Thus, we have in total $N^{tot} = N^{da} \times N^{id} \times N^{w}$ scenarios, which are assumed to have the same probability of realization. Note that the real-time wind output scenario set, i.e. S^{w}, is updated with the reduced forecast uncertainties when bidding into the markets that are cleared closer to real-time. As depicted in

Fig. 2.2, the real-time wind generation scenario sets generated by the aggregator when bidding into the DAM and IDA1, IDA2, IDA3 and IDA4 are S^{w1}, S^{w2}, S^{w3} and S^{w4}, respectively.

As the information is revealed sequentially, the scenario structure described above is fed into a multi-stage stochastic optimization model. It is important to mention the non-anticipativity characteristic of the multi-stage stochastic programming formulation, which means that if realizations of stochastic processes are identical up to a certain stage, then their decision variables must be identical up to that stage [30]. The structure of the proposed multi-stage optimization model is as follows [18, 21]:

- In electricity markets, producers and consumers must decide their supply and demand curves, respectively. As depicted in Fig. 2.2, shortly before 11:00 on the day (i.e., day $d-1$) before the delivery day, as a prosumer, the aggregator submits its Day-ahead (DA) supply and demand curves considering the initial wind forecast scenarios S^{w1} for 00:00 to 24:00 of the next day (i.e., day d). The submitted supply and demand curves consist of the price-quantity pairs (one for each DA price scenario) derived by the solution of the proposed problem. Both curves are unique (scenario independent) for each hour of the scheduling period, i.e. they are the same for all possible realizations of stochastic variables in the following stages.
- After the revelation of the DAM prices, the accepted quantity of the aggregator's biddings in the DAM is known (based on the submitted supply and demand curves). Then after the closure of the DAM and shortly before the closure of the IDA1, the aggregator updates the forecast of the wind generation outputs for hours 0:00 to 24:00 of the delivery day d considering the information newly arrived between the DAM and the closure IDA1, i.e. the realized wind generations between 11:00 and 23:00 of day $d-1$. Based on the updated forecast and the realized DA results, the aggregator fixes the realized biddings into the DAM and re-optimizes the bids for the following IDAs so as to correct its resources' schedules. The bidding processes for IDA2-IDA4 are modeled similarly to that for IDA1.

- After the IDA1 is cleared and shortly before the closure of the IDA2, the aggregator updates the forecast of the wind generation outputs for hours 5:00 to 24:00 of the delivery day d considering the wind output realizations between the closure times of IDA1 and IDA2, i.e. 0:00-4:00 of day d. Based on the updated information, the aggregator fixes the biddings accepted by the DAM and the IDA1 and then re-optimizes the bids for the following IDAs so as to correct its resources' schedules.
- After the IDA2 is cleared and shortly before the closure of the IDA3, the aggregator updates the forecast of the wind generation outputs for hours 8:00 to 24:00 of the delivery day d considering the wind output realizations between the closure times of IDA2 and IDA3, i.e. 4:00-7:00 of day d. Based on the updated information, the aggregator fixes the bidding quantities accepted by the DAM and IDA1-IDA2 and then re-optimizes the bids for the following IDAs so as to correct its resources' schedules.
- After the IDA3 is cleared and shortly before the closure of the IDA4, the aggregator updates the forecast of the wind generation outputs for hours 13:00 to 24:00 of the delivery day d considering the wind output realizations between the closure times of IDA3 and IDA4, i.e. 7:00-12:00 of day d. Based on the updated information, the aggregator fixes the bidding quantities cleared by the DAM and IDA1-3 and then re-optimizes the bids for IDAs4 so as to correct its resources' schedules.
- For each hour of the delivery day d, after the DAM and all the IDAs related to that hour are cleared, i.e. the total accepted DAM and IDM supply and demand quantities submitted by the aggregator for that hour are known, the aggregator decides on the Real-time (RT) dispatch of all units within the aggregator.

Note that when the aggregator submits the supply and demand curves to the DAM at 11:00 for day $d-1$, it has to forecast the wind output for 00:00 to 24:00 of the following day (i.e., day d), 13-37 hours in advance. When bidding into the IDAi ($i \in \{1,2,3,4\}$), the historical wind output between the closures of the DAM and the IDAi is realized, and thus can be used to improve the hourly wind forecast for the delivery day. In other words, the aggregator bids into the IDAi with a reduced wind uncertainty level than that for the DAM and the previous IDAs. However, due to the lack of data, as shown in Fig. 2.2,

the aggregator is assumed to bid into the DAM and the IDA1 considering an identical set of wind scenarios, i.e. S^{w1}. In other words, the wind scenarios are not improved/updated between 11:00 and 23:00 on day $d-1$.

2.4 Mathematical Formulation

As introduced in Section 2.2, the aggregator consists of four different types of components, namely loads, storage devices, dispatchable and variable generation units (i.e. wind units), as shown in Fig. 2.1. It participates in the day-ahead, intraday and balancing markets. To optimize the trading strategies of the aggregator, all types of devices as well as how they are coordinated and the market environment in which they participate need to be modeled.

2.4.1 Aggregator Modeling

Dispatchable Generation Unit

The power output of the dispatchable generation unit $P^{\text{g}}_{t,\omega}$ at time t for scenario ω is limited by the maximum and the minimum power output $P^{\text{g,max}}$ and $P^{\text{g,min}}$, and the maximum ramp rate $r^{\text{g,max}}$, i.e.,

$$u^{\text{g}}_{t,\omega} P^{\text{g,min}} \leq P^{\text{g}}_{t,\omega} \leq u^{\text{g}}_{t,\omega} P^{\text{g,max}} \tag{2.1}$$

$$|P^{\text{g}}_{t,\omega} - P^{\text{g}}_{t-1,\omega}| \leq r^{\text{g,max}} \tag{2.2}$$

where u^{g} is a binary variable denoting the on or off status of the generator. The startup and shut down statuses are denoted by two binary variables y^{g} and z^{g}, which are restricted by

$$y^{\text{g}}_{t,\omega} - z^{\text{g}}_{t,\omega} = u^{\text{g}}_{t,\omega} - u^{\text{g}}_{t-1,\omega} \tag{2.3}$$

$$y^{\text{g}}_{t,\omega} + z^{\text{g}}_{t,\omega} \leq 1 \tag{2.4}$$

ensuring that the dispatchable generation unit may not operate in startup and shut down modes simultaneously.

The total generation cost of the dispatchable unit consists of two parts: 1) the startup and shut down cost C^{SUD} and 2) the production cost C^{OP} that is approximated with a piece-wise linear function based on [31, 32], which consists of a fixed production cost and the total marginal production costs over

N^{b} production blocks. Mathematically,

$$C^{\mathrm{SUD}}_{t,\omega} = c^{\mathrm{su}} y^{\mathrm{g}}_{t,\omega} + c^{\mathrm{sd}} z^{\mathrm{g}}_{t,\omega} \tag{2.5}$$

$$C^{\mathrm{OP}}_{t,\omega} = c^{\mathrm{foc}} u^{\mathrm{g}}_{t,\omega} + \sum_{b=1}^{N^{\mathrm{b}}} c^{\mathrm{voc}}_{b} P^{\mathrm{g}}_{t,\omega,b} \tag{2.6}$$

where c^{su}, c^{sd}, c^{foc} and c^{voc} are constants. Variable $P^{\mathrm{g}}_{t,\omega,b}$ is the power produced by the dispatchable generation unit at time t for scenario ω and production block b and it is related to the total power output of the dispatchable unit with the following equation:

$$P^{\mathrm{g}}_{t,\omega} = P^{\mathrm{g,min}} u^{\mathrm{g}}_{t,\omega} + \sum_{b=1}^{N^{\mathrm{b}}} P^{\mathrm{g}}_{t,\omega,b} \tag{2.7}$$

$$0 \leq P^{\mathrm{g}}_{t,\omega,b} \leq \Delta P^{\mathrm{g}}_{b} \tag{2.8}$$

where $\Delta P^{\mathrm{g}}_{b}$ is the maximum power that could be produced by the dispatchable unit for production block b.

Storage Device

A generic storage model is applied. The minimum and the maximum stored energy of the storage are defined by $E^{\mathrm{s,min}}$ and $E^{\mathrm{s,max}}$, while the maximum inflow and outflow of the storage are indicated by $P^{\mathrm{ch,max}}$ and $P^{\mathrm{dis,max}}$, respectively. This results in the following set of equations:

$$E^{\mathrm{s,min}} \leq E^{\mathrm{s}}_{t,\omega} \leq E^{\mathrm{s,max}} \tag{2.9}$$

$$0 \leq P^{\mathrm{ch}}_{t,\omega} \leq P^{\mathrm{ch,max}} \tag{2.10}$$

$$0 \leq P^{\mathrm{dis}}_{t,\omega} \leq P^{\mathrm{dis,max}} \tag{2.11}$$

where E^{s}, P^{ch} and P^{dis} indicate the stored energy, charging and discharging power of the storage, respectively. Finally, the relationship of storage levels for two consecutive time steps are defined by

$$E^{\mathrm{s}}_{t,\omega} = E^{\mathrm{s}}_{t-1,\omega} + \eta^{\mathrm{s}} P^{\mathrm{ch}}_{t,\omega} \Delta t - P^{\mathrm{dis}}_{t,\omega} \Delta t / \eta^{\mathrm{s}} \tag{2.12}$$

where η^{s} indicates the one-way conversion efficiency of the storage unit and Δt is the length of one time step.

Load

It is assumed that parts of the aggregator's loads are flexible and participate in the Demand Response Program (DRP) through load shifting from the initial load estimation l^{est} (including both flexible and inflexible loads). The final scheduled load profile is given by

$$l^{\text{sch}}_{t,\omega} = l^{\text{est}}_{t} + r^{\text{lu}}_{t,\omega} - r^{\text{ld}}_{t,\omega} \tag{2.13}$$

where r^{lu} and r^{ld} indicate the load increase and decrease, respectively. The load increase and decrease are determined considering the following constraints: 1) the load increase or decrease cannot exceed the maximum load allowed to be shifted for each hour denoted by l^{dr} (defined by the DRP contract signed between the aggregator and the consumers); 2) the load decrease is limited by the current energy consumption $l^{\text{est,flex}}$ of the flexible portion of the total load; and 3) the load increase cannot exceed the difference between the maximum energy consumption $l^{\text{lsh,max}}$ (i.e. capacity) of the flexible load and the current energy consumption of the flexible load. Mathematically, r^{lu} and r^{ld} are enforced to satisfy the following equations [33]:

$$0 \leq r^{\text{ld}}_{t,\omega} \leq l^{\text{dr}} u^{\text{ld}}_{t,\omega} \tag{2.14}$$

$$0 \leq r^{\text{lu}}_{t,\omega} \leq l^{\text{dr}} u^{\text{lu}}_{t,\omega} \tag{2.15}$$

$$0 \leq r^{\text{ld}}_{t,\omega} \leq l^{\text{est,flex}}_{t} u^{\text{ld}}_{t,\omega} \tag{2.16}$$

$$0 \leq r^{\text{lu}}_{t,\omega} \leq (l^{\text{lsh,max}} - l^{\text{est,flex}}_{t}) u^{\text{lu}}_{t,\omega} \tag{2.17}$$

$$u^{\text{ld}}_{t,\omega} + u^{\text{lu}}_{t,\omega} \leq 1 \tag{2.18}$$

where u^{lu} and u^{ld} are binary variables indicating the load increase or decrease, respectively. The last equation ensures that only one of u^{lu} or u^{ld} is 1. Furthermore, for each day starting at time t_0, the total daily shifted load defined as the sum of absolute values of the load decreases and increases over the day is

restricted by an upper limit, i.e.,

$$\sum_{t=t_0}^{t_0+24} (r_{t,\omega}^{\text{lu}} + r_{t,\omega}^{\text{ld}})\Delta t \leq E^{\text{lsh,max}} \tag{2.19}$$

Additionally, it is required that the total daily energy consumption should not be changed, i.e.,

$$\sum_{t=t_0}^{t_0+24} (r_{t,\omega}^{\text{lu}} - r_{t,\omega}^{\text{ld}}) = 0 \tag{2.20}$$

Under the assumption that the DRP is based on the long-term contracts with consumers, the cost for the DRP is therefore neglected.

Aggregator's Portfolio

The aggregator along with the sequential markets (i.e., the DAM, the IDM and the BM) constitutes a closed energy system that must be balanced at each time step. This means that the amount of energy that is generated from both the dispatchable and wind power plants and drawn from the storage units minus the amount of energy that is consumed by the load and used to charge the storage units must be equal to the exchange in spot electricity markets for each time step, i.e.

$$P_{t,\omega}^{\text{g}} + P_{t,\omega}^{\text{w}} + P_{t,\omega}^{\text{dis}} - l_{t,\omega}^{\text{sch}} - P_{t,\omega}^{\text{ch}} = q_{t,\omega}^{\text{DA}} + q_{t,\omega}^{\text{ID}} + q_{t,\omega}^{\text{BM+}} - q_{t,\omega}^{\text{BM-}} \tag{2.21}$$

where P^{w} is the power output of the wind unit, $q^{\text{BM+}}$ and $q^{\text{BM-}}$ are the positive and negative imbalances. The aggregator's DAM and IDM bidding quantities q^{DA} and q^{ID} are defined as

$$q_{t,\omega}^{\text{DA}} = q_{t,\omega}^{\text{DAs}} - q_{t,\omega}^{\text{DAb}} \tag{2.22}$$

$$q_{t,\omega}^{\text{ID}} = q_{t,\omega}^{\text{IDs}} - q_{t,\omega}^{\text{IDb}} \tag{2.23}$$

where q^{DAs} and q^{DAb} are the non-negative DAM supply and demand quantities, while q^{IDs} and q^{IDb} are the non-negative IDM supply and demand quantities.

2.4.2 Formulation of the Electricity Markets

Day-ahead Market

We decompose the aggregator's DA bidding curve $(q^{\mathrm{DA}}_{t,\omega}, pr^{\mathrm{DA}}_{t,\omega})$, into a supply curve $(q^{\mathrm{DAs}}_{t,\omega}, pr^{\mathrm{DA}}_{t,\omega})$ and a demand curve $(q^{\mathrm{DAb}}_{t,\omega}, pr^{\mathrm{DA}}_{t,\omega})$, where each block of the supply and demand curves is associated with one scenario of the DAM price pr^{DA}. The non-decreasing (non-increasing) characteristic of the resulting supply (demand) curve is ensured by

$$q^{\mathrm{DAs}}_{t,\omega} \leq q^{\mathrm{DAs}}_{t,\omega'} \qquad \forall t, \forall \omega, \omega' : \qquad pr^{\mathrm{DA}}_{t,\omega} \leq pr^{\mathrm{DA}}_{t,\omega'} \tag{2.24}$$

$$q^{\mathrm{DAb}}_{t,\omega} \leq q^{\mathrm{DAb}}_{t,\omega'} \qquad \forall t, \forall \omega, \omega' : \qquad pr^{\mathrm{DA}}_{t,\omega} \geq pr^{\mathrm{DA}}_{t,\omega'} \tag{2.25}$$

The non-anticipativity of the DAM decisions is enforced by

$$q^{\mathrm{DAs}}_{t,\omega} = q^{\mathrm{DAs}}_{t,\omega'} \qquad \forall t, \forall \omega, \omega' : \qquad pr^{\mathrm{DA}}_{t,\omega} = pr^{\mathrm{DA}}_{t,\omega'} \tag{2.26}$$

$$q^{\mathrm{DAb}}_{t,\omega} = q^{\mathrm{DAb}}_{t,\omega'} \qquad \forall t, \forall \omega, \omega' : \qquad pr^{\mathrm{DA}}_{t,\omega} = pr^{\mathrm{DA}}_{t,\omega'} \tag{2.27}$$

which forces the DA decisions to be the same in all scenarios with identical DAM prices. In other words, the hourly DA supply (demand) curve is unique, irrespective of the market prices and wind output realizations [30].

Intraday Market

As depicted in Fig. 2.2, four intraday auctions that are cleared at 23:00 on day $d-1$, 4:00, 7:00 and 12:00 on day d respectively, are considered. The IDAs are modeled in a similar way as the DAM, except that their gate closure times are closer to real-time delivery and the biddings into the IDAs are exposed to a reduced level of the wind output uncertainty. Besides the non-decreasing (non-increasing) characteristic, the hourly supply (demand) curve submitted to each IDA is unique, i.e. independent of the realizations of the IDA prices and the real-time wind outputs. Consequently, for each IDAi, the decisions (points on the supply/demand curve) should be equal in all scenarios with identical realizations of uncertainties up to IDAi, i.e. DAM prices, IDAs prices and wind

outputs between the DAM and the corresponding IDA. This is modeled as

$$q^{\text{IDs}}_{t,\omega,i} \leq q^{\text{IDs}}_{t,\omega',i} \qquad \forall t, \forall \omega, \omega' : \quad pr^{\text{ID}}_{t,\omega} \leq pr^{\text{ID}}_{t,\omega'} \tag{2.28}$$

$$q^{\text{IDb}}_{t,\omega,i} \leq q^{\text{IDb}}_{t,\omega',i} \qquad \forall t, \forall \omega, \omega' : \quad pr^{\text{ID}}_{t,\omega} \geq pr^{\text{ID}}_{t,\omega'} \tag{2.29}$$

$$q^{\text{IDs}}_{t,\omega,i} = q^{\text{IDs}}_{t,\omega',i} \qquad \forall t, \forall \omega, \omega' : \quad pr^{\text{DA}}_{t,\omega} = pr^{\text{DA}}_{t,\omega'} \tag{2.30}$$

$$\forall t, \forall \omega, \omega' : \quad pr^{\text{ID}}_{t,\omega} = pr^{\text{ID}}_{t,\omega'} \tag{2.31}$$

$$q^{\text{IDb}}_{t,\omega,i} = q^{\text{IDb}}_{t,\omega',i} \qquad \forall t, \forall \omega, \omega' : \quad pr^{\text{DA}}_{t,\omega} = pr^{\text{DA}}_{t,\omega'} \tag{2.32}$$

$$\forall t, \forall \omega, \omega' : \quad pr^{\text{ID}}_{t,\omega} = pr^{\text{ID}}_{t,\omega'} \tag{2.33}$$

Note that the IDA prices are not dependent on the IDA index i as the market prices for all IDAs are assumed to be the same (see subsection 2.2.2 for more details). Variables q^{IDs} and q^{IDb} are the aggregator's supply and demand quantities for IDAi with

$$\sum_{i=1}^{N^{\text{ida}}} q^{\text{IDs}}_{t,\omega,i} = q^{\text{IDs}}_{t,\omega} \tag{2.34}$$

$$\sum_{i=1}^{N^{\text{ida}}} q^{\text{IDb}}_{t,\omega,i} = q^{\text{IDb}}_{t,\omega} \tag{2.35}$$

where N^{ida} is the total number of IDAs, i.e. four in this work. As mentioned in Section 2.2.2, the considered power delivery periods for the four IDAs are assumed to be 00:00-24:00, 5:00-24:00, 8:00-24:00 and 13:00-24:00 for the delivery day, respectively. Therefore, the bidding quantities for the periods that are not considered by the corresponding IDA should be set to zero, i.e.

$$q^{\text{IDs/b}}_{t,\omega,2} = 0, \qquad t_0 \leq t \leq t_0 + 4 \tag{2.36}$$

$$q^{\text{IDs/b}}_{t,\omega,3} = 0, \qquad t_0 \leq t \leq t_0 + 7 \tag{2.37}$$

$$q^{\text{IDs/b}}_{t,\omega,4} = 0, \qquad t_0 \leq t \leq t_0 + 12 \tag{2.38}$$

Although the total intraday trading volume increases continuously in recent years, it is still low compared to the total energy traded in the DAM. According to the data published in [34], the total energy traded in the EPEX spot markets in 2019 amounted to 593.2 TWh, of which 501.6 TWh are from the DAM trad-

ing, whereas the volume of the IDM trading for the same year is equal to the remaining 91.6 TWh (i.e., 83.2 TWh from intraday continuous trading and 8.4 TWh from intraday auctions). Based on this fact, a parameter γ^{ID} is defined to limit the trading volume in the IDM according to

$$\sum_{t=1}^{T} q_{t,\omega}^{\text{ID}} \leq \gamma^{\text{ID}} \sum_{t=1}^{T} q_{t,\omega}^{\text{DA}} \tag{2.39}$$

where T is the simulation horizon.

Balancing Market

Balancing market prices are modeled following a two-price settlement scheme, which is commonly applied in European electricity markets. Compared to a single-price imbalance price settlement scheme, where imbalance prices are irrespective of wether the balance group is in deficit or surplus, the imbalance prices in a two-price system are determined according to the deviation direction of a balance group. The price of the positive imbalance, i.e. the price of selling electricity in the BM in the case of surplus generation or deficit consumption, is defined by $pr^{\text{BM+}}$ and the price of the negative imbalance, i.e. the price of purchasing electricity in the BM under the situation of deficit generation or surplus consumption, is defined by $pr^{\text{BM-}}$. In this work, we assume that the hourly BM price is dependent on the DAM and IDM prices of that hour and therefore the uncertainty concerning the BM price is not considered. This is defined by the following equation, which ensures that the aggregator can only sell (purchase) electricity in the BM at a price lower (higher) than the corresponding day-ahead and intraday market prices [29]:

$$pr_{t,\omega}^{\text{BM+}} = a_1 \cdot \min\{pr_{t,\omega}^{\text{DA}},\ pr_{t,\omega}^{\text{ID}}\} \qquad \forall t, \forall \omega \tag{2.40}$$

$$pr_{t,\omega}^{\text{BM-}} = a_2 \cdot \max\{pr_{t,\omega}^{\text{DA}},\ pr_{t,\omega}^{\text{ID}}\} \qquad \forall t, \forall \omega \tag{2.41}$$

where a_1 and a_2 are all positive constants with $0 \leq a_1 \leq 1$ and $a_2 \geq 1$.

2.4.3 Formulation of Risk Constraints

Additionally, trade-offs have to be made between the expected profit and the impact of uncertainty. Hence, the objective function consists of two parts: one

maximizing the expected profit R of the aggregator, and the other minimizing the risk exposure to uncertainties using the Conditional Value at Risk (CVaR) [35] of the expected profits, i.e.

$$\max \left\{ (1-\beta)R + \beta(\zeta - \frac{1}{1-\alpha}\sum_{\omega=1}^{N^{\text{tot}}} \xi_\omega \zeta_\omega) \right\} \tag{2.42}$$

where ξ_ω represents the realization probability of scenario ω with in total N^{tot} scenarios considered; β is a weighting parameter with $\beta \in [0,1]$; α is the confidence level with $\alpha \in (0,1)$; ζ and ζ_ω are auxiliary variables restricted by

$$\begin{aligned} \zeta - R_\omega &\leq \zeta_\omega \\ \zeta_\omega &\geq 0 \end{aligned} \tag{2.43}$$

where R_ω is the profit of scenario ω with $\sum_{\omega=1}^{N^{\text{tot}}} \xi_\omega R_\omega = R$.

2.4.4 Formulation of the Optimization Problem

The total profits of the aggregator comprise the profits from participating in the day-ahead market, the intraday market and the balancing market minus the generation costs. Mathematically,

$$\begin{aligned} R = \sum_{t=1}^{T}\sum_{\omega=1}^{N^{\text{tot}}} \xi_\omega (&pr_{t,\omega}^{\text{DA}} q_{t,\omega}^{\text{DA}} + pr_{t,\omega}^{\text{ID}} q_{t,\omega}^{\text{ID}} - pr_{t,\omega}^{\text{BM-}} q_{t,\omega}^{\text{BM-}} + pr_{t,\omega}^{\text{BM+}} q_{t,\omega}^{\text{BM+}} \\ &- C_{t,\omega}^{\text{OP}} - C_{t,\omega}^{\text{SUD}}) \end{aligned} \tag{2.44}$$

Note that only generation costs of the conventional units are considered, while the generation costs of variable generation units (i.e. wind units) and storage devices are assumed to be zero.

Finally, the optimization problem is formulated as:

$$\max \left\{ (1-\beta)R + \beta(\zeta - \frac{1}{1-\alpha}\sum_{\omega=1}^{N^{\text{tot}}} \xi_\omega \zeta_\omega) \right\} \tag{2.45}$$

s.t. Constraints (2.1)-(2.43)

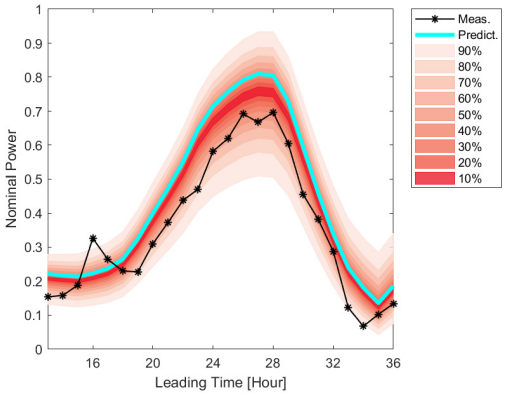

Figure 2.3: Example probabilistic forecasts generated using the method from [1] with the 13-hour to 36-hour ahead lead time along with the day-ahead point forecast and the real-time measurement data for the simulation day.

where constraints regarding different components of the aggregator (i.e. storage, load, dispatchable and variable generation units), different electricity markets are given in (2.1)-(2.41), and the constraints concerning risk control are given in (2.43).

2.5 Wind Scenario Generation

To optimize the trading strategies of the aggregator in sequential electricity markets that have different gate closure times, forecasts of wind should be generated in a way to account for the development of the forecast uncertainties over time (i.e., a reduced level of wind output uncertainty should be considered when bidding into the market that is cleared closer to the real-time delivery). We therefore generate the scenarios for wind forecasts using the method proposed in [1, 36] to account for the interdependence of forecast errors with different lead times and to better simulate the development of wind forecasts in reality. Based on the available historical forecast and measurement data, it is proposed by [1, 36] to convert the series of the forecast errors to a multivariate Gaussian random variable, whose interdependence structure is then described by a unique covariance matrix. We applied the method by setting

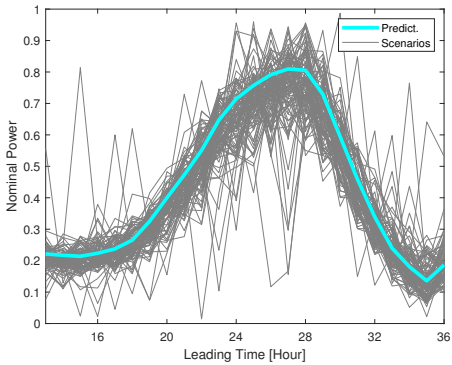

Figure 2.4: Example day-ahead wind forecast scenarios generated using the method from [1] along with the day-ahead point forecast data from Nord Pool for the same time period as Fig. 2.3.

the forgetting factor that permits an adaptive tracking of the interdependence structure of prediction errors to 0.995, which is identical to the value used in [1]. The resulting probabilistic forecast of the real-time wind generation takes the form of a predictive distribution over 9 quantiles ranging from 10% to 90% with an increment of 10%. As an example, the probabilistic forecast for the simulation day with the lead time from 13-hour to 36-hour ahead along with the DA point forecasts and the real-time measurements based on the Nord Pool 2016 data for Denmark [37] is presented in the form of a fan chart in Fig. 2.3. In addition, 100 real-time wind output scenarios generated using the method from [1] along with the DA point forecast for the same time period are shown in Fig. 2.4. These real-time wind output scenarios have a lead time from 13-hour to 36-hour ahead, which corresponds to the wind output scenario S^{w1} faced by the DAM and the IDA1 biddings. Wind scenarios S^{w2}, S^{w3} and S^{w4}, which are used when bidding into the IDA2-IDA4, are updated based on the corresponding newly arrived wind output realization information. Due to the lack of data to generate wind output scenarios with shorter lead times, the wind scenarios are updated by selecting the wind scenarios that have the highest forecast accuracy[4] for the revealed wind output realizations for the delivery day d. To be more specific, the aggregator bids into the DAM and IDA1 using

[4]The forecast accuracy is estimated using the mean squared error.

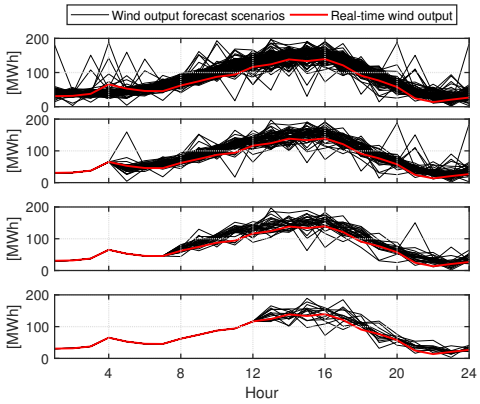

Figure 2.5: Updated wind generation scenarios over different bidding stages along with the realized wind output at real-time. From top to down the figures correspond to the real-time wind output scenarios S^{w1}, S^{w2}, S^{w3} and S^{w4}.

the initial wind output scenario set S^{w1} built with a lead time from 13-hour to 36-hour ahead by applying the method in [1, 36]. When bidding into the IDA2 shortly before 4:00 on the delivery day d, the updated wind scenario set S^{w2} is built by selecting the N^{w2} wind scenarios in S^{w1} that achieve the highest forecast accuracy for the forecast period 0:00 to 4:00 on day d, where N^{w2} is the number of scenarios included in scenario set S^{w2}. Similarly, based on the realizations of the real-time wind outputs, wind scenario sets S^{w3} and S^{w4} are generated by selecting the scenarios that obtain the highest forecast accuracy for the periods 0:00-7:00 and 0:00-12:00 on day d, respectively.

Figure 2.5 shows the resulting wind scenarios (i.e. S^{w1}, S^{w2}, S^{w3} and S^{w4}) corresponding to the four bidding stages[5] generated following the process described above. It can be observed that a shorter lead time enables a reduced forecast uncertainty.

[5]DAM and IDA1 are combined as one bidding stage due to the assumption of identical real-time wind output scenarios, while IDA2-IDA4 are considered as the second, third and the fourth bidding stages, respectively.

Table 2.1: Parameters of units within the aggregator.

Category	Parameter	Adopted Value
Wind	Capacity	200 MW
	Marginal cost	0 EUR/MWh
Battery Storage	Capacity	240 MWh
	Max./min. energy level	240/20 MWh
	Initial energy level	0 MWh
	Max. charging/discharging power	120 MW
	Charging/discharging efficiency	90%
Dispatchable Generator	Capacity	120 MW
	Max./min. production level	120/40 MW
	Initial production level	40 MW
	Startup/shutdown cost	800/100 EUR
	Fixed operational cost	1000 EUR
	Marginal cost	40-60 MW: 23.5 EUR/MWh
		60-80 MW: 31.5 EUR/MWh
		80-100 MW: 45.6 EUR/MWh
		100-120 MW: 72.3 EUR/MWh
DRP	Max. hourly shiftable power	30 MW
	Max. daily shiftable energy	150 MWh
	Max. consumption of flexible load	72 MW

2.6 Case Study

In this section, we first show the results considering the aggregator's participation only in the DAM and the BM, i.e. no IDM is considered. Then we investigate the impacts of including different numbers of IDAs and the influence of the modeled intraday trading limits.

2.6.1 Input Data

The proposed methodology is implemented using the MATLAB toolbox Yalmip [38]. Information of the units per category within the aggregator is provided in Table 2.1, where the parameters of the dispatchable generation unit are modified based on the data from [32]. All units considered are aggregated and consist of several individual generators, loads or storage devices. The load (including the DRP information) is from the example in [33] and the estimation of the total load as well as the flexible load is shown in Appendix 9.3.

Market price forecasting is outside the scope of this thesis, we therefore simulate the scenarios of the market prices based on the historical data obtained from EPEX. These data are publicly available [39] and correspond to the DAM

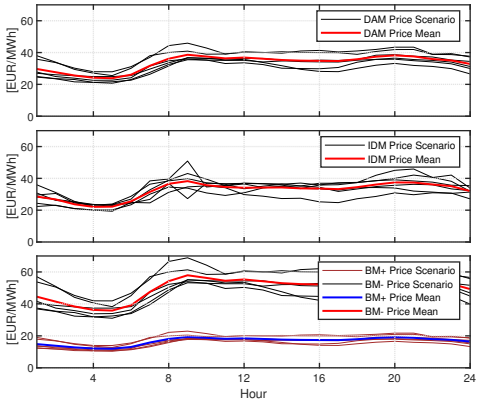

Figure 2.6: Scenarios for day-ahead, intraday and balancing market prices.

and IDM prices that occurred on the Tuesdays from August 2016 to September 2016. As mentioned in subsection 2.2.2, the market price of all IDAs are assumed to be the same so as to focus on the certainty gain effect brought by the IDM trading. The number of market price scenarios are six and the average DAM and IDM prices for this period were 33.45 EUR/MWh and 32.39 EUR/MWh, respectively. Balancing market prices are difficult to predict or simulate and the rules for calculating the balancing market prices vary from market to market, we therefore set the parameters for the balancing market price as $a_1 = 0.5$ and $a_2 = 1.5$ so as to possibly avoid the arbitrage opportunities between the BM and the DAM or the IDM. Scenarios for the DAM, the IDM and the BM prices are shown in Fig. 2.6. Scenarios for the real-time wind output is generated based on the data from Nord Pool [37] following the process described in Section 2.5. The number for the RT wind output scenario sets S^{w1}, S^{w2}, S^{w3} and S^{w4} are set as 100, 50, 25 and 13, respectively.

The confidence level α for calculating the CVaR is set to 0.95, while the weighting parameter β is set as 0 (i.e., the aggregator is assumed to be risk-neutral) for the Baseline scenario and sensitivity analysis is conducted for simulating different values of β between 0 and 0.8. The simulation is carried out for one day (i.e., 24 hours), but due to the low computational efficiency, the simulation horizon can be expanded in a straightforward way.

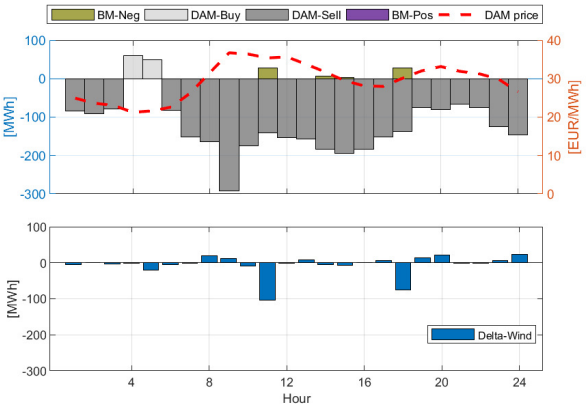

Figure 2.7: Single scenario analysis for the aggregator participating only in the day-ahead and the balancing markets: market trading behaviors are shown in the top figure; deviations of the wind generation of the considered scenario from the expected wind generation of all scenarios named as "Delta-Wind" are shown in the bottom figure.

2.6.2 Results: Analysis of the Day-ahead Market Behavior

In this section, we analyze the results considering that the aggregator only participates in the DAM and the BM, i.e. no IDM is considered. To better illustrate the results, we first show the results of one example scenario, then the benefits of coordinating different types of units are analyzed. Finally, to analyze the influence of the risk appetite of the aggregator, sensitivity analyses are conducted by applying different values of β (the aggregator is assumed to be risk-neutral in the Baseline scenario with β set to 0).

Single Scenario Analysis

Figure 2.7 shows the market trading behaviors of the aggregator in an example scenario (i.e., top figure) together with the deviations of the wind generation of the considered scenario from the expected wind generation of all scenarios named as "Delta-Wind" (i.e., bottom figure). Focusing on the top figure that depicts the trading behaviors of the aggregator, it is seen that generally the aggregator is a market seller as it generates more than it consumes, and

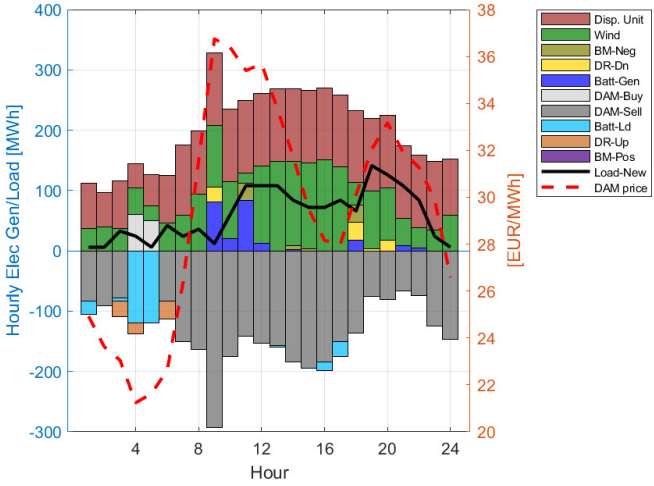

Figure 2.8: Single scenario analysis for the aggregator participating only in the day-ahead and the balancing markets: optimal real-time dispatch of different units within the aggregator as well as the aggregator's market biddings and the rescheduled hourly load named as "Load-New".

it trades in the market according to the "buy low, sell high" strategy. Futhermore, since BM prices are always unfavorable to DAM prices, balancing energy should only be used for covering deviations between scheduled electricity and actually produced electricity. This is confirmed by the observation that the negative imbalance occurs mainly in hours 11 and 18 when the wind generation level of the considered scenario is much lower than that of the expected wind generation (i.e., Delta-Wind is negative). However, the imbalance quantities are limited compared to the wind deviation (i.e., Delta-Wind). This is likely to be explained by the coordination of different units within the aggregator and is further analyzed using Fig. 2.8, which shows the real-time dispatch of different units as well as the market biddings and the rescheduled hourly load (i.e., Load-New) of the aggregator. Combining Fig. 2.7 and Fig. 2.8, we can see that both the storage device and the flexible load operate mainly in response to the DAM prices and the wind output deviation. More specifically, on one hand, the flexible load (the storage device) shifts up (charges) during the lower price

Table 2.2: Impacts of coordinations on the profit obtained by each unit within the aggregator and the total aggregator profit.

	Dispatchable unit	Wind	Storage	Load	Total
Without coordination [EUR]	27'141	63'761	983	-50'905	40'981
With coordination [EUR]	22'434	72'587		-51'373	43'648 (+6.5%)

Negative values indicate the costs.

period, i.e. hours 3, 4 and 6 (hours 1, 3-5), and shifts down (discharges) during the high price period, i.e. hours 9, 19-20 (hours 9-12); on the other hand, the flexible load and the storage device also operates in order to possibly reduce the imbalances caused by the wind output deviation. For example, despite the comparably low DAM price level in hour 18, the flexible load shifts down and the storage device discharges so as to reduce the large negative wind deviations during that hour. Similarly, the dispatchable generation unit ramps up and down considering the impact of the DAM prices and the wind generation deviation. It is also worth noting that even during the period when market prices are lower than the marginal cost of the first production block (i.e. 23.5 EUR/MWh) of the dispatchable generator, i.e., hour 3-5, the dispatchable generator still stays online and operates at a low level due to the effects of startup and shut-down costs.

Benefits of Coordination

The benefits of the coordination between different units within the aggregator are already shown in the previous section, to quantify these benefits, we compare the profits obtained with and without considering the coordination of different units. In the case without coordinations, each unit is assumed to operate and bid into the market aiming to maximize its own profits without considering the impact on the total profits of the aggregator. Results of these two cases are listed down in Table 2.2, where positive and negative values indicate the profits and costs, respectively. Note that it is difficult to separate the profits achieved by each single unit in the case with coordination. The profits obtained by the dispatchable unit are calculated as the sum of the product of the DAM price and the generation minus the total generation costs over the simulation horizon, the profits for the load unit are calculated as the sum of the negative load consumption multiplied by the DAM price, while the remain-

ing profits of the aggregator are assumed to be generated together by the wind and the storage units. It can be observed in Table 2.2 that compared to the case without coordination the total aggregator profits increase by 6.5% in the case with coordination, however, this is at the cost of decreasing the profits earned by the dispatchable unit and the load unit. Hence, it is important to design an appropriate mechanism to distribute the total profits of the aggregator to the different units within it in a fair and an efficient way. The work in [40] addresses the problem of profit allocation between an energy storage aggregator and its constituent storage units by using a Nash Bargaining Process.

Impact of Risk Control

In this section, the optimization problem (2.45) is solved applying different values of the weighting parameter β with $\beta \in [0, 1]$, and the impact of risk control is analyzed by comparing the resulting DA bidding curves, imbalances and the total profits of the aggregator. As a reminder, the aggregator is more risk-averse with an increasing value of β.

The aggregator bids into the DAM with a bidding curve, which consists of a series of price-quantity pairs and are independent of the DA price realizations. The DA bidding curve of the aggregator under the risk-neutral case (i.e. $\beta = 0$) and the risk-averse case (i.e. $\beta = 0.8$) for example hours 9, 10 and 11 are shown in Fig. 2.9. It can be seen that the lowest price at which the aggregator is willing to supply varies between hours, which is likely due to the different expectation of electricity prices for different hours. Comparing the risk-neutral case (i.e. $\beta = 0$) to the risk-averse case (i.e. $\beta = 0.8$), in general the aggregator prefers to offer less in the DAM when it becomes more risk-averse.

To further investigate the impacts of risk control, we plot the development of imbalances and the profits with β increasing from 0 to 0.8 with a step of 0.1 in Fig. 2.10. It shows that in general the negative imbalance decreases with the increasing level of risk aversion, while the change of positive imbalances is negligible. Furthermore, the total aggregator profit decreases and the CVaR increases as the risk exposure decreases. The trade-off between the risk exposure and the profits helps to hedge against uncertainty when participating in sequential electricity markets.

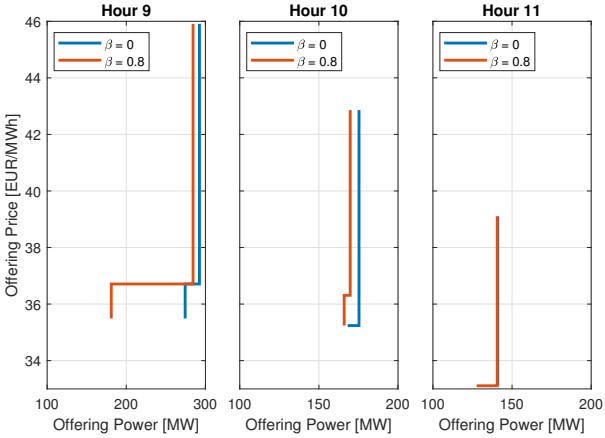

Figure 2.9: Day-ahead bidding curves of the aggregator under $\beta = 0$ and $\beta = 0.8$ for example hours 9, 10 and 11.

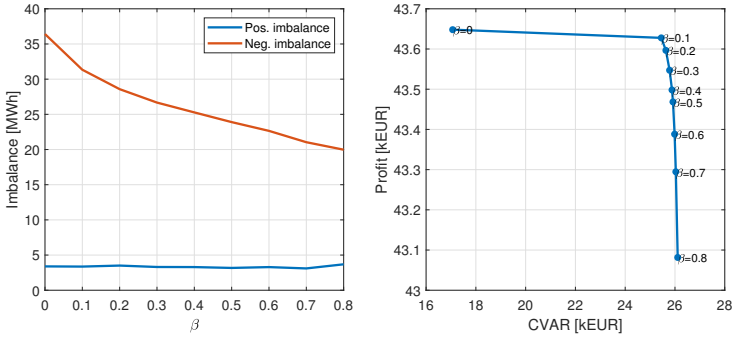

Figure 2.10: Impacts of risk aversion on the expected imbalance quantities (i.e., left figure) and the aggregator profits (i.e., right figure).

2.6.3 Results: Impacts of the Intraday Market

In this section, the impacts of including the IDM as well as the number of the considered IDAs are investigated. In order to compare the results of including different numbers of IDAs in a reasonable way, we carried out the simulations based on a rolling horizon approach, which is capable of solving a multi-stage problem periodically considering the additional information available at each

Table 2.3: Impacts of including different numbers of intraday auctions.

	1 IDA	2 IDAs	3 IDAs	4 IDAs
Expected profit [kEUR]	34.4	34.8	35.2	36.9
Expected imbalance cost [kEUR]	16.6	15.8	14.9	9.9
Expected net imbalance [MWh]	-293	-280	-263	-146

stage. The simulations are conducted in a rolling manner following the steps below:

- Step 1: The optimization problem (2.45) is solved considering the initial wind output forecast scenario S^{w1} and without considering IDA2-IDA4 (i.e., bidding quantities for IDA2-IDA4 are set to be zero).
- Step 2: The resulting optimized DAM and the IDA1 decisions from step 1 are then fixed and fed back to the model. The optimization problem (2.45) is solved again by fixing the biddings into the DAM and the IDA1, replacing S^{w1} with the updated wind scenario S^{w2} and including the possibility to bid into the IDA2.
- Step 3: The resulting optimized IDA2 decisions from step 2 are then fixed and fed back to the model. The optimization problem (2.45) is solved again by fixing all biddings into the DAM and IDA1-IDA2, replacing S^{w2} with the updated wind scenario S^{w3} and including the possibility to bid into the IDA3.
- Step 4: The resulting optimized IDA3 decisions from step 3 are then fixed and fed back to the model. The optimization problem (2.45) is solved again by fixing the biddings into the DAM and IDA1-IDA3, replacing S^{w3} with the updated wind scenario S^{w4} and including the possibility to bid into the IDA4.

Table 2.3 compares the expected profits, the imbalance costs and the net imbalance quantities considering different numbers of IDAs. The resulting profits, the imbalance quantities and costs of the aggregator considering different number of IDAs are calculated using the actual realized wind output for the simulation day, while the real-time dispatch of the aggregator is the expected value over the considered scenarios. Results for considering one to four IDAs are obtained by carrying out step 1, step 1-2, steps 1-3 and steps 1-4, respectively.

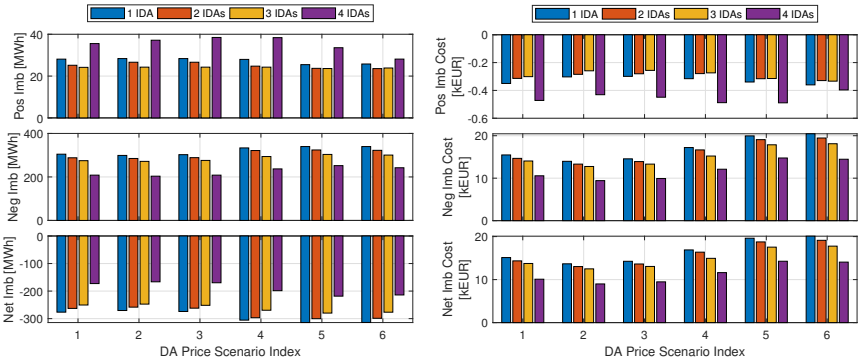

(a) Imbalance Quantity **(b)** Imbalance Cost

Figure 2.11: Realized imbalance quantity and cost developments at real-time considering different numbers of intraday auctions.

Comparing the results considering different numbers of IDAs, it can be seen that the expected profit increases and the imbalance costs and quantities decrease, as more IDAs are considered. This is due to the fact that the gate closure time is closer to the real-time delivery from IDA1 to IDA4, which provides additional opportunities for the aggregator to adjust its positions with reduced uncertainties of the real-time wind generation outputs. When looking at the positive and negative imbalance quantities and costs for each individual DAM price scenario shown in Fig. 2.11, it can be observed that although the positive imbalance increases when IDA4 is considered, in general both the imbalance quantities and the imbalance costs are significantly reduced in all DAM price scenarios.

To further analyze how this certainty gain effect is realized, we compare the resulting expected real-time dispatch and the market biddings of the aggregator considering one and four IDAs for an identical DAM price scenario. The differences of the results considering four IDAs and one IDA are depicted in Fig. 2.12, with the results for the case considering one IDA serving as the reference values. The wind deviation is defined as the difference of the expected wind generation over the most updated scenarios considered in the four IDAs and one IDA cases, i.e. difference of the expected wind generations over wind

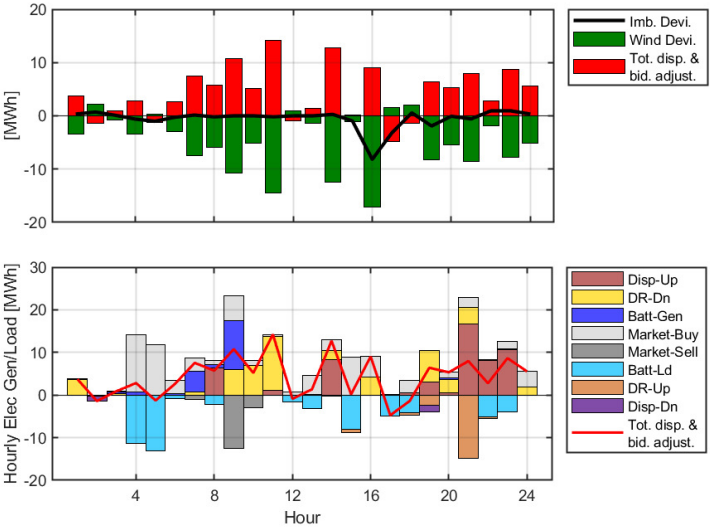

Figure 2.12: Re-dispatch of the units and the adjustment of the market biddings under an example day-ahead market price scenario, as a reaction to the updated wind forecasts considering four intraday auctions compared to the case considering only one intraday auction.

scenarios S^{w1} and S^{w4}. A positive (negative) wind deviation means that based on the updated wind scenario the wind unit is expected to generate more (less) than what is predicted in the original wind scenario, which could lead to positive (negative) real-time imbalances assuming that the updated scenario is more accurate and the dispatch and the market biddings of the aggregator remain unchanged. Similarly, the imbalance deviation and the bidding deviation are the differences of the resulting expected net imbalance quantity (i.e., positive imbalance minus negative imbalance) and the net supply quantity (i.e., market sale minus market purchase) for all considered markets in these two cases (i.e., DAM and IDA1 when one IDA is considered, and DAM and IDA1-IDA4 when four IDAs are considered). The top figures of Fig. 2.12 shows that the aggregator adjusts the market biddings and the dispatch of the units[6] in a

[6]The total dispatch and market bidding adjustment of the aggregator is defined as the difference between the resulting net generation and net market purchase considering four IDAs and one IDA, respectively.

Table 2.4: Effects of the intraday market trading limit.

ID trading limit	Expected aggregator profit [EUR]	Net imbalance [MWh]
Unlimited	45'249	Neg. imb. 48.2
30%	44'211 (-2%)	Neg. imb. 67.3 (+40%)
20%	43'276 (-4%)	Neg. imb. 76.4 (+59%)
10%	41'983 (-7%)	Neg. imb. 76.5 (+59%)

way so as to possibly eliminate the impacts of the wind forecast deviation using the updated wind scenario information. This leads to the in general much lower imbalance deviations than what could be caused by the wind forecast deviation. The bottom figure shows how each type of unit within the aggregator contributes to the total dispatch and market bidding adjustments of the aggregator.

2.6.4 Results: Effects of the Intraday Market Trading Limit

The effects of the intraday trading limit are analyzed in this section. Table 2.4 compares the expected profit and net imbalance quantities considering 10%, 20% and 30% IDM trading limits or no trading limits. As defined by constraint (2.39), for each scenario the energy traded in the IDM for the simulation horizon (i.e. 24 hours) is thus limited to 10%, 20% and 30% of the energy traded in the DAM or not limited. The changes of the results under different Intraday (ID) trading limits using the unlimited case results as a reference are shown in parentheses. As expected, a tighter restriction on the ID trading volumes results in a decrease on the aggregator profits and an increase on the net imbalance quantity, whereas it is worth noting that the relative changes are dependent on the assumptions made for the DAM and the IDM prices.

2.7 Limitations and Future Work

This work has several limitations and a few of which are highlighted in this section. First, several assumptions are made to simplify the intraday market tradings. It is assumed that the aggregator participates in the intraday-market only for the purpose to reduce the potential real-time imbalance costs, while other motivations for intraday tradings such as arbitrage across different markets [13] are not considered. To eliminate the arbitrage opportunities across

different intraday auctions or between the intraday and balancing markets so as to focus on the influence of additional intraday auctions on imbalance costs, identical market prices are assumed for all intraday auctions and the balancing market prices are modeled to be always unfavorable to the day-ahead and intraday market prices. Furthermore, considering the low liquidity of the intraday market, we adopt a constant value to limit the aggregator's bidding quantities that can be submitted to the intraday market. However, the intraday market trading in real-world is limited due to multiple factors, such as the transmission capacity limit, generation mix of the electricity system (especially the share of variable energy resources and hydro power plants), the volatility of the intraday market price, the pricing scheme of the imbalance etc., which can hardly be simplified as a single number. Future work should model the intraday market trading quantity in a more appropriate way to take the above mentioned factors into account, which though might require additional input data and implementation efforts. Additionally, the tradings in sequential markets are modeled in a way without considering the preference of the traders. However, in reality it was found that most trades are carried out shortly before the gate closure to use the updated renewable forecast information with short forecast horizons [13], which might be more expensive as it requires the rescheduling of dispatchable units in short time. A future version should therefore incorporate this characteristic into the modeling.

Second, the day-ahead, intraday and balancing market prices are modeled using limited number of scenarios based on historical data. In future work, a proper method is required to predict the electricity prices in sequential electricity markets while accounting for the correlations of prices between different markets and the influence of market rules. Example forecasting methods for this purpose include Auto-regressive Integrated Moving Average (ARIMA) [41], Generalized Autoregressive Conditional Heteroskedastic (GARCH) [42] and Artificial Neural Network (ANN) [43], etc.

Third, the wind forecast error scenarios are generated based on the historical aggregated country-wide data from Denmark, provided by Nord Pool. Due to the statistical smoothing effects when aggregating wind generation data especially for regions with significant amount of wind capacities installed [44], the generation forecast errors for the wind units within the considered aggregator

cannot be well represented (i.e. are underestimated) by using the country-wide dataset. Moreover, due to the lack of data, only the day-ahead forecast scenarios with 13-hour to 36-hour ahead lead time are generated based on the probabilistic method proposed in [1]. Updating the wind forecast when bidding closer to the delivery time is simplified as selecting the most accurate scenarios from the day-ahead forecast scenarios. This compromise, although still reflects the certainty gain effect to some extent, can be improved by using a more complete dataset and generating a new set of scenarios applying the method from [1] shortly before the closure of each considered trading floor. Thus, future work should use a more realistic and complete dataset that is consistent with the modeled wind capacity.

Fourth, we estimate the load profiles as well as the demand response programs using the synthetic data from [33] that undoubtedly deviate from real-world data. Future work should utilize realistic load patterns and demand response contracts.

Fifth, the sizes of the units within the aggregator are fixed and are not optimized, but the results might be different under different assumptions of the sizes of the units. The optimal dispatch and trading strategy model should therefore be integrated into a generation investment model to assess the impacts of sizing, more about this topic will be discussed in the second part of the thesis.

Lastly, the simulation horizon is limited to one day thereby neglecting the seasonal fluctuations. Furthermore, the volatility of the day-to-day profit as well as the generation of wind and PV units is high. Hence, it would be interesting to expand the time horizon and simulate multiple days across different seasons.

2.8 Summary and Conclusions

A stochastic programming methodology to derive optimal trading strategies for an aggregator participating in sequential electricity markets is presented. The benefits of participating in sequential markets and including more intraday trading auctions are examined by applying a rolling horizon approach, which enables the adjustment of the dispatch and market bidding decisions using the updated information closer to real-time.

The coordination of different units within the aggregator realizes higher flexibility provisions and increased total profits for the aggregator, although this might reduce the individual profit of some unit. The risk control is conducted to assure a certain risk level when designing optimal trading strategies and in general the aggregator prefers to offer less in the day-ahead market when it becomes more risk-averse. Simulation results considering different numbers of intraday auctions show that the presented rolling-horizon optimization method enables the aggregator to modify the dispatch schedules and market biddings based on the updated information. As a result, the integration of more trading floors results in an increase in the aggregator profits, guaranteeing at the same time lower imbalance quantities.

Chapter 3

Dispatch Optimization of the Aggregator as a Price-maker

In this chapter, we investigate the impact of considering market power on the optimal dispatch and trading strategies of a hybrid wind-solar aggregator. A stochastic bi-level model is presented to derive optimal offering strategies for the aggregator, who participates as a price-maker in both the day-ahead and intraday markets, and a deviator in the balancing market. The upper-level represents the profit maximization problem of the aggregator, while the two lower-levels represent the market clearing problems of the day-ahead and the intraday markets, respectively. The problem considered is stochastic and subject to different levels of uncertainties. Uncertainties concerning intraday rivals' offers are modeled using scenarios, while the uncertainty of the variable generation output is taken into consideration by formulating chance constraints. The stochastic bi-level optimization problem is then solved by being transformed into a mixed-integer linear programming model using the Karush-Kuhn-Tucker optimality conditions and the strong duality theory. A case study based on a modified Swiss system demonstrates the effectiveness of the proposed model. Sensitivity analyses are conducted to investigate the impacts of the aggregator's market share, the import electricity prices, the price elasticity of the system demand curve, and the generation mix of the aggregator on the offering strategy and the profits of the aggregator as well as the market results. Finally, the effect of incorporating the variable generation output using chance constraints is analyzed. This chapter is based on [45].

3.1 Introduction

3.1.1 Motivation and Related Work

In recent years, driven by its contributions to enabling a sustainable energy future, the penetration of Variable Renewable Energy (VRE), such as wind power and solar power, has increased dramatically. Furthermore, governmental policies contribute to further expansions of the VRE capacities. As a result, the market share of VRE in some countries is high enough (e.g. wind power plants in Denmark) to enable them to bid strategically and to exercise market power[7] so as to make more profits. Although VRE is challenging to dispatch and difficult to forecast, due to the continuous decreasing subsidies, VRE are forced to trade in the same market environment as conventional generators. To better exploit the economic value of VRE, the aggregation of VRE of different technologies and at different locations is of great interest to the power plant operators and owners, since it results in smoothing effects on the aggregated generation outputs especially when the power plants are spatially distributed. It also enables small-sized variable generation power plants especially distributed wind and solar power plants to participate in the electricity markets. It is therefore important to answer the question of what would be the optimal offering strategy for a VRE aggregator considering its market power. The VRE aggregator considered in this chapter consists of wind and Photovoltaic (PV) units and it will be referred to as a hybrid aggregator or an aggregator in the following context.

A lot of work has been done on the topic. Optimal bidding strategies have been developed for wind producers [15, 47, 48, 49, 50], PV power plants [51] or virtual power plants [23, 25, 33] in recent years. Several works design bidding strategies considering the producer's market power in different markets. For example, the work in [48] presents a bi-level model to optimize the trading strategies for a wind producer that acts as a price-taker in the Day-ahead Market (DAM) and as a price-maker in the Balancing Market (BM), while references [49, 50] model the market power of a wind producer in both the DAM and the BM. A stochastic bi-level model to optimize the pool strategy of a price-

[7] Following the definition in [46], market power is defined as the ability to profitably alter prices away from competitive levels.

maker storage system in the day-ahead (including the reserve market) and balancing markets is proposed in [52].

While most of the work targets at developing strategies considering only two conventional electricity markets, i.e. day-ahead and balancing market, as mentioned in the previous chapter, the Intraday Market (IDM) is more interesting to variable generation units as it is cleared closer to the real-time delivery, which provides the opportunities for the VRE operators to modify the dispatch schedules with reduced forecast uncertainties. The works [15] and [47] determine the offering strategies for a wind power plant considering a complete market structure (day-ahead, intraday and balancing markets), but the wind power plant is modeled as a price-taker in all trading floors. However, since the trading volume of the IDM is generally lower than that of the DAM, the IDM price is more vulnerable to the aggregator's offers and the market power of the aggregator should be taken into account in IDMs. As a result, there is a lack of studies taking into account the market power of variable generation units in both day-ahead and intraday markets. However, with the further expansion of VRE capacities and the deepening interests of VRE producers in market participation, this is becoming increasingly important.

The focus of this chapter is on a hybrid aggregator which is modeled as price-makers in both the DAM and the IDM, and as deviators in the BM. Different uncertainties concerning VRE power outputs and IDM rivals' offers are considered. In order to account for VRE forecast deviations in a comprehensive way and at the same time ease the computational burden resulting from a large number of scenarios, probabilistic constraints (i.e., chance constraints) are employed. Uncertainties regarding IDM rival producers' offers are modeled using scenarios. The goal of this chapter is therefore threefold: to optimize the offering strategies for a hybrid aggregator in a multi-market environment, to investigate the impacts of the aggregator's offerings on electricity markets and to study the effects of different uncertainties on the results.

Consequently, the contributions of this chapter are:

1. To propose a stochastic bi-level model that allows strategic offerings for a hybrid wind and PV aggregator that acts as a price-maker in both day-ahead and intraday markets, and as a deviator in the balancing market.

2. To model the uncertainty regarding wind and PV productions using the probabilistic constraint and combine it with stochastic optimization.
3. To validate the model using a modified Swiss system and conduct sensitivity analyses to investigate the impacts of the aggregator's market share, the import electricity prices, the price elasticity of the system demand curve and the generation mix of the aggregator.

3.1.2 Chapter Organization

The remainder of this chapter is organized as follows: the problem descriptions and main model assumptions are presented in Section 3.2, and the mathematical formulations of the proposed optimization model are given in Section 3.3. Section 3.4 describes the test system for the case study and the results are shown in Section 3.5. Finally, limitations and the future work are discussed in Section 3.6, and conclusions are drawn in Section 3.7.

3.2 Problem Descriptions and Model Assumptions

In this section, we first introduce the multi-market environment that the hybrid aggregator is involved in and illustrate how the uncertainties are incorporated. Afterwards, the proposed bi-level model and the main modeling assumptions are described.

3.2.1 Multi-market Environment

Similar to the market environment defined in the previous chapter, the hybrid aggregator is assumed to participate in an electricity market that is organized around three major trading floors: the day-ahead, the intraday and the balancing markets, as illustrated in Fig. 3.1. The day-ahead market is assumed to be cleared at 11:00 on day $d-1$, i.e. the day before the delivery day d, in a uniform auction, while the intraday market is simplified as a single intraday auction that is cleared shortly before the delivery day (i.e. the day before delivery at 23:00). Finally, the balancing market is designed to compensate the difference between the scheduled and the measured energy. In this context, it is assumed that all imbalances can be corrected through the balancing market.

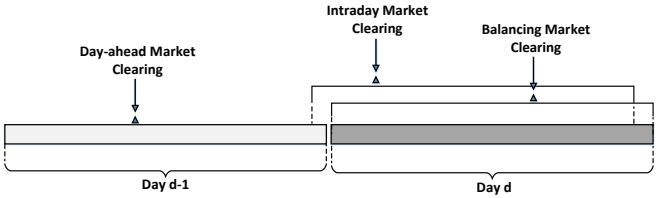

Figure 3.1: Structure of the sequential spot electricity markets.

3.2.2 Uncertainty Characterization

The hybrid aggregator faces different levels of uncertainties such as the rival producers' offers, demands' bids and the power outputs of VRE. In this model, we neglect uncertainties regarding demands' bids as demands are in general inelastic. It is however straightforward to incorporate this into the model and a sensitivity analysis is conducted to assess the impact of the price elasticity of demands. Additionally, rivals' offers in the day-ahead market are assumed to be deterministic and are modeled based on the rival units' marginal costs and available capacities, while the uncertainty concerning rivals' intraday offers are modeled using scenarios. This is based on the fact that intraday market prices are more volatile, as they reflect events which were not foreseen on the day before the delivery. Furthermore, to reach a compromise between accuracy and computational time, instead of using scenarios, the VRE output uncertainty is taken into consideration by formulating probabilistic constraints. The VRE output forecast error is modeled assuming that it is subject to the Gaussian distribution. The resulting chance constraints are analytically reformulated into the deterministic ones without adding computational complexity to the original problem. A method to model the uncertainties in a more realistic way without requiring to specify the distribution of the random variables will be presented in the following chapter. Note that since the BM prices are in general difficult to simulate and forecasting the BM prices is beyond the scope of this thesis, BM prices are modeled using a function of the DAM and IDM prices and therefore uncertainties concerning the BM prices are not considered.

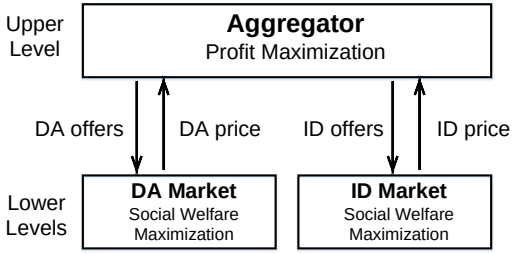

Figure 3.2: Structure of the bi-level model.

3.2.3 Stochastic Bi-level Model

The hybrid aggregator aims to maximize its profits by participating in all three trading floors, i.e. the day-ahead, the intraday and the balancing markets. As mentioned, the hybrid aggregator is assumed to act as a price-maker in both day-ahead and intraday markets, and as a deviator in the balancing market. The offering strategy is formulated as a stochastic bi-level optimization problem, which is shown in Fig. 3.2. The upper-level represents the aggregator's profit maximization problem, while the two lower-levels represent the day-ahead and the intraday market clearing problems, respectively.

The bi-level model is formulated as a Mathematical Program with Equilibrium Constraints (MPEC), by replacing the two lower level problems with their first-order Karush-Kuhn-Tucker (KKT) conditions and integrating them into the upper level problem. Then the resulting MPEC model is further transformed into a Mixed-Integer Linear Programming (MILP) using the KKT optimality conditions and strong duality theory [20, 53].

3.2.4 Model Assumptions

The main assumptions made in this chapter are summarized as follows:

- The hybrid aggregator is assumed to participate in an electricity market that is organized around three major trading floors: the day-ahead, the intraday and the balancing markets.
- An auction-based intraday trading that is based on uniform pricing is assumed, while instead of four Intraday (ID) trading floors that are as-

sumed in Chapter 2, only one ID auction is considered as the focus of this chapter is to analyze the impact of market power.

- Due to the lack of data, identical DAM and IDM participants are assumed. Based on the fact that the total energy traded in the IDM is much less than that in the DAM [34], the supply quantity of each producer as well as the demand quantities for the DAM and the IDM are assumed to be 90% and 10% of the total supply and demand quantities for the DAM and the IDM together.
- The aggregator is assumed to be the only one in the market that could bid strategically, i.e. all rival producers are assumed to be non-strategic producers with offering curves constructed based on their corresponding marginal costs and available capacities. While rivals' offers in the day-ahead market are assumed to be deterministic, uncertainties concerning rivals' intraday offers are modeled using scenarios.
- Both the DAM and the IDM demands are assumed to be inelastic in the Baseline scenario, while a sensitivity scenario is simulated to investigate the influence of the price elasticity of demand.
- The BM prices are assumed to be independent of the aggregator's position, i.e. the aggregator is a price-taker in the balancing market. This assumption, however, might need to be reconsidered when the aggregator accounts for a significant share of the market. Moreover, it is assumed that all imbalances can be corrected through the balancing market.
- The simulated modified Swiss electricity system is assumed to be uncongested, i.e. no network constraints are considered, which is consistent with the zonal pricing scheme of the European electricity markets.
- The cross-border transmission is modeled as a non-strategic rival producer, while sensitivity analyses are conducted to analyze the impact of the import electricity's offering prices.

Note that the simulated electricity system and the market environment are a simplification of a much more complex reality.

3.3 Mathematical Formulation

In this section, we first present the mathematical formulation of the deterministic bi-level optimization model and how it can be reformulated as a MILP

model. Then, the final formulation of the proposed stochastic MILP model is described by integrating the modeling of uncertainties.

3.3.1 Upper Level Formulation

The Upper-Level (UL) problem is the aggregator's profit maximization problem and is defined by (3.1a)-(3.1f). The objective function represents the aggregator's profit, which comprises the profits from the day-ahead, the intraday and the balancing markets. Note that the generation costs for the wind and PV units within the aggregator are assumed to be zero. Mathematically,

$$\max \sum_{t=1}^{T} \left(\lambda_t^{\mathrm{DA}} P_t^{\mathrm{DA}} + \lambda_t^{\mathrm{ID}} P_t^{\mathrm{ID}} + pr_t^{\mathrm{BM}} P_t^{\mathrm{BM}} \right) \tag{3.1a}$$

where λ_t^{DA} and λ_t^{ID} are the day-ahead and intraday market clearing prices at time t, P_t^{DA} and P_t^{ID} are the dispatch quantities of the aggregator in the day-ahead and intraday markets. The term $pr^{\mathrm{BM}} P^{\mathrm{BM}}$ is equal to $pr^{\mathrm{BM+}} P^{\mathrm{BM+}} - pr^{\mathrm{BM-}} P^{\mathrm{BM-}}$, where $pr^{\mathrm{BM+}}/pr^{\mathrm{BM-}}$ and $P^{\mathrm{BM+}}/P^{\mathrm{BM-}}$ denote the positive/negative balancing prices and quantities. The simulation horizon is denoted by T.

The aggregator's total dispatched quantities in all three markets should be equal to the aggregator's real-time outputs, which are the sum of wind outputs P^{W} and PV outputs P^{S}. The real-time wind and PV outputs are limited by the wind forecast P^{Wf} and PV forecast P^{Sf} in the case of perfect forecast, respectively. Mathematically,

$$P_t^{\mathrm{W}} + P_t^{\mathrm{S}} = P_t^{\mathrm{DA}} + P_t^{\mathrm{ID}} + P_t^{\mathrm{BM}} \tag{3.1b}$$

$$0 \leq P_t^{\mathrm{W}} \leq P_t^{\mathrm{Wf}} \tag{3.1c}$$

$$0 \leq P_t^{\mathrm{S}} \leq P_t^{\mathrm{Sf}} \tag{3.1d}$$

Furthermore, as the considered aggregator has no ability to store energy, it is assumed that it cannot purchase energy from the market[8]. The minimum offer quantity is equal to zero, while the maximum offer quantities Q^{DA} and Q^{ID} that the aggregator submits to the day-ahead and intraday markets are limited to

[8]The possibility of virtual bidding, which refers to the trading of electricity without physically producing or consuming the electricity, is not considered.

the total wind and PV installed capacities $P^{\text{Wc}} + P^{\text{Sc}}$, i.e.,

$$0 \leq Q_t^{\text{DA}} \leq P^{\text{Wc}} + P^{\text{Sc}} \tag{3.1e}$$

$$0 \leq Q_t^{\text{ID}} \leq P^{\text{Wc}} + P^{\text{Sc}} \tag{3.1f}$$

3.3.2 Lower Level Formulation

As mentioned, the two Lower-Level (LL) problems represent the market clearings of the day-ahead and intraday markets. As the derivation for offering strategies in the IDMs is analogous to the derivation of the ones in the DAM, only the lower-level problem of the DAMs is described here. It is assumed that results of IDMs are independent from DAMs.

The objective of the LL problem is to maximize the social welfare, as expressed by

$$\max_{\alpha_t^{\text{DA}}, P_t^{\text{DA}}} \sum_{t=1}^{T} \sum_{m=1}^{N^{\text{m}}} \lambda_{t,m}^{\text{DA,D}} P_{t,m}^{\text{DA,D}} - \sum_{t=1}^{T} \sum_{j=1}^{N^{\text{j}}} \sum_{b=1}^{N^{\text{b}}} \lambda_{t,j,b}^{\text{DA,O}} P_{t,j,b}^{\text{DA,O}} - \sum_{t=1}^{T} \alpha_t^{\text{DA}} P_t^{\text{DA}} \tag{3.2a}$$

where $P_{t,m}^{\text{DA,D}}$ and $\lambda_{t,m}^{\text{DA,D}}$ is the consumers' Day-ahead (DA) price-quantity pair of bidding block m at time t, while $\lambda_{t,j,b}^{\text{DA,O}}$ and $P_{t,j,b}^{\text{DA,O}}$ is the DA price-quantity pair of offering block b of rival producer j at time t. The number of consumers' demand bidding blocks, the number of rival producers and the number of the rival producers' offering blocks are denoted as N^{m}, N^{j} and N^{b}, respectively. Finally, α^{DA} and P^{DA} is the DA price-quantity pair of the aggregator. The LL problem is subject to two types of constraints: 1) offering and bidding quantities' minimum/maximum limits expressed by (3.2b)-(3.2d); and 2) the power balance constraint (3.2e) which forces the summation of DAM dispatched offering quantities to be equal to the DAM dispatched bidding quantities for each

time step, i.e.

$$0 \leq P_t^{\mathrm{DA}} \leq Q_t^{\mathrm{DA}} \quad : \mu_t^{\mathrm{DAmin}},\ \mu_t^{\mathrm{DAmax}} \tag{3.2b}$$

$$0 \leq P_{t,j,b}^{\mathrm{DA,O}} \leq P_{t,j,b}^{\mathrm{DA,Omax}} \quad : \mu_{t,j,b}^{\mathrm{DA,Omin}},\ \mu_{t,j,b}^{\mathrm{DA,Omax}} \tag{3.2c}$$

$$0 \leq P_{t,m}^{\mathrm{DA,D}} \leq P_{t,m}^{\mathrm{DA,Dmax}} \quad : \mu_{t,m}^{\mathrm{DA,Dmin}},\ \mu_{t,m}^{\mathrm{DA,Dmax}} \tag{3.2d}$$

$$P_t^{\mathrm{DA}} + \sum_{j=1}^{N^{\mathrm{j}}} \sum_{b=1}^{N^{\mathrm{b}}} P_{t,j,b}^{\mathrm{DA,O}} - \sum_{m=1}^{N^{\mathrm{m}}} P_{t,m}^{\mathrm{DA,D}} = 0 \quad : \lambda_t^{\mathrm{DA}} \tag{3.2e}$$

where $P^{\mathrm{DA,Omax}}$ and $P^{\mathrm{DA,Dmax}}$ are the maximum DAM offering quantities of the rival producers and the maximum bidding quantities of the demand. The dual variables are denoted following a colon after each corresponding equation. Note that P^{DA} indicates the power that the aggregator expects to be dispatched for, which is an outcome of the lower-level market clearing problem as it models the dispatch of the market. The total power that the aggregator is dispatched for is the summation over all offering or bidding blocks. The same holds for $P^{\mathrm{DA,O}}$ and $P^{\mathrm{DA,D}}$.

3.3.3 Bi-level Formulation with Two Lower Levels

Thus, the overall bi-level problem can be formulated as:

$$\text{UL:} \quad \max \sum_{t=1}^{T} \left(\lambda_t^{\mathrm{DA}} P_t^{\mathrm{DA}} + \lambda_t^{\mathrm{ID}} P_t^{\mathrm{ID}} + pr_t^{\mathrm{BM}} P_t^{\mathrm{BM}} \right)$$

s.t. (3.1b)-(3.1f)

$$\text{LL1:} \quad \underset{\alpha_t^{\mathrm{DA}}, P_t^{\mathrm{DA}}}{\operatorname{argmax}} \sum_{t=1}^{T} \sum_{m=1}^{N^{\mathrm{m}}} \lambda_{t,m}^{\mathrm{DA,D}} P_{t,m}^{\mathrm{DA,D}} - \sum_{t=1}^{T} \sum_{j=1}^{N^{\mathrm{j}}} \sum_{b=1}^{N^{\mathrm{b}}} \lambda_{t,j,b}^{\mathrm{DA,O}} P_{t,j,b}^{\mathrm{DA,O}} - \sum_{t=1}^{T} \alpha_t^{\mathrm{DA}} P_t^{\mathrm{DA}}$$

s.t. (3.2b)-(3.2e)

$$\text{LL2:} \quad \underset{\alpha_t^{\mathrm{ID}}, P_t^{\mathrm{ID}}}{\operatorname{argmax}} \sum_{t=1}^{T} \sum_{m=1}^{N^{\mathrm{m}}} \lambda_{t,m}^{\mathrm{ID,D}} P_{t,m}^{\mathrm{ID,D}} - \sum_{t=1}^{T} \sum_{j=1}^{N^{\mathrm{j}}} \sum_{b=1}^{N^{\mathrm{b}}} \lambda_{t,j,b}^{\mathrm{ID,O}} P_{t,j,b}^{\mathrm{ID,O}} - \sum_{t=1}^{T} \alpha_t^{\mathrm{IDM}} P_t^{\mathrm{ID}}$$

s.t. equivalent ID constraints of (3.2b)-(3.2e)

3.3.4 Mathematical Program with Equilibrium Constraints (MPEC) Formulation

As the lower-level problem (3.2) is convex, it can be replaced by the following set of KKT conditions:

$$\alpha_t^{\mathrm{DA}} - \lambda_t^{\mathrm{DA}} + \mu_t^{\mathrm{DAmax}} - \mu_t^{\mathrm{DAmin}} = 0 \tag{3.3a}$$
$$\lambda_{t,j,b}^{\mathrm{DA,O}} - \lambda_t^{\mathrm{DA}} + \mu_{t,j,b}^{\mathrm{DA,Omax}} - \mu_{t,j,b}^{\mathrm{DA,Omin}} = 0 \tag{3.3b}$$
$$\lambda_{t,m}^{\mathrm{DA,D}} - \lambda_t^{\mathrm{DA}} - \mu_{t,m}^{\mathrm{DA,Dmax}} + \mu_{t,m}^{\mathrm{DA,Dmin}} = 0 \tag{3.3c}$$
$$0 \leq P_t^{\mathrm{DA}} \perp \mu_t^{\mathrm{DAmin}} \geq 0 \tag{3.3d}$$
$$0 \leq P_{t,j,b}^{\mathrm{DA,O}} \perp \mu_{t,j,b}^{\mathrm{DA,Omin}} \geq 0 \tag{3.3e}$$
$$0 \leq P_{t,m}^{\mathrm{DA,D}} \perp \mu_{t,m}^{\mathrm{DA,Dmin}} \geq 0 \tag{3.3f}$$
$$0 \leq (Q_t^{\mathrm{DA}} - P_t^{\mathrm{DA}}) \perp \mu_t^{\mathrm{DAmax}} \geq 0 \tag{3.3g}$$
$$0 \leq (P_{t,j,b}^{\mathrm{DA,Omax}} - P_{t,j,b}^{\mathrm{DA,O}}) \perp \mu_{t,j,b}^{\mathrm{DA,Omax}} \geq 0 \tag{3.3h}$$
$$0 \leq (P_{t,m}^{\mathrm{DA,Dmax}} - P_{t,m}^{\mathrm{DA,D}}) \perp \mu_{t,m}^{\mathrm{DA,Dmax}} \geq 0 \tag{3.3i}$$
$$P_t^{\mathrm{DA}} + \sum_{j=1}^{N^{\mathrm{j}}} \sum_{b=1}^{N^{\mathrm{b}}} P_{t,j,b}^{\mathrm{DA,O}} - \sum_{m=1}^{N^{\mathrm{m}}} P_{t,m}^{\mathrm{DA,D}} = 0 \tag{3.3j}$$

where (3.3a)-(3.3c) are stationary conditions. Inequalities on the left-hand side and the right-hand side of (3.3d)-(3.3i) declare the feasibility of the primal and dual problems, respectively.

Thus, the resulting MPEC formulation is:

$$\max \sum_{t=1}^{T} \left(\lambda_t^{\mathrm{DA}} P_t^{\mathrm{DA}} + \lambda_t^{\mathrm{ID}} P_t^{\mathrm{ID}} + pr_t^{\mathrm{BM}} P_t^{\mathrm{BM}} \right) \tag{3.4a}$$
$$\text{s.t.} \quad \text{(3.1b)-(3.1f)} \tag{3.4b}$$
$$\text{DAM KKT conditions (3.3a)-(3.3j)} \tag{3.4c}$$
$$\text{IDM KKT conditions equivalent to (3.3a)-(3.3j)} \tag{3.4d}$$

3.3.5 Mixed-integer Linear Programming (MILP) Formulation

Note that the resulting MPEC is a non-linear and non-convex optimization problem that is difficult to solve. On one hand, the non-linearity of the MPEC

is caused by the complementarity conditions (3.3d)-(3.3i) and the equivalent IDM conditions. On the other hand, it is due to the non-linear part $\lambda_t^{\mathrm{DA}} P_t^{\mathrm{DA}}$ and $\lambda_t^{\mathrm{ID}} P_t^{\mathrm{ID}}$ in the objective function. Hence, in the following the problem is transformed into a MILP formulation.

First, the equations including the perpendicularity operator "$\perp$" are linearized using binary variables [54]:

$$0 \leq P_t^{\mathrm{DA}} \leq M_1 u_t^{\mathrm{DA1}} \tag{3.5a}$$
$$0 \leq P_{t,j,b}^{\mathrm{DA,O}} \leq M_2 u_{t,j,b}^{\mathrm{DA,O1}} \tag{3.5b}$$
$$0 \leq P_{t,m}^{\mathrm{DA,D}} \leq M_3 u_{t,m}^{\mathrm{DA,D1}} \tag{3.5c}$$
$$0 \leq \mu_t^{\mathrm{DAmin}} \leq M_4 (1 - u_t^{\mathrm{DA1}}) \tag{3.5d}$$
$$0 \leq \mu_{t,j,b}^{\mathrm{DA,Omin}} \leq M_5 (1 - u_{t,j,b}^{\mathrm{DA,O1}}) \tag{3.5e}$$
$$0 \leq \mu_{t,m}^{\mathrm{DA,Dmin}} \leq M_6 (1 - u_{t,m}^{\mathrm{DA,D1}}) \tag{3.5f}$$
$$0 \leq Q_t^{\mathrm{DA}} - P_t^{\mathrm{DA}} \leq M_7 u_t^{\mathrm{DA2}} \tag{3.5g}$$
$$0 \leq P_{t,j,b}^{\mathrm{DA,Omax}} - P_{t,j,b}^{\mathrm{DA,O}} \leq M_8 u_{t,j,b}^{\mathrm{DA,O2}} \tag{3.5h}$$
$$0 \leq P_{t,m}^{\mathrm{DA,Dmax}} - P_{t,m}^{\mathrm{DA,D}} \leq M_9 u_{t,m}^{\mathrm{DA,D2}} \tag{3.5i}$$
$$0 \leq \mu_t^{\mathrm{DAmax}} \leq M_{10} (1 - u_t^{\mathrm{DA2}}) \tag{3.5j}$$
$$0 \leq \mu_{t,j,b}^{\mathrm{DA,Omax}} \leq M_{11} (1 - u_{t,j,b}^{\mathrm{DA,O2}}) \tag{3.5k}$$
$$0 \leq \mu_{t,m}^{\mathrm{Dmax}} \leq M_{12} (1 - u_{t,m}^{\mathrm{DA,D2}}) \tag{3.5l}$$
$$u_t^{\mathrm{DA1}}, u_{t,j,b}^{\mathrm{DA,O1}}, u_{t,m}^{\mathrm{DA,D1}}, u_t^{\mathrm{DA2}}, u_{t,j,b}^{\mathrm{DA,O2}}, u_{t,m}^{\mathrm{DA,D2}} \in \{0,1\} \tag{3.5m}$$

where $M_{1,2,\ldots,12}$ are large enough constants.

Second, the non-linear part $\lambda^{\mathrm{DA}} P^{\mathrm{DA}}$ and $\lambda^{\mathrm{ID}} P^{\mathrm{ID}}$ in the objective function are linearized by applying the strong duality theorem to the lower-level problems and using some of the KKT conditions stated before. According to the strong duality theorem, the primal optimal objective and the dual optimal objective is equal, which means that for the DA market clearing problem the following

holds:

$$\begin{aligned}
&\sum_{t=1}^{T}\sum_{m=1}^{N^{\mathrm{m}}}\lambda_{t,m}^{\mathrm{DA,D}}P_{t,m}^{\mathrm{DA,D}}-\sum_{t=1}^{T}\sum_{j=1}^{N^{\mathrm{j}}}\sum_{b=1}^{N^{\mathrm{b}}}\lambda_{t,j,b}^{\mathrm{DA,O}}P_{t,j,b}^{\mathrm{DA,O}}-\sum_{t=1}^{T}\alpha_t^{\mathrm{DA}}P_t^{\mathrm{DA}}\\
=&\sum_{t=1}^{T}\mu_t^{\mathrm{DAmax}}Q_t^{\mathrm{DA}}+\sum_{t=1}^{T}\sum_{j=1}^{N^{\mathrm{j}}}\sum_{b=1}^{N^{\mathrm{b}}}\mu_{t,j,b}^{\mathrm{DA,Omax}}P_{t,j,b}^{\mathrm{DA,Omax}}\\
&+\sum_{t=1}^{T}\sum_{m=1}^{N^{\mathrm{m}}}\mu_{t,m}^{\mathrm{DA,Dmax}}P_{t,m}^{\mathrm{DA,Dmax}}
\end{aligned}\tag{3.6}$$

By reformulating (3.3a), (3.3d) and (3.3g), we obtain

$$\sum_{t=1}^{T}\alpha_t^{\mathrm{DA}}P_t^{\mathrm{DA}}=\sum_{t=1}^{T}P_t^{\mathrm{DA}}(\lambda_t^{\mathrm{DA}}-\mu_t^{\mathrm{DAmax}}+\mu_t^{\mathrm{DAmin}})\tag{3.7}$$

$$P_t^{\mathrm{DA}}\mu_t^{\mathrm{DAmin}}=0\tag{3.8}$$

$$P_t^{\mathrm{DA}}\mu_t^{\mathrm{DAmax}}=Q_t^{\mathrm{DA}}\mu_t^{\mathrm{DAmax}}\tag{3.9}$$

Substituting (3.8) and (3.9) into (3.7) yields

$$\sum_{t=1}^{T}\alpha_t^{\mathrm{DA}}P_t^{\mathrm{DA}}=\sum_{t=1}^{T}\lambda_t^{\mathrm{DA}}P_t^{\mathrm{DA}}-\sum_{t=1}^{T}\mu_t^{\mathrm{DAmax}}Q_t^{\mathrm{DA}}\tag{3.10}$$

and with (3.6), we have

$$\begin{aligned}
\sum_{t=1}^{T}\lambda_t^{\mathrm{DA}}P_t^{\mathrm{DA}}=&-\sum_{t=1}^{T}\sum_{j=1}^{N^{\mathrm{j}}}\sum_{b=1}^{N^{\mathrm{b}}}\lambda_{t,j,b}^{\mathrm{DA,O}}P_{t,j,b}^{\mathrm{DA,O}}+\sum_{t=1}^{T}\sum_{m=1}^{N^{\mathrm{m}}}\lambda_{t,m}^{\mathrm{DA,D}}P_{t,m}^{\mathrm{DA,D}}\\
&-\sum_{t=1}^{T}\sum_{j=1}^{N^{\mathrm{j}}}\sum_{b=1}^{N^{\mathrm{b}}}\mu_{t,j,b}^{\mathrm{DA,Omax}}P_{t,j,b}^{\mathrm{DA,Omax}}-\sum_{t=1}^{T}\sum_{m=1}^{N^{\mathrm{m}}}\mu_{t,m}^{\mathrm{DA,Dmax}}P_{t,m}^{\mathrm{DA,Dmax}}
\end{aligned}\tag{3.11}$$

With the linearization of the KKT complementarity conditions, the linearized form of $\lambda_t^{\mathrm{DA}}P_t^{\mathrm{DA}}$ in (3.11), as well as the equivalent linearization for the IDM LL problem, the MPEC model is converted to an MILP model. It can be written as:

$$
\begin{aligned}
\max \quad & \sum_{t=1}^{T} pr_t^{\mathrm{BM}} P_t^{\mathrm{BM}} \\
& + \sum_{t=1}^{T} \sum_{m=1}^{N^{\mathrm{m}}} \left(\lambda_{t,m}^{\mathrm{DA,D}} P_{t,m}^{\mathrm{DA,D}} - \mu_{t,m}^{\mathrm{DA,Dmax}} P_{t,m}^{\mathrm{DA,Dmax}} \right) \\
& - \sum_{t=1}^{T} \sum_{j=1}^{N^{\mathrm{j}}} \sum_{b=1}^{N^{\mathrm{b}}} \left(\mu_{t,j,b}^{\mathrm{DA,Omax}} P_{t,j,b}^{\mathrm{DA,Omax}} + \lambda_{t,j,b}^{\mathrm{DA,O}} P_{t,j,b}^{\mathrm{DA,O}} \right) \\
& + \sum_{t=1}^{T} \sum_{m=1}^{N^{\mathrm{m}}} \left(\lambda_{t,m}^{\mathrm{ID,D}} P_{t,m}^{\mathrm{ID,D}} - \mu_{t,m}^{\mathrm{ID,Dmax}} P_{t,m}^{\mathrm{ID,Dmax}} \right) \\
& - \sum_{t=1}^{T} \sum_{j=1}^{N^{\mathrm{j}}} \sum_{b=1}^{N^{\mathrm{b}}} \left(\mu_{t,j,b}^{\mathrm{ID,Omax}} P_{t,j,b}^{\mathrm{ID,Omax}} + \lambda_{t,j,b}^{\mathrm{ID,O}} P_{t,j,b}^{\mathrm{ID,O}} \right) && \text{(3.12a)} \\
\text{s.t.} \quad & \text{(3.1b)-(3.1f)} && \text{(3.12b)} \\
& \text{KKT conditions (3.3a)-(3.3c), (3.3j) for DAM} && \text{(3.12c)} \\
& \text{KKT conditions for IDM equivalent to} \\
& \text{(3.3a)-(3.3c), (3.3j)} && \text{(3.12d)} \\
& \text{Linearized complementarity constraints} \\
& \text{(3.5a)-(3.5m) for DAM} && \text{(3.12e)} \\
& \text{Linearized complementarity constraints} \\
& \text{for IDM equivalent to (3.5a)-(3.5m)} && \text{(3.12f)}
\end{aligned}
$$

With the deterministic formulation of the problem, now various uncertainty levels need to be considered. As mentioned in Section 3.2, uncertainties concerning rivals' offers in the IDM are modeled using scenarios, while the VRE output uncertainties are modeled using probabilistic constraints. The details of the uncertainty modeling will be discussed in the following paragraphs.

3.3.6 Modeling Variable Generation Output Uncertainties Using Probabilistic Constraints

VRE output fluctuates significantly and the variation from one hour to another can be large. In this part, we assume that the VRE output is not known in

advance, but rather is a random variable and is represented as the sum of the VRE forecast and the forecast error:

$$P_t^{\mathrm{W}} = P_t^{\mathrm{Wf}} + \Delta P_t^{\mathrm{W}} \tag{3.13}$$

$$P_t^{\mathrm{S}} = P_t^{\mathrm{Sf}} + \Delta P_t^{\mathrm{S}} \tag{3.14}$$

where P^{W} and P^{S} are the actual wind and PV outputs, ΔP^{W} and ΔP^{S} are the wind and PV generation forecast errors. The DA wind and PV forecast errors are modeled as Gaussian random variables with mean zero and standard deviations σ^{W} and σ^{S}, i.e. $\Delta P_t^{\mathrm{W}} \sim \mathcal{N}(0, (\sigma_t^{\mathrm{W}})^2)$ and $\Delta P_t^{\mathrm{S}} \sim \mathcal{N}(0, (\sigma_t^{\mathrm{S}})^2)$.

The chance-constrained power balance equation for the upper-level, i.e. constraint (3.1b), is now formulated as

$$\mathbb{P}\left[P_t^{\mathrm{DA}} + P_t^{\mathrm{ID}} + P_t^{\mathrm{BM}} \leq P_t^{\mathrm{W}} + P_t^{\mathrm{S}}\right] \geq 1 - \epsilon \tag{3.15}$$

With (3.13) and (3.14) we obtain

$$\mathbb{P}\left[P_t^{\mathrm{DA}} + P_t^{\mathrm{ID}} + P_t^{\mathrm{BM}} \leq P_t^{\mathrm{Wf}} + \Delta P_t^{\mathrm{W}} + P_t^{\mathrm{Sf}} + \Delta P_t^{\mathrm{S}}\right] \geq 1 - \epsilon \tag{3.16}$$

where ϵ denotes the violation probability. The constraint can be reformulated analytically into a deterministic equation [55]:

$$P_t^{\mathrm{DA}} + P_t^{\mathrm{ID}} + P_t^{\mathrm{BM}} \leq P_t^{\mathrm{Wf}} + P_t^{\mathrm{Sf}} - \Phi^{-1}(1-\epsilon)\left[\sqrt{(\sigma_t^{\mathrm{W}})^2 + (\sigma_t^{\mathrm{S}})^2}\right] \tag{3.17}$$

where Φ is the probability distribution function.

The inverse of the cumulative distribution function is the quantile function, and the quantile function of the standard Gaussian distribution is called the "probit function", which can be expressed in terms of the inverse error function:

$$\Phi^{-1}(p) = \sqrt{2} \cdot \mathrm{erf}^{-1}(2p-1), \quad p \in (0,1) \tag{3.18}$$

Thus, (3.17) becomes:

$$P_t^{\mathrm{DA}} + P_t^{\mathrm{ID}} + P_t^{\mathrm{BM}} \leq P_t^{\mathrm{Wf}} + P_t^{\mathrm{Sf}} - \sqrt{2}\mathrm{erf}^{-1}(1-2\epsilon)\left[\sqrt{(\sigma_t^{\mathrm{W}})^2 + (\sigma_t^{\mathrm{S}})^2}\right] \tag{3.19}$$

which can replace (3.1b) without adding computational complexity.

3.3.7 Modeling Market Uncertainties using Scenarios

As the price elasticity of demand is close to zero, and the DA offering prices are assumed to be close to the marginal costs, only the uncertainty regarding rival producers' IDM offers is considered.

The final stochastic bi-level model with probabilistic constraints is as follows:

$$\max \quad \sum_{t=1}^{T}\sum_{\omega=1}^{N^{\omega}} \alpha_{\omega}\left(\lambda^{\mathrm{DA}}_{t,\omega}P^{\mathrm{DA}}_{t,\omega} + \lambda^{\mathrm{ID}}_{t,\omega}P^{\mathrm{ID}}_{t,\omega} - pr^{\mathrm{BM}}_{t,\omega}P^{\mathrm{BM}}_{t,\omega}\right) \tag{3.20a}$$

$$\text{s.t.} \quad \text{(3.1b)-(3.1f), (3.19)}, \quad \forall\omega \tag{3.20b}$$

$$\text{KKT conditions (3.3a)-(3.3c), (3.3j) for DA}, \quad \forall\omega \tag{3.20c}$$

$$\text{KKT conditions for IDM equivalent to (3.3a)-(3.3c), (3.3j)}, \quad \forall\omega \tag{3.20d}$$

$$\text{Linearized complementarity constraints (3.5a)-(3.5m) for DA}, \quad \forall\omega \tag{3.20e}$$

$$\text{Linearized complementarity constraints for IDM equivalent to (3.5a)-(3.5m)}, \quad \forall\omega \tag{3.20f}$$

$$P^{\mathrm{DA}}_{t,\omega'} = P^{\mathrm{DA}}_{t,\omega}, \quad \forall\omega,\omega' \tag{3.20g}$$

$$Q^{\mathrm{DA}}_{t,\omega'} = Q^{\mathrm{DA}}_{t,\omega}, \quad \forall\omega,\omega' \tag{3.20h}$$

$$\lambda^{\mathrm{DA}}_{t,\omega'} = \lambda^{\mathrm{DA}}_{t,\omega}, \quad \forall\omega,\omega' \tag{3.20i}$$

$$P^{\mathrm{ID}}_{t,\omega} \leq P^{\mathrm{ID}}_{t,\omega'}, \quad \forall\omega,\omega' : \ \lambda^{\mathrm{ID}}_{t,\omega} \leq \lambda^{\mathrm{ID}}_{t,\omega'} \tag{3.20j}$$

where α_{ω} is the realization possibility of scenario ω and N^{ω} indicates the total numbers of scenarios considered. Note that constraints (3.20b)-(3.20f) are all dependent on scenario index ω. Equations (3.20g)-(3.20i) force the non-anticipativity of DA decisions, while (3.20j) ensures the non-decreasing characteristic of the resulting ID offer curves. It should be mentioned that the consideration of consumers' bids' uncertainties can be incorporated into the formulation without incurring large additional computational cost.

3.4 Case Study - Test System

The proposed methodology is implemented using the MATLAB toolbox Yalmip [38] and is applied to a modified Swiss system. Since a one-year simulation is computationally expensive, the model is simulated for four selected weeks in 2016, namely the first weeks of January, April, July and October, each representing one season. Thus, all data used for the case study are from this period and the corresponding 28-day simulation results are presented.

The simulated system comprises 15 generation technology types with a total maximum capacity of 22'599 MW. Table 3.1 lists the installed capacities and the marginal cost assumptions for each technology type simulated for the modified Swiss system. Note that the assumed marginal cost includes both the variable operational cost and the fuel cost. In addition, subsidies for processing the waste are considered for the waste incinerators [3]. Units with the same technology type are merged and are assumed to submit the identical offering curves to the electricity market. Capacity factors of all units except hydro, wind and PV are assumed to be one. The capacity factors that are applied for different types of hydro power plants in different seasons are based on the data from [56] and the adopted values for the simulation are summarized in Table 3.2. All hydro power plants are modeled as normal generation units, i.e. the pumping and turbining behaviors are not modeled.

Table 3.1: Parameters of the units simulated for the modified Swiss system.

Unit types	Capacity [MW]	Marginal price [CHF/MWh]	Source
Nuclear	2'865	29.1	[57, 58]
Run-of-river hydro	3'957	9.5	[56]
Storage hydro	7'957	11.0	[56]
Pumped hydro	4'655	9.0	[56]
PV	2'492	2.7	[59, 60]
Wind	75	2.5	[60, 61]
Biogas plant	10	65.0	[62, 63, 64]
Waste incinerator	266	2.5	[3, 65]
Gas turbine	71	86.7	[3, 60, 65, 66, 67]
Waste wood	6	2.0	[62, 66]
Oil	3	240.7	[3, 60, 65]
Gas CHP	3	60.0	[58, 62]
Wood CHP	133	30.2	[3, 62, 65]
Biogas CHP	81	65.0	[63, 64, 65]
Oil CHP	25	240.7	[3, 60, 62]

Table 3.2: Capacity factors for different types of hydro power plants.

	Winter	Spring	Summer	Autumn
Run-of-river hydro	0.23	0.44	0.68	0.44
Storage hydro	0.28	0.23	0.14	0.23
Pumped hydro	0.20	0.15	0.10	0.13

As shown in Table 3.1, the Swiss power system is highly dependent on the supply of hydro power plants and with the gradual nuclear phase-out the hydro power already accounts for more than half of the Swiss electricity supply [65]. Since the generation of the hydro power plants is seasonal, the Swiss electricity system is not self-sufficient during seasons with low hydro power outputs (i.e., winter seasons). Thanks to the central location and the up to 9 GW cross-border transmission capacities of Switzerland, which is substantial considering its around 10 GW peak demand [68], the Swiss system demand deficits are able to be partly satisfied through imports from neighboring countries. As the modeling of the cross-border trading is beyond the scope of this thesis, the modified Swiss system is simplified by assuming that there is sufficient import energy available. The import electricity is modeled as a rival unit with the maximum capacity of 5000 MW and offering prices at around 65 CHF/MWh, which is a simplification of a highly complex reality. In reality, the cross-border electricity exchange quantity and price curves vary over time and are influenced by multiple factors, such as the seasons, the availability of transmission capacities, the trading country especially its generation mix and the energy path. Furthermore, the modeled Swiss electricity system is assumed to be uncongested, i.e. the network constraints are not considered.

Demands are assumed to be price inelastic for both the DAM and the IDM, i.e. the demand is independent of market prices. The total system demand is modeled based on the data from [69] with an hourly maximum and minimum load of 9'358 MW and 5'450 MW, respectively. Market participants for the IDM are assumed to be the same as those for the DAM, but the maximum offering quantities of all market participants as well as the demand quantities for the DAM and the IDM are assumed to be 90% and 10% of that for the DAM and IDM in total. This is based on the fact that the total energy traded in the Swiss IDM is much less than the energy traded in the DAM [29]. As the rival produc-

ers' offering quantities and prices for the market are confidential and hardly available, we consider that all rival producers are non-strategic producers with offering curves constructed based on their available capacities and marginal costs. To be more specific, the offering curve for each non-strategic unit consists of four blocks. Under the assumption that in a competitive market each market participant will offer close to its marginal cost, the offering price for each block is set to 1, 1.05, 1.1 and 1.15 times of the unit's marginal cost while the corresponding offering quantity for each block is set to 60%, 20%, 10% and 10% of the unit's total available offering quantity. Since the IDM prices are more volatile than the DAM prices, we consider 20 scenarios to represent the uncertainty concerning rivals' offering prices in the IDM. The IDM offering price of rival unit type j for block b under scenario ω is simulated as

$$\lambda^{\text{ID,O}}_{t,j,b,\omega} = \lambda^{\text{DA,O}}_{t,j,b}(1 + \epsilon^{\text{ID}}_{j,\omega}) \tag{3.21}$$

where ϵ^{ID} follows a Gaussian distribution, i.e. $\epsilon^{\text{ID}} \sim \mathcal{N}(\mu^{\text{ID}}, (\sigma^{\text{ID}})^2)$ with the mean μ^{ID} and the standard deviation σ^{ID} set to 0 and 0.3, respectively. These offering price scenarios are associated with equal realization probability (i.e., 5%). The aggregated hourly average DAM offering curve of all rival producers along with the hourly average inelastic DA demand curve is shown in Fig. 3.3, while the aggregated hourly average IDM offering curves of the rival producers under different scenarios and the hourly average inelastic ID demand curve are shown in Fig. 3.4. Note that for the offering curves shown in Fig. 3.3 and Fig. 3.4 the capacity factors of all units are set to the corresponding annual average values.

The positive and negative imbalance prices (i.e., $pr^{\text{BM+}}$ and $pr^{\text{BM-}}$) are modeled based on the hourly DAM and IDM prices in the case when the market share of the aggregator is zero, i.e. pr^{DA} and pr^{ID}. Mathematically,

$$\begin{aligned} pr^{\text{BM+}}_{t,\omega} &= a_1 \cdot \min\{pr^{\text{DA}}_{t,\omega},\ pr^{\text{ID}}_{t,\omega}\} \qquad \forall t, \forall \omega \\ pr^{\text{BM-}}_{t,\omega} &= a_2 \cdot \max\{pr^{\text{DA}}_{t,\omega},\ pr^{\text{ID}}_{t,\omega}\} \qquad \forall t, \forall \omega \end{aligned} \tag{3.22}$$

where a_1 and a_2 are constants and are set to 0.7 and 1.3 based on the values provided in [70]. The hourly positive and negative imbalance prices, as well as the average DAM and IDM prices over all IDM offering price scenarios con-

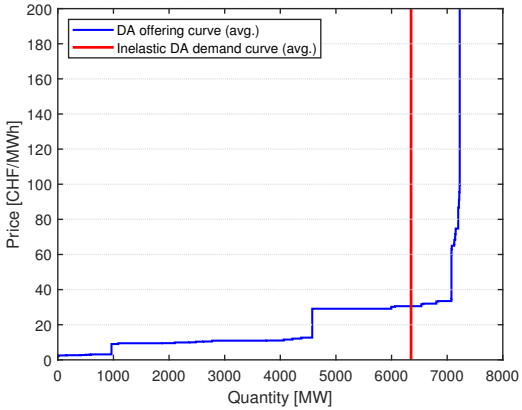

Figure 3.3: Average aggregated hourly day-ahead offering curve of rival producers and an inelastic demand curve with the demand quantity equaling to the average hourly day-ahead market demand quantity.

sidering zero market share of the aggregator (i.e. pr^{DA} and pr^{ID}) for the four representative weeks are shown in Fig. 3.5.

Finally, the strategic hybrid aggregator is assumed to be an aggregated portfolio of several wind and PV power plants. The maximum generation output of the wind and PV are calculated based on the corresponding wind and PV market shares, which are defined as the ratio of the wind and PV generation to the total system demand over the four-week simulation horizon, respectively. Note that the strategic hybrid aggregator is introduced to the market to replace the existing capacities in the system, i.e., as the market share of the aggregator increases, the market share of other non-strategic units decreases correspondingly while keeping the total supply of all strategic and non-strategic units (excluding the imports) the same.

The hourly capacity factors of wind and PV units for the four representative weeks are modeled based on the data from Renewables.ninja [71] and are shown in Fig. 3.6. These capacity factors are applied to both the wind and PV units within the aggregator and the existing non-strategic wind and PV units modeled in the system. The violation probability ϵ used in the probabilistic constraint is chosen to be 5% [55].

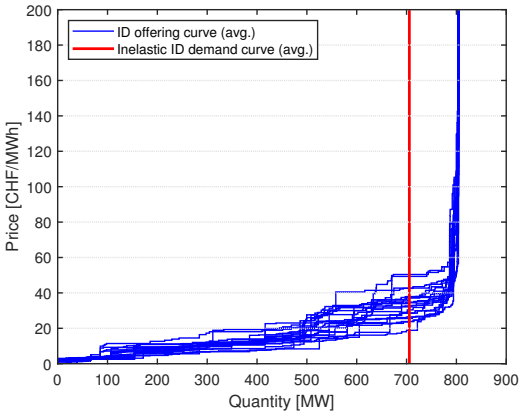

Figure 3.4: Average aggregated hourly intraday offering curves of rival producers under different intraday market offering price scenarios and an intraday market inelastic demand curve with the demand quantity equaling to the hourly average of the intraday market demand quantity.

3.5 Case Study - Results

In this section, we first validate the effectiveness of the proposed model by comparing a strategic aggregator using the presented method to a non-strategic aggregator in the Baseline scenario, where the optimization is carried out considering only the uncertainty regarding the IDM offerings of the rival producers. The strategic aggregator optimizes both the offering quantities and prices aiming to maximize its total profits, whereas the non-strategic aggregator is assumed to offer all forecasted power to the DAM and the IDM at a price of zero. Then to investigate how the results are affected by our assumptions, we show the results of conducting a set of one-at-a-time sensitivity analyses of the aggregator's market share, the price of the import electricity, the price elasticity of the demand, the generation mix of the aggregator and the forecast uncertainty while keeping the remaining parameters equal to the Baseline scenario value. Parameters modeled in the Baseline and the sensitivity scenarios are summarized in Table 3.3.

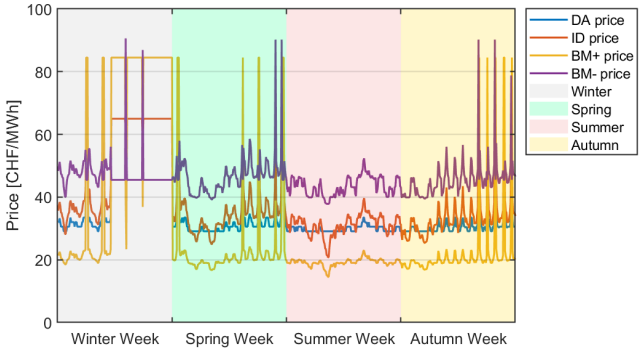

Figure 3.5: The hourly average positive and negative imbalance prices, as well as the day-ahead and intraday market prices over all intraday price scenarios considering only the offering of the non-strategic rivals for the four representative weeks corresponding to four seasons (from left to right: winter, spring, summer, autumn).

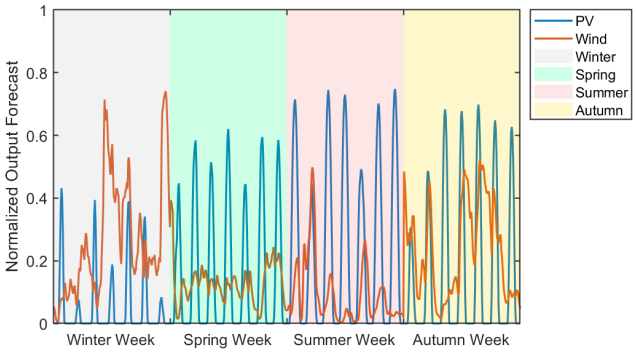

Figure 3.6: Hourly capacity factors of wind and PV units for four weeks corresponding to four seasons (from left to right: winter, spring, summer, autumn).

3.5.1 Strategic offering vs. Non-strategic offering

In this section, we compare the results of the strategic and non-strategic offerings in the Baseline scenario.

Figure 3.7 shows the DA offering quantities and the resulting DAM clearing prices of a winter, a spring, a summer and an autumn day under strategic

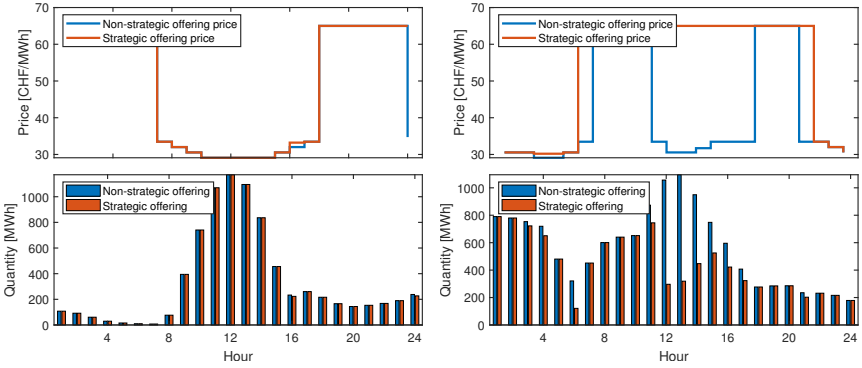

(a) A Winter Day **(b)** A Spring Day

(c) A Summer Day **(d)** An Autumn Day

Figure 3.7: Day-ahead offering quantities and the resulting market clearing prices for strategic and non-strategic offerings in the Baseline scenario for four selected days from four seasons.

Table 3.3: Modeled input parameters in the Baseline and the sensitivity scenarios.

Parameter	Baseline value	Sensitivity analysis value
Import electricity offering price	65 CHF/MWh	97.5 CHF/MWh, 130 CHF/MWh
Standard deviation of forecast errors	0%	0~30%
Demand bidding curve	price inelastic	increased elasticity
Aggregator market share	10%	0%-35%
Wind share within the aggregator	50%	0~100%
PV share within the aggregator	50%	0~100%

and non-strategic offerings. In general, the strategic aggregator manages to increase the market prices by withholding its offering quantities for some hours during the day. This can be observed for example in hours 11-17 in Fig. 3.7b and hour 12 in Fig. 3.7c where strategic offering quantities are lower than non-strategic quantities, resulting in an increase of the market prices during these hours. However, it can be observed that in most of the hours the DA offering quantities and the resulting DA market clearing prices under strategic offerings are identical to those under the non-strategic offerings. This is due to the fact that on one hand the market power (i.e. the ability to alter the market price) of the strategic aggregator is influenced by a lot of factors, such as the market share of the aggregator, the demand elasticity and the market price cap etc. More details of these influencing factors will be discussed in the following sections. On the other hand, the strategic aggregator always faces a price-volume trade-off, which means that it can choose to be dispatched for a higher quantity and at a lower price, or it can choose to be dispatched for a lower quantity and at a higher price [72]. Whenever the revenues earned in the latter case are higher than the revenues earned in the former case, the aggregator will exercise the market power and withhold the capacity by either offering part of the available capacities at higher prices or offering less quantities than the available capacities.

Furthermore, it can be noticed that the maximum DAM price of the four selected days does not exceed 65 CHF/MWh, which is the marginal cost assumed for the import electricity. The DAM prices remain at this level during the winter and the spring seasons, when the output of the hydro power plants and PV power plants are in general low, e.g. hours 1-7 and 18-24 in Fig. 3.7a as well as hours 8-11 and 18-20 in Fig. 3.7b. This is due to the assumption that the im-

port electricity is sufficient enough to meet the system demand deficit. More specifically, when part of the system demand is satisfied by the imported electricity, i.e. the total offering quantities within the system that are associated with an offering price below 65 CHF/MWh (i.e. the import electricity offering price) are lower than the corresponding system demand, the market clearing price will remain at the import electricity offering price. Furthermore, it can be seen that the strategic aggregator does not withhold the capacity whenever the market clearing price under the non-strategic offering reaches the offering price of the import electricity. This is because the offering price of the import electricity acts similar to a price cap under the assumption that sufficient import electricity is available, the aggregator therefore cannot further increase the market price by withholding the capacity in this case. The impact of the import electricity price is further analyzed by conducting sensitivity analyses and the results are discussed in the following sections.

Figure 3.8 shows the average IDM offering quantities and the resulting IDM clearing prices over all ID offering price scenarios under the strategic and non-strategic offerings for the same four days that are considered in Fig. 3.7. It shows that the IDM clearing prices are more volatile than the DAM clearing prices as the uncertainties of the IDM offerings of other participants in the market are incorporated. Furthermore, it can be seen that the strategic aggregator exercises the market power, i.e. withholds the outputs, more frequently that it does in the DAM. This is likely due to the fact that with the incorporated uncertainties, the aggregator needs to withhold less quantity to increase the market clearing price to the level of the next-highest offer in the market.

3.5.2 Impacts of the Market Share

In this section, we analyze the impact of the aggregator's market share, which is defined as the ratio of the total aggregator's generation to the total system demand over the four representative weeks. Table 3.4 shows the results considering market shares of the aggregator increasing from 0% to 35% with a step of 5% in the strategic and non-strategic offering cases, respectively. Same as the Baseline scenario, it is assumed that both the wind and the PV units contribute to the same amount of market share of the aggregator, which is specified in the table. It shows that both increase and decrease in DAM prices are observed in

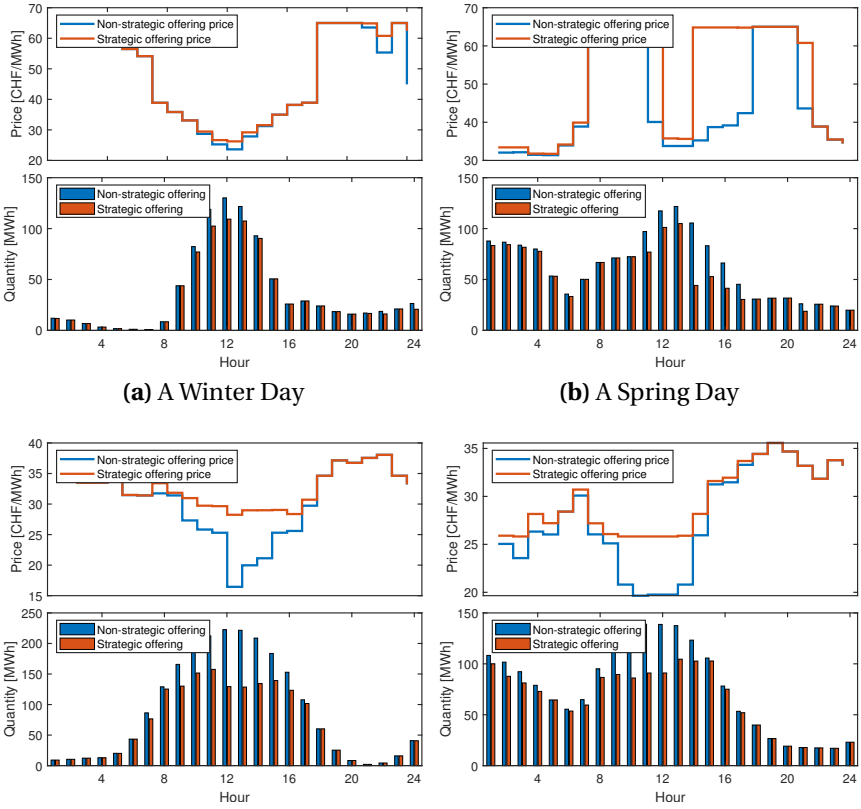

(a) A Winter Day

(b) A Spring Day

(c) A Summer Day

(d) An Autumn Day

Figure 3.8: Average intraday offering quantities and the resulting market clearing prices for strategic and non-strategic offerings in the Baseline scenario for four selected days from four seasons.

Table 3.4: Impact of the aggregator's market share on day-ahead market prices and the aggregator profit.

Results for Non-strategic Offering							
Market share [%]			**Average DAM weekly price [CHF/MWh]**				**Aggregator**
Tot.	**Wind**	**PV**	**Week 1**	**Week 2**	**Week 3**	**Week 4**	**profit [mCHF]**
0	0	0	50.43	32.97	29.77	32.07	n/a
5	2.5	2.5	50.26	34.60	29.06	32.29	9.54
10*	5	5	52.94	35.85	28.50	31.76	17.82
15	7.5	7.5	53.47	37.90	29.56	31.38	24.71
20	10	10	53.67	38.89	32.97	30.88	30.42
25	12.5	12.5	52.55	40.21	36.00	32.23	35.39
30	15	15	52.21	42.83	36.14	33.73	40.28
35	17.5	17.5	51.58	44.19	36.42	33.88	44.97

Results for Strategic Offering							
Market share [%]			**Average DAM weekly price [CHF/MWh]**				**Aggregator**
Tot.	**Wind**	**PV**	**Week 1**	**Week 2**	**Week 3**	**Week 4**	**profit [mCHF]**
0	0	0	50.43	32.97	29.77	32.07	n/a
5	2.5	2.5	53.46	37.28	30.32	34.54	9.96 (+4.4%)
10*	5	5	58.16	43.10	31.94	37.19	20.25 (+13.7%)
15	7.5	7.5	62.28	48.06	38.60	41.55	30.98 (+25.3%)
20	10	10	63.30	55.11	46.48	48.41	42.48 (+39.7%)
25	12.5	12.5	64.57	60.55	57.47	58.00	55.20 (+56.0%)
30	15	15	65.00	62.44	61.37	60.52	68.81 (+70.8%)
35	17.5	17.5	65.02	64.15	63.08	64.57	82.64 (+83.8%)

* Baseline value.
Note that values in () are the increase in profits of the aggregator in the case of strategic offering compared to that of non-strategic offering under the same market share.

the case of non-strategic offering. This is likely due to the mixed impacts of a few factors: 1) with the increasing market share of the non-strategic aggregator, an increasing amount of offering quantities are submitted to the market at price zero, which could have a negative impact on the market prices during these hours; 2) based on the definition of the market share, the non-strategic aggregator's market share increases as a replacement of the existing capacities within the system. As a result of the diurnal and seasonal pattern of the aggregator's output, more demand needs to be satisfied by the import electricity during the periods of low aggregator generations (e.g. winter), the electricity market prices during these hours are thus increased since the import electricity offering price is in general higher than the average market price. Moreover, with the increasing market share, the price increase in the case of strategic offerings is stronger than that in the case of non-strategic offerings. This is because the aggregator exerts the market power and succeeds in increasing

Table 3.5: Impact of the aggregator's market share on market revenues and costs.

Market share [%]			Revenue [mCHF]		Cost [mCHF]	
Tot.	**Wind**	**PV**	**Aggregator**	**Rival producers**	**Demand**	**Import**
0	0	0	n/a	172.82	178.19	5.37
5	2.5	2.5	9.96	175.44	190.34	5.20
10*	5	5	20.25	183.36	207.85	5.54
15	7.5	7.5	30.98	197.36	231.28	6.65
20	10	10	42.48	213.92	257.59	8.72
25	12.5	12.5	55.20	232.66	287.59	12.01
30	15	15	68.81	227.49	297.21	16.04
35	17.5	17.5	82.63	219.96	305.14	20.70

* Baseline value.

market prices by withholding the outputs. When comparing the total expected profits (including the profits from all markets) of the strategic and the non-strategic aggregators considering different values of the market share. It is notable that the profit of the strategic aggregator grows at a higher rate than the profit of the non-strategic aggregator. More specifically, with the aggregator market share changing from 5% to 35%, the aggregator's profit in the case of strategic offering is from 4.4% higher to 83.8% higher than the aggregator's profit in the corresponding non-strategic offering case. This is due to the fact that the non-strategic aggregator offers into the market at price zero. When its market share increases, market clearing prices drop dramatically during the periods when the aggregator generations are high. In contrast, the strategic aggregator has more market power and more control of the market price by withholding big amounts of the output when the market share increases. Results for IDM price changes under different market shares of the aggregator are not shown, but as the market participants for the DAM and IDM are assumed to be identical, the findings of the IDM results are in general consistent with those of the DAM.

We further analyze the impact of market shares by showing the revenues and costs of different market participants under different values of market shares in the case of strategic offerings in Table 3.5. The numbers shown include the revenues and costs incurred in both the DAM and the IDM. Note that the revenues shown for the strategic aggregator are identical to the profits shown in Table 3.4, as no generation cost is considered for the aggregator and the wind

Table 3.6: Impact of the import electricity price.

Import offering price [CHF/MWh]	Average DAM weekly price [CHF/MWh]				Aggregator profit [mCHF]	Aggregator offer DAM & IDM [TWh]
	Week 1	Week 2	Week 3	Week 4		
65*	58.16	43.10	31.94	37.19	20.25	0.44
97.5	82.18	52.58	32.80	43.35	23.94	0.43
130	107.39	64.38	34.49	50.12	27.86	0.42

* Baseline value.

and PV outputs are assumed to be perfectly forecasted in the Baseline scenario. The results show that both the revenues of the strategic aggregator and the rival producers increase as the aggregator's market share increases from 0% to 25%, even though the aggregator's market share increases as a replacement of the existing capacities in the system. This can be explained by the increasing average market prices shown in Table 3.4, which leads to more revenues for each MWh of quantities offered to the market and could possibly recover the losses caused by the reduced offering quantities. The revenues of the rival producers decrease after the market share of the aggregator reaches 25%, which means that additional revenues generated by the further increase in market prices are not sufficient enough to recover the losses incurred by the reduced market share. It is worth noting that since the import electricity offering price acts similar to a price cap under the assumption that there is sufficient import energy available, import offering price therefore limits the market price increase and the revenues earned by the producers in the market (i.e., market participants who offer to supply the electricity). In general, the total revenues earned by all producers within the system increase as the market share of the strategic aggregator increases, however, as shown in Table 3.5, this increase is at the cost of increasing costs for the demand and for the imports, which might not be favored by the system regulators and policy makers. Moreover, although in reality the demand is in general inelastic to the price changes in the short run, its price elasticity increases in the long run [73], which means that as a result of the high market clearing prices and producer surplus in the long run part of the demand might turn to alternative energy sources.

3.5.3 Impacts of the Import Electricity Price

To analyze the impact of the assumption on the import electricity offering prices, we conduct the sensitivity scenarios by increasing the import offering

Table 3.7: Impact of the price elasticity of demand.

Demand	Average price [CHF/MWh]		Producer revenue [mCHF]		Demand cost	Aggregator DAM & IDM offer
	DAM	IDM	Aggregator	Rivals	[mCHF]	[TWh]
Inelastic*	42.60	42.56	20.25	183.36	207.85	0.44
Increased elasticity	36.95	37.92	19.05	156.85	164.54	0.51

* Baseline value.

prices to 150% and 200% of the value assumed in the Baseline scenario (i.e. 65 CHF/MWh). The results are shown in Table 3.6[9]. It is obvious that the DAM prices increase significantly with the increase of the import electricity price. This is because with the increasing import price the strategic aggregator has more incentives to exercise the market power, i.e. it has more space to increase the market price by withholding the outputs, This can be justified by the increasing aggregator profits and the decreasing total offering quantities to the markets shown in Table 3.6. Furthermore, this phenomenon is more pronounced during winter when there is less spare capacity in the system.

3.5.4 Impacts of the Price Elasticity of Demand

According to the work in [74], demand elasticity can contribute to mitigating the strategic bidding behavior of the producers. In addition, despite the in general low price elasticity of demand, even a small increase in demand elasticity can result in appreciable improvement of the market performance. To analyze how the assumption of the price elasticity of demand impacts the offering behaviors of the aggregator and the market results, in this section we simulate a sensitivity scenario, i.e. a scenario with increased demand elasticity. In this scenario, for each hour the total demand is assumed to consist of two parts: a) inflexible demand, which accounts for 90% of the total demand; b) flexible demand, which accounts for the remaining 10% of the demand. The short-term price elasticity of the flexible demand part is assumed to be -0.3 based on [73], which means that for each 1% increase (decrease) in electricity price, the demand quantity will decrease (increase) 0.3%. Note that the values are only taken for illustration purposes and in reality they may vary across sectors, seasons, hours and regions, etc. As shown in Table 3.7, with the increasing price elasticity of demand, the market clearing prices and the producers' rev-

[9] IDM market results are similar to the results of the DAM and therefore are not shown.

Table 3.8: Impact of the aggregator's generation mix.

Results for Non-strategic Offering				
Share [%]		Average price [CHF/MWh]		Aggregator
Wind	PV	DAM	IDM	profit [mCHF]
100%	**0%**	35.48	37.18	18.13
80%	**20%**	36.15	37.66	18.61
60%	**40%**	36.91	38.34	18.52
40%	**60%**	37.49	38.87	16.76
20%	**80%**	37.62	39.23	14.12
0%	**100%**	38.18	39.75	10.96

Results for Strategic Offering				
Share [%]		Average price [CHF/MWh]		Aggregator
Wind	PV	DAM	IDM	profit [mCHF]
100%	**0%**	42.56	42.48	22.20
80%	**20%**	42.43	42.43	21.71
60%	**40%**	42.42	42.36	20.81
40%	**60%**	42.82	42.76	19.61
20%	**80%**	43.09	43.21	18.10
0%	**100%**	43.08	44.03	16.22

enues decrease whereas the demand costs decrease. This is because with the increased price elasticity of demand the strategic aggregator has less incentive to exercise the market power as further increase the market price could reduce the consumption of demand. Thus, the aggregator increases the total offering quantities to the DAM and the IDM from 0.44 TWh in the inelastic demand case to 0.51 TWh in the increased elasticity demand case. In general, introducing the elasticity to the demand side could shift the additional surplus due to the exercise of market power from the supply side to the demand side, which could increase the efficiency of the market. This observation is consistent with the findings of [74].

3.5.5 Impacts of the Generation Mix of the Aggregator

In this section, the impact of the aggregator's generation mix, i.e. the share of wind and PV generation within the aggregator, on the market power and the resulting profits of the aggregator are analyzed. To do so, we simulate the sensitivity scenarios by changing the (total generation) share of wind and PV units within the aggregator from 0% to 100% with a step of 20%, while keeping the market share of the aggregator the same as the Baseline scenario, i.e. 10%.

The results under both the non-strategic offerings and the strategic offerings are shown in Table 3.8.

It can be seen that in both the strategic and non-strategic offering cases, in general the market price slightly increases as the share of wind decreases. Furthermore, while the aggregator achieves the highest profits when the share of wind and PV is around 80%:20% in the case of non-strategic offering, the strategic aggregator obtains the highest profits when the share of wind is 100%. To better understand the reasons behind this, we plot the average hourly DAM and IDM offering quantities and the resulting market clearing prices for strategic and non-strategic offerings over the four representative weeks under two extreme cases, namely the 100% wind case and the 100% PV case in Fig. 3.9. It can be seen that in general the DAM results are similar to the IDM results except that more capacities are withheld in the IDM. When focusing on the results of 100% PV in the case of strategic offerings, it is noticeable that due to the diurnal pattern of the PV generation, the strategic aggregator needs to withhold significant amount of capacity during the hours with high PV generation so as to possibly eliminate the negative impact of the concentrated generation on the market clearing price. In contrast, in the case of 100% wind under strategic offering, as the aggregator generation is more evenly distributed across different hours of the day, the aggregator withholds the capacity in almost all hours of the day and with less quantities to be withheld for each hour in order to make a good price-volume trade-off. As a result, the aggregator has more incentives and flexibilities to exercise market power and therefore achieve higher profits, when the aggregator generation is more evenly distributed between hours, i.e. when the share of wind is higher. In the case of non-strategic offering, under the assumption that the aggregator submits all forecasted output at a price of zero, higher profits can be achieved when the generations of the aggregator match well with the profile of the demands. Additionally, this is also influenced by the available capacities of existing producers in the system.

3.5.6 Impacts of the Forecast Uncertainty

In this section, we analyze the impact of wind and PV generation forecast errors by carrying out simulations with the forecast error standard deviations (i.e. σ^{W} and σ^{S}) increased from 5% to 30% of the corresponding wind and PV

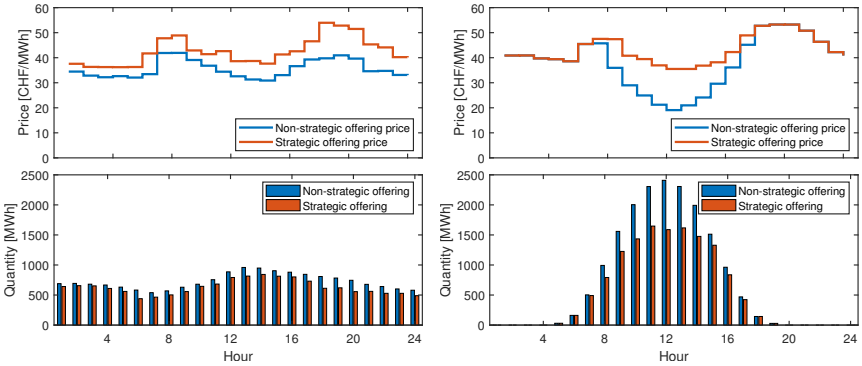

(a) DAM - 100% Wind **(b)** DAM - 100% PV

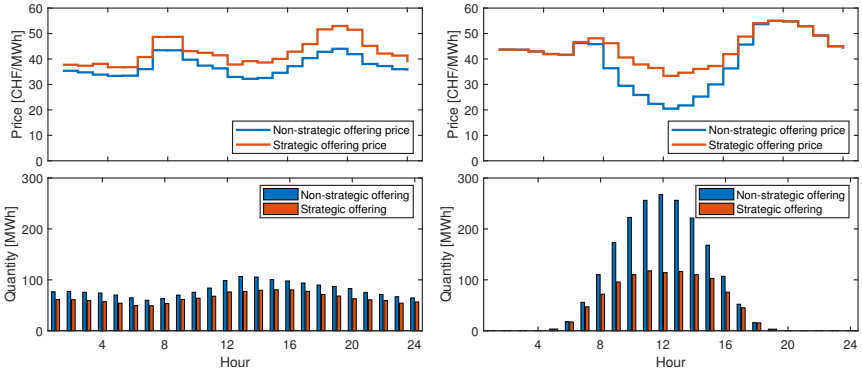

(c) IDM - 100% Wind **(d)** IDM - 100% PV

Figure 3.9: Average hourly day-ahead and intraday market offering quantities and the resulting market clearing prices for strategic and non-strategic offerings over the four representative weeks under two extreme generation mix cases: 100% wind and 100% PV.

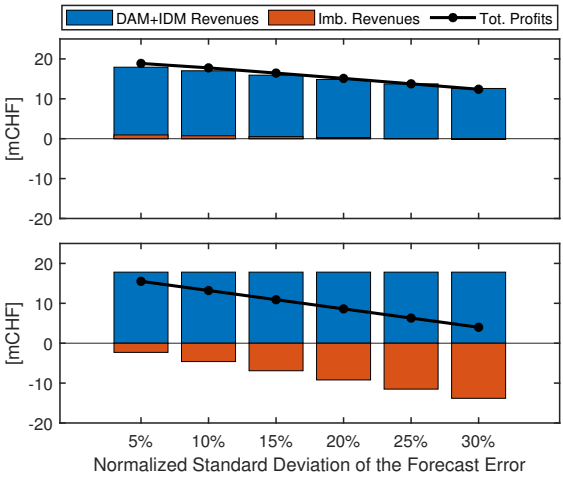

Figure 3.10: Impacts of forecast uncertainty on the aggregator profits: results under the strategic offering are shown in the top figure; results under the non-strategic offering are shown in the bottom figure.

generation forecast, while other parameters remain unchanged as the Baseline scenario. Values of σ^{W} and σ^{S} are assumed to be the same for each of the simulated sensitivity scenarios.

The resulting revenues from the DAM, the IDM and the BM as well as the total profits of the aggregator over the four representative weeks under the strategic offering and the non-strategic offering are shown in Fig. 3.10. It can be seen that in the case of strategic offering the aggregator's revenues from the DAM and IDM and the total profits decrease as the considered standard deviations increase from 5% to 30%, while the imbalance cost only slightly increases (i.e. revenues from the balancing market slightly decreases). This is because with the increasing values of σ^{W} and σ^{S} more conservative offering strategies are adopted, i.e. the aggregator offers less to the DAM and the IDM, so as to possibly avoid high costs in the balancing market. In contrast, in the case of non-strategic offering, since the aggregator always offers all forecasted power to the DAM and the IDM at zero prices, the revenues from the DAM and the IDM are the same for different values of σ^{W} and σ^{S}. However, the deviation of the forecast from the real-time output increases as σ^{W} and σ^{S} increase, leading

to the increasing imbalance costs and decreasing total profits of the aggregator. Comparing the results of the strategic and the non-strategic offering cases, while the total profits for the strategic offering case decrease from 18.9 mCHF to 11.2 mCHF by 41%, the total profits for the non-strategic offering case decrease from 15.5 mCHF to 4.0 mCHF by 74%, which shows the importance of integrating forecast uncertainties into the offering strategies.

3.6 Limitations and Future Work

This work has several limitations and a few of which are highlighted in this section. First, the market environment is simplified assuming that the aggregator is the only one that could bid strategically in the market. Moreover, the market participants of the day-ahead and intraday markets are assumed to be identical, which might not be the case in reality as the motivations for participating in these two markets are different. A future version should model a more realistic market environment by introducing competitions among multiple strategic producers using an equilibrium model, and differentiate the participants in different electricity markets.

Second, the uncertainties of wind and PV generation forecasts are incorporated using the chance constraints, which are reformulated assuming that the forecast errors are Gaussian distributed. However, the distributions of the wind and PV forecast errors in the real world are found to deviate substantially from the standard Gaussian distribution [75, 76]. A more realistic method to model the uncertainty without requiring the full knowledge of the uncertainty distribution will be presented in the following chapters.

Third, the network constraints including both the transmission limits within the modified Swiss electricity system and the cross-border transmission limits are not considered. However, the network constraints are expected to have a significant impact on the incentive to exercise market power as the network constraints limit the ability of producers in other areas to respond to the price changes [72]. Depending on whether the price zone that the aggregator is located in is importing electricity from or exporting electricity to the neighboring price zones, the aggregator might intend to increase the local market price by making the transmission limit binding or not binding through the exercise of market power.

Fourth, the balancing market prices are assumed to be independent of the forecast errors introduced by the aggregator, however, this assumption might not hold when the market share of the aggregator is high enough to influence the day-ahead and intraday market prices. Future work should include a more realistic modeling of the balancing market price and consider the mutual influence between the aggregator's forecast errors and the balancing market prices.

3.7 Summary and Conclusions

A stochastic bi-level model to derive optimal offering strategies for a hybrid aggregator that consists of wind and PV units and acts as a price-maker in both the day-ahead and intraday markets is presented. Uncertainties regarding the intraday market offers from rival producers are incorporated using scenarios, whereas the uncertainties of the wind and PV outputs are modeled using chance constraints.

The proposed offering strategy enables the aggregator to offer more efficiently into the markets and therefore to make more profits than the non-strategic aggregator. As the market share increases, the aggregator has more market power to increase the market price by withholding the output. As a result, the total profits for the aggregator grow at a higher speed than its market share increase, which however is at the cost of increasing system demand and import costs. In addition, the impact of import electricity offering prices is investigated, as under the assumption that the modified Swiss electricity system is not self-sufficient and the import electricity is sufficiently enough to supply the demand deficits, the import electricity price works similar to the market price cap. Results show that increasing the assumed import electricity offering price will increase the profits of the aggregator as it gives the strategic aggregator more space to exert market power. This phenomenon is more pronounced during winter when there is less capacity available in the system due to the low output level of hydro power plants, which are the main electricity suppliers in the system. Besides the market price cap, the ability to exercise the market power is also limited by the price elasticity of the demand curve. Results show that increasing the price elasticity of the demand curve could shift the additional producer surplus generated by exercising the market power from the supply side back to the demand side, which increases the market efficiency.

With regard to the influence of the wind and PV generation mix of the aggregator, due to the diurnal pattern of the PV generation, an increasing share of PV limits the opportunities to exert market power to the high PV generation periods, i.e. noon time. The total profits of the aggregator therefore decrease when the share of the PV generation increases in a hybrid aggregator that consists of wind and PV units. Finally, the incorporated wind and PV forecast uncertainty using chance constraints assures a certain risk level when designing the optimal offering strategies.

Chapter 4

Modeling Uncertainty using Distributionally Robust Optimization

The main challenge for variable renewable energy is to deal with the generation output uncertainty. To model this uncertainty more realistically and adequately, in this chapter, we present a two-stage distributionally robust model to derive optimal bidding strategies for an aggregated wind power plant that participates as a price-maker in the day-ahead market and a deviator in the balancing market. The market power is realized using a bi-level model. The uncertainty in wind generation output is characterized by an ambiguity set that defines a family of possible uncertainty distributions, and the optimal decision is robust to the expectation over the worst-case distribution. A case study based on a modified Swiss system verifies the effectiveness of the proposed distributionally robust optimization model. Out-of-sample analyses are conducted to compare its performance to that of a deterministic optimization model, a robust and a stochastic optimization model. This chapter is based on [77].

4.1 Introduction

4.1.1 Motivation and Related Work

The penetration of Variable Renewable Energy (VRE) (e.g. wind power and solar power) has increased dramatically in recent years, driven by the favorable governmental policies and its contributions to enabling a sustainable energy future. However, their intermittent and uncertain nature poses great challenges to both the VRE operators and the electricity system operators. Due to the continuous decreasing subsidies, VRE is forced to trade in the same market environment as conventional generators, although it is challenging to dispatch and difficult to forecast. While the optimal bidding strategy of wind or Photovoltaic (PV) units in sequential markets as a price-taker [15] or as a price-maker [45, 49, 78] as presented in Chapter 2 and Chapter 3 has been studied extensively, the distribution of uncertain VRE generation forecast errors was often assumed to be known. Most of the work assumes that the wind and PV generation forecast errors are subject to Gaussian distribution (e.g. [55, 79, 80, 81]), while beta and Weibull distributions have been applied as well (e.g. [48]). Nevertheless, it has been shown that these assumed distributions differ greatly from the wind and PV generation forecast errors in reality [75,76]. It is therefore important to answer the question of what would be the optimal offering strategy for VRE considering the forecast uncertainties are modeled in a proper way. In this chapter, a bidding strategy for an aggregated price-maker Wind Power Plant (WPP) based on Ditributionally Robust Optimization (DRO) is proposed. Note that the work in this chapter focuses primarily on wind power plants, however, the presented approaches are also applicable for PV power plants.

DRO falls into the general category of Stochastic Optimization (SO). Traditionally, SO incorporates uncertainties in the form of random variables and corresponding scenarios generated by using Monte Carlo simulations or probability distributions. The minimization/maximization of the objective function is then carried out over these scenarios. However, with an increasing number of random variables and scenarios, the problem quickly grows to unmanageable sizes. Moreover, an exact uncertainty distribution that is rarely available is required for SO. Robust Optimization (RO) [82] on the other hand has attracted a lot of attention due to its tractability and robustness. In this approach, it is not

necessary to know the probability distributions of the random variables but the worst case is considered. Nevertheless, it achieves results that are robust against parameter uncertainties requiring limited computation time while the resulting optimal solutions are often over-conservative. Different from RO and SO, DRO does not require the knowledge of exact distribution of uncertainties and it considers the uncertainty in distributions using an ambiguity set, which is constructed based on partial distributional information such as moment statistics or uncertainty range. Based on the fact that historical realizations of random variables are usually accessible, statistical data (e.g. expectation, standard deviation etc.) needed for building the ambiguity set is generally readily available. In this way, DRO can avoid over-conservative solutions by effectively extracting statistical features from empirical data, without requiring the specific probability distribution. While the solutions in RO are optimized against the worst-case realization, DRO seeks to protect against the worst-case distribution. To summarize, generally DRO acts as intermediary between SO and RO and achieves acceptable optimality with reasonable computational effort.

At the moment, the most popular method applied to optimize bidding strategies is stochastic optimization, e.g. [25] and [33]. However, as already mentioned, stochastic optimization often suffers from high computational complexity resulting from a large number of scenarios. Even though there are studies researching scenario reduction algorithms [83, 84], the applicability of stochastic optimization can also be limited by the fact that the uncertainty distribution is not always available.

Instead of requiring the knowledge of the uncertainty distribution, robust optimization is used to obtain a bidding strategy that optimizes the worst-case scenario over an uncertainty set, e.g. in [85] and [86]. RO is often computationally tractable as it requires only the range of possible variations of the random variable, but the performance of robust optimization is restricted by its conservativeness. To take advantage of both stochastic optimization and robust optimization, the work in [87] models the wind and price uncertainties by confidence bounds and scenarios, respectively. It combines adaptive robust optimization and stochastic programming to solve the offering problem of a virtual power plant.

By minimizing the worst-case expected cost, DRO aims to optimize problems under uncertainty taking both the risk and the ambiguity into account [88]. In DRO, the worst-case is taken over an ambiguity set, i.e. a family of distributions characterized through certain known properties of the unknown data-generating distribution [89]. In recent years, the method became popular again and research regarding a tractable framework and formulation for DRO has been carried out [88, 90, 91, 92]. Particularly, a Linear Decision Rule (LDR) that restricts the adaptive decisions to be affinely dependent on the uncertain parameters is used to enable tractability. To increase the flexibility of LDR functions, an enhanced LDR method that restricts the adaptive decisions to be affinely dependent on both the primary and the newly introduced auxiliary random variables, was also proposed in [88].

Lately, DRO has been applied to power system problems [93, 94, 95, 96]. In [93], a DRO model based on the enhanced LDR method was proposed to solve a unit commitment problem considering uncertain wind power generation. In [95], the same method is applied to solve the optimal power flow (OPF) problem considering uncertainties from wind power generation and load-based reserves, and DRO and a chance-constrained approach are compared. The work in [94] is an extension of the approach presented in [93] where the ambiguity set is extended by including non-linear functions and considering statistic characteristics such as the standard deviation. Finally, it is reformulated as a mixed-integer convex optimization problem with second-order cone constraints. Different from the method described above, [96] proposed another distributionally robust optimization model to solve the energy and reserve dispatch problem. It is modeled as a semi-definite programming problem and the delayed constraint generation algorithm was used to solve it in a tractable manner.

Some work has been done in terms of comparing DRO with RO and SO methods. It is shown in [91] and [96] that generally DRO outperforms RO as more statistical information is included, however, the DRO model is also more difficult to solve. The work in [97] demonstrates that in terms of the objective value, DRO is more conservative than the traditional SO as SO only accounts for the reference distribution, but the SO model also results in the highest computational time. Furthermore, both [91] and [97] concluded that compared to the

SO model, the DRO model stands out as being more reliable, i.e. its optimal solution is insensitive to probability distribution function (PDF) perturbations.

To our knowledge, however, there is a lack of studies dealing with optimizing bidding strategies using distributionally robust optimization. In this chapter, a bi-level model is developed to optimize the bidding strategy of a price-maker wind aggregator under uncertainty. It is formulated as a two-stage optimization problem: the Day-ahead (DA) bidding is the "here-and-now" first-stage decision and the real-time dispatch is the "wait-and-see" second-stage decision. The objective of the wind aggregator is to maximize the sum of its day-ahead profits and the expected worst-case Balancing Market (BM) profits over the ambiguity set. It is assumed that the wind aggregator acts as a price-maker in the Day-ahead Market (DAM), and as a deviator in the BM. To guarantee the tractability, the second-stage decisions are assumed to be linearly dependent on random variables by using the enhanced LDR method proposed in [88]. Following the linearization process presented in Chapter 3, the two-stage bi-level problem is solved by being transformed into a Mixed-Integer Linear Programming (MILP) model using the Karush-Kuhn-Tucker (KKT) optimality conditions and strong duality theory.

Consequently, the contributions of this chapter are:

1. To propose a two-stage DRO model to optimize the offering strategies of a wind aggregator that acts as a price-maker in the DAM, and as a deviator in the balancing market.
2. To validate the model using a modified Swiss system and compare the results of the DRO model to that of a Deterministic Optimization (DO) model, a RO model and a SO model.

4.1.2 Chapter Organization

The remainder of the chapter is organized as follows: the main model assumptions are described in Section 4.2. The mathematical formulations and the proposed optimization model are presented in Section 4.3. Section 4.4 provides an analysis for a case study based on a modified Swiss electricity system. The limitations and future work are discussed in Section 4.5. Finally, conclusions are drawn in Section 4.6.

4.2 Model Assumptions

The main modeling assumptions for this chapter are summarized as follows:

- The wind aggregator is assumed to participate in the day-ahead and the balancing markets, while the DAM demand is assumed to be price inelastic, i.e. the demand quantity does not respond to the price changes.
- All producers other than the strategic wind aggregator are assumed to be fully competitive and offer their productions at their marginal costs. If the market power of multiple strategic producers are considered and modeled in the market, the model will be an equilibrium problem with equilibrium constraints. This extension is beyond the scope of this thesis and is left for future research.
- The BM prices are assumed to be independent of the aggregator's position, i.e. the aggregator is a price-taker in the balancing market. This assumption, however, might need to be reconsidered when the aggregator accounts for a significant share of the market. Moreover, it is assumed that all imbalances can be corrected through the balancing market.
- The simulated modified Swiss electricity system is assumed to be uncongested, i.e. no network constraints are considered, which is consistent with the zonal pricing scheme of the European electricity markets. Futhermore, the cross-border transmission is modeled as a non-strategic rival producer with sufficient transmission capacity.
- The wind turbines in this work are assumed to be the ones receiving investment subsidies or negligible output subsidies, thus the effects of output subsidies on offering strategies are not considered. When considering output subsidies, the market power through capacity withholding will be limited and the offering strategy will change depending on whether the extra profits realized by wind curtailments are more than the benefits from output subsidies or not. The impact of the output subsidies on strategic biddings will be analyzed in Chapter 5.

4.3 Formulation of the Optimization Problem

This section presents the derivation of the distributionally robust optimization formulation of a wind aggregator's bidding problem. Similar to Chap-

ter 3, the market power of the aggregator is modeled using a bi-level structure. The upper-level represents the wind aggregator's profit maximization problem, while the lower-level represents the DAM clearing.

In the upper level model, the wind aggregator makes its offering decisions (i.e. one price-quantity pair $(\alpha_t^{\text{DA}}, Q_t^{\text{DA}})$ for each time step t) using the lower-level outcome, namely the day-ahead market clearing prices λ_t^{DA}, as an input. On the other hand, the lower level model clears the DAM by maximizing the social welfare using the bidding quantities as an input and communicates the resulting market clearing prices to the upper-level model. As we only consider the uncertainty of real-time wind generations, the DA bidding is unique in the balancing market whereas the balancing market dispatch depends on the actual wind generation realization. In Section 4.3.1 and 4.3.2, we first present the general formulation of the bi-level optimization model and then show how it can be reformulated as a MILP model using KKT conditions and duality theory. However, the problem is intractable as it requires computing a solution for all possible realizations of the wind generation output uncertainty. Therefore, in Section 4.3.3, a tractable two-stage bi-level MILP model is derived by approximating the second-stage decisions using enhanced LDR, while the wind generation output uncertainty is modeled using an ambiguity set, where the family of distributions is characterized by statistical parameters calculated from the historical data. Note that only uncertainties regarding real-time wind outputs are considered here, it is however straightforward to incorporate other uncertainties into the model.

4.3.1 Bi-level Bidding Model

The strategic bidding model is formulated using a bi-level structure.

Upper-level Formulation

The Upper-Level (UL) problem is the wind aggregator's profit maximization problem, i.e. it maximizes the profits obtained from the DAM and the BM. Note that the generation cost for wind is assumed to be zero. Mathematically, the objective function is given by

$$\max \sum_{t=1}^{T} \left(\lambda_t^{\text{DA}} P_t^{\text{DA}} + pr_t^{\text{BM}} P_t^{\text{BM}} \right) \tag{4.1a}$$

where P_t^{DA} is the DA dispatched quantity for time step t and λ_t^{DA} is the market clearing price. The term $pr^{\text{BM}} P^{\text{BM}}$ equals to $pr^{\text{BM+}} P^{\text{BM+}} - pr^{\text{BM-}} P^{\text{BM-}}$, where $pr_t^{\text{BM+/-}}$ and $P_t^{\text{BM+/-}}$ denote the prices and quantities for positive/negative imbalances, respectively. Balancing market prices are modeled as constants and the values are chosen such that it is guaranteed that the wind aggregator can only sell (purchase) electricity in the BM at a price lower (higher) than the corresponding DAM price [15]. Variable T indicates the simulation time horizon.

It is assumed that the wind aggregator cannot purchase energy from the market. The minimum offer quantity is therefore set to zero, and the maximum offer quantities of the wind aggregator are limited by its capacity P^{Wc}. Mathematically,

$$0 \leq Q_t^{\text{DA}} \leq P^{\text{Wc}} \tag{4.1b}$$

Note that while Q^{DA} is the quantity that is offered to the market, P^{DA} indicates the power that the wind aggregator expects to be dispatched for, which is an outcome of the lower-level market clearing problem as it models the dispatch of the market.

The wind aggregator along with the DAM and the BM constitute a closed energy system that must be balanced at each time period. This means that the actual wind generation P^{W} must be equal to the total exchange in the electricity markets, while P^{W} is limited by the sum of wind forecasts P^{Wf} and forecast error δ, and the imbalance quantities must be non-negative:

$$P_t^{\text{DA}} + P_t^{\text{BM}} = P_t^{\text{W}} \tag{4.1c}$$

$$P_t^{\text{W}} \leq P_t^{\text{Wf}} + \delta_t \tag{4.1d}$$

$$P_t^{\text{BM}} = P_t^{\text{BM+}} - P_t^{\text{BM-}} \tag{4.1e}$$

$$P_t^{\text{BM+}}, P_t^{\text{BM-}} \geq 0 \tag{4.1f}$$

where free wind curtailment is assumed. The modeling of the forecast error δ will be elaborated in the following section.

Lower-level Formulation

The Lower-Level (LL) represents the day-ahead market clearing and the objective is to maximize the social welfare, as expressed by

$$\max_{\alpha_t^{\mathrm{DA}}, P_t^{\mathrm{DA}}} \sum_{t=1}^{T} \sum_{m=1}^{N^{\mathrm{m}}} \lambda_{t,m}^{\mathrm{DA,D}} P_{t,m}^{\mathrm{DA,D}} - \sum_{t=1}^{T} \alpha_t^{\mathrm{DA}} P_t^{\mathrm{DA}} - \sum_{t=1}^{T} \sum_{j=1}^{N^{\mathrm{j}}} \sum_{b=1}^{N^{\mathrm{b}}} \lambda_{t,j,b}^{\mathrm{DA,O}} P_{t,j,b}^{\mathrm{DA,O}} \quad (4.2a)$$

where α^{DA} and P^{DA} are the day-ahead offering price and the dispatched DA offering quantity of the wind aggregator. Variables $\lambda_{t,j,b}^{\mathrm{DA,O}}$ and $P_{t,j,b}^{\mathrm{DA,O}}$ are the offering price and the day-ahead dispatched offering quantity for block b of rival producer j at time t, while $\lambda_{t,m}^{\mathrm{DA,D}}$ and $P_{t,m}^{\mathrm{DA,D}}$ are the bidding price and the dispatched day-ahead bidding quantity for bidding block m of the consumer. The number of consumers' demand bidding blocks, the number of rival producers and the number of the rival producers' offering blocks are indicated by N^{m}, N^{j} and N^{b}, respectively. As the rival producers' offering quantities and prices for the market are hardly available, we consider that they are non-strategic producers with offering price-quantity pairs constructed based on their corresponding marginal costs and available capacities.

The LL problem is subject to two types of constraints: 1) the upper and lower limits on the offering quantities of the producers and the bidding quantities of the demands; and 2) the power balance constraint which enforces that the summations of the production quantities are equal to the load dispatch quantities for each time step, i.e.

$$0 \leq P_t^{\mathrm{DA}} \leq Q_t^{\mathrm{DA}} \quad : \ \mu_t^{\mathrm{DAmin}}, \ \mu_t^{\mathrm{DAmax}} \quad (4.2b)$$

$$0 \leq P_{t,j,b}^{\mathrm{DA,O}} \leq P_{t,j,b}^{\mathrm{DA,Omax}} \quad : \ \mu_{t,j,b}^{\mathrm{DA,Omin}}, \ \mu_{t,j,b}^{\mathrm{DA,Omax}} \quad (4.2c)$$

$$0 \leq P_{t,m}^{\mathrm{DA,D}} \leq P_{t,m}^{\mathrm{DA,Dmax}} \quad : \ \mu_{t,m}^{\mathrm{DA,Dmin}}, \ \mu_{t,m}^{\mathrm{DA,Dmax}} \quad (4.2d)$$

$$\sum_{m=1}^{N^{\mathrm{m}}} P_{t,m}^{\mathrm{DA,D}} - \sum_{j=1}^{N^{\mathrm{j}}} \sum_{b=1}^{N^{\mathrm{b}}} P_{t,j,b}^{\mathrm{DA,O}} - P_t^{\mathrm{DA}} = 0 \quad : \ \lambda_t^{\mathrm{DA}} \quad (4.2e)$$

The dual variables are denoted following a colon after each corresponding equation.

4.3.2 Linearization of the Bidding Model

As the linearization process is similar to what has been presented in Chapter 3, a brief version is presented here for the completeness of the mathematical formulations. For more details of the reformulation and linearization process, please refer to Chapter 3. For readers who have read Chapter 3, it is suggested to skip the linearization process and directly jump to the resulting linearized MILP model (4.6).

The bi-level model is formulated as a mathematical program with equilibrium constraints (Mathematical Program with Equilibrium Constraints (MPEC)), by replacing the lower level problem with the first-order KKT conditions and integrating them into the upper level problem.

The stationary and the equality constraints are:

$$\sum_{m=1}^{N^{\mathrm{m}}} P_{t,m}^{\mathrm{DA,D}} - \sum_{j=1}^{N^{\mathrm{j}}} \sum_{b=1}^{N^{\mathrm{b}}} P_{t,j,b}^{\mathrm{DA,O}} - P_t^{\mathrm{DA}} = 0 \tag{4.3a}$$

$$\alpha_t^{\mathrm{DA}} - \lambda_t^{\mathrm{DA}} + \mu_t^{\mathrm{DAmax}} - \mu_t^{\mathrm{DAmin}} = 0 \tag{4.3b}$$

$$\lambda_{t,j,b}^{\mathrm{DA,O}} - \lambda_t^{\mathrm{DA}} + \mu_{t,j,b}^{\mathrm{DA,Omax}} - \mu_{t,j,b}^{\mathrm{DA,Omin}} = 0 \tag{4.3c}$$

$$-\lambda_{t,m}^{\mathrm{DA,D}} + \lambda_t^{\mathrm{DA}} + \mu_{t,m}^{\mathrm{DA,Dmax}} - \mu_{t,m}^{\mathrm{DA,Dmin}} = 0 \tag{4.3d}$$

$$0 \leq P_t^{\mathrm{DA}} \perp \mu_t^{\mathrm{DAmin}} \geq 0 \tag{4.3e}$$

$$0 \leq P_{t,j,b}^{\mathrm{DA,O}} \perp \mu_{t,j,b}^{\mathrm{DA,Omin}} \geq 0 \tag{4.3f}$$

$$0 \leq P_{t,m}^{\mathrm{DA,D}} \perp \mu_{t,m}^{\mathrm{DA,Dmin}} \geq 0 \tag{4.3g}$$

$$0 \leq (Q_t^{\mathrm{DA}} - P_t^{\mathrm{DA}}) \perp \mu_t^{\mathrm{DAmax}} \geq 0 \tag{4.3h}$$

$$0 \leq (P_{t,j,b}^{\mathrm{DA,Omax}} - P_{t,j,b}^{\mathrm{DA,O}}) \perp \mu_{t,j,b}^{\mathrm{DA,Omax}} \geq 0 \tag{4.3i}$$

$$0 \leq (P_{t,m}^{\mathrm{DA,Dmax}} - P_{t,m}^{\mathrm{DA,D}}) \perp \mu_{t,m}^{\mathrm{DA,Dmax}} \geq 0 \tag{4.3j}$$

Note that the resulting MPEC is a non-linear and non-convex optimization problem. On one hand, the non-linearity of the MPEC is caused by the complementarity conditions (4.3e)-(4.3j). On the other hand, it is due to the non-linear part $\lambda^{\mathrm{DA}} P^{\mathrm{DA}}$ in the objective function (4.1a). To reduce the problem complexity, in the following the problem is transformed into a MILP.

First of all, complementarity conditions (4.3e)-(4.3j) are linearized using the "Big-M" method [53, 98]. For example, equation (4.3e) is reformulated as:

$$0 \leq P_t^{\mathrm{DA}} \quad \leq M_1 z_t^{\mathrm{DA}} \tag{4.4a}$$

$$0 \leq \mu_t^{\mathrm{DAmin}} \leq M_2(1 - z_t^{\mathrm{DA}}) \tag{4.4b}$$

where $M_{1,2}$ are large enough constants and z^{DA} is a binary variable. The same method is used for linearizing (4.3f)-(4.3j). Furthermore, the objective function (4.1) is linearized by applying the strong duality theorem to the lower-level problem and using some of the KKT conditions stated before. The non-linear part $\lambda^{\mathrm{DA}} P^{\mathrm{DA}}$ is linearized as follows:

$$\begin{aligned} Z^{\mathrm{DA}} &= \sum_{t=1}^{T} \lambda_t^{\mathrm{DA}} P_t^{\mathrm{DA}} \\ &= -\sum_{t=1}^{T} \sum_{j=1}^{N^{\mathrm{j}}} \sum_{b=1}^{N^{\mathrm{b}}} \left(\lambda_{t,j,b}^{\mathrm{DA,O}} P_{t,j,b}^{\mathrm{DA,O}} + \mu_{t,j,b}^{\mathrm{DA,Omax}} P_{t,j,b}^{\mathrm{DA,Omax}}\right) \\ &\quad + \sum_{t=1}^{T} \sum_{m=1}^{N^{\mathrm{m}}} \left(\lambda_{t,m}^{\mathrm{DA,D}} P_{t,m}^{\mathrm{DA,D}} - \mu_{t,m}^{\mathrm{DA,Dmax}} P_{t,m}^{\mathrm{DA,Dmax}}\right) \end{aligned} \tag{4.5}$$

With linearizations of the KKT complementarity conditions and the linearized form of $\sum_{t=1}^{T} \lambda^{\mathrm{DA}} P^{\mathrm{DA}}$ in (4.5), the MPEC model is converted into an MILP

model. It can be written as:

$$\begin{aligned}
\max \quad & -\sum_{t=1}^{T}\sum_{j=1}^{N^{\mathrm{j}}}\sum_{b=1}^{N^{\mathrm{b}}}\left(\lambda_{t,j,b}^{\mathrm{DA,O}}P_{t,j,b}^{\mathrm{DA,O}}+\mu_{t,j,b}^{\mathrm{DA,Omax}}P_{t,j,b}^{\mathrm{DA,Omax}}\right) \\
& +\sum_{t=1}^{T}\sum_{m=1}^{N^{\mathrm{m}}}\left(\lambda_{t,m}^{\mathrm{DA,D}}P_{t,m}^{\mathrm{DA,D}}-\mu_{t,m}^{\mathrm{DA,Dmax}}P_{t,m}^{\mathrm{DA,Dmax}}\right) \\
& +\sum_{t=1}^{T}pr_{t}^{\mathrm{BM}}P_{t}^{\mathrm{BM}} && \text{(4.6a)} \\
\text{s.t.} \quad & \text{(4.1b)-(4.1f)} && \text{(4.6b)} \\
& \text{KKT conditions (4.3a)-(4.3d)} && \text{(4.6c)} \\
& \text{Linearized form of equations (4.3e)-(4.3j)} && \text{(4.6d)}
\end{aligned}$$

4.3.3 Modelling of Wind Uncertainty

In this section, we will discuss how to use DRO to model the wind uncertainty. We first rewrite (4.6) in following compact form:

$$\begin{aligned}
& \min \ \left\{\boldsymbol{o}^{\mathsf{T}}\boldsymbol{x}+\phi(\boldsymbol{x},\boldsymbol{\delta})\right\} \\
& \text{s.t.} \quad \boldsymbol{x}\in\boldsymbol{X_f}
\end{aligned} \tag{4.7}$$

where $\boldsymbol{o}^{\mathsf{T}}\boldsymbol{x}$ is the first-stage cost and the adaptive second-stage cost is expressed as $\phi(\boldsymbol{x},\boldsymbol{\delta})$, i.e. a function of the first-stage decision matrix $\boldsymbol{x}=\{\boldsymbol{\alpha}^{\mathrm{DA}},\boldsymbol{Q}^{\mathrm{DA}},\boldsymbol{P}^{\mathrm{DA}},\boldsymbol{P}^{\mathrm{DA,D}},\boldsymbol{P}^{\mathrm{DA,O}},\boldsymbol{\lambda}^{\mathrm{DA}},\boldsymbol{\mu}^{\mathrm{DAmin}},\boldsymbol{\mu}^{\mathrm{DAmax}},\boldsymbol{\mu}^{\mathrm{DA,Omin}},\boldsymbol{\mu}^{\mathrm{DA,Omax}},\boldsymbol{\mu}^{\mathrm{DA,Dmin}},\boldsymbol{\mu}^{\mathrm{DA,Dmax}}\}$ and the realizations of the random vector $\boldsymbol{\delta}$. The set $\boldsymbol{X_f}$ represents the feasibility region of the first-stage decision $\boldsymbol{x}$ defined by equations (4.6b)-(4.6d).

SO Formulation

In traditional SO, random vector $\boldsymbol{\delta}$ is described by a set of scenarios that are drawn from a known distribution I and the objective is to optimize the first-stage cost plus the expectation over the optimal second-stage cost $H(\boldsymbol{x},\boldsymbol{\delta})$:

$$\phi(\boldsymbol{x},\boldsymbol{\delta})=\mathbb{E}_I\left\{H(\boldsymbol{x},\boldsymbol{\delta})\right\} \tag{4.8}$$

where $H(\boldsymbol{x}, \boldsymbol{\delta})$ is expressed as:

$$H(\boldsymbol{x}, \boldsymbol{\delta}) = \min \left\{ -\sum_{t=1}^{T} pr_t^{\text{BM}} P_t^{\text{BM}} \right\} \quad \text{s.t.} \quad \text{Constraints (4.1c)-(4.1f)} \tag{4.9}$$

RO Formulation

In RO, $\boldsymbol{\delta}$ is described by an uncertainty set U, and the objective is to optimize the first-stage cost plus the worst-case optimal second-stage cost, i.e.,

$$\phi(\boldsymbol{x}, \boldsymbol{\delta}) = \sup_{\delta \in U} \left\{ H(\boldsymbol{x}, \boldsymbol{\delta}) \right\} \tag{4.10}$$

DRO Formulation

DRO combines the characteristics of both RO and SO, i.e. in DRO, the probability distribution I of the random vector $\boldsymbol{\delta}$ is uncertain and it belongs to an ambiguity set F which will be explained later. The second-stage cost is reformulated as the worst-case expectation over a family of distributions:

$$\phi(\boldsymbol{x}, \boldsymbol{\delta}) = \sup_{I \in F} \mathbb{E}_I \left\{ H(\boldsymbol{x}, \boldsymbol{\delta}) \right\} \tag{4.11}$$

Thus, the second-stage problem based on DRO can be written as:

$$\phi(\boldsymbol{x}, \boldsymbol{\delta}) = \min \sup_{I \in F} \mathbb{E}_I \left\{ -\sum_{t=1}^{T} pr_t^{\text{BM}} P_t^{\text{BM}} \right\} \quad \text{s.t.} \quad \text{Constraints (4.1c)-(4.1f)} \tag{4.12}$$

Modelling Ambiguity Set As mentioned, the Probability Distribution Function (PDF) of $\boldsymbol{\delta}$, namely I, is uncertain and it belongs to an ambiguity set F, which represents a family of distributions sharing some common statistical features (e.g. expectation, deviation, variance, etc.). Similar to the classical RO problems, the tractability of a DRO problem is also dependent on the choice of the ambiguity set. In this work, we focus on a standard ambiguity set where the family of distributions are characterized by a group of second-order cone

representable constraints and a linear support set. This is because the robust counterpart corresponding to a second-order cone uncertainty set is at most a Second-order Cone Program (SOCP), which can be solved by off-the-shelf solvers [88]. The ambiguity set modelled in this work is:

$$F = \left\{ I: \begin{array}{l} \mathbb{E}_I[\delta_t] = 0 \\ \mathbb{E}_I[|\delta_t|] \leq \gamma_{1,t} \\ \mathbb{E}_I[(\delta_t)^2] \leq \gamma_{2,t} \\ Pr(\boldsymbol{\delta} \in \mathscr{W}) = 1 \end{array} \right\}$$

The first line ensures that the expectation of δ_t for each time point t is zero, while the second and third lines guarantee that the expected absolute deviation and variance are limited to $\gamma_{1,t}$ and $\gamma_{2,t}$, respectively. The last equation implies that all realizations of $\boldsymbol{\delta}$ belong to a support set $\mathscr{W}$ defined as:

$$\mathscr{W} = \{\delta_t^{\min} \leq \delta_t \leq \delta_t^{\max}\}$$

where $\delta_t^{\min}$ and $\delta_t^{\max}$ indicate the lower and upper bounds of δ_t. As the expectation terms in the second and third constraints are difficult to compute, based on the lifting theorem proposed in [99], a set of auxiliary random variables $\boldsymbol{u} = \{\boldsymbol{u_1}, \boldsymbol{u_2}\}$ is introduced to set bounds and achieve an ambiguity set that has only linear expectation constraints, namely the lifted ambiguity set G. The lifted ambiguity set and the second-order cone representable extended uncertainty set are defined as:

$$G = \left\{ J: \begin{array}{l} \mathbb{E}_J[\delta_t] = 0 \\ \mathbb{E}_J[u_{1,t}] \leq \gamma_{1,t} \\ \mathbb{E}_J[u_{2,t}] \leq \gamma_{2,t} \\ Pr\{(\boldsymbol{\delta}, \boldsymbol{u}) \in \overline{\mathscr{W}}\} = 1 \end{array} \right\}$$

$$\overline{\mathscr{W}} = \left\{ \begin{array}{c} \delta_t^{\min} \leq \delta_t \leq \delta_t^{\max} \\ |\delta_t| \leq u_{1,t} \\ (\delta_t)^2 \leq u_{2,t} \\ u_{1,t} \leq u_{1,t}^{\max} = \max\{\delta_t^{\max}, -\delta_t^{\min}\} \\ u_{2,t} \leq u_{2,t}^{\max} = \max\{(\delta_t^{\max})^2, (\delta_t^{\min})^2\} \end{array} \right\}$$

where the second and third lines in $\overline{\mathscr{W}}$ set u_1 and u_2 as upper bounds for $|\delta|$ and $(\delta)^2$, so that the second and third constraints in F and in G are equivalent. To make the support set less conservative, the fourth and fifth lines in $\overline{\mathscr{W}}$ limit u_1 and u_2 to the worst-case [93], which can be calculated using historical data.

With constraints on random vectors $\boldsymbol{\delta}$ and $\boldsymbol{u}$ in the lifted ambiguity set G, the inner maximization problem of (4.12) can be reformulated as:

$$\sup_{J \in G} \mathbb{E}_J \left\{ -\sum_{t=1}^{T} pr_t^{\text{BM}} P_t^{\text{BM}} \right\}$$

$$= \sup \int_{\overline{\mathscr{W}}} -\sum_{t=1}^{T} pr_t^{\text{BM}} P_t^{\text{BM}} \, df(\boldsymbol{\delta}, \boldsymbol{u}) \tag{4.13a}$$

$$\text{s.t.} \quad \int_{\overline{\mathscr{W}}} \boldsymbol{\delta} df(\boldsymbol{\delta}, \boldsymbol{u}) = 0 \qquad : \boldsymbol{\rho} \tag{4.13b}$$

$$\int_{\overline{\mathscr{W}}} \boldsymbol{u} df(\boldsymbol{\delta}, \boldsymbol{u}) \leq \boldsymbol{\gamma} \qquad : \boldsymbol{\beta} \tag{4.13c}$$

$$\int_{\overline{\mathscr{W}}} df(\boldsymbol{\delta}, \boldsymbol{u}) \;\; = \mathbf{1} \qquad : \boldsymbol{\eta} \tag{4.13d}$$

$$f(\boldsymbol{\delta}, \boldsymbol{u}) \geq 0, \qquad \forall (\boldsymbol{\delta}, \boldsymbol{u}) \in \overline{\mathscr{W}} \tag{4.13e}$$

$$\text{Constraints (4.1c)-(4.1f)} \tag{4.13f}$$

where $f(\boldsymbol{\delta}, \boldsymbol{u})$ is the probability density function and the dual variables are denoted following a colon after each corresponding equation. Equations (4.13b)-(4.13d) are equivalent to the four lines in set G. Problem (4.13) is known as a Continuous Linear Programming (CLP) problem. Based on the Lagrange duality theory for CLP problems presented in [100] and [101], the corresponding Lagrange dual function of (4.13a)-(4.13e) is defined as the supreme of the La-

grangian over $f(\boldsymbol{\delta}, \boldsymbol{u})$:

$$\begin{aligned} L(\boldsymbol{\delta}, \boldsymbol{u}) = \sup \; \{ & \int_{\overline{\mathscr{W}}} - \sum_{t=1}^{T} pr_t^{\mathrm{BM}} P_t^{\mathrm{BM}} df(\boldsymbol{\delta}, \boldsymbol{u}) - \rho \int_{\overline{\mathscr{W}}} \boldsymbol{\delta} df(\boldsymbol{\delta}, \boldsymbol{u}) \\ & - \boldsymbol{\eta}(\int_{\overline{\mathscr{W}}} df(\boldsymbol{\delta}, \boldsymbol{u}) - \mathbf{1}) - \boldsymbol{\beta}(\int_{\overline{\mathscr{W}}} \boldsymbol{u} df(\boldsymbol{\delta}, \boldsymbol{u}) - \boldsymbol{\gamma})\} \\ = \sup \; \{ & \int_{\overline{\mathscr{W}}} (- \sum_{t=1}^{T} pr_t^{\mathrm{BM}} P_t^{\mathrm{BM}} - \boldsymbol{\eta} - \boldsymbol{\rho}\boldsymbol{\delta} - \boldsymbol{\beta}\boldsymbol{u}) df(\boldsymbol{\delta}, \boldsymbol{u}) \\ & + \boldsymbol{\eta} + \boldsymbol{\gamma}\boldsymbol{\beta}\} \end{aligned} \tag{4.14}$$

Depending on the value of $\boldsymbol{\delta}$ and $\boldsymbol{u}$, this can be:

$$L(\boldsymbol{\delta}, \boldsymbol{u}) = \begin{cases} \boldsymbol{\eta} + \boldsymbol{\gamma}\boldsymbol{\beta} & \text{if } \; \boldsymbol{\eta} + \boldsymbol{\rho}\boldsymbol{\delta} + \boldsymbol{\beta}\boldsymbol{u} \geq - \sum_{t=1}^{T} pr_t^{\mathrm{BM}} P_t^{\mathrm{BM}}, \\ +\infty & \text{otherwise.} \end{cases}$$

Thus, the Lagrange dual problem is defined as

$$\begin{aligned} \min \quad & \boldsymbol{\eta} + \boldsymbol{\gamma}\boldsymbol{\beta} \\ \text{s.t.} \quad & \boldsymbol{\beta} \geq 0 \\ & \boldsymbol{\eta} + \boldsymbol{\rho}\boldsymbol{\delta} + \boldsymbol{\beta}\boldsymbol{u} \geq - \sum_{t=1}^{T} pr_t^{\mathrm{BM}} P_t^{\mathrm{BM}} \\ & \text{Constraints (4.1c)-(4.1f)} \end{aligned} \tag{4.15}$$

Thus, combining (4.15) with the first-stage constraints and objective, the overall two-stage maximization problem is:

$$\max \ \boldsymbol{Z}^{\text{DA}} - \boldsymbol{\eta} - \boldsymbol{\gamma}\boldsymbol{\beta} \tag{4.16a}$$

$$\text{s.t.} \quad \boldsymbol{\beta} \geq 0 \tag{4.16b}$$

$$\boldsymbol{\eta} + \boldsymbol{\rho}\boldsymbol{\delta} + \boldsymbol{\beta}\boldsymbol{u} \geq -\sum_{t=1}^{T} pr_t^{\text{BM}} P_t^{\text{BM}} \tag{4.16c}$$

$$\text{Constraints (4.1b)-(4.1f)} \tag{4.16d}$$

$$\text{Constraints (4.3a)-(4.3d)} \tag{4.16e}$$

$$\text{Linearized form of equations (4.3e)-(4.3j)} \tag{4.16f}$$

However, constraints (4.16c) and (4.16d) are in general intractable, as it requires solving recourse problems over all outcomes of uncertain parameters [102]. Thus, an appropriate decision rule should be applied to solve the problem via approximation.

Approximate Reformulation using Enhanced LDR We first approximate the second-stage decision $\{P^{\text{BM+}}, P^{\text{BM-}}\}$ by using the linear affine functions of the random vector $\boldsymbol{\delta}$ and auxiliary random vector $\boldsymbol{u}$:

$$\begin{aligned} P_t^{\text{BM+}} &= k_t^0 + k_t^1\delta_t + k_t^2 u_{1,t} + k_t^3 u_{2,t} \\ P_t^{\text{BM-}} &= l_t^0 + l_t^1\delta_t + l_t^2 u_{1,t} + l_t^3 u_{2,t} \end{aligned} \tag{4.17}$$

Substituting (4.17) into constraints (4.16c)-(4.16d), the following problem results

$$\max \quad \boldsymbol{Z}^{\text{DA}} - \boldsymbol{\eta} - \boldsymbol{\gamma}\boldsymbol{\beta} \tag{4.18a}$$

$$\text{s.t.} \quad \boldsymbol{\beta} \geq 0 \tag{4.18b}$$

$$\begin{aligned}\boldsymbol{\eta} + \boldsymbol{\rho}\boldsymbol{\delta} + \boldsymbol{\beta}\boldsymbol{u} \geq \sum_{t=1}^{T} & pr_t^{\text{BM-}}(l_t^0 + l_t^1\delta_t + l_t^2 u_{1,t} + l_t^3 u_{2,t}) \\ & - pr_t^{\text{BM+}}(k_t^0 + k_t^1\delta_t + k_t^2 u_{1,t} + k_t^3 u_{2,t})\end{aligned} \tag{4.18c}$$

$$\begin{aligned}P_t^{\text{DA}} + (k_t^0 + k_t^1\delta_t + k_t^2 u_{1,t} + k_t^3 u_{2,t}) \\ - (l_t^0 + l_t^1\delta_t + l_t^2 u_{1,t} + l_t^3 u_{2,t}) = P_t^{\text{W}}\end{aligned} \tag{4.18d}$$

$$-P_t^{\text{W}} \geq -P_t^{\text{Wf}} - \delta_t \tag{4.18e}$$

$$k_t^0 + k_t^1\delta_t + k_t^2 u_{1,t} + k_t^3 u_{2,t} \geq 0 \tag{4.18f}$$

$$l_t^0 + l_t^1\delta_t + l_t^2 u_{1,t} + l_t^3 u_{2,t} \quad \geq 0 \tag{4.18g}$$

Constraints (4.1b), (4.3a)-(4.3d) (4.18h)

Linearized form of equations (4.3e)-(4.3j) (4.18i)

Constraints (4.18d)-(4.18g) correspond to (4.16d) in the considered problem which are on the other hand equivalent to (4.1c)-(4.1f). Instead of iterating over all possible random variable realizations, (4.18) minimizes the objective by optimizing the coefficients of the enhanced LDR, i.e. $k^{0\sim3}$ and $l^{0\sim3}$. As constraints (4.18c)-(4.18g) include uncertainty variables $\boldsymbol{\delta}$ and $\boldsymbol{u}$ that are restricted by the uncertainty set $\overline{\mathscr{W}}$, they should be reformulated considering the constraints in $\overline{\mathscr{W}}$. For example, by moving all terms to the left side, constraint (4.18c) can be written as the following worst-case optimization problem that is subject to the constraints in $\overline{\mathscr{W}}$:

$$\begin{aligned}\min_{J\in G} \{\boldsymbol{\eta} + \boldsymbol{\rho}\boldsymbol{\delta} + \boldsymbol{\beta}\boldsymbol{u} - [\sum_{t=1}^{T} & (pr_t^{\text{BM-}} l_t^0 - pr_t^{\text{BM+}} k_t^0) \\ & + (pr_t^{\text{BM-}} l_t^1 - pr_t^{\text{BM+}} k_t^1)\delta_t + (pr_t^{\text{BM-}} l_t^2 - pr_t^{\text{BM+}} k_t^2) u_{1,t} \\ & + (pr_t^{\text{BM-}} l_t^3 - pr_t^{\text{BM+}} k_t^3) u_{2,t}]\} \geq 0\end{aligned} \tag{4.19}$$

$$
\begin{aligned}
\text{s.t.} \quad \left\| -\boldsymbol{\delta} + \boldsymbol{\delta}^{\min} + 1 \right\| &\leq \boldsymbol{\delta} - \boldsymbol{\delta}^{\min} + 1 && : \boldsymbol{\pi^1}, \boldsymbol{\zeta^1} \\
\left\| \boldsymbol{\delta} - \boldsymbol{\delta}^{\max} + 1 \right\| &\leq -\boldsymbol{\delta} + \boldsymbol{\delta}^{\max} + 1 && : \boldsymbol{\pi^2}, \boldsymbol{\zeta^2} \\
\left\| \boldsymbol{\delta} - \boldsymbol{u_1} + 1 \right\| &\leq -\boldsymbol{\delta} + \boldsymbol{u_1} + 1 && : \boldsymbol{\pi^3}, \boldsymbol{\zeta^3} \\
\left\| 0 \right\| &\leq \boldsymbol{u_1} && : \boldsymbol{\pi^4}, \boldsymbol{\zeta^4} \\
\left\| \boldsymbol{u_1} \right\| &\leq \boldsymbol{u_1^{\max}} && : \boldsymbol{\pi^5}, \boldsymbol{\zeta^5} \\
\left\| \begin{pmatrix} \frac{1-\boldsymbol{u_2}}{2} \\ \boldsymbol{\delta} \end{pmatrix} \right\| &\leq \frac{\boldsymbol{u_2} + 1}{2} && : \boldsymbol{\pi^6}, \boldsymbol{\zeta^6} \\
\left\| \boldsymbol{u_2} \right\| &\leq \boldsymbol{u_2^{\max}} && : \boldsymbol{\pi^7}, \boldsymbol{\zeta^7}
\end{aligned}
\tag{4.20}
$$

where $\boldsymbol{\pi^{1\sim7}}$ and $\boldsymbol{\zeta^{1\sim7}}$ are the corresponding dual variables.

We first rewrite the objective function in (4.19) in a compact form $g^{\text{primal}}(\boldsymbol{\delta}, \boldsymbol{u})$, then the following equivalences are satisfied.

$$
\begin{aligned}
& \min \left\{ g^{\text{primal}}(\boldsymbol{\delta}, \boldsymbol{u}) \right\} && \geq 0 && (4.21) \\
\Leftrightarrow\ & \max \left\{ g^{\text{dual}}(\boldsymbol{\pi}, \boldsymbol{\zeta}) \right\} && \geq 0 && (4.22) \\
\Leftrightarrow\ & \exists\, \boldsymbol{\pi}, \boldsymbol{\zeta} :\ g^{\text{dual}}(\boldsymbol{\pi}, \boldsymbol{\zeta}) && \geq 0 && (4.23)
\end{aligned}
$$

where $g^{\text{dual}}(\boldsymbol{\pi}, \boldsymbol{\zeta})$ represents the dual objective function.

The first equivalence is obtained by applying the Lagrange duality theory to the primal SOCP (4.19) and (4.20) [100], [103]. As stated by the strong duality theorem, the solution to the primal (minimization) problem is always equal to the solution to the associated dual (maximization) problem. The second equivalence holds as the feasible set of the primal minimization problem is not empty [103]. Finally, to integrate (4.19) and (4.20) into (4.18), the following constraints derived using duality theory are formulated:

$$
\begin{aligned}
\boldsymbol{\eta} + \sum_{t=1}^{T} \Big[& pr_t^{\text{BM+}} k_t^0 - pr_t^{\text{BM-}} l_t^0 \\
& - \left(\delta_t^{\min 1} \pi_t^1 + \delta_t^{\min 2} \zeta_t^1 + \delta_t^{\max 1} \pi_t^2 + \delta_t^{\max 2} \zeta_t^2 \right. \\
& \left. + \pi_t^3 + \zeta_t^3 + u_{1,t}^{\max} \zeta_t^5 + [1/2, 0] \pi_t^6 + \frac{\zeta_t^6}{2} + u_{2,t}^{\max} \zeta_t^7 \right) \Big] \geq 0
\end{aligned}
\tag{4.24a}
$$

$$-\pi_t^1 + \zeta_t^1 + \pi_t^2 - \zeta_t^2 + \pi_t^3 - \zeta_t^3 + [0,1]\pi_t^6 = \rho_t + pr_t^{\text{BM+}} k_t^1 - pr_t^{\text{BM-}} l_t^1 \tag{4.24b}$$

$$-\pi_t^3 + \zeta_t^3 + \zeta_t^4 + \pi_t^5 = \beta_t^1 + pr^{\text{BM+}} k_t^2 - pr^{\text{BM-}} l_t^2 \tag{4.24c}$$

$$[-1/2,0]\pi_t^6 + \frac{\zeta_t^6}{2} + \pi_t^7 = \beta_t^2 + pr^{\text{BM+}} k_t^3 - pr^{\text{BM-}} l_t^3 \tag{4.24d}$$

$$\|\pi_t^n\| \leq \zeta_t^n,\ 0 \leq \zeta_t^n,\ n = 1,2,...,7 \tag{4.24e}$$

Constraint (4.18d)-(4.18g) can be rewritten following the similar process as that for constraint (4.18c). As (4.18d)-(4.18e) are equivalent to

$$-P_t^{\text{DA}} - (k_t^0 + k_t^1\delta_t + k_t^2 u_{1,t} + k_t^3 u_{2,t}) + (l_t^0 + l_t^1\delta_t + l_t^2 u_{1,t} + l_t^3 u_{2,t}) \geq -P_t^{\text{Wf}} - \delta_t \tag{4.25}$$

and can be reformulated as:

$$-P_t^{\text{DA}} - k_t^0 + l_t^0 + P_t^{\text{Wf}} - (\delta_t^{\min 1}\pi_t^{a1} + \delta_t^{\min 2}\zeta_t^{a1} + \delta_t^{\max 1}\pi_t^{a2} + \delta_t^{\max 2}\zeta_t^{a2} + \pi_t^{a3} + \zeta_t^{a3} + u_{1,t}^{\max}\zeta_t^{a5} + [1/2,0]\pi_t^{a6} + \frac{\zeta_t^{a6}}{2} + u_{2,t}^{\max}\zeta_t^{a7})] \geq 0 \tag{4.26a}$$

$$-\pi_t^{a1} + \zeta_t^{a1} + \pi_t^{a2} - \zeta_t^{a2} + \pi_t^{a3} - \zeta_t^{a3} + [0,1]\pi_t^{a6} = 1 - k_t^1 + l_t^1 \tag{4.26b}$$

$$-\pi_t^{a3} + \zeta_t^{a3} + \zeta_t^{a4} + \pi_t^{a5} = -k_t^2 + l_t^2 \tag{4.26c}$$

$$[-1/2,0]\pi_t^{a6} + \frac{\zeta_t^{a6}}{2} + \pi_t^{a7} = -k_t^3 + l_t^3 \tag{4.26d}$$

$$\|\pi_t^{an}\| \leq \zeta_t^{an},\ 0 \leq \zeta_t^{an},\ n = 1,2,...,7 \tag{4.26e}$$

Constraints (4.18f) is reformulated as

$$k_t^0 - (\delta_t^{\min 1}\pi_t^{b1} + \delta_t^{\min 2}\zeta_t^{b1} + \delta_t^{\max 1}\pi_t^{b2} + \delta_t^{\max 2}\zeta_t^{b2} + \pi_t^{b3} + \zeta_t^{b3} + u_{1,t}^{\max}\zeta_t^{b5} + [1/2,0]\pi_t^{b6} + \frac{\zeta_t^{b6}}{2} + u_{2,t}^{\max}\zeta_t^{b7})] \geq 0 \tag{4.27a}$$

$$-\pi_t^{b1} + \zeta_t^{b1} + \pi_t^{b2} - \zeta_t^{b2} + \pi_t^{b3} - \zeta_t^{b3} + [0,1]\pi_t^{b6} = k_t^1 \tag{4.27b}$$

$$-\pi_t^{b3} + \zeta_t^{b3} + \zeta_t^{b4} + \pi_t^{b5} = k_t^2 \tag{4.27c}$$

$$[-1/2,0]\pi_t^{b6} + \frac{\zeta_t^{b6}}{2} + \pi_t^{b7} = k_t^3 \tag{4.27d}$$

$$\|\pi_t^{bn}\| \leq \zeta_t^{bn},\ 0 \leq \zeta_t^{bn},\ n = 1,2,...,7 \tag{4.27e}$$

Constraints (4.18g) is reformulated as

$$l_t^0 - (\delta_t^{\min 1}\pi_t^{c1} + \delta_t^{\min 2}\zeta_t^{c1} + \delta_t^{\max 1}\pi_t^{c2} + \delta_t^{\max 2}\zeta_t^{c2} + \pi_t^{c3} + \zeta_t^{c3} + u_{1,t}^{\max}\zeta_t^{c5} + [1/2,0]\pi_t^{c6} + \frac{\zeta_t^{c6}}{2} + u_{2,t}^{\max}\zeta_t^{c7})] \geq 0 \tag{4.28a}$$

$$-\pi_t^{c1} + \zeta_t^{c1} + \pi_t^{c2} - \zeta_t^{c2} + \pi_t^{c3} - \zeta_t^{c3} + [0,1]\pi_t^{c6} = l_t^1 \tag{4.28b}$$

$$-\pi_t^{c3} + \zeta_t^{c3} + \zeta_t^{c4} + \pi_t^{c5} = l_t^2 \tag{4.28c}$$

$$[-1/2,0]\pi_t^{c6} + \frac{\zeta_t^{c6}}{2} + \pi_t^{c7} = l_t^3 \tag{4.28d}$$

$$\|\pi_t^{cn}\| \leq \zeta_t^{cn},\ 0 \leq \zeta_t^{cn},\ n = 1,2,...,7 \tag{4.28e}$$

where $\delta_t^{\min 1}$, $\delta_t^{\min 2}$, $\delta_t^{\max 1}$ and $\delta_t^{\max 2}$ in equations above are assigned to $\delta_t^{\min} + 1$, $-\delta_t^{\min} + 1$, $-\delta_t^{\max} + 1$ and $\delta_t^{\max} + 1$, respectively.

Thus, the final optimization problem is:

$$\max\ Z^{\mathrm{DA}} - \boldsymbol{\eta} - \boldsymbol{\gamma\beta}$$

s.t. $\boldsymbol{\beta} \geq 0$

Constraints (4.24a)-(4.28e)

Constraints (4.1b), (4.3a)-(4.3d)

Linearized form of equations (4.3e)-(4.3j)

4.4 Case Study

4.4.1 Input Data

The proposed methodology is applied to a modified Swiss system, with details of the system given in Chapter 3. Same as the definition provided in Chap-

ter 3, the market share of the wind aggregator is defined as the ratio of the total generation of the aggregator to the total system demand over the simulation horizon. Furthermore, the strategic aggregator is introduced to the market to replace the existing capacities in the system. In other words, the market share of other non-strategic units decreases as the market share of the aggregator increases so as to keep the same total supply within the system. Considering the time consumed by running the SO model, the simulation horizon is set as 24 hours with an hourly resolution. However, it is worth mentioning that as the optimization problem is time-decoupled, theoretically the computational burdens for running the DRO, SO and the RO models for each single step are not influenced by the expansion of the time horizon. All simulations are conducted on a Windows 10 machine with Intel(R) Xeon(R) Gold 6154 CPU @ 3.00 GHz and 479 GB memory. All optimization models are established by Yalmip [38] in MATLAB and solved with Gurobi.

In the Baseline scenario, the market share of the aggregator is set as 10% , while the samples of the nominal wind output forecast errors are generated using the random number generation function in Matlab under Gaussian distribution with zero mean and 10% standard deviation. The wind forecast error is calculated as the product of the nominal wind forecast error and the capacity of the wind aggregator. 1000 samples of wind output forecast error δ are generated for each time step, and we assume that the upper and lower bounds of δ used to construct the uncertainty set for DRO, the empirical mean, the mean absolute deviation and standard deviation used to build the ambiguity set for DRO are calculated based on the sample data.

4.4.2 Results

In this section, we first validate the effectiveness of the LDR applied by the DRO model by comparing the LDR approximation of the second-stage decisions with the fitting curves of the second-stage decisions obtained by simulating the SO model under the same simulation assumptions. Then we conduct sensitivity analyses to investigate the impacts of wind aggregator's market shares and the wind output forecast errors' standard deviations. In the end, the performance of the DRO model is compared to that of the DO, RO and SO models

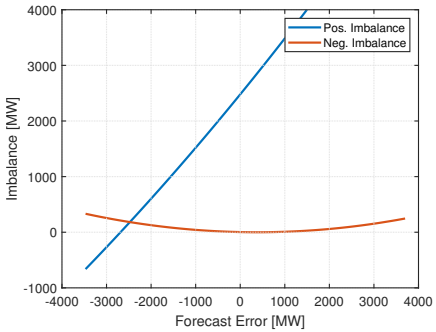

Figure 4.1: Approximation of the optimal second-stage decisions, i.e. positive and negative imbalances, using the enhanced linear decision rule applied by the distributionally robust optimization model.

from the perspective of the computational time, the expected and the worst-case out-of-sample results.

Enhanced linear decision rule approximation

In this section, the performance of approximating the second-stage decisions (i.e. positive and negative imbalance quantities) using the enhanced linear decision rule defined by equation (4.17) is evaluated. To do so, we compare the results of running both the DRO and SO models assuming 10% wind aggregator market share with forecast errors generated under Gaussian distribution with zero mean and 0.25 standard deviation. Note that the SO results are selected to serve as benchmark results as SO has complete information of the uncertainty set, it is without doubt that the resulting optimal second-stage decisions of SO are superior to that of RO and DRO. Moreover, 200 scenarios are considered by running the SO model due to the computational time consumed by SO, more about this will be discussed in the last part of the results section.

Figure 4.1 shows the results of DRO by applying the LDR for an example hour. It can be seen that the positive imbalances are a lot higher than the negative imbalances, even in the case when the forecast error is slightly below zero. This result corresponds to the fact that the proposed DRO bidding strategy is in general risk-averse, as it optimizes the result under the worst-case expectation over the uncertain distributions. Moreover, as the negative imbalance price (i.e. 144 CHF/MWh for the example hour) is in general much higher than the

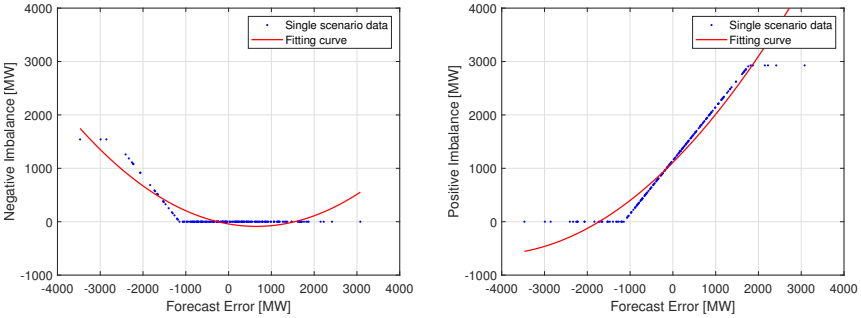

(a) Negative imbalances **(b)** Positive imbalances

Figure 4.2: Approximation of the optimal second-stage decisions, i.e. positive and negative imbalances, using the results of stochastic optimization.

positive imbalance price (i.e. 10 CHF/MWh for the example hour), the wind aggregator will always bid lower in the DAM so as to avoid high negative imbalance costs at real-time.

Figure 4.2 shows the optimal second-stage decisions of SO and overlying them with the corresponding second-degree polynomial curves fitting to determine the relationship of the optimal second-stage decisions and the simulated forecast errors. Comparing Fig. 4.1 and Fig. 4.2, it can be observed that the enhanced LDR provides a good approximation as the approximation curves of DRO and the fitting curves of SO have very similar patterns.

Impacts of Market Share

To analyze the impacts of the market share on the trading strategies of the wind aggregator, we conduct simulations considering the aggregator's market share increases from 5% to 20% with a step of 5%, while the samples of forecast errors are generated randomly using the Gaussian distribution with zero mean and 0.1 standard deviation, which is the same as the Baseline scenario. For better illustrations, we run the SO model and the DO model[10], i.e. bidding into the market without considering the potential DA forecast errors, under the same simulation setup and use their results as the benchmark results. Fig-

[10]The DO model is built by setting the upper and lower bounds of the forecast errors in the RO model to zero.

ure 4.3 shows the resulting DA offers and the DAM prices of these three models, i.e. the DO, SO and DRO models under different market shares. Note that as mentioned before, the market share of the aggregator increases as a replacement of the capacity of other units in the system. Comparing the resulting DA offering quantities of the DO model to the corresponding DA wind generation forecasts, it can be seen that the wind aggregator exerts market power by withholding the capacity at all considered market share levels, while more market power is exercised (i.e. more outputs withheld) with the increased market share. Furthermore, when comparing the results of DO, DRO and SO, it is obvious that as the aggregator market share increases, both the SO and the DRO offering strategies become more risk-seeking and the difference between DA bidding quantities of the DRO and the SO decreases. When the aggregator market share reaches 20% (i.e. Fig. 4.3d), the offering strategies of the three considered models, i.e. DO, SO and DRO models, become identical.

The resulting profits of the DRO model considering 5% to 20% wind aggregator market shares are given in Table 4.1. It shows that the profits from the DAM increases at a rate that is lower than the market share increase. This can be explained by the fact that, as shown in Fig. 4.3, for most of the hours the market prices remain at around 65 CHF/MWh, i.e. the offering price of the assumed to be sufficient import electricity[11], and the aggregator can hardly further increase the market price using the increasing market power brought by the increasing market share. Furthermore, the BM profits slightly increase with the increasing market share, the changes in DAM and BM profits together result in a total profit that increases almost proportionally with the market share.

Effects of forecast error's variance

To investigate how the day-ahead bidding behaviors of the aggregator are influenced by the variance of the wind forecast errors, we conduct simulations using forecast errors generated under Gaussian distributions with mean zero and Standard Deviations (SDs) increased from 0.05 to 0.3 with a step of 0.05. Figure 4.4 shows the resulting aggregator's DA offering quantities and the DA

[11] The market prices are high as the considered simulation day is a day from the winter season, when the demand is relatively higher and the supply that is dominated by hydro power plants is comparatively lower than other seasons.

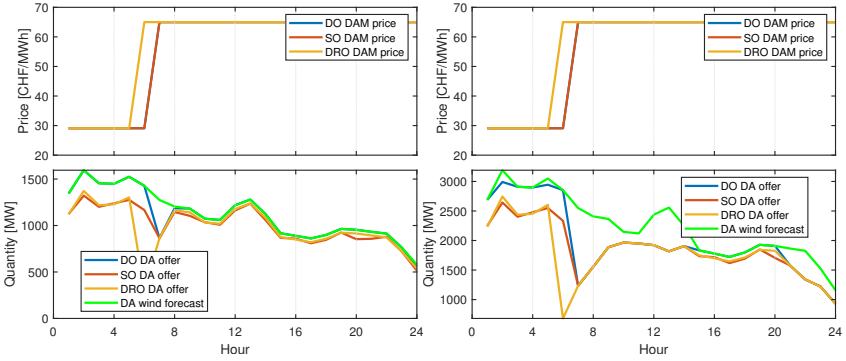

(a) Market Share - 5% **(b)** Market Share - 10%

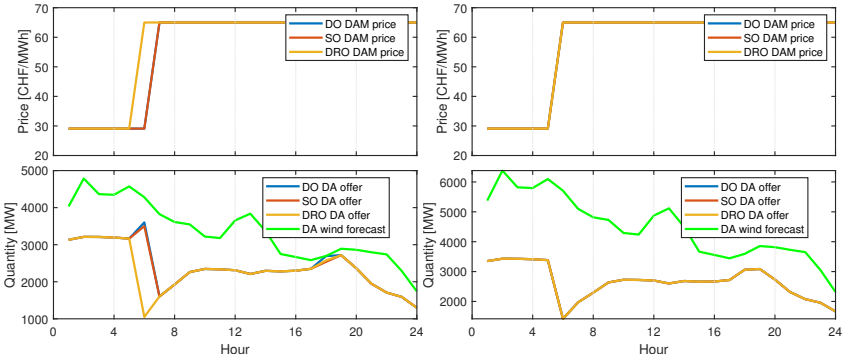

(c) Market Share - 15% **(d)** Market Share - 20%

Figure 4.3: Resulting day-ahead offers of the deterministic, stochastic and the distributionally robust optimization models assuming the aggregator market share as 5%, 10%, 15% and 20%.

Table 4.1: Market profits resulted by the distributionally robust optimization model under different aggregator market shares

Market share	DAM profit [mCHF]	BM profit [mCHF]	Total profit [mCHF]
5%	1.31	-0.21	1.10
10%	2.34 (+79%)	-0.26	2.08 (+89%)
15%	3.03 (+132%)	-0.13	2.90 (+164%)
20%	3.53 (+170%)	0.11	3.64 (+231%)

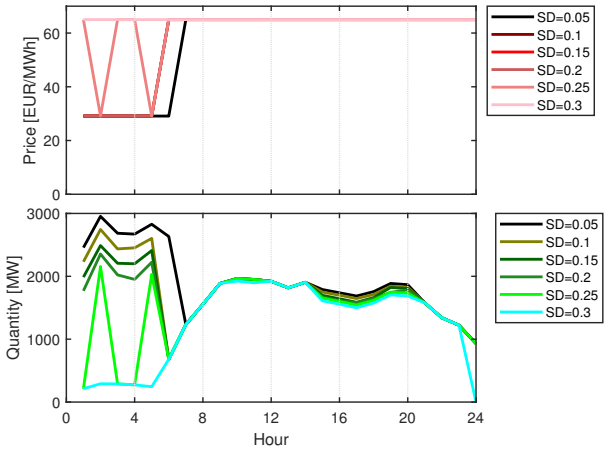

Figure 4.4: Aggregator's day-ahead offering quantities and the resulting day-ahead market prices with 10% market share and forecast errors generated under Gaussian distributions with mean zero and standard deviations ranging from 0.05 to 0.3.

market clearing prices under 10% wind aggregator market share with different values of SDs. It is obvious that as the SD increases, the aggregator offers less so as to consider the worst forecast error distribution. Moreover, the resulting DA market price increases as the aggregated market supply curve is shifting to the left with less offered by the wind aggregator.

Comparison of different optimization methods

To compare the performance of deterministic optimization, stochastic optimization, robust optimization and distributionally robust optimization in a reasonable way, we carry out the following simulations:

1. For each time step, generate scenarios using the random number generation function under Gaussian distributions with mean zero and standard deviations set as 0.05, 0.1, 0.15 and 0.2, respectively. 2000 scenarios are generated for each time step under each of the considered Gaussian distributions and are split evenly into two sets, i.e. set 1 and set 2, each contains 1000 samples for each time step. Set 1 serves as the training set to optimize the DA decisions and set 2 serves as the out-of-sample test set to validate the optimality of the methods. To investigate the performance of the methods in the case when the actual distribution of the forecast errors deviates from the simulated one, additional out-of-sample scenarios under two different distributions, namely the uniform distribution and the beta distribution, with mean zero and SDs set as 0.05, 0.1, 0.15 and 0.2 are generated. Finally, set 2 includes 9 subsets of scenarios under Gaussian, uniform and beta distributions with zero mean and SDs from 0.05 to 0.2, while each subset contains 1000 samples for each time step. Distributions of the forecast errors included in the training set 1 and the out-of-sample test set 2 are shown in Fig. 4.5.
2. With the information of set 1, we assume that the upper and lower bounds of the forecast error δ that are used to construct the uncertainty set for RO and DRO, the empirical mean, the mean absolute deviation and standard deviation that are used to build the ambiguity set for DRO are calculated based on the sample data from set 1. Then we optimize the decisions using the DO, SO, RO and DRO models. Note that the SO model is solved using only 200 scenarios from set 1, since further increasing the scenario number significantly increases the computational burden and also results in memory issues[12].
3. Fix the resulting optimal DA decisions achieved by DO, SO, RO and DRO and calculate the real-time decisions (i.e. positive and negative imbalance quantities) using the out-of-sample scenarios of set 2. Compare the performances of different models by calculating the expected and the worst-case out-of-sample profits.

[12] When increasing the number of scenarios above 200, some of the simulation cases cannot be solved within 24 hours using the SO model even by relaxing the optimality gap.

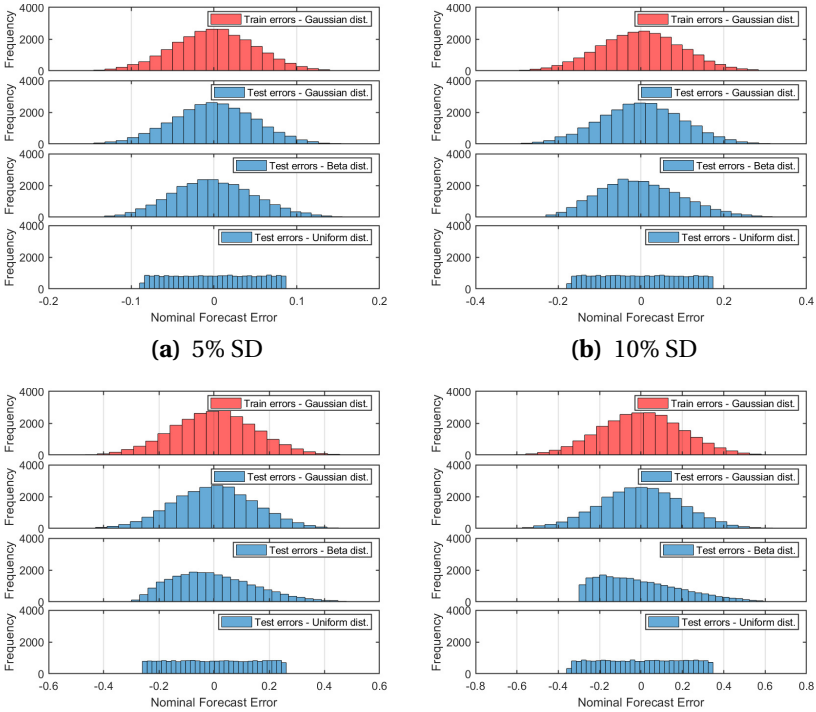

(a) 5% SD **(b)** 10% SD

(c) 15% SD **(d)** 20% SD

Figure 4.5: Distribution of forecast errors included in the training set 1 and in the out-of-sample test set 2 with mean zero and standard deviations ranging from 0.05 to 0.2 with a step of 0.05.

Here, we limit the number of scenarios generated to build the uncertainty and ambiguity sets for RO and DRO to 1000, as continuously increasing the number does not affect the result too much. However, it is worth noting that the computational complexity of both the RO and the DRO models is not influenced by the number of scenarios. The optimality gap is set to 0.01% for all optimization models except for the SO model, whose optimality gap is set to be 0.3% to ensure that for each simulated case the model can be solved within a reasonable time (i.e., maximum one hour for solving the model for one time step).

Table 4.2: Comparison of aggregator's expected simulation profits, the expected and the worst-case out-of-sample profits with standard deviations ranging from 0.05 to 0.2 resulted by deterministic, robust, distributionally robust and stochastic optimization models.

SD	Method	Sim. profit [mCHF]	Expected out-of-sample profit [mCHF]			Worst-case out-of-sample profit [mCHF]		
		Gaussian	Gaussian	Beta	Uniform	Gaussian	Beta	Uniform
0.05	DO	2.53	2.39	2.39	2.38	0.82	1.00	1.75
	RO	1.87	2.03	2.03	2.04	1.77*	1.86*	1.94*
	DRO	2.35	2.41*	2.42*	2.41*	0.96	1.14	1.89
	SO	2.42	2.41*	2.42*	2.41*	-0.97	-0.78	-0.03
0.1	DO	2.53	2.19	2.19	2.15	-1.66	-0.35	0.61
	RO	0.94	1.28	1.28	1.28	0.65*	1.03*	1.10*
	DRO	2.08	2.24*	2.25*	2.22	-1.20	0.03	0.96
	SO	2.24	2.24*	2.25*	2.23*	-3.19	-1.88	-0.92
0.15	DO	2.53	1.95	1.95	1.89	-3.55	-1.11	-0.66
	RO	0.35	0.81	0.81	0.81	-0.06*	0.50*	0.53*
	DRO	1.80	2.04*	2.07*	2.00*	-2.87	-0.48	-2.32
	SO	2.06	2.04*	2.06	2.00*	-4.71	-2.32	-1.94
0.2	DO	2.53	1.70	1.70	1.62	-4.32	-1.22	-1.92
	RO	0.04	0.57	0.57	0.57	-0.03*	0.25*	0.20*
	DRO	1.53	1.83*	1.86*	1.78*	-3.50	-0.51	-1.18
	SO	1.85	1.83*	1.86*	1.78*	-5.23	-5.24	-2.91

For each simulation case, the best out-of-sample results, i.e. the highest expected profits and highest worst-case profits, among all are marked with *.

Table 4.2 compares the aggregator's expected simulation profits with forecast errors modeled using training set 1, the expected and the worst-case out-of-sample profits calculated using samples under different distributions from test set 2 with SDs ranging from 0.05 to 0.2 resulted by running the DO, RO, DRO and SO models. The market share of the aggregator is assumed to be 10%. The best out-of-sample results for each simulation case are marked with *. Moreover, to be consistent with the optimality gap set for simulations, the number of digits for the results shown is set as two.

Compared to RO, DRO and SO, DO has the best simulation results in all cases as it does not account for the potential forecast errors and the resulting imbalances costs. However, as expected, similar profits cannot be achieved by DO during the out-of-sample test due to the incurred high imbalance costs, and the situation worsens with the increasing value of the SD. As a result, both the expected and the worst-case out-of-sample profits obtained by DO are com-

paratively lower among all models in all simulated cases, which strengthens the importance of integrating forecast uncertainties into modeling.

We further compare the expected out-of-sample profits of all models. It can be observed that the best results are always achieved by either the DRO or the SO model or both of them, whereas the results differences between these two models are negligible. The high profits achieved by DRO shows that the performance of the model can be improved by incorporating statistical information of the uncertainty distribution. It is without doubt that the SO model performs the best when the out-of-sample scenarios are generated under the same distribution as the one used to build the training set, i.e. Gaussian distribution. Nevertheless, the SO model also delivers good performance under beta and uniform distributions, which seem to be against the expectation that the performance of SO will deteriorate when the actual distribution of the uncertainties deviates from the simulated one. Furthermore, when comparing the performance of SO as well as other optimization models under different distributions, limited differences in terms of the expected out-of-sample profits are observed. This is likely to be explained by the fixed mean and standard deviation values under all distributions in both the training and the test sets. As shown in Fig. 4.5, the weighted average values of the forecast error samples under different distributions are close to zero, which is verified by calculating the mean of the forecast error samples under different distributions. Since the out-of-sample BM prices are deterministic[13] and the imbalance quantities are linearly related to the forecast errors, the expected imbalance costs, which are calculated as the sum of the product of the BM price and the corresponding imbalance quantity, are comparable under different out-of-sample distributions. For a better illustration, we plot the distributions of imbalance quantities under Gaussian, beta and uniform distributions resulted by distributionally robust optimization, stochastic optimization and robust optimization models under two extreme SD cases, i.e. SD=0.05 and SD=0.2 in Fig. 4.6. It can be seen that the distributions of imbalance quantities under different out-of-sample forecast error distributions are similar. The similar imbalance costs therefore

[13]The DA decisions including the the DAM prices are fixed during the out-of-sample test. The BM prices, which are modeled as a function of the DAM prices, are thus deterministic.

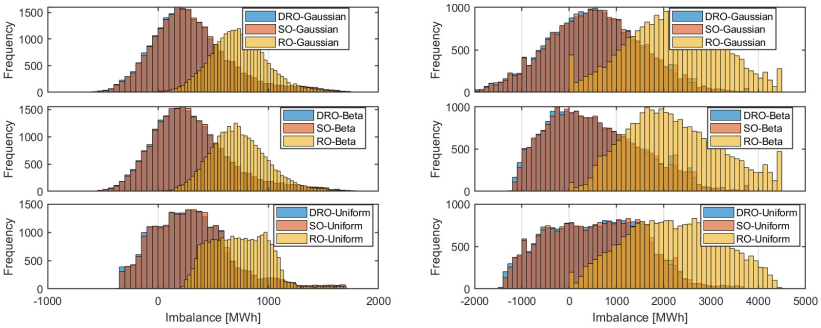

(a) 5% SD **(b)** 20% SD

Figure 4.6: Distributions for the resulting imbalance quantities of distributionally robust optimization, stochastic optimization and robust optimization models assuming that the forecast errors are subject to Gaussian, beta and uniform distributions with standard deviations set as 0.05 and 0.2.

lead to the similar expected out-of-sample profits under different distributions for each optimization model.

However, when focusing on the worst-case out-of-sample profits, the results differ a lot under different out-of-sample distributions, which can be explained by the different values of worst-case forecast errors and the resulting different worst-case imbalance quantities under different distributions (see Fig. 4.5 and Fig. 4.6). Furthermore, it can be noticed that RO achieves the highest worst-case profits during the out-of-sample test in all cases, as its decisions are optimized against the worst case with almost no negative imbalance penalties incurred at real-time (see Fig. 4.6). Compared to RO, DRO is less conservative as its decisions are immune against a family of distributions, the worst-case performance of DRO is therefore not as good as RO but still much better than that of DO and SO.

Comparing the results under different SDs, it can be seen that in general the resulting simulation and out-of-sample test profits of all models decrease with the increasing SD. In addition, compared to RO and DRO, the worst-case out-of-sample profits of the SO model are more sensitive to the variance of the forecast errors, i.e. the worst-case profit decreases dramatically with the

Table 4.3: Problem size and the average computational time for solving the optimization problem of one time step using different methods.

	DO	RO	DRO	SO
Variable No.	122 (46 integer)	121 (46 integer)	279 (46 integer)	24'001 (9'200 integer)
Constraint No.	217	216	347 (28 quadratic)	47'777
Computation time (s)	2	2	2	243

Robust optimization was solved using the integrated module in Yalmip [38].

increasing SD, since the SO decisions are optimized only considering the expected objective value under all scenarios.

The problem size and the average computational time consumed by DO, RO, DRO and the SO model considering 200 scenarios for solving the problem for one time step are compared in Table 4.3. As mentioned, the optimization problem is time decoupled, i.e. the complexity of the problem does not increase with the expansion of the time horizon. It can be seen that although the DRO model is more complex than the DO and RO models, i.e. it has more variables and constraints including additional quadratic constraints, due to the limited problem size, the average computational time of running the DRO model is the same as that of running the RO and DRO models. In contrast, solving the SO model in average consumes much more time as the problem size is much bigger, though only 200 scenarios are considered for the simulation.

To summarize, compared to SO and RO, DRO achieves a good trade-off between the expected and the worst-case performance, with the computational effort that is comparable to that of using RO and DO. The DRO model is therefore more appropriate in cases with large amount of uncertainty realizations data available but the unknown probability distribution of the uncertainty.

4.5 Limitations and Future Work

This work has several limitations and a few of which are highlighted in this section. First, the ambiguity set for distributionally robust optimization is constructed considering the mean, the mean absolute deviation and the standard deviation of the wind output forecast errors. Thus, the symmetry and the degree of peakedness of the distribution, which are important to characterize the wind forecast error distributions [76], are not captured. A future version of

the ambiguity set could incorporate skewness and kurtosis to describe these two characteristics. In order to consider the correlation of the forecast errors between different time steps, the covariance matrix could be included in the ambiguity set, which will however increase the computational complexity of the method. An alternative approach, which incorporates the correlation of wind forecast errors between hours without adding the computational complexity, is presented in Chapter 5. Moreover, instead of using synthetic wind forecast errors, it is more interesting to estimate the performance of the model using real-world data.

Second, the aggregator is assumed to be the only market participant that could act strategically. For future work, a more realistic market environment can be modeled by introducing competitions among multiple strategic producers using an Equilibrium Problem with Equilibrium Constraints (EPEC) model. Furthermore, the assumptions related to the number of wind power producers in the system should be gradually relaxed, which allows to assess the market value and the strategic positioning of the price-maker aggregator not only with respect to its size but also to its correlation with the aggregate wind power production in the system.

Third, a simple version of linear decision rule is applied in this work, which might not always deliver a good approximation. To reduce the approximation error, an extended version of the simple linear decision rule, such as the segregated linear decision rule that introduces a piece-wise linear approximation of the uncertainties [104], can be applied.

4.6 Summary and Conclusions

In this chapter, a distributionally robust optimization method is presented to optimize the bidding strategies for a wind aggregator, who participates as a price-maker in the day-ahead market and a deviator in the balancing market.

The enhanced linear decision rule that is applied by the distributionally robust optimization model provides a good approximation of the second-stage decisions, which is verified by comparing the approximation curves to the fitting curves obtained by stochastic optimization. Sensitivity analyses regarding the market share of the aggregator and the standard deviation of the forecast errors show that aggregator is more risk-seeking with increasing market

shares and it offers less to the day-ahead market when the standard deviation of the wind output forecast error increases. Furthermore, we compare the performance of distributionally robust optimization with two extensively applied methods, i.e. stochastic optimization and robust optimization, as well as the deterministic method that does not consider the potential forecast errors. Based on the out-of-sample test results, it is shown that distributionally robust optimization outperforms robust optimization in the expected profits with comparable computational efforts, and it achieves similar results as stochastic optimization with much less computational time. Compared to the results of other models, deterministic optimization model does not deliver a good performance in any of the simulated cases, which shows the importance of uncertainty modeling.

Chapter 5

The Integration of Storage Units

This chapter expands the work in Chapter 3 and Chapter 4 by integrating the storage units into the aggregator. Hence, distributionally robust optimal bidding strategies for a wind-storage aggregator that participates as a price-maker in the day-ahead market and a deviator in the balancing market are derived. To improve the performance of the method, we use an Auto-regressive Moving Average (ARMA) model to learn the auto-correlations and the cross-correlations of historical forecast errors and generate the day-ahead forecast error scenarios in a rolling manner. Then the potential distributions of the uncertain forecast errors are described by extracting the statistical information of these scenarios. A case study based on one-year Nord Pool data validates the effectiveness of the model. In addition, the impact of output-based renewable subsidies and aggregation levels are investigated. Finally, the value of integrating storage units is assessed by comparing the performance of a wind-storage aggregator to that of a wind aggregator in all simulated cases. Two benchmark cases, namely the perfect information case and the deterministic case, are used to analyze the performance of the model. In the deterministic case, the aggregator is assumed to bid at the day-ahead forecast without considering potential forecast errors. Results show that the model performance can be improved by applying the ARMA model. Moreover, both the distributionally robust optimization models with and without ARMA outperform the deterministic benchmark case. This chapter is based on [105].

5.1 Introduction

5.1.1 Motivation and Related Work

As mentioned in previous chapters, the intermittent and uncertain nature of Variable Renewable Energy (VRE) poses great challenges to VRE operators and electricity system operators. These challenges can be approached mainly in two ways: 1) incorporate the uncertainties into the modeling to take preventive steps in the bidding process; 2) combine different energy resources (especially storage units) to compensate for the imbalances of individual units. In Chapter 4, we've already tried tackling the uncertainty problem following the idea of option 1) by applying Ditributionally Robust Optimization (DRO), which enables to incorporate the uncertainty in a more realistic way. To further alleviate the problem following the principle of option 2), wind and Photovoltaic (PV) units can be combined with storage units in order to compensate for the their variable and uncertain generation outputs. Due to the advancement in storage industries in terms of costs and technologies, the combination of VRE (which consists mainly of wind and solar energy) and storage units has drawn significant attention in recent years and is viewed as a viable option to overcome these challenges. The operators of such hybrid systems will be referred to as aggregators in the following context.

In this chapter, we expand the work in the Chapter 4 and focus on addressing the following questions:

- As wind and PV units have zero marginal costs and enjoy subsidies, what is the aggregator's optimal bidding strategy with and without considering the output subsidies and how does it impact the market?
- How does the level of aggregation affect the market?
- How can the effects brought by wind and PV output forecast uncertainties be mitigated?
- What is the benefit of combining wind or PV units with storage units?

The benefit of bidding hybrid energy resources in a coordinated way has been verified in Chapter 2 and in the literatures [25, 106, 107]. It is shown that higher efficiency and lower costs can be achieved through the coordination. The main advantage of combining storage units with solar or wind is to alleviate the real-time imbalances caused by generation forecast errors and to en-

able arbitrage in different markets. Under the assumption that the size of the aggregator is not large enough to impact the market, the aggregator is modeled as a price-taker in most of the work. However, the realization of large-scale virtual power plants and hybrid projects (e.g. Tesla's Virtual Power Plant (VPP) project in South Australia and Arizona Public Service's solar-storage hybrid project) shows that the market power of these aggregators cannot be neglected in the near future. The authors of [23, 86, 87] propose methods to optimize the offering strategy of virtual power plants, while uncertainties are considered using point estimation, robust optimization and adaptive robust optimization, respectively. In [108], the wind-storage aggregator is modeled as a price-maker using the residual demand curve, whereas uncertainties are modelled using a limited number of scenarios and the simulation is carried out only for a few days of the year thereby neglecting the seasonal fluctuations and uncertainties of the variable resources. An analysis regarding market interactions between different types of market participants, e.g. storage, wind and conventional units, is provided in [109].

To fill the identified gaps in the existing research, in this chapter, distributionally robust optimal bidding strategies for a price-maker wind-storage aggregator that participates in the day-ahead and balancing markets are derived. Consequently, the contributions of this chapter are:

1. To propose a two-stage DRO model to optimize the bidding strategies of a wind-storage aggregator that acts as a price-maker in the Day-ahead Market (DAM), and as a deviator in the balancing market.
2. To improve the performance of the model using an ARMA model to learn the auto-correlations and the cross-correlations of historical forecast errors and to generate the day-ahead forecast error scenarios in a rolling manner. Finally, the potential distributions of the uncertain forecast errors are described by extracting the statistical information of these scenarios.
3. To validate the model using one year worth of data of Nord Pool and compare the results to two benchmark cases, namely the perfect information case and the deterministic case (i.e. bidding at the day-ahead forecast without considering potential forecast errors).

5.1.2 Chapter Organization

The remainder of the chapter is organized as follows: the main model assumptions are described in Section 5.2. The mathematical formulations and the proposed optimization model are presented in Section 5.3. Section 5.4 provides an analysis for a case study based on one-year Nord Pool data. Limitations and future work are discussed in Section 5.5. Finally, conclusions are drawn in Section 5.6.

5.2 Model Assumptions

The main assumptions made in this chapter are summarized as follows:

- The wind-storage aggregator is assumed to participate as a price-maker in the day-ahead and a deviator the balancing markets.
- The aggregator is assumed to be the only one that could bid strategically into the market. The rival producers and consumers are modeled through the historical Nord Pool supply and demand curves of 2018. For each hour, due to the computational limit, the original supply (offering) and demand (bidding) curves that consist of up to nearly 1000 blocks are approximated focusing on bids and offers near the original market clearing point. The resulting approximated supply and demand curves for rival producers and the consumers have a maximum of 79 blocks.
- The Balancing Market (BM) prices are assumed to be independent of the aggregator's position, i.e. the aggregator is a price-taker in the balancing market. This assumption, however, might need to be reconsidered when the aggregator accounts for a significant share of the market. Moreover, it is assumed that all imbalances can be corrected through the balancing market.
- The simulated electricity system is assumed to be uncongested, i.e. no network constraints are considered, which is consistent with the zonal pricing scheme of the European electricity markets.

Note that the simulated electricity system and the market environment are a simplification of a much more complex reality.

5.3 Mathematical Formulation

In this section, we extend the distributionally robust optimization formulation of a wind aggregator bidding problem presented in previous chapters to that of a wind-storage aggregator bidding problem. Note that the formulations presented will focus on the changes required for this extension.

5.3.1 Bi-level Bidding Model

The trading strategy is formulated as a bi-level optimization problem.

Upper-level Formulation

The Upper-Level (UL) problem is the aggregator's profit maximization problem, i.e. it maximizes the profits obtained from the DAM and the BM:

$$\max \sum_{t=1}^{T} \left(\lambda_t^{\text{DA}} (P_t^{\text{DAs}} - P_t^{\text{DAb}}) + pr_t^{\text{BM+}} P_t^{\text{BM+}} - pr_t^{\text{BM-}} P_t^{\text{BM-}} \right) \tag{5.1a}$$

where P_t^{DAs} and P_t^{DAb} are the dispatched Day-ahead (DA) supply and demand quantity of the aggregator for time step t, and λ^{DA} is the DA market clearing price. The positive/negative imbalance prices and quantities are denoted by $pr^{\text{BM+/-}}$ and $P^{\text{BM+/-}}$. The simulation horizon is denoted by T.

The upper-level problem is subject to two groups of constraints: the market constraints and the operational constraints. Market constraints include the limits on the supply and demand quantity Q^{DAs} and Q^{DAb} of the aggregator. Note that while Q^{DAs} and Q^{DAb} are the supply and demand quantities that are submitted to the market, P^{DAs} and P^{DAb} indicate the power that the aggregator expects to be dispatched for, which are the outcomes of the lower-level market clearing problem. The submitted DA supply quantity Q^{DAs} of the aggregator is restricted by the sum of the capacity of the wind P^{Wc} and the maximum discharging rate of the storage $P^{\text{dis,max}}$, while its submitted DA demand quantity Q^{DAb} is limited by the maximum charging rate of the storage $P^{\text{ch,max}}$, i.e.

$$0 \leq Q_t^{\text{DAs}} \leq P^{\text{Wc}} + P^{\text{dis,max}} \tag{5.1b}$$

$$0 \leq Q_t^{\text{DAb}} \leq P^{\text{ch,max}} \tag{5.1c}$$

The real-time output of the wind unit is equal to the sum of the wind output forecast P^{Wf} and the wind output forecast error δ, i.e.,

$$0 \leq P_t^{\text{W}} \leq P_t^{\text{Wf}} + \delta_t \tag{5.1d}$$

where modeling of the forecast error δ will be elaborated in following sections.

For storage units, the real-time charging and discharging powers P^{ch} and P^{dis} are non-negative and are limited by the maximum charging and discharging rates $P^{\text{ch,max}}$ and $P^{\text{dis,max}}$. The storage level E^{s} is required to be in the range of $[E^{\text{s,min}}, E^{\text{s,max}}]$. Mathematically,

$$0 \leq P_t^{\text{dis/ch}} \leq p^{\text{dis/ch,max}} \tag{5.1e}$$

$$E^{\text{s,min}} \leq E_t^{\text{s}} \leq E^{\text{s,max}} \tag{5.1f}$$

In addition, the storage levels of the two consecutive time steps are defined by:

$$E_{t+1}^{\text{s}} = E_t^{\text{s}} + \eta^{\text{s}} P_t^{\text{ch}} \Delta t - P_t^{\text{dis}} \Delta t / \eta^{\text{s}} \tag{5.1g}$$

where η^{s} is the one-way efficiency.

As all the deviations of the aggregator are assumed to be cleared in the BM, the real-time output of the aggregator must be equal to the total market exchange in the DAM and the BM for each time period, i.e.,

$$P_t^{\text{DAs}} - P_t^{\text{DAb}} + P_t^{\text{BM+}} - P_t^{\text{BM-}} = P_t^{\text{W}} + P_t^{\text{dis}} - P_t^{\text{ch}} \tag{5.1h}$$

$$P_t^{\text{BM+}}, P_t^{\text{BM-}} \geq 0 \tag{5.1i}$$

Lower-level Formulation

The Lower-Level (LL) represents the day-ahead market clearing problem and the objective is to maximize the social welfare, as expressed by

$$\max_{\alpha_t^{\text{DAs/b}}, P_t^{\text{DAs/b}}} \sum_{t=1}^{T} (\alpha_t^{\text{DAb}} P_t^{\text{DAb}} + \sum_{m=1}^{N^{\text{m}}} \lambda_{t,m}^{\text{DA,D}} P_{t,m}^{\text{DA,D}} - \alpha_t^{\text{DAs}} P_t^{\text{DAs}} - \sum_{j=1}^{N^{\text{j}}} \sum_{b=1}^{N^{\text{b}}} \lambda_{t,j,b}^{\text{DA,O}} P_{t,j,b}^{\text{DA,O}}) \tag{5.2a}$$

where α^{DAs} and α^{DAb} are the offering and bidding price of the aggregator. Variables $\lambda^{\text{DA,O}}_{t,j,b}$ and $P^{\text{DA,O}}_{t,j,b}$ are the offering price and dispatched offering quantity for block b of rival producer j at time t, while $\lambda^{\text{DA,D}}_{t,m}$ and $P^{\text{DA,D}}_{t,m}$ are the bidding price and dispatched bidding quantity of consumer's bidding block m at time t. The number of consumers' demand bidding blocks, the number of rival producers and the number of the rival producers' offering blocks are indicated by N^{m}, N^{j} and N^{b}, respectively.

The LL problem is subject to two types of constraints: upper and lower limits on bidding quantities and the power balance constraint which enforces the summations of the DAM dispatched supply quantities equal to the dispatched demand quantities for each time step, i.e.

$$0 \leq P^{\text{DAs}}_{t} \leq Q^{\text{DAs}}_{t} \quad : \ \mu^{\text{DAsmin}}_{t},\ \mu^{\text{DAsmax}}_{t} \tag{5.2b}$$

$$0 \leq P^{\text{DAb}}_{t} \leq Q^{\text{DAb}}_{t} \quad : \ \mu^{\text{DAbmin}}_{t},\ \mu^{\text{DAbmax}}_{t} \tag{5.2c}$$

$$0 \leq P^{\text{DA,O}}_{t,j,b} \leq P^{\text{DA,Omax}}_{t,j,b} \quad : \ \mu^{\text{DA,Omin}}_{t,j,b},\ \mu^{\text{DA,Omax}}_{t,j,b} \tag{5.2d}$$

$$0 \leq P^{\text{DA,D}}_{t,m} \leq P^{\text{DA,Dmax}}_{t,m} \quad : \ \mu^{\text{DA,Dmin}}_{t,m},\ \mu^{\text{DA,Dmax}}_{t,m} \tag{5.2e}$$

$$\sum_{m=1}^{N^{\text{m}}} P^{\text{DA,D}}_{t,m} + P^{\text{DAb}}_{t} - P^{\text{DAs}}_{t} - \sum_{j=1}^{N^{\text{j}}} \sum_{b=1}^{N^{\text{b}}} P^{\text{DA,O}}_{t,j,b} = 0 : \ \lambda^{\text{DA}}_{t} \tag{5.2f}$$

where variables after the columns are the corresponding dual variables.

Following the linearization and reformulation process presented in Chapter 3, the bi-level problem can finally be reformulated as a Mixed-Integer Lin-

ear Programming (MILP) problem as follows:

$$\begin{aligned}
\min \quad & \sum_{t=1}^{T}\sum_{j=1}^{N^{\mathrm{j}}}\sum_{b=1}^{N^{\mathrm{b}}}\left(\lambda_{t,j,b}^{\mathrm{DA,O}}P_{t,j,b}^{\mathrm{DA,O}}+\mu_{t,j,b}^{\mathrm{DA,Omax}}P_{t,j,b}^{\mathrm{DA,Omax}}\right) \\
& -\sum_{t=1}^{T}\sum_{m=1}^{N^{\mathrm{m}}}\left(\lambda_{t,m}^{\mathrm{DA,D}}P_{t,m}^{\mathrm{DA,D}}-\mu_{t,m}^{\mathrm{DA,Dmax}}P_{t,m}^{\mathrm{DA,Dmax}}\right) \\
& -\sum_{t=1}^{T}pr_{t}^{\mathrm{BM+}}P_{t}^{\mathrm{BM+}}+\sum_{t=1}^{T}pr_{t}^{\mathrm{BM\text{-}}}P_{t}^{\mathrm{BM\text{-}}} && \text{(5.3a)} \\
\text{s.t.} \quad & \text{Upper-level constraints (5.1b)-(5.1i)} && \text{(5.3b)} \\
& \text{Linearized reformulations of LL problem (5.2)} && \text{(5.3c)}
\end{aligned}$$

5.3.2 Modelling of Uncertainty

Since the forecast error δ in (5.1d) is subject to uncertainty, problem (5.3) is in general intractable as the optimal real-time decisions need to be found by looping over all possible realizations of δ. Therefore, we first use the linear decision rule to approximate the real-time decisions $\{P^{\mathrm{BM+/\text{-}}}, P^{\mathrm{W}}, E^{\mathrm{s}}, P^{\mathrm{ch/dis}}\}$ using an affine function of the forecast error:

$$P_{t}^{\mathrm{BM+}}=k_{t,0}^{\mathrm{BM+}}+k_{t,1}^{\mathrm{BM+}}\delta_{t} \tag{5.4}$$
$$P_{t}^{\mathrm{BM\text{-}}}=k_{t,0}^{\mathrm{BM\text{-}}}+k_{t,1}^{\mathrm{BM\text{-}}}\delta_{t} \tag{5.5}$$
$$P_{t}^{\mathrm{W}}=k_{t,0}^{\mathrm{W}}+k_{t,1}^{\mathrm{W}}\delta_{t} \tag{5.6}$$
$$E_{t}^{\mathrm{s}}=k_{t,0}^{\mathrm{s}}+k_{t,1}^{\mathrm{s}}\delta_{t} \tag{5.7}$$
$$P_{t}^{\mathrm{ch}}=k_{t,0}^{\mathrm{ch}}+k_{t,1}^{\mathrm{ch}}\delta_{t} \tag{5.8}$$
$$P_{t}^{\mathrm{dis}}=k_{t,0}^{\mathrm{dis}}+k_{t,1}^{\mathrm{dis}}\delta_{t} \tag{5.9}$$

As mentioned, different from Stochastic Optimization (SO) that describes the uncertainty using finite scenarios, DRO incorporates the uncertainty by describing the possible distributions I of the uncertainty using an ambiguity set F. The ambiguity set describes the common statistical information shared by

all possible distributions. The ambiguity set considered in this work, i.e.

$$F = \left\{ I: \begin{array}{c} \mathbb{E}_I[\delta_t] = 0 \\ \mathbb{E}_I[|\delta_t|] \leq \gamma_t \\ Pr(\boldsymbol{\delta} \in \mathscr{W}) = 1 \end{array} \right\}$$

restricts the expectation and mean absolute deviation of the random vector $\boldsymbol{\delta}$ to 0 and $\boldsymbol{\gamma}$, respectively. The last line requires that all realizations of $\boldsymbol{\delta}$ should be within the uncertainty set $\mathscr{W}$, which defines the upper and lower limits of $\boldsymbol{\delta}$ as follows:

$$\mathscr{W} = \{\delta_t^{\min} \leq \delta_t \leq \delta_t^{\max}\}$$

Note that in order to lower the computational burden, only linear constraints are considered in F. To guarantee the tractability of the problem and to increase the flexibility of the linear decision rule, an auxiliary variable u_t for each time step t is introduced [99] and the ambiguity set and the uncertainty set are reformulated as $\overline{F}$ and $\overline{\mathscr{W}}$ given by

$$\overline{F} = \left\{ J: \begin{array}{c} \mathbb{E}_J[\delta_t] = 0 \\ \mathbb{E}_J[u_t] \leq \gamma_t \\ Pr\{(\boldsymbol{\delta}, \boldsymbol{u}) \in \overline{\mathscr{W}}\} = 1 \end{array} \right\}$$

$$\overline{\mathscr{W}} = \left\{ \begin{array}{c} \delta_t^{\min} \leq \delta_t \leq \delta_t^{\max} \\ |\delta_t| \leq u_t \\ u_t \leq u_t^{\max} = \max\{\delta_t^{\max}, -\delta_t^{\min}\} \end{array} \right\}$$

Correspondingly, the affine functions of the real-time decisions are rewritten as follows:

$$P_t^{\text{BM+}} = k_{t,0}^{\text{BM+}} + k_{t,1}^{\text{BM+}}\delta_t + k_{t,2}^{\text{BM+}}u_t \tag{5.10}$$

$$P_t^{\text{BM-}} = k_{t,0}^{\text{BM-}} + k_{t,1}^{\text{BM-}}\delta_t + k_{t,2}^{\text{BM-}}u_t \tag{5.11}$$

$$P_t^{\text{W}} = k_{t,0}^{\text{W}} + k_{t,1}^{\text{W}}\delta_t + k_{t,2}^{\text{W}}u_t \tag{5.12}$$

$$E_t^{\text{s}} = k_{t,0}^{\text{s}} + k_{t,1}^{\text{s}}\delta_t + k_{t,2}^{\text{s}}u_t \tag{5.13}$$

$$P_t^{\text{ch}} = k_{t,0}^{\text{ch}} + k_{t,1}^{\text{ch}}\delta_t + k_{t,2}^{\text{ch}}u_t \tag{5.14}$$

$$P_t^{\text{dis}} = k_{t,0}^{\text{dis}} + k_{t,1}^{\text{dis}}\delta_t + k_{t,2}^{\text{dis}}u_t \tag{5.15}$$

To integrate the modeling of uncertainty described above into problem (5.3), we first write (5.3) in a compact form:

$$\min_{\boldsymbol{x}} \quad \Theta(\boldsymbol{x}) + \phi(\boldsymbol{x}, \boldsymbol{\delta}) \tag{5.16a}$$

$$\text{s.t.} \quad \boldsymbol{x} \in \boldsymbol{X_f} \tag{5.16b}$$

$$\boldsymbol{A}(\boldsymbol{\delta}) + \boldsymbol{B}\boldsymbol{y}(\boldsymbol{\delta}, \boldsymbol{u}) \leq \boldsymbol{D}(\boldsymbol{\delta}) \tag{5.16c}$$

where $\boldsymbol{x} = \{P^{\text{DAs/b}}, \alpha^{\text{DAs/b}}, Q^{\text{DAs/b}}, \lambda^{\text{DA}}, P^{\text{DA,O}}, P^{\text{DA,D}}\}$ represents the first-stage decisions, $\Theta(\boldsymbol{x})$ and $\phi(\boldsymbol{x}, \boldsymbol{\delta})$ correspond to the first-stage term (i.e., the day-ahead market cost) and the second-stage term (i.e., the balancing market cost) in the objective function (5.3a), respectively. The feasibility region of $\boldsymbol{x}$ based on constraints (5.1b)-(5.1c) and (5.1h) in (5.3b) and constraint (5.3c) is defined by $\boldsymbol{X_f}$. Constraint (5.16c) corresponds to real-time constraints (5.1d)-(5.1i) in (5.3b). Following the principle of DRO, i.e. the decisions should be optimized against the expectation of the worst-case distribution, the second-stage optimization problem is formulated as:

$$\phi(\boldsymbol{x}, \boldsymbol{\delta}) = \min_{\boldsymbol{k_t^{0,1,2}}} \sup_{J \in \overline{F}} \mathbb{E}_{\mathbf{J}} \left\{ \sum_{t=1}^{T} C_t^{\text{bm}}(\boldsymbol{\delta}, \boldsymbol{u}) \right\} \tag{5.17a}$$

$$\text{s.t.} \quad \boldsymbol{A}(\boldsymbol{\delta}) + \boldsymbol{B}\boldsymbol{y}(\boldsymbol{\delta}, \boldsymbol{u}) \leq \boldsymbol{D}(\boldsymbol{\delta}) \tag{5.17b}$$

where $C_t^{\text{bm}}(\boldsymbol{\delta}, \boldsymbol{u})$ equals $pr_t^{\text{BM-}} P_t^{\text{BM-}}(\boldsymbol{\delta}, \boldsymbol{u}) - pr_t^{\text{BM+}} P_t^{\text{BM+}}(\boldsymbol{\delta}, \boldsymbol{u})$. This problem can be solved by optimizing the linear decision rule parameters, i.e. $\{k^{\text{BM+}}, k^{\text{BM-}}, k^{\text{W}}, k^{\text{s}}, k^{\text{ch}}, k^{\text{dis}}\}$. As $\boldsymbol{\delta}$ and $\boldsymbol{u}$ are subject to constraints in $\overline{F}$, the inner problem of (5.17) can be reformulated as:

$$\sup_{J \in \overline{F}} \mathbb{E}_{\mathbf{J}} \left\{ \sum_{t=1}^{T} C_t^{\text{bm}}(\boldsymbol{\delta}, \boldsymbol{u}) \right\}$$

$$= \sup \int_{\overline{\mathscr{W}}} \sum_{t=1}^{T} C_t^{\text{bm}}(\boldsymbol{\delta}, \boldsymbol{u}) df(\boldsymbol{\delta}, \boldsymbol{u}) \tag{5.18a}$$

$$\text{s.t.} \int_{\overline{\mathscr{W}}} \boldsymbol{\delta} df(\boldsymbol{\delta}, \boldsymbol{u}) = 0 \qquad : \boldsymbol{\rho} \tag{5.18b}$$

$$\int_{\overline{\mathscr{W}}} \boldsymbol{u} df(\boldsymbol{\delta}, \boldsymbol{u}) \leq \boldsymbol{\gamma} \qquad : \boldsymbol{\beta} \tag{5.18c}$$

$$\int_{\overline{\mathscr{W}}} df(\boldsymbol{\delta}, \boldsymbol{u}) = 1 \qquad : \eta \tag{5.18d}$$

$$f(\boldsymbol{\delta}, \boldsymbol{u}) \geq 0, \qquad \forall (\boldsymbol{\delta}, \boldsymbol{u}) \in \overline{\mathscr{W}} \tag{5.18e}$$

$$\boldsymbol{A}(\boldsymbol{\delta}) + \boldsymbol{B}\boldsymbol{y}(\boldsymbol{\delta}, \boldsymbol{u}) \leq \boldsymbol{D}(\boldsymbol{\delta}) \tag{5.18f}$$

where $\boldsymbol{\rho}$, $\boldsymbol{\beta}$ and η are the corresponding dual variables, $f(\boldsymbol{\delta}, \boldsymbol{u})$ is the probability density function. Finally, according to duality theory [100], we rewrite (5.16) as follows by replacing the second-stage problem with its dual form:

$$\min \quad \Theta(\boldsymbol{x}) + \eta + \boldsymbol{\gamma}\boldsymbol{\beta} \tag{5.19a}$$

$$\text{s.t.} \quad \boldsymbol{\beta} \geq 0 \tag{5.19b}$$

$$\eta + \boldsymbol{\rho}\boldsymbol{\delta} + \boldsymbol{\beta}\boldsymbol{u} \geq \sum_{t=1}^{T} C_t^{\text{bm}}(\boldsymbol{\delta}, \boldsymbol{u}) \tag{5.19c}$$

$$\boldsymbol{A}(\boldsymbol{\delta}) + \boldsymbol{B}\boldsymbol{y}(\boldsymbol{\delta}, \boldsymbol{u}) \leq \boldsymbol{D}(\boldsymbol{\delta}) \tag{5.19d}$$

$$\boldsymbol{x} \in \boldsymbol{X_f} \tag{5.19e}$$

where $\boldsymbol{\delta}$-related and $\boldsymbol{u}$-related equations, i.e. (5.19c) and (5.19d), also need to satisfy the constraints in $\overline{\mathscr{W}}$. Constraints (5.19c) and (5.19d) are fulfilled only if the worst-case is fulfilled. Taking (5.19c) as an example, it can be reformulated

as:

$$\min \{\eta + \boldsymbol{\rho\delta} + \boldsymbol{\beta u} - \sum_{t=1}^{T} C_t^{\text{bm}}(\boldsymbol{\delta}, \boldsymbol{u})\} \geq 0 \tag{5.20a}$$

$$\text{s.t.} \quad \boldsymbol{\delta}^{\min} \leq \boldsymbol{\delta} \leq \boldsymbol{\delta}^{\max} \quad : \boldsymbol{\pi^1}, \boldsymbol{\pi^2} \tag{5.20b}$$

$$-\boldsymbol{u} \leq \boldsymbol{\delta} \leq \boldsymbol{u} \quad : \boldsymbol{\pi^3}, \boldsymbol{\pi^4} \tag{5.20c}$$

$$\boldsymbol{u} \leq \boldsymbol{u}^{\max} \quad : \boldsymbol{\pi^5} \tag{5.20d}$$

where $\boldsymbol{\pi^{1\sim5}}$ are the corresponding dual variables. Using the Linear Decision Rule (LDR) approximation (5.4) in (5.20) to linearize the term $\sum_{t=1}^{T} C_t^{\text{bm}}(\boldsymbol{\delta}, \boldsymbol{u})$, the resulting dual equivalence of (5.20) is:

$$\max \ \eta + \sum_{t=1}^{T} \left[pr_t^{\text{BM+}} k_{t,0}^{\text{BM+}} - pr_t^{\text{BM-}} k_{t,0}^{\text{BM-}} + \left(\delta_t^{\min} \pi_t^1 - \delta_t^{\max} \pi_t^2 - u_t^{\max} \pi_t^5 \right) \right] \tag{5.21a}$$

$$\text{s.t.} \quad \sum_{t=1}^{T} (\pi_t^1 - \pi_t^2 + \pi_t^3 - \pi_t^4) = \sum_{t=1}^{T} (\rho_t + pr_t^{\text{BM+}} k_{t,1}^{\text{BM+}} - pr_t^{\text{BM-}} k_{t,1}^{\text{BM-}}) \tag{5.21b}$$

$$\sum_{t=1}^{T} (\pi_t^3 + \pi_t^4 - \pi_t^5) = \sum_{t=1}^{T} (\beta_t + pr_t^{\text{BM+}} k_{t,2}^{\text{BM+}} - pr_t^{\text{BM-}} k_{t,2}^{\text{BM-}}) \tag{5.21c}$$

$$\pi_t^n \geq 0, \ n = 1, 2, ..., 5 \tag{5.21d}$$

Applying the strong duality theory, (5.21a) is equivalent to:

$$\eta + \sum_{t=1}^{T} \left[pr_t^{\text{BM+}} k_{t,0}^{\text{BM+}} - pr_t^{\text{BM-}} k_{t,0}^{\text{BM-}} + \left(\delta_t^{\min} \pi_t^1 - \delta_t^{\max} \pi_t^2 - u_t^{\max} \pi_t^5 \right) \right] \geq 0 \tag{5.22}$$

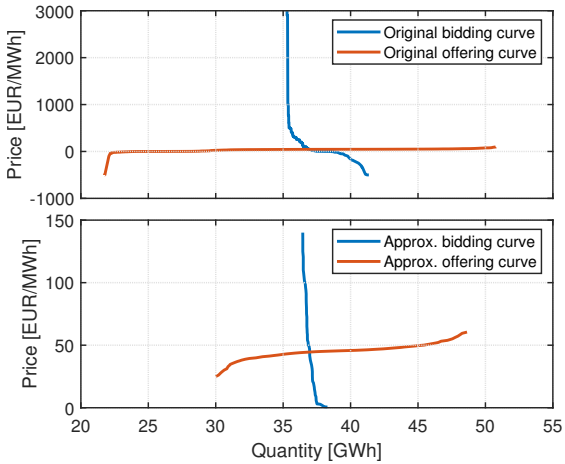

Figure 5.1: Comparison of the original market offering/bidding curves and the approximated offering/bidding curves for an example hour.

Constraint (5.19d) can be reformulated following a similar process and the final optimization problem is:

$$\min \ \Theta(\boldsymbol{x}) + \eta + \boldsymbol{\gamma}\boldsymbol{\beta}$$

s.t. $\boldsymbol{\beta} \geq 0$

Constraints (5.21b)-(5.21d) and (5.22) that are equivalent to (5.19c)

Reformulated constraints equivalent to (5.1d)-(5.1i) in (5.19d)

$\boldsymbol{x} \in \boldsymbol{X_f}$

5.4 Case Study

5.4.1 Input Data

Parameters of the wind-storage aggregator are listed in Table 5.1. Supply and

Table 5.1: Parameters of the wind-storage aggregator

$E^{s,max}$	$E^{s,min}$	E^{s}_{1}, E^{s}_{T+1}	η^{s}	$p^{ch/dis,max}$	P^{Wc}
100 MWh	10 MWh	50 MWh	0.95	100 MW	250 MW

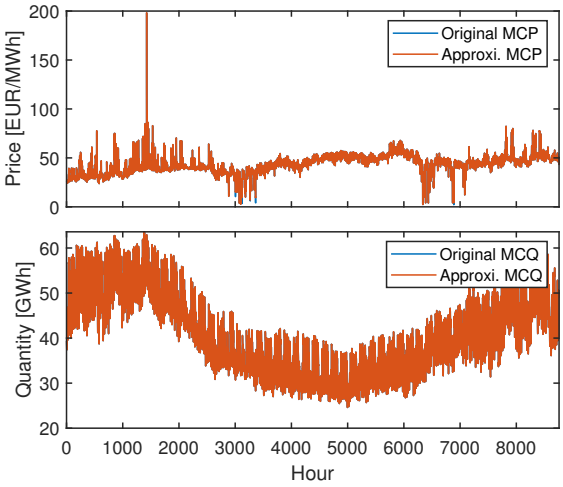

Figure 5.2: Comparison of the original and the approximated market clearing prices and quantities for the simulation year 2018.

demand curves are based on the Nord Pool market clearing data of 2018. For each hour the original supply (offering) and demand (bidding) curves consist of up to nearly 1000 blocks, due to the computational limit, the original supply (offering) and demand (bidding) curves are approximated focusing on the bids and offers near the original market clearing point. The resulting approximated supply and demand curves for each hour consist of a maximum of 79 blocks. To visualize the results, Fig. 5.1 shows the original and the approximated DAM offering and bidding curves for an example hour. The original and the resulting approximated day-ahead market clearing prices as well as quantities are shown in Fig. 5.2.

In order to simulate the case for Denmark, the total Nord Pool system-level bidding and offering quantities are scaled down by a factor of 0.08 while the prices remain unchanged. The scaling results in maximum hourly demand quantity ranges from 2'026 MW to 5'302 MW. The wind forecast and real-time output data are from the Denmark region in 2018. For each simulation day in 2018, the scenarios to build the ambiguity set are generated based on the 2017 data and all the data of 2018 before that simulation day.

Different from the assumptions made in previous chapters, the aggregator is in general[14] assumed to participate in the market without replacing the market share of the existing market participants. In other words, the aggregator enters the market by adding its offers and bids to the existing offering and bidding curves. Due to the price suppression effect when introducing the aggregator into the market, balancing market prices are modified as follows to guarantee that the aggregator can only sell (purchase) electricity in the balancing market at a price lower (higher) than the DAM price:

$$pr_t^{\text{BM+}} = \min\left\{pr_t^{\text{BM+0}},\ a_1 \cdot (pr_t^{\text{DA}} - p_1)\right\}$$
$$pr_t^{\text{BM-}} = \max\left\{pr_t^{\text{BM-0}},\ a_2 \cdot (pr_t^{\text{DA}} + p_2)\right\}$$

where $pr^{\text{BM-0}}$, $pr^{\text{BM+0}}$ and pr^{DA} are the original negative imbalance, positive imbalance and DA market clearing prices from Nord Pool. Constants a_1 and a_2 are set to 0.8 and 1.2, price adjustments p_1 and p_2 are set to 10 EUR/MWh based on the values provided in [29]. Based on the renewable subsidy scheme published by the Danish Energy Agency in 2017 [110] and considering the fact that the subsidies are subject to further decrease in the future, a conservative subsidy level of 13 EUR/MWh which corresponds to 100 DKK/MWh [15] is assumed when analyzing the impact of subsidies.

5.4.2 Results

The results section consists of three parts. In the first part, a perfect forecast for the wind generation is assumed, which means that only the DAM without a balancing market is considered. Under this assumption, the impacts of market power and subsidies for a wind aggregator and a wind-storage aggregator are analyzed. In addition, the influence of aggregating existing wind producers in the market is investigated. In the second part, the effects of forecast errors are analyzed. and the deviations caused by forecast errors that cannot be balanced by the storage are assumed to be cleared in the balancing market. Finally, in the last part, the value of storage units is investigated by comparing the results with and without the integration of storage units in all simulated cases.

[14] An exception is when analyzing the impact of aggregation, details will be given in the corresponding subsection.

[15] The exchange rate is assumed to be 0.13 EUR/DKK.

All the results shown in this section are from the simulation over 8760 hours of the examined year 2018. No subsidies are considered except in the cases for analyzing the impact of subsidies.

Impacts of market power

In this section, we analyze the impacts of the aggregator's market power by simulating four cases detailed as follows:

- **PT1**: the price-taker case, i.e. the aggregator bids all forecasted output at a price of zero. The aggregator only consists of wind units.
- **PT2**: the price-taker case, i.e. the aggregator bids all forecasted output at a price of zero. The aggregator consists of both wind and storage units.
- **PM1**: the price-maker case, i.e. the aggregator maximizes its profits by optimizing both the bidding price and the quantity, taking into account their impacts on the market. The aggregator only consists of wind units.
- **PM2**: the price-maker case, i.e. the aggregator maximizes its profits by optimizing both the bidding price and the quantity, taking into account their impacts on the market. The aggregator consists of both wind and storage units.

Table 5.2 shows the results for the four cases described above along with the **Base** case, which corresponds to the case without the market participation of the wind-storage aggregator, i.e. the actually realized market results. Social welfare is calculated based on (5.2a), which is equal to the total payoffs of all market participants. The demand satisfaction rate is defined as the ratio of the total dispatched demand quantities to the total demand bidding quantities submitted into the market. The curtailment rate of the aggregator is the ratio of the wind output that is not offered to the market to the total wind outputs. These definitions also apply to the results presented in the following sections.

As wind units have near-zero marginal costs, by introducing the wind-storage aggregator to the market, both the social welfare and the demand satisfaction rate in the system are increased while the average DAM price decreases compared to the Base case.

Comparing the results of the price-maker cases (i.e., PM1 and PM2) to those of the corresponding price-taker cases (i.e., PT1 and PT2), it can be seen that the aggregator achieves higher profits in the price-maker cases. This is because

Table 5.2: Impacts of market power.

Case	Social welfare [mEUR]	Demand satisfaction rate [%]	Average DAM price [EUR/MWh]	Aggregator		
				Profit [mEUR]	Market share [%]	Curtailment [%]
Base	2598.89	98.002	44.04	n/a	n/a	n/a
PT1	2624.34	98.065	42.36	24.68	2.08	0
PT2	2624.34	98.064	42.36	24.69	2.08	0
PM1	2599.52	98.062	42.52	24.82	2.06	1.09
PM2	2599.44	98.060	42.63	25.12	2.06	0.65

the price-maker strategies consider the impact of their offerings and biddings on the market, higher profits are therefore obtained by softening the price decrease using wind curtailments. However, there is limited space for exerting market power as the demand coverage rate is high, in addition the ability of the aggregator to exercise market power is limited by its market share.

Figure 5.3 shows the offering strategies and the resulting Market Clearing Prices (MCPs) of PT2 and PM2 for four selected weeks corresponding to four seasons in 2018, all starting from a Monday[16]. Comparing the MCPs of different seasons, it can be seen that the prices are more volatile and in general lower during the winter and spring weeks [111], which is likely due to the fact that the share of wind generation in Nord Pool (which consists of mainly Nordic countries) is relatively high during winter and spring seasons when the wind blows strongly.

Furthermore, in contrast to the PT2 case, it can be seen that the suppressing effect of the market price caused by the increasing wind penetration can be mitigated by exerting market power in the PM2 case. To be more specific, the aggregator in the PM2 case manages to withhold the generation output to increase the market price when it results in more profits, e.g. the beginning of days 5 and 6 in Fig. 5.3c and the beginning of day 3 in Fig. 5.3d. Results for PT1 and PM1, while are not shown here, are similar to those of PT2 and PM2, respectively. In addition, the results in Table 5.2 show that the integration of storage units helps the aggregator to achieve more profits with less wind outputs being curtailed. However, the difference is negligible in the price-taker case (i.e. PT1 vs. PT2) as storage units are barely used in this case (i.e. PT2).

[16]The market clearing prices on the first days of the winter and the spring weeks are relatively low as they correspond to January 1st and April 2nd in 2018, which are holidays.

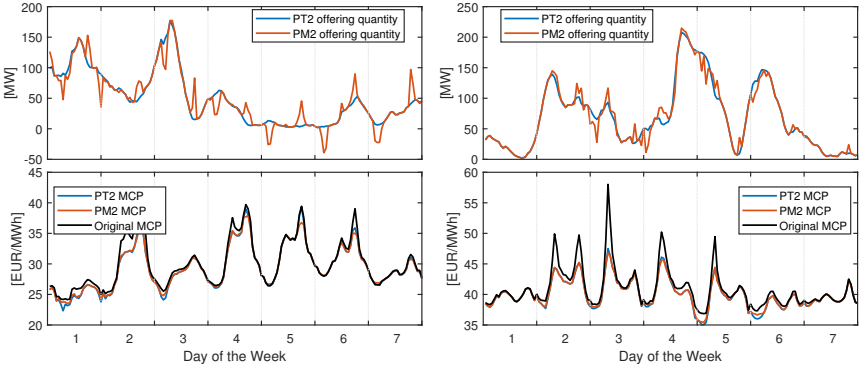

(a) A Winter Week

(b) A Spring Week

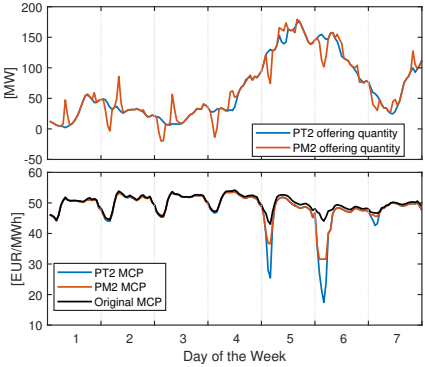

(c) A Summer Week

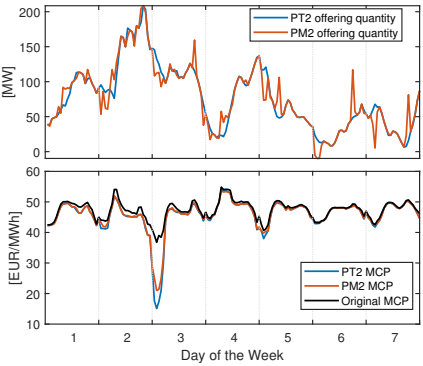

(d) An Autumn Week

Figure 5.3: Comparison of the offering quantities (i.e., top figure) and the resulting market clearing prices of PT2 and PM2 (i.e., bottom figure) for four selected weeks in 2018 corresponding to four seasons. All weeks start from a Monday.

This means that in the case of PT2, making the arbitrage using the price spread between peaks and troughs alone is not sufficient to support profitable battery operations. To better explore how batteries help to make more profits in the price-maker case (i.e. PM2), in Fig. 5.4 the storage operations of PM2 for the same four weeks in 2018 as those presented in Fig. 5.3 are shown. A mutual influence between the storage operations and the MCPs can be observed: on one hand the storage units charge (discharge) during low (high) price periods; on the other hand, the charging/discharging behaviors of the storage units help to smooth the total generation of the aggregator and also the resulting MCP.

Small differences are observed when comparing the results of the four different cases (i.e. PT1, PT2, PM1 and PM2) and this can be explained by the following reasons: 1) the market power of the aggregator is limited by its size, i.e. the market share. Given the maximum hourly load bidding ranging from 2026 MW to 5302 MW and an average capacity factor of wind as 0.28, assuming 98% of the demand is met, the market share for a 250 MW wind power plant ranges from 1.35% to 3.53%; 2) other market suppliers are considered to be non-strategic and most of their offers center on prices around 40 EUR/MWh, which further limits the aggregator's ability to exercise the market power; c) as perfect forecast is assumed for the cases shown in this section, the value of storage is underestimated as it can only be used to shift wind generation from low price to high price periods and to reduce the wind curtailments.

Effects of subsidies

As the aggregator often exerts market power by withholding generation capacity, output-based subsidies are only paid if the generator actually provides generation. Hence, the aggregator needs to balance the usage of market power by withholding output and the receipt of subsidies for production.

Table 5.3: Effects of output-based subsidies.

Case	Social welfare [mEUR]	Average DAM price [EUR/MWh]	Aggregator			
			Profit [mEUR]	Subsidy [mEUR]	Market share [%]	Curtailment [%]
PM1	2599.52	42.52	24.82	n/a	2.06	1.09
PM1sub	2599.59	42.43	24.75	7.98	2.08	0.22
PM2	2599.44	42.63	25.12	n/a	2.05	0.65
PM2sub	2599.46	42.59	25.06	7.97	2.06	0.28

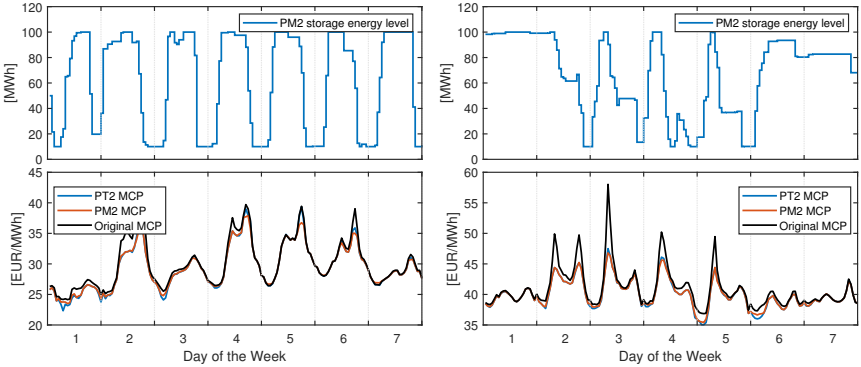

(a) A Winter Week

(b) A Spring Week

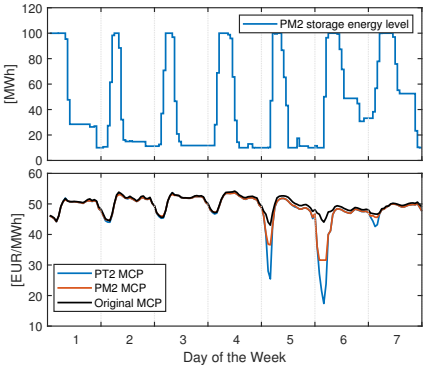

(c) A Summer Week

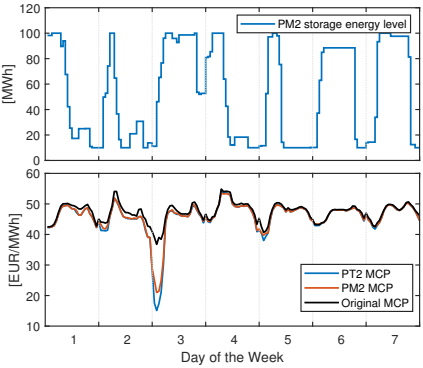

(d) An Autumn Week

Figure 5.4: The top figure shows the storage operations in the case of PM2 for the four selected weeks; the bottom figure illustrates the original market clearing prices and the market clearing prices of PT2 and PM2 for the four selected weeks. All weeks start from a Monday.

In this section, effects of subsidies on the aggregator's bidding strategy and the market results are analyzed by simulating two additional cases, i.e. the price-maker case without and with storage units considering the payment of subsidies, which are named as **PM1sub** and **PM2sub**, respectively. These two cases (i.e., PM1sub and PM2sub) are then compared to the corresponding price-maker cases without subsidies defined before, i.e. PM1 and PM2. As mentioned in Section 5.4.1, a subsidy level of 13 EUR/MWh is assumed for the wind generation. Table 5.3 compares the results of these four cases. It illustrates that less wind is curtailed when considering subsidies, which leads to lower market prices. Moreover, the total social welfare increases in the case considering subsidies, but the increase is negligible when it is compared to the subsidies that are paid to the aggregator.

Effects of the aggregation level

As companies such as Statkraft [112] are working on grouping existing wind, solar and storage units into large virtual power plants, it is thus important to study the impact if some of the existing units in the market are aggregated. In this section, we investigate the impact of aggregating existing wind power plants in the market on these wind power plants' profits and on the market results. It is assumed that the existing wind turbines in the market are the ones that offer near-zero prices. When aggregated, instead of offering at prices zero, they can influence the market by exercising the market power. It is worth noting that instead of introducing new producers to the market as what is simulated in previous sections, the aggregation is assumed to be applied to the existing wind power plants (i.e., the ones that offer near-zero prices) in the system. Furthermore, no storage units are considered in this section.

Table 5.4: Effects of the aggregation level.

Case	Social welfare [mEUR]	Demand satisfaction rate [%]	Average DAM price [EUR/MWh]	Aggregator		
				Profit [mEUR]	Curtailment [%]	Unit profit [EUR/MW]
Base	2598.86	98.002	44.04	n/a	n/a	n/a
PM1agg1	2596.83	98.002	44.05	5.25	0.04	105'036
PM1agg2	2594.76	98.002	44.06	10.51	0.10	105'065
PM1agg3	2592.69	98.002	44.08	15.77	0.17	105'102
PM1agg4	2590.59	98.002	44.12	21.03	0.29	105'160
PM1agg5	2588.42	98.001	44.22	26.32	0.51	105'263

Table 5.4 shows the results considering different aggregation levels, where cases **PM1agg1** to **PM1agg5** correspond to an aggregation of 50 MW to 250 MW of wind capacities with a step of 50 MW. As defined before, the Base case corresponds to the original actually realized market results. The results show that as the aggregation level increases, the market prices increase as the aggregator can better exert market power to its benefit by curtailing more wind outputs, which leads to higher unit profits per MW capacity. Therefore, for units that have near zero marginal costs in the market, such as small wind or PV units, their profits can be increased through aggregation. However, for market operators, as both the demand satisfaction rate and the social welfare in general decrease with the increasing level of aggregation, possible regulations should be introduced to maintain the market efficiency.

Effects of forecast errors

In this section, we investigate the effects of DA wind forecast errors by simulating and comparing the results of the following four cases:

- **Benchmark1**: The aggregator optimizes the biddings to the market with perfect information of the real-time wind generation.
- **Benchmark2**: The aggregator optimizes the biddings to the market according to the original DA wind forecast without considering potential forecast errors at real-time.
- **DRO**: The aggregator optimizes the biddings to the market considering potential forecast errors using an ambiguity set constructed using the historical wind forecast error data over 2014-2017 clustered on a monthly basis[17].
- **DRO_ARMA**: An ARMA model is applied trying to learn the historical forecast error and improve the performance of the model following four steps: a) Build the ARMA model by learning the auto-correlations and the cross-correlations of historical forecast errors; b) Use the ARMA model to generate scenarios of the forecast errors of the next day based on historical data until the the day before; c) Correct the forecast errors using the mean value of the generated forecast error scenarios so as to keep the expectation of the forecast error equal to zero and update the

[17] The statistical properties of the nominal wind forecast errors for the same hour in the same month of the year are assumed to be the same.

Table 5.5: Day-ahead forecast improvements using the ARMA model.

	Mean absolute percentage error [%]	Mean absolute deviation [MW]
Original DA forecast	33.65	1079
ARMA corrected forecast	29.79	1058

DA forecast; d) Similar to case DRO, construct the monthly based ambiguity set based on the corrected forecast errors and then optimizes the offerings and biddings to the market considering potential forecast errors using this updated ambiguity set and the updated forecast.

ARMA model is applied to generate scenarios of the wind forecast error as it can capture the cross-correlations of the data and generate numerous sample paths of the wind forecast errors while retaining the same probabilistic properties, such as the variance of the error and the distribution of the length of the crossing-time distributions [113]. Implementations of the ARMA model to simulate wind forecast errors can be found in a lot of works such as [113, 114, 115]. Same as the model simulated in [115, 116], a simple ARMA(1,1) model is applied since increasing the order of the model does not substantially improve the results. However, the results might be different when different wind datasets are used. Comparison of the performance of the forecast before and after using the ARMA model is illustrated in Table 5.5.

Results of the above described four cases with and without considering the integration of storage units are shown in Table 5.6. For each case, the uncertainty capture rate is calculated as the ratio of the aggregator's profits in this case to the aggregator's profits in the corresponding Benchmark1 case, i.e. the perfect information case. Note that the results of Benchmark1 without/with storage units differ from the results of case PM1/PM2 under perfect information shown in the previous sections as the balancing market is considered in Benchmark1 case and the arbitrage between the DAM and balancing market is allowed, which is however limited due to unfavorable imbalance prices. Comparing the results of Benchmark2, DRO and DRO_ARMA, it can be seen that DRO_ARMA achieves the highest profits, which is mainly due to the decrease of imbalance costs. Moreover, compared to Benchmark2, both DRO and DRO_ARMA consider the potential forecast errors and do not overbid into

Table 5.6: Impact of the forecast error.

Results without Storage Units					
Case	**Avg. DAM price [EUR/MWh]**	**DAM profit [mEUR]**	**BM profit [mEUR]**	**Tot. profit [mEUR]**	**Uncertainty capture [%]**
Benchmark1	42.76	22.90	1.34	24.24	100
Benchmark2	42.48	25.05	-2.30	22.74	93.83
DRO	42.64	24.91	-2.04	22.86	94.32
DRO_ARMA	42.68	23.96	-0.94	23.02	94.96

Results with Storage Units					
Case	**Avg. DAM price [EUR/MWh]**	**DAM profit [mEUR]**	**BM profit [mEUR]**	**Tot. profit [mEUR]**	**Uncertainty capture [%]**
Benchmark1	42.82	23.83	0.97	24.80	100
Benchmark2	42.60	25.35	-1.72	23.62	95.27
DRO	42.73	25.16	-1.44	23.73	95.68
DRO_ARMA	42.78	24.15	-0.27	23.88	96.30

the DAM, therefore the DAM prices in these two cases are higher, resulting in relatively higher profit for each MW bidding into the DAM. When using the ARMA model to learn the forecast error and then simulate the future path of the forecast errors, significant improvements of the results can be observed.

Value of storage units

In this section, the value of integrating storage units are analyzed by comparing the cases with and without storage units analyzed in the previous sections. As stated, storage units can contribute to increasing the aggregator's profits by: 1) charging and discharging to alleviate the price suppressing effect caused by wind penetration, as illustrated in the section to analyze the impact of market power; 2) reducing the imbalances due to forecast errors through real-time operations. These two effects can be verified by Fig. 5.5, which shows the real-time storage operations as well as the DA market clearing prices of an example week of the simulation year in the DRO case. It can be seen that in general the battery mainly discharges in the morning when the market price peaks and charges at night when the DAM prices are relatively low. In addition, the charging/discharging behaviors are also influenced by the wind forecast errors. For example, on day 4 of the example week, the battery charges in the afternoon and discharges at night so as to possibly alleviate the impacts of wind forecast errors, although the market prices in the afternoon are relatively higher than the prices at night.

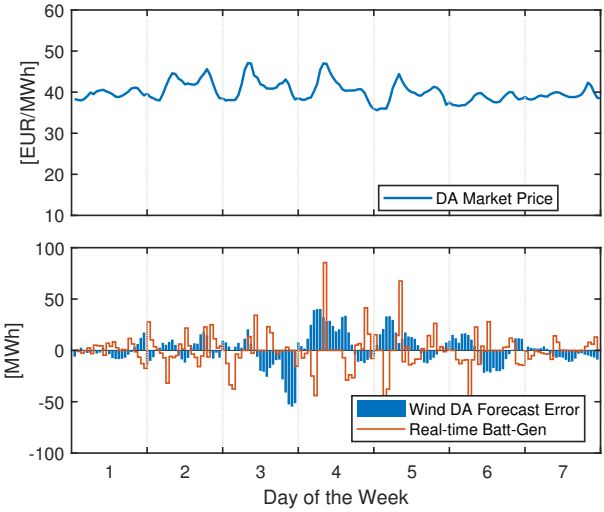

Figure 5.5: The real-time battery operations along with the day-ahead market price and the day-ahead wind forecast error of the DRO case over an example week. The battery operations are influenced by both the day-ahead market prices and the day-ahead wind forecast errors.

To better quantify the benefits of integrating storage units, the profits of different cases with and without storage units in Table 5.2 and Table 5.6 are listed again in Table 5.7, where the first row corresponds to the results of the PM1 and PM2 cases in Table 5.2, the second to the fifth rows correspond to the results in Table 5.6. Furthermore, as it is interesting to know whether it is profitable to invest in storage units, i.e. if the benefits justify the investment, the value of storage and the maximum acceptable investment cost of the storage units are calculated to answer this question. The value of per kWh storage val_s^{unit} equals the yearly profit difference between the corresponding case with and without storage divided by the capacity of the storage unit. The maximum acceptable investment cost c_s^{inv} for the storage unit is calculated by

$$c_s^{\text{inv}} = val_s^{\text{unit}} \frac{1 - 1/(1+r)^{lt}}{r} \tag{5.23}$$

Table 5.7: Comparison of the aggregator's profits in cases with and without storage units along with the resulting maximum acceptable investment cost of the storage unit.

Case	Profit without storage [mEUR]	Profit with storage [mEUR]	Value per unit storage [EUR/kWh/year]	Max. acceptable investment cost [EUR/kWh]
PM	24.82	25.12	3.03	31.42
Benchmark1	24.24	24.80	5.59	58.03
Benchmark2	22.74	23.62	8.81	91.47
DRO	22.86	23.73	8.66	89.91
DRO_ARMA	23.02	23.88	8.63	89.58

where r and lt denote the discount rate and the storage unit's lifetime, which are assumed to be 5% and 15 years, respectively.

Comparing the results of different cases, it is obvious that the profits of the aggregator increase when integrating storage units. PM and Benchmark 1 cases are under the assumption of perfect information, while forecast errors are simulated for the Benchmark2, DRO and DRO_ARMA cases. Comparing the value of per unit storage of these two groups of cases, it can be seen that the storage unit plays an important role in reducing the imbalance costs as the unit profit is more than doubled or almost doubled when accounting for forecast errors, depending on whether taking PM or Benchmark 1 as the reference case. Moreover, the corresponding maximum acceptable unit investment cost reaches a level of 90 EUR/kWh, which is below the current cost of the 1-hour utility-scale battery storage (i.e. 601 USD/kWh) [117] and requires a significant decrease. However, considering the multi-applications of the storage units such as the additional participation in the reserve market and the trend of decreasing battery prices, investments in battery storage could still possibly be profitable in the not so distant future or even today [118].

5.5 Limitations and Future Work

This work has several limitations and a few of which are highlighted in this section. First, the statistical information of the wind forecast errors for the wind aggregator is calculated based on the historical Denmark wind data at the country level, without accounting for the fact that in general the forecast errors can be reduced when aggregating the data from multiple sites. The work in [44]

identifies the statistical smoothing effects when aggregating wind generation data for a region with spatially distributed wind farms, and it is found that the improvement of the prediction is noticeable even for small regions and only few sites. Future work should model the locations and the sizes of the wind power plants within the aggregator in a more realistic way and use a dataset that is consistent with the modeled locations and sizes.

Second, the balancing market prices are assumed to be independent of the aggregator's imbalance positions. However, this assumption might not be valid when the aggregator accounts for a significant share in the market. In other words, with the increasing market share of the aggregator, the influence of the aggregator's imbalance positions on the balancing market prices cannot be neglected. Future work should include modeling the mutual influences of the forecast errors of the aggregator and the balancing market prices.

Third, the total wind capacity and the storage energy capacity are fixed, i.e. they are not optimized. Furthermore, the C-rate of the storage units are fixed to be one-hour. Nevertheless, the resulting profits of the aggregator and the resulting values of integrating the storage units might change when different assumptions regarding the wind and storage capacities are made. A future version should interface the presented model with an investment model that aims to optimize the size of each unit. The second part of the thesis will focus on optimizing the investment decisions of an aggregator in a market environment.

5.6 Summary and Conclusions

A stochastic distributionally robust optimization model to derive optimal bidding strategies for a wind-storage aggregator is presented in this chapter. Compared to the price-taker strategy, the price-maker strategy can achieve higher profits as it considers the potential impacts on the market. The integration of storage units can further strengthen this effect. Furthermore, numerical results suggest that considering the output-based subsidies reduces the aggregator's motivation to exert market power, which increases the resulting social welfare. However, the increase in social welfare is not comparable to the subsidies paid to the power plants. When simulating the cases of aggregating existing wind power plants in the system, results show that higher aggregation levels result in

higher unit revenues, but at the cost of a decrease in social welfare and the demand satisfaction rate. The analysis of the forecast uncertainty shows that the proposed distributionally robust optimization model can achieve higher profits than the benchmark case of bidding at the day-ahead forecast. Additionally, the application of the ARMA model can further improve the performance of the model.

Part II

Stochastic Investment Optimization in a Market Environment

Chapter 6

Investment Optimization considering Joint Reserve and Energy Market Participation

In this chapter, an optimization model is presented to optimize the generation mix and the operations of a distributed energy resource aggregator jointly to satisfy the demand and policy targets while minimizing the total costs. The components considered in the aggregator include the distributed storage units, demand response programs, variable and dispatchable generation units. In order to better exploit the economic value of the distributed energy resources, their participation in reserve and energy markets is considered. As the investment and market bidding decisions are made sequentially, a multi-stage stochastic programming model is formulated to minimize the sum of the long-term investment cost and the short-term cost. The latter includes the fixed and variable operating cost, fuel costs, emission cost, and market participation cost. A case study demonstrates the effectiveness of the proposed model, shows the benefits of market participation and coordinated bidding, analyzes the impact of different reserve market products, and finally investigates the influences of the policy targets and demand response programs. This chapter is based on [119].

6.1 Introduction

6.1.1 Motivation and Related Work

The potential demand gap that is mainly due to the policies such as nuclear or coal phase-out urgently requires new generation investments in power systems. Driven by favorable government policies and ambitious renewable generation penetration and emission reduction targets, the electricity industry worldwide is experiencing three major changes: electrification, decentralization and digitization. All these trends provide opportunities to invest in Distributed Energy Resources (DERs) including the Demand Response Programs (DRPs). On the one hand it is beneficial to the system as it reduces grid losses and possibly decreases or defers capacity investments, on the other hand it provides customers more economical energy solutions and chances to make profits by participating in the supply and demand balancing process. These effects are strengthened by the ongoing decrease in costs of DERs such as Photovoltaic (PV) or storage units. In order to fully utilize the economic value of DERs' investments, aggregation is of great interest as it enables DERs to participate in the electricity markets and to provide grid services (e.g. reserve provision). Without considering the possibility of energy arbitrage and reserve provisions, values of DER investments are underestimated. As lots of system operators such as California Independent System Operator (CAISO) have already implemented rules or consider to do so to allow DERs' market participation, it is important to address the research question of what would be the optimal generation mix and operational decisions of DERs considering their participation in the markets.

With the increasing penetration of DERs such as storage devices, wind and PV generation units in recent years, modern generation expansion planning models of DERs are more complex and focus on one or the coordinated planning of several DER technologies. For example, [120] and [121] investigate the effects of electric vehicles' penetration. References [122] and [123] focus on the integration of Demand Response (DR), while [124] and [125] consider the incorporation of both DR and storage investments. In [126,127,128], approaches for planning and operating renewable energies and storage devices are proposed whereas in [129] a planning method to decide on optimal locations, sizes and

mix of both dispatchable and intermittent distributed generation is presented, with renewable outputs' uncertainties incorporated using robust optimization. The authors of [130] propose a method that considers a comprehensive configuration of microgrids with DRP, considering solar, wind and battery as the candidate technologies. As a result, most of the existing models only target the optimization of investment decisions considering limited options of candidate technologies and without considering their participation in electricity markets. However, because of the uncertain nature of variable generation outputs, it is important to consider the coordination of different units already in the planning phase to support their integration. Furthermore, as DERs are expected to participate in markets and contribute flexibility, it is important to consider their market participation to exploit the economic value of DER investments.

Furthermore, limited by the computational complexity, traditional generation expansion planning models often adopt the sliced load duration curve [131] to approximate the temporal characteristics of the load profile. Despite the computational tractability, this method on one hand cannot preserve the chronology to reflect the correlation of demand and variable generation outputs; on the other hand it does not allow the modeling of the inter-temporal operational decisions (e.g. operations of storage units). As shown in [132, 133], the temporal details have a significant impact on investment decisions and the impacts increase with the increasing share of Renewable Energy Sources (RESs). Although attempts have been made to model the variations in demand and supply while maintaining the computational efficiency by using representative days [134, 135], the number of the days are limited and they are often selected using some simple heuristics.

Consequently, the goal of this chapter is to optimize the investment decisions of a DER aggregator by optimizing the operational decisions over the full 8760 hours for each examined year. The aggregator is assumed to have access to both the reserve and the energy markets.

6.1.2 Chapter Organization

The remainder of this chapter is organized as follows: the problem description and the main modeling assumptions are given in Section 6.2, mathematical formulations and the proposed optimization model are presented in Section

6.3. Section 6.4 presents the results of a case study. Limitations and future work are discussed in Section 6.5. Finally, conclusions are drawn in Section 6.6.

6.2 Problem Description and Model Assumptions

The considered investment model aims to optimize the investment decisions of a distributed energy resources mix for an examined year (i.e., 2020, 2030, 2040 and 2050) using an hourly resolution. Given the electricity market prices, the model trades-off between investing in local distributed energy resources and purchasing electricity from the wholesale market to satisfy the demands and the policy targets, while minimizing the total costs. The trade-off is realized by jointly optimizing the investments and operations of a DER aggregator considering different types of storage units, variable and dispatchable generation units, and the DRP, while taking the participation into the energy and reserve markets into consideration. The planner, which also acts as an aggregator, is assumed to have full control over all units and have access to demand response. It integrates the characteristics of diverse units into a single entity and generates a single dispatch portfolio. Aggregation is done to take advantage of a variety of DERs and to contribute efficiently to covering the flexibility needs of the system. To lower the computational burden, a static planning for a particular year is modeled.

Similar to the Swiss market structure, it is assumed that the reserve capacity market is cleared one-week ahead, while the energy market is cleared one day ahead. The aggregator acts as a price-taker and a uniform pricing scheme is assumed in both markets. Given the market prices as inputs, the optimal decisions to be made are the purchase/sale from/to the energy market and the optimal capacity bidding into the reserve market. The real-time reserve activation is simulated using the historical activation rate. Note that all units except for the variable generation units are assumed to be able to provide reserves.

The structure of the multi-stage optimization model is:

- 1st stage: The aggregator optimizes investment decisions for the examined year (i.e. how much should be invested for each type of units).
- 2nd & 3rd stage: The second and the third stages correspond to two markets: reserve and energy markets. Following a realistic market structure, the aggregator first decides its bids into the reserve market and then to the energy

market. All units are assumed to participate in the Day-ahead (DA) energy market and all units except variable generation units are assumed to have access to the reserve market. Note that only a general form of reserve is considered in this work.

- 4th stage: Finally, re-dispatch occurs due to reserve activation at real-time, while deviations caused by DA variable generation forecast errors are cleared in the balancing market.

The main modeling assumptions considered in this chapter are summarized as follows:

- The aggregator is assumed to have access to both the energy and the reserve markets, and only a general form of reserve is considered. Participation in the long-term future markets is not considered.
- To limit the computational complexity, a static investment model for a particular year is simulated. Furthermore, a green-field investment is modeled for each examined year, i.e. investments in previous years are not considered.
- Uncertainties regarding wind and PV outputs are incorporated using robust optimization.
- No subsidies such as the investment subsidies or feed-in tariffs for renewables are modeled.
- It is assumed that the investment decisions are made by a central planner, i.e. the aggregator. Although it might not be the case in reality, the results could offer the aggregator and the policy-makers the insights about what would be the optimal generation mix in terms of the cost considering the given demand and policy targets [136].

6.3 Mathematical Formulation

In this section, we first describe the constraints for each stage of the multi-stage stochastic optimization problem, then we present the overall objective function and the final optimization problem.

1st-stage Constraints

For the examined investment year, the investment capacity x_i^{inv} in candidate unit type i has to be non-negative:

$$0 \leq x_i^{\text{inv}}, \quad \forall i \in I \tag{6.1}$$

where I is the set of candidate unit types.

2nd- and 3rd-stage Constraints

Since only uncertainties in the DA forecast of variable generation are considered, both the week-ahead reserve capacity bidding and the day-ahead energy bidding are optimized taking into account the day-ahead variable generation forecasts.

Dispatchable Generation Unit We use G to indicate the set of dispatchable generation unit types. The DA scheduled output $p_{g,t}^{\text{da}}$ at time t of dispatchable generation unit type g with $g \in G$ considering the full downward reserve capacity activation is non-negative, while the maximum output considering the full upward reserve capacity activation is limited by the invested capacity x_g^{inv}. Mathematically,

$$p_{g,t}^{\text{da}} - q_{g,t}^{\text{RD}} \geq 0 \tag{6.2}$$

$$p_{g,t}^{\text{da}} + q_{g,t}^{\text{RU}} \leq x_g^{\text{inv}} \tag{6.3}$$

$$q_{g,t}^{\text{RU}},\ q_{g,t}^{\text{RD}} \geq 0 \tag{6.4}$$

where q_g^{RU} and q_g^{RD} denote the upward and downward reserve capacity contributed by the dispatchable generation unit g, respectively.

Variable Generation Unit The DA output $p_{v,t}^{\text{da}}$ of variable generation unit v where $v \in V$ is non-negative and limited by the product of the investment capacity and the generation forecasts in percentage $p_{v,t}^{\text{f}}$:

$$0 \leq p_{v,t}^{\text{da}} \leq x_v^{\text{inv}} p_{v,t}^{\text{f}} \tag{6.5}$$

It is assumed that variable generation output can be curtailed with a direct cost of zero.

Battery Storage Unit Let S denote the set of candidate storage unit types. The DA scheduled stored energy $E_{s,t}^{\text{da}}$ of the storage unit s with $s \in S$ at time t is non-negative and limited by the invested battery energy capacity x_s^{inv}, while the initial stored energy is set by (6.7). The relationship of the energy storage levels of two consecutive time steps is defined by (6.8), with DA charging and discharging powers denoted by $p_s^{\text{ch,da}}$ and $p_s^{\text{dis,da}}$, respectively.

$$0 \leq E_{s,t}^{\text{da}} \leq x_s^{\text{inv}} \tag{6.6}$$

$$E_{s,1}^{\text{da}} = E_s^{\text{ini}} x_s^{\text{inv}} \tag{6.7}$$

$$E_{s,t}^{\text{da}} = (1-\zeta_s) E_{s,t-1}^{\text{da}} + \eta_s p_{s,t}^{\text{ch,da}} \Delta t - \eta_s^{-1} p_{s,t}^{\text{dis,da}} \Delta t \tag{6.8}$$

where Δt is the time step length, ζ_s and η_s indicate the self-discharging rate and one-way efficiency.

To ensure that the charging and discharging powers of the battery units are within the limits in the case of full up-/downward reserve capacity activation, constraints (6.9) and (6.10) are defined. More specifically, the sum of the DA charging minus the discharging plus the activation of the full downward reserve capacity q_s^{RD} is limited by the maximum charging power $p_s^{\text{ch,max}}$, while the sum of the DA discharging minus charging plus the activation of the full upward reserve capacity q_s^{RU} is limited by the maximum discharging power $p_s^{\text{dis,max}}$. Furthermore, constraints (6.11) and (6.12) guarantee that the stored energy of the storage unit is within the range in case of full reserve activation occurs, where τ^{RM} is the duration of reserve provision. Mathematically,

$$p_{s,t}^{\text{ch,da}} - p_{s,t}^{\text{dis,da}} + q_{s,t}^{\text{RD}} \leq p_s^{\text{ch,max}} x_s^{\text{inv}} \tag{6.9}$$

$$p_{s,t}^{\text{dis,da}} - p_{s,t}^{\text{ch,da}} + q_{s,t}^{\text{RU}} \leq p_s^{\text{dis,max}} x_s^{\text{inv}} \tag{6.10}$$

$$E_{s,t}^{\text{da}} - \tau^{\text{RM}} \eta_s^{-1} q_{s,t}^{\text{RU}} \geq 0 \tag{6.11}$$

$$E_{s,t}^{\text{da}} + \tau^{\text{RM}} \eta_s q_{s,t}^{\text{RD}} \leq x_s^{\text{inv}} \tag{6.12}$$

$$p_{s,t}^{\text{ch,da}},\ p_{s,t}^{\text{dis,da}},\ q_{s,t}^{\text{RU}},\ q_{s,t}^{\text{RD}} \geq 0 \tag{6.13}$$

Different from other units, in the case that only upward-reserve or downward-reserve is activated over a period of time, the cumulative effects of continuous discharging or charging would result in an empty or a fully-charged battery in extreme cases, which does not allow the further discharging or charging. To guarantee the reserve provision in these cases, additional constraints are enforced to limit the day-ahead scheduled energy stored in the battery to be within an energy band $[E^{\text{self,min}}, E^{\text{self,max}}]$, and in addition to limit the reserve capacity $q_{s,t}^{\text{RU/RD}}$ provided by the storage to only a fraction β^{res} of the maximum charging/discharging power [137], i.e.,

$$E_s^{\text{self,min}} x_s^{\text{inv}} \leq E_{s,t}^{\text{da}} \leq E_s^{\text{self,max}} x_s^{\text{inv}} \tag{6.14}$$

$$0 \leq q_{s,t}^{\text{RU}} \leq p_s^{\text{dis,max}} \beta_s^{\text{res}} x_s^{\text{inv}} \tag{6.15}$$

$$0 \leq q_{s,t}^{\text{RD}} \leq p_s^{\text{ch,max}} \beta_s^{\text{res}} x_s^{\text{inv}} \tag{6.16}$$

Load To ensure the full reserve capacity to be provided by the load unit l for each time step, the absolute value of the day-ahead load shifting $l^{\text{sh,da}}$ plus/minus the downward/upward reserve $q_l^{\text{RD/RU}}$ is limited to the maximum hourly load shifting, which is defined as a fraction $\beta^{\text{sh,max}}$ of the load estimation l^{est}. Furthermore, the load consumption for each day starting at time t_0 are required to be constant before and after the shifting. Mathematically,

$$l_t^{\text{sh,da}} - q_{l,t}^{\text{RU}} \geq -\beta^{\text{sh,max}} l_t^{\text{est}} \tag{6.17}$$

$$l_t^{\text{sh,da}} + q_{l,t}^{\text{RD}} \leq \beta^{\text{sh,max}} l_t^{\text{est}} \tag{6.18}$$

$$\sum_{t=t_0}^{t_0+24} l_t^{\text{sh,da}} = 0 \tag{6.19}$$

$$q_{l,t}^{\text{RU}},\ q_{l,t}^{\text{RD}} \geq 0 \tag{6.20}$$

Policy Constraints A self-sufficiency rate target β^{ss} and a renewable target β^{res} are set to guarantee that a certain amount of the load is served by local

generation and local renewable resources, i.e.

$$\sum_{t=1}^{T}\sum_{i\in I} p_{i,t}^{\text{da}} \geq \beta^{\text{ss}} \sum_{t=1}^{T} l_t^{\text{est}} \tag{6.21}$$

$$\sum_{t=1}^{T}\sum_{i\in I^{\text{res}}} p_{i,t}^{\text{da}} \geq \beta^{\text{res}} \sum_{t=1}^{T} l_t^{\text{est}} \tag{6.22}$$

where I^{res} is the set of the renewable unit categories.

Power Balance Constraint For each time step, the DA bidding quantity q^{DA} needs to equal the DA scheduled generation of all units minus the sum of the load estimation and the scheduled load shifting, i.e.

$$\sum_{g\in G} p_{g,t}^{\text{da}} + \sum_{v\in V} p_{v,t}^{\text{da}} + \sum_{s\in S}(p_{s,t}^{\text{dis,da}} - p_{s,t}^{\text{ch,da}}) - (l_t^{\text{est}} + l_t^{\text{sh,da}}) = q_t^{\text{DA}} \tag{6.23}$$

Market Constraints The power that is exchanged between the aggregator and the system considering the reserve provision is set to be limited by the transformer capacity. As the transformer is rarely fully loaded in reality for security reasons, the transformer capacity is estimated by the aggregator's peak demand $l^{\text{est,max}}$ multiplied by a factor γ^{ex} that is greater than one, i.e.

$$q_{g,t}^{\text{RU}} + q_{s,t}^{\text{RU}} + q_{l,t}^{\text{RU}} = q_t^{\text{RU}} \tag{6.24}$$

$$q_{g,t}^{\text{RD}} + q_{s,t}^{\text{RD}} + q_{l,t}^{\text{RD}} = q_t^{\text{RD}} \tag{6.25}$$

$$q_t^{\text{RU}} + q_t^{\text{DA}} \leq \gamma^{\text{ex}} l^{\text{est,max}} \tag{6.26}$$

$$q_t^{\text{RD}} - q_t^{\text{DA}} \leq \gamma^{\text{ex}} l^{\text{est,max}} \tag{6.27}$$

In addition, the reserve bidding capacity is generally required to to be provided for a certain period of time (e.g. one week):

$$q_t^{\text{RU}} = q_{t_0^{\text{res}}}^{\text{RU}} \quad \text{for} \quad \forall t \in [t_0^{\text{res}}, t_0^{\text{res}} + \Delta^{\text{res}}] \tag{6.28}$$

$$q_t^{\text{RD}} = q_{t_0^{\text{res}}}^{\text{RD}} \quad \text{for} \quad \forall t \in [t_0^{\text{res}}, t_0^{\text{res}} + \Delta^{\text{res}}] \tag{6.29}$$

where t_0^{res} is the starting time point of each reserve bidding period and Δ^{res} is the minimum time length of the reserve provision. Moreover, constraint (6.30) needs to be enforced if the reserve bidding is required to be symmetric.

$$q_t^{\text{RU}} = q_t^{\text{RD}} \tag{6.30}$$

4th-stage Constraints

At real-time, re-dispatch is required due to the realization of day-ahead variable generation forecast error δ and the upward/downward reserve activation $q_i^{\text{RUact/RDact}}$ for unit i with $i \in \{s, l, g\}$. Therefore, real-time dispatchable generation p_g, load l and variable generation p_v are given by

$$p_{g,t} = p_{g,t}^{\text{da}} + q_{g,t}^{\text{RUact}} - q_{g,t}^{\text{RDact}} \tag{6.31}$$

$$l_t = l_t^{\text{est}} + l_t^{\text{sh,da}} + q_{l,t}^{\text{RDact}} - q_{l,t}^{\text{RUact}} \tag{6.32}$$

$$0 \leq p_{v,t} \leq x_v^{\text{inv}}(p_{v,t}^{\text{f}} + \delta_{v,t}) \tag{6.33}$$

where the variable generation is assumed to be curtailed at a cost of zero. Similarly, the real-time storage charging p_s^{ch}, discharging p_s^{dis} and the storage level E_s are defined as follows:

$$0 \leq E_{s,t} \leq x_s^{\text{inv}} \tag{6.34}$$

$$0 \leq p_{s,t}^{\text{ch}} \leq p_s^{\text{ch,max}} x_s^{\text{inv}} \tag{6.35}$$

$$0 \leq p_{s,t}^{\text{dis}} \leq p_s^{\text{dis,max}} x_s^{\text{inv}} \tag{6.36}$$

$$p_{s,t}^{\text{dis}} - p_{s,t}^{\text{ch}} = p_{s,t}^{\text{dis,da}} - p_{s,t}^{\text{ch,da}} + q_{s,t}^{\text{RUact}} - q_{s,t}^{\text{RDact}} \tag{6.37}$$

$$E_{s,1} = E_s^{\text{ini}} x_s^{\text{inv}} \tag{6.38}$$

$$E_{s,t} = (1 - \zeta_s) E_{s,t-1} + \eta_s p_{s,t}^{\text{ch}} \Delta t - \eta_s^{-1} p_{s,t}^{\text{dis}} \Delta t \tag{6.39}$$

Note that limitations on the constant daily load consumption is not required at real-time, since reserve activation is generally small, almost symmetric over long-time and hardly predictable. Moreover, adding the constraint may result in extra imbalance costs that should not be undertaken by reserve providers.

The real-time power balance equation

$$\sum_{g\in G} p_{g,t} + \sum_{v\in V} p_{v,t} + \sum_{s\in S} (p_{s,t}^{\text{dis}} - p_{s,t}^{\text{ch}}) - l_t = q_t^{\text{DA}} + q_t^{\text{BM}} + q_t^{\text{RUact}} - q_t^{\text{RDact}} \tag{6.40}$$

ensures that the sum of the market exchange equals the real time generation of all units minus the final load. In this equation, we have used

$$q_t^{\text{BM}} = q_t^{\text{BM+}} - q_t^{\text{BM-}} \text{ with } q_t^{\text{BM+}}, q_t^{\text{BM-}} \geq 0 \tag{6.41}$$

$$q_t^{\text{RDact}} = q_{l,t}^{\text{RDact}} + q_{g,t}^{\text{RDact}} + q_{s,t}^{\text{RDact}} \tag{6.42}$$

$$q_t^{\text{RUact}} = q_{l,t}^{\text{RUact}} + q_{g,t}^{\text{RUact}} + q_{s,t}^{\text{RUact}} \tag{6.43}$$

where $q^{\text{BM+}}$ and $q^{\text{BM-}}$ are the positive and negative imbalances. The reserve activation is modeled as the product of the reserve bidding capacity and the corresponding historical reserve activation rate.

Objective

The objective of the problem is to minimize the sum of the annualized investment cost C^{inv}, the fixed and variable operating costs C^{foc} and C^{voc}, the day-ahead energy market costs C^{DAM}, the reserve market costs C^{RM} and the balancing market costs C^{BM} over the simulation horizon, i.e.

$$C^{\text{inv}} = \sum_{i\in I} \alpha_i^{\text{ann}} c_i^{\text{inv}} x_i^{\text{inv}} \tag{6.44}$$

$$C^{\text{foc}} = \sum_{i\in I} c_i^{\text{foc}} x_i^{\text{inv}} \tag{6.45}$$

$$C_t^{\text{voc}} = \sum_{i\in I} (c_i^{\text{voc}} + c_i^{\text{fuel}}) p_{i,t} \tag{6.46}$$

$$C_t^{\text{DAM}} = -pr_t^{\text{DA}} q_t^{\text{DA}} \tag{6.47}$$

$$C_t^{\text{RM}} = -pr_t^{\text{cRU}} q_t^{\text{RU}} - pr_t^{\text{cRD}} q_t^{\text{RD}} - pr_t^{\text{aRU}} q_t^{\text{RUact}} + pr_t^{\text{aRD}} q_t^{\text{RDact}} \tag{6.48}$$

$$C_t^{\text{BM}} = -pr_t^{\text{BM+}} q_t^{\text{BM+}} + pr_t^{\text{BM-}} q_t^{\text{BM-}} \tag{6.49}$$

where investment, fuel, fixed and variable operating cost parameters are denoted by c^{inv}, c^{fuel}, c^{foc} and c^{voc}, while pr^{DA}, $pr^{\text{cRU/D}}$, $pr^{\text{aRU/D}}$ and $pr^{\text{BM+/-}}$ are the day-ahead market, reserve capacity, reserve energy and positive/negative

imbalance price parameters. Note that the reserve market costs comprise the costs related to the procurement of the reserve capacity and the costs related to the reserve energy activation. Parameter α^{ann} is the annuity factor computed by $\frac{r}{1-1/(1+r)^{lt}}$ with r and lt denoting the Weighted Average Cost of Capital (WACC) and the candidate unit's lifetime. Finally, the optimization problem can be written as:

$$\begin{aligned} &\min\ C^{\text{inv}} + C^{\text{foc}} + \alpha^{\text{d}} \sum_{t=1}^{T} (C_t^{\text{voc}} + C_t^{\text{DAM}} + C_t^{\text{RM}} + C_t^{\text{BM}}) \\ &\text{s.t.}\quad \text{Constraints (6.1)-(6.49)} \end{aligned} \tag{6.50}$$

where T is the total number of hours of all selected days and α^{d} equals the number of days of the examined year divided by the number of representative days. In this work, we optimize the investment and operational decisions considering the full 8760 hours of the year, α^{d} is therefore equal to one.

6.4 Case Study

6.4.1 Input Data

The case study is simulated using the 2018 load and price data published by Elia (Belgium's electricity system operator) [138]. The cost parameters for the considered unit types of the aggregator are listed in Table 6.1. The initial storage level of the battery is set to 50%. Note that the costs shown in Table 6.1 are given as ranges since they vary according to the considered investment year (i.e., 2020, 2030, 2040 and 2050). Details of the costs over all considered investment years are provided in Appendix 9.3.

Input parameters modeled in the Baseline scenario as well as the sensitivity scenarios including electricity market prices and the WACC assumption are summarized in Table 6.2. The total Elia grid demand is scaled down by a factor of 0.003 to serve as the simulated demand of the aggregator and the resulting hourly peak and minimum load for simulation are 39.7 MW and 20.5 MW, respectively.

Table 6.1: Parameters of candidate units.

Category	Unit type	Parameter	Adopted value	Source
Variable Generation Unit	**PV**	Investment cost	677'000~1'481'000 EUR/MW	[2]
		Fixed operational cost	5'000~10'000 EUR/MW-year	[2]
		Variable operational cost	0 EUR/MWh	[2]
		Lifetime	30 years	[2]
	Wind (land-based)	Investment cost	1'458'000 ~2'219'000 EUR/MW	[2]
		Fixed operational cost	28'000~36'000 EUR/MW-year	[2]
		Variable operational cost	0 EUR/MWh	[2]
		Lifetime	30 years	[2]
Battery Storage Unit	**Battery (2-hour)**	Investment cost	154'000~364'000 EUR/MWh	[2]
		Fixed operational cost	13'000~31'000 EUR/MW-year	[2]
		Lifetime	15 years	[2]
		Depth of discharge	100%	[2]
		Roundtrip efficiency	85%	[2]
		Lifetime	15 years	[2]
Dispatchable Generation Unit	**CHP**	Investment cost	1'346'000~1'564'000 EUR/MWp	[3]
		Fixed operational cost	0 EUR/MW-year	[3]
		Variable operational cost	16~17 EUR/MWh	[3]
		Fuel cost	56~110 EUR/MWh	[3]
		Electrical efficiency	0.37~0.40	[3]
		Thermal efficiency	0.47~0.50	[3]
		Boiler efficiency	0.75	[139]
		Gas price	86~117 EUR/MWh	[3]
		Lifetime	20 years	[3]

Original values are converted to Euros based on the exchange rates of 0.91 EUR/CHF and 0.85 EUR/USD.
Fuel cost for Combined Heat and Power (CHP) units are calculated based on the equation from [139], i.e. $\frac{pr^{\text{gas}}}{\eta^{\text{e}}}(1 - \frac{\eta^{\text{th}}}{\eta^{\text{b}}})$, where pr^{gas}, η^{e}, η^{th}, η^{b} are the gas price, the electrical, thermal and the boiler efficiencies of the CHP unit.

6.4.2 Results

In this section, we first validate the effectiveness of the proposed model by analyzing the results of the Baseline scenario. Then to account for the uncertainties that our results are subject to, we conduct a set of one-at-a-time sensitivity analyses related to market participation, reserve bidding requirement, policy targets, the demand response shifting potential and the forecast error respectively, while keeping the remaining parameters equal to the Baseline scenario values. Note that as the considered investment model is static and aims to minimize the total cost for the examined year, all costs or profits shown in this section are the annualized values.

Analysis of the Baseline Scenario

In the Baseline scenario, we run the model assuming the investment year as 2020, 2030, 2040 and 2050, respectively. More specifically, we run the static

Table 6.2: Input parameters and market prices for modeling.

Parameter	Baseline value	Sensitivity analysis	Source
Self-sufficiency target	80%	0~100%	n/a
Renewable target	50%	0~100%	n/a
Worst-case nominal DA forecast error	0%	0~40%	n/a
Transmission limit	120 % of peak demand	n/a	n/a
Time length of reserve product	168 hrs	4, 8, 16, 24, 168 hrs	Elia
Symmetry of reserve product	Symmetric	Asymmetric	n/a
Battery day-ahead energy band	[0.2,0.8]	n/a	[137]
Battery reserve bidding limit	80%	n/a	n/a
Avg. reserve activation rate	Downward: 10% Upward: 8%	n/a	Elia
Day-ahead market price	-32~499 EUR/MWh	n/a	Elia
Reserve capacity price	3~18 EUR/MW	n/a	Elia
Reserve activation price	Downward: 0~79 EUR/MWh Upward: 0~149 EUR/MWh	n/a	Elia
DR shifting limits	10% of load estimation	0%, 20%	[140]
WACC	4%	n/a	[141]

investment model for each investment year without considering any investments in previous years (i.e., a greenfield investment is simulated for each investment year). As given in Table 6.2, all forecasts are assumed to be perfect in the Baseline scenario, and the renewable and the self-sufficiency target are set to 50% and 80%. Note that sensitivity analyses will be conducted in the following sections to investigate the impacts of the policy targets. Furthermore, the aggregator is assumed to participate in both reserve and energy markets, while reserve bidding quantities need to be symmetric, i.e. up- and downward reserve bidding quantities are equal, with a provisioning time of one week.

Figure 6.1 shows the installed capacity and the annual generation by technology type for investment years 2020 to 2050 for the Baseline scenario. It can be observed that the aggregator invests as much as the Self-suffiency (SS) target requires (i.e., SS target constraint is binding) for all considered years, which means that purchasing electricity from the wholesale markets is more attractive compared to investing in self-generations. This is mainly due to the fact that 1) the electricity market prices are assumed to be constant over the years without considering the influence of fuel cost or emission cost increase; and 2) subsidy policies such as the heat credits for CHP units or investment subsidies for wind and PV units are not considered, which might lead to different results. Futhermore, it shows that the renewable generation surpasses the renewable target from 2030 onwards. More specifically, while the optimal generation mix

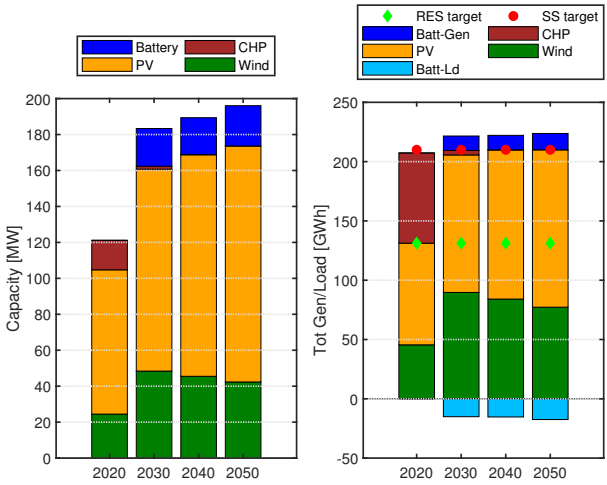

Figure 6.1: Comparison of the annual generation and the installed capacity by technology type for years 2020, 2030, 2040 and 2050 under the Baseline scenario.

to meet both the renewable and the SS targets in 2020 is achieved with a similar output share of CHP, wind and PV, the optimal generation mix is dominated by renewables (i.e., wind and PV) after 2030. These observations can be attributed to a combination of technological improvements and cost declines of renewables. However, this growth of renewable investments is not evenly distributed between wind and PV. After an increase in both wind and PV investments in 2030, PV gradually replace wind in the optimal generation mix after 2030. This is because compared to the cost decrease for wind units a larger cost decrease is projected for PV units in future years. The battery units start to be invested in 2030, which is likely due to the drastic cost reduction betweens 2020 and 2030 (see Appendix 9.3 for more details). The investment in CHP units decreases over the years and no CHP units are invested after 2030 as a result of its high operating and fuel costs and the projected cost reductions of renewables.

To present the results for the generation and load dispatch on the daily and hourly timescales, the optimal real-time dispatch results of one example winter and an example summer week both starting from a Monday for 2020 and 2050 are shown in Figs. 6.2-6.3. The hourly results for electricity generation by tech-

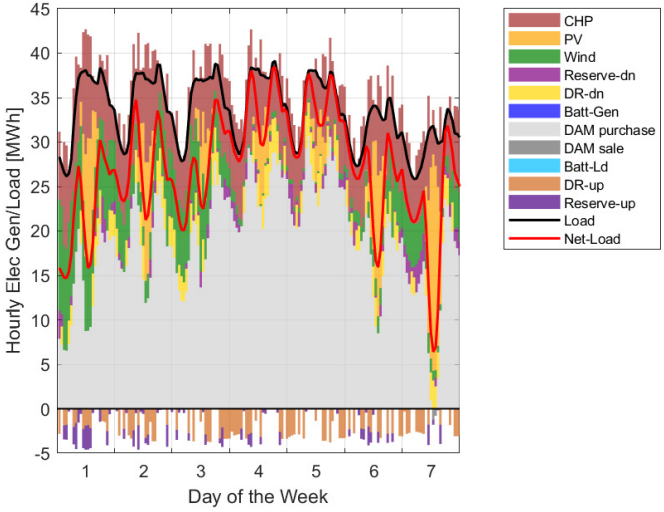

(a) 2020 - Winter

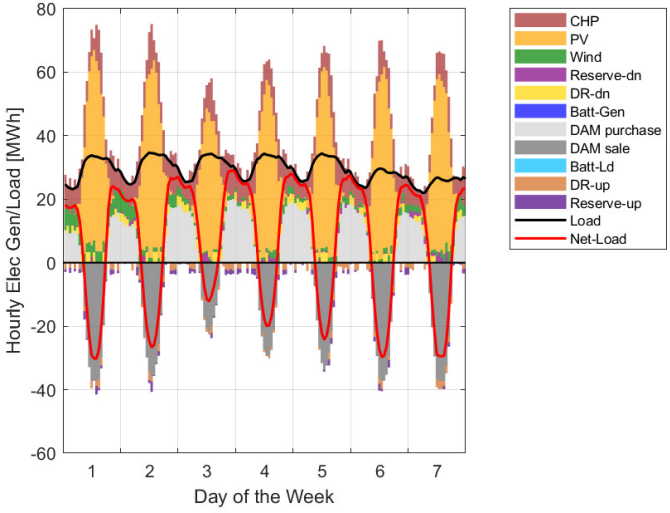

(b) 2020 - Summer

Figure 6.2: The hourly generation by technology type over an example winter and summer week for 2020 under the Baseline scenario.

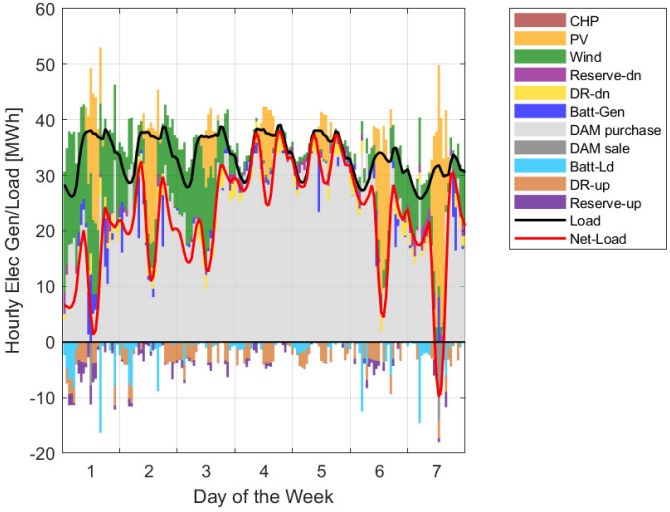

(a) 2050 - Winter

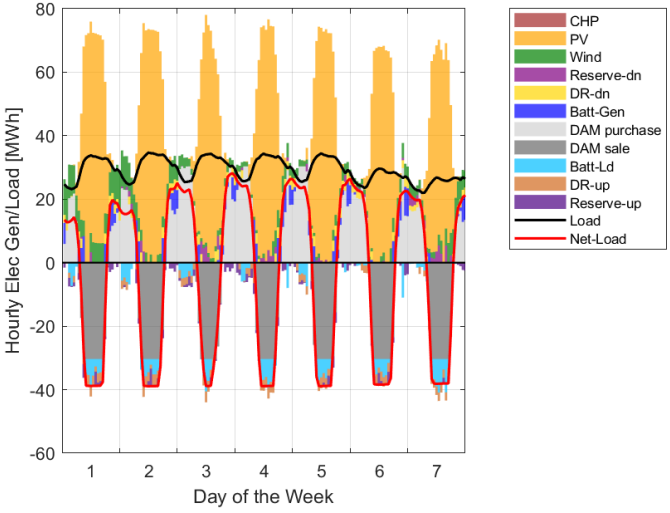

(b) 2050 - Summer

Figure 6.3: The hourly generation by technology type over an example winter and summer week for 2050 under the Baseline scenario.

nology type, the DA market exchange, reserve activations, original load and net load[18] are presented, where storage discharging/charging is represented by positive/negative values. During the winter week (i.e., Fig. 6.2a and Fig. 6.3a), the net load is mostly positive and the aggregator mainly purchases the electricity from the wholesale market. During the summer week (i.e., Fig. 6.2b and Fig. 6.3b), the net load repeats the plunge and the recovery pattern from day to day and the aggregator switches between selling electricity to and purchasing electricity from the market. This dynamic behavior of the net load is mainly due to the diurnal pattern of the PV generation that is more strengthened by the high solar irradiation during summer. Compared to 2020, this phenomenon is more pronounced in 2050 when more PV capacities are installed. The need for flexible resources to match the highly dynamic pattern of the net load during the summer weeks are mainly satisfied by the flexibilities provided by:

- Battery storage units: The battery units (in 2050) mainly charge (discharge) during negative (positive) net load hours to absorb the excess generation (satisfy the demand deficit). However, exceptions are observed in the early morning of the summer week of 2050 when the battery still charges even though the net load is positive. This is because of the low electricity prices during this period (see Fig. 6.4), the battery charges so as to discharge later during high electricity price periods.
- CHP units: The CHP units (in 2020) mainly ramp up (down) during positive (negative) net load hours;
- DR: Similar to the battery units, DR helps to balance the variations of the net load and to reduce the total aggregator cost by shifting the load from high electricity price and high net load hours to the low electricity price and low net load periods (see Fig. 6.4 for the impact of electricity prices);
- Electricity exchange with the market: In general, the aggregator sells (purchases) electricity to (from) the market during the period of the negative (positive) net load, while respecting the transmission capacity limit.

To summarize, the dispatch of different resources within the aggregator and the market exchange behaviors of the aggregator are highly impacted by the net load variations, but they are also influenced by the hourly electricity prices.

[18] Net load is defined as the load minus the variable generation, i.e. Net Load = Load - (Wind + PV generation).

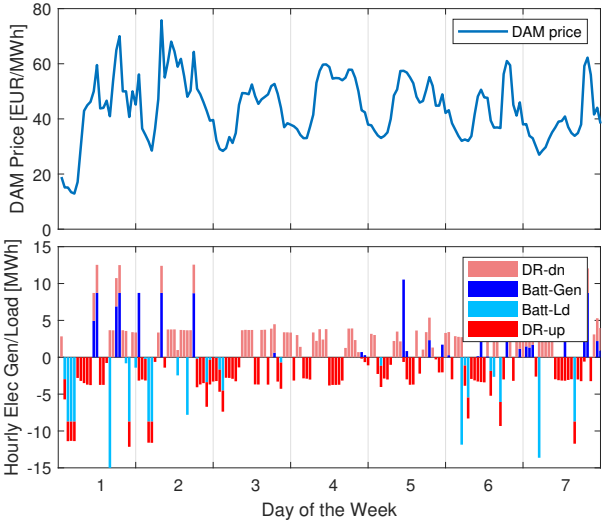

(a) 2050 - Winter

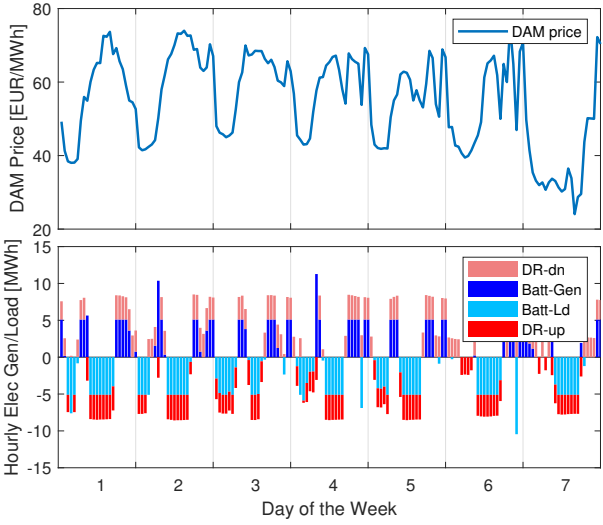

(b) 2050 - Summer

Figure 6.4: Day-ahead dispatch of battery and demand response programs over an example winter and summer week for 2050 along with the day-ahead market prices for the same period under the Baseline scenario.

To visualize the impact of Day-ahead Market (DAM) prices on the dispatch of DR and battery units, we plot the DA dispatch of the battery and the DR over an example winter and a summer week for 2050 along with the DAM prices for the same period under the Baseline scenario in Fig. 6.4. Results for other investment years can be found in Appendix 9.3. It shows that during the example winter week in general both the battery units and the DR shift demand from the high DAM price hours to hours with comparatively lower DAM prices to reduce the total cost of purchasing electricity from the wholesale market. However, different behaviors can be observed in the example summer week: the battery charges and the DR shifts up mainly during the noon time when the electricity market price is generally high. This is because the PV generation during the noon time of the summer week is so high that the energy injection from the aggregator to the grid already reaches the transmission capacity limit. Hence, batteries charge and the DR shifts up the load to absorb the excess PV generation, and then discharge and shifts down during evening hours when there is no PV generation. In this way, the aggregator reduces the electricity cost by decreasing the renewable curtailment. In general the battery behaves similarly to the DR, but exceptions may occur since the DA scheduled State of Charge (SOC) of the battery is limited by the day-ahead energy band and the DR up and down shiftings are limited by the maximum hourly shifting potential and the constant daily consumption constraint.

Figure 6.5 shows the DA and Real-time (RT) battery operations and its reserve capacity biddings as well as the reserve activations over an example winter and summer week for 2050 under the Baseline scenario, where the upward/downward reserve capacity procurement and activation are represented by positive/negative values. Results for other investment years can be found in Appendix 9.3. When comparing the battery dispatch between the example summer and the example winter weeks, it can be noticed that in general the SOC of the battery during the summer week follows a pattern of increasing during the day and then decreasing at night, which is consistent with the diurnal pattern of the PV generation. Furthermore, it can be seen that the RT battery operation deviates from the DA schedule due to the reserve activation, but thanks to the limits on the DA SOC and the reserve provision quantity, the battery units are able to provide continuous net upward reserves or downward

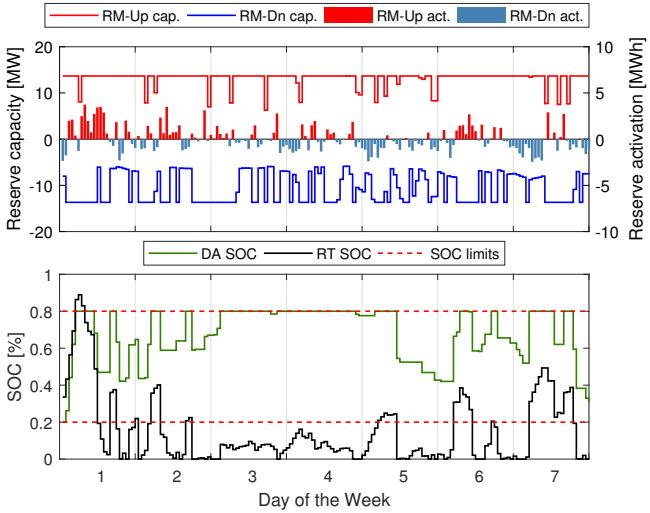

(a) 2050 - Winter

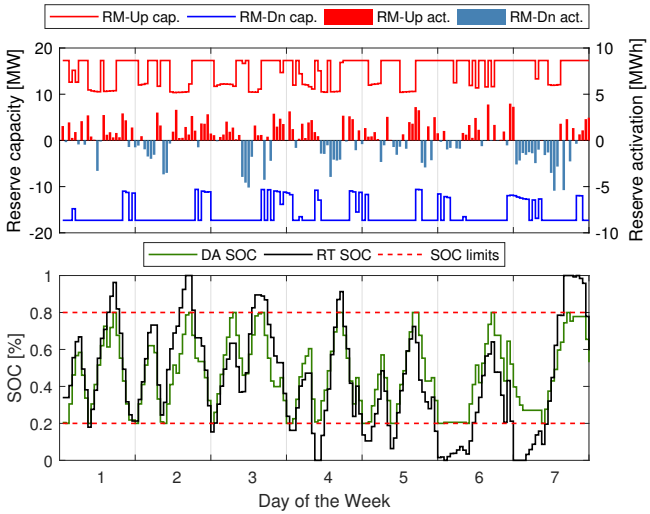

(b) 2050 - Summer

Figure 6.5: Day-ahead and real-time battery operations, reserve capacity biddings as well as the reserve activations over an example winter and summer week for years 2050 under the Baseline scenario.

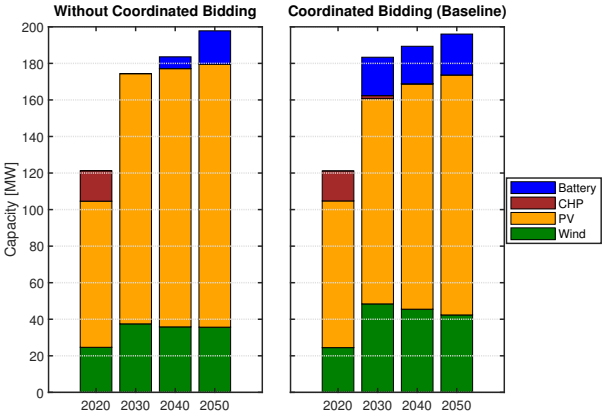

Figure 6.6: Impacts of coordinated bidding on the investments decisions.

reserves for some time. In addition, the battery units adjust their biddings into the reserve capacity market according to the day-ahead and real-time SOC levels. The time-varying reserve bidding of the battery units is enabled by the coordinated dispatch of different units within the aggregator. More specifically, instead of fulfilling the reserve bidding requirement by each of the single unit, the dispatch coordination of different energy resources enables the time-varying reserve bidding of each single unit while satisfying the market requirements through the aggregated bidding.

Effects of coordinated bidding

To quantify the impacts of coordinated aggregator bidding, we simulate two cases: one with coordinated bidding and one without. More specifically, in the case without coordinated bidding the market requirements such as the symmetric reserve bidding with a minimum provisioning time of one week should be fulfilled by the bids of each energy resource within the aggregator, while they only have to be satisfied by the aggregator's bids in the case with coordinated bidding.

Figure 6.6 shows the investment capacity per technology type for investment years 2020 to 2050 in the case with and without coordinated biddings. We can see that compared to the case without coordinated bidding, the battery investments increase significantly from 2030 to 2050 while both increase and de-

Table 6.3: Comparison of the results with and without coordinated bidding considering the same investment decisions.

Results without Coordinated Bidding							
Year	**Tot. cost [mEUR]**	**Op. cost [mEUR]**	**DAM cost [mEUR]**	**RM profit [mEUR]**	**RM bidding [MW]**		
					Battery	**DR**	**CHP**
2020	20.15	7.31	3.00	2.05	0	2.13	7.05
2030	15.75	3.96	3.07	2.36	17.8 (42%*)	1.78	0.19
2040	14.36	3.38	3.06	2.26	17.2 (41%*)	1.71	0
2050	12.89	3.01	2.98	2.35	17.5 (41%*)	1.46	0

Results with Coordinated Bidding							
Year	**Tot. cost [mEUR]**	**Op. cost [mEUR]**	**DAM cost [mEUR]**	**RM profit [mEUR]**	**RM bidding [MW]**		
					Battery	**DR**	**CHP**
2020	20.00	7.18	2.99	2.07	0	2.53	6.84
2030	14.67	4.06	3.07	3.48	27.4 (65%*)	2.25	0.46
2040	13.46	3.39	3.10	3.16	25.3 (61%*)	2.16	0
2050	11.99	3.01	3.06	3.29	27.1 (60%*)	1.76	0

*: Percentage share of the corresponding installed battery power capacity.
Reserve market bidding capacities shown are the average of the up- and downward values.

crease are observed for PV and wind investments in the case with coordinated bidding.

To better investigate and illustrate the reasons behind, we run the simulations without coordinated bidding with the investment decisions fixed as the values in the Baseline scenario (i.e., investment decisions resulted by coordinated bidding). Results with and without coordinated bidding considering the same investment decisions are compared in Table 6.3. It shows that the coordinated bidding results in less total costs for the aggregator, which is mainly due to the increasing profits from the reserve market, while changes in the operating and DAM costs are negligible. When focusing on the reserve bidding quantities in these two cases, it can be seen that the coordinated bidding in general allows higher bidding quantities into the reserve market. Moreover, it is obvious that the percentage share of the battery power capacity (marked with $*$ in the table) that bids into the reserve market significantly increases in the case with coordinated bidding. This in turn increases the profitability of the investments in battery storage units and could explain the increasing battery investments shown in Fig. 6.6.

Table 6.4: Impacts of different reserve products on investments and costs.

Impacts of different Reserve Products for 2020							
Symmetry of bids	n/a	Sym.	Asym.				
Provisioning time	n/a	1-week	1-week	24-hr	16-hr	8-hr	4-hr
Total cost [mEUR]	21.19	20.00	19.14	18.93	18.82	18.52	18.38
DAM cost [mEUR]	2.25	2.99	1.86	1.55	1.43	1.11	1.03
RM profit [mEUR]	n/a	2.07	3.86	4.72	4.95	5.32	5.44
RM profit from CHP [mEUR]	n/a	1.44	3.30	4.16	4.38	4.72	4.82
RM profit from storage [mEUR]	n/a	n/a	n/a	n/a	n/a	n/a	n/a
RM profit from DR [mEUR]	n/a	0.63	0.56	0.55	0.57	0.60	0.62
CHP investment [MW]	13.3	16.4	30.7	37.7	39.3	42.0	42.5
Wind investment [MW]	8.6	24.5	38.9	44.1	45.2	44.5	44.7
PV investment [MW]	107.7	80.3	55.2	46.1	44.2	45.4	45.1
Battery investment [MWh]	0	0	0	0	0	0	0

Impacts of different Reserve Products for 2050							
Symmetry of bids	n/a	Sym.	Asym.				
Provisioning time	n/a	1-week	1-week	24-hr	16-hr	8-hr	4-hr
Total cost [mEUR]	13.16	11.99	11.47	10.95	10.68	9.81	9.58
DAM cost [mEUR]	3.02	3.06	3.14	3.14	3.06	2.94	2.87
RM profit [mEUR]	n/a	3.29	5.20	6.29	6.41	7.77	8.06
RM profit from CHP [mEUR]	n/a	n/a	n/a	n/a	n/a	n/a	n/a
RM profit from storage [mEUR]	n/a	2.94	4.83	5.81	6.00	7.35	7.63
RM profit from DR [mEUR]	n/a	0.35	0.37	0.48	0.41	0.42	0.43
CHP investment [MW]	0	0	0	0	0	0	0
Wind investment [MW]	26.6	42.4	52.6	53.9	46.00	34.1	32.9
PV investment [MW]	161.8	131.3	110.3	106.8	119.3	139.4	141.3
Battery investment [MWh]	0	44.8	72.7	88.6	95.3	122.8	127.6

Effects of market participation and different reserve products

Following the roadmaps of various transmission system operators such as Swissgrid [142], reserve products are expected to have shorter provisioning times and more flexible bidding structures in the future. In this section, simulations assuming different available reserve products are carried out to analyze their impacts on investment decisions and the aggregator's total costs.

Table 6.4 shows the results considering the availability of different reserve products along with the results of only participating in the DAM (i.e., the first column of the table) for years 2020 and 2050. Comparing the cases with and without considering the participation in the reserve market, it can be seen that the total cost of the aggregator increases and the economic viability of battery units decreases when only considering the DAM participation. More specifically, no battery is invested in 2020 or 2050 when the Reserve Market (RM) participation is not considered, which means that the profits from the arbi-

trage using the price spread in the DAM are not sufficient enough to cover the total battery costs, even considering the projected cost reductions by 2050. This result might change if the assumption of the battery cost changes. When comparing the investment decisions considering different reserve products for one specific year, in general, the availability of more flexible reserve products encourages the investments in units that are able to provide the reserves, e.g. the CHP units in 2020 and the batteries in 2050. Furthermore, both introducing the asymmetric reserve products and shortening the minimum reserve provisioning time decrease the total aggregator costs by realizing more profits from the reserve market. However, the benefit of introducing more flexible reserve products for the battery storage and the CHP units is limited, since storage units in general bid upward and downward reserves closer to half of the energy capacity and CHP units prefer to bid downward reserves closer to their generation outputs. Although the more flexible reserve products are expected to mostly benefit the reserve bidding of flexible loads, both increase and decrease in RM profits from DR are observed in Table 6.4. This is because the aggregator coordinates the dispatch of different resources in order to minimize the total cost of the aggregator, which might not necessarily minimize the cost that each single unit faces. It is therefore important to research on how to allocate the total profits to each unit within the aggregator [143, 144], which is however beyond the scope of this thesis.

Impacts of policy targets

In the Baseline scenario, we assume a 50% RES target and a 80% SS target. As shown by the investment results in the Baseline scenario, these two targets (especially the SS target constraint) are binding most of the time. To analyze the impact of the policy targets, we simulate two sensitivity scenarios: 1) assuming 0-100% RES target with a step of 10% while keeping the SS target same as the Baseline scenario (i.e. 80%); 2) assuming 0-100% SS target with a step of 10% while keeping the RES target same as the Baseline scenario (i.e. 50%).

Figure 6.7 shows the results of sensitivity analysis 1), namely the sensitivity analysis against the RES target for 2020 and 2050. The results can be analyzed by splitting the RES target into two ranges:

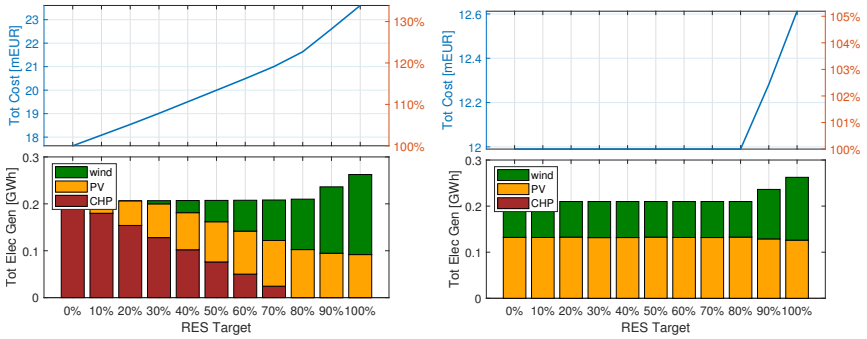

(a) 2020 **(b)** 2050

Figure 6.7: Comparison of the total generation and costs for 2020 and 2050 under different renewable targets. Data shown are from simulations of applying the renewable target from 0% to 100% while keeping the remaining parameters equal to the Baseline scenario value.

- RES target ranges from 0% to 80% (i.e. RES target value lower or equal to the 80% Baseline SS target value): It can be seen that in 2020, when increasing the RES target from 0% to 80%, the total cost increases and the total generations from CHP are gradually replaced by wind and PV investments. This is due to the fact that in 2020 it is economic viable to meet the SS target by investing in CHP units, the investments in wind and PV thus increase with the RES target increase with the RES target binding all the time. In contrast, in 2050, both the optimal generation mix and the total cost are unchanged when increasing the RES target from 0% to 80%. This is because with the projected cost reduction it is more profitable to invest in wind and PV units to meet the SS target in 2050, the RES target therefore is not binding when it is lower than or equal to the SS target.
- RES target ranges from 90% to 100% (i.e. RES target value greater than the 80% Baseline SS target value): The total cost increases by around 10% and 5% in 2020 and 2050, respectively. The wind generation increases while the PV generation is almost unchanged when the RES target increases from 90% to 100%. Further increasing the RES target does not increase the generations of wind and PV simultaneously, as the PV generation is likely to be limited

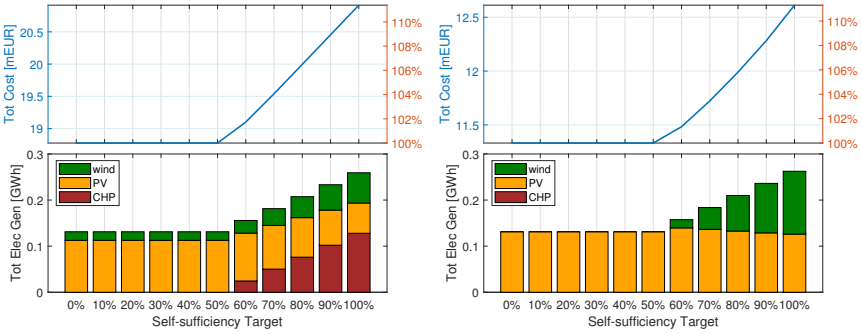

(a) 2020 **(b)** 2050

Figure 6.8: Comparison of the total generation and costs for 2020 and 2050 under different self-sufficiency targets. Data shown are from simulation of applying the self-sufficiency target from 0% to 100% while keeping the remaining parameters equal to the Baseline scenario values.

by the transmission capacity. More specifically, the diurnal pattern of the PV generation profile in general increases the peak electricity injection into the grid, which might result in curtailments when the transmission limit is reached.

Similarly, Fig. 6.8 shows the results of the sensitivity analysis against the SS target. It can be seen that while the optimal investment portfolio remains the same with the SS target ranging from 0% to 50% (i.e. the Baseline RES target value) for both 2020 and 2050, further increasing the SS target results in significant increase in wind and/or CHP investments, which is likely due to their comparatively higher annual generation outputs.

In general, both increasing the RES target and increasing the SS target result in higher aggregator costs, as compared to investing in local generations it is more favorable to purchase the electricity from the wholesale market. While the cost change in percentage for increasing the SS target from 0% to 100% (using the cost at 0% SS target as the reference) is similar for 2020 and 2050 (around 12% cost increase for both years), this is not the case when changing the RES target. The aggregator cost increases by around 35% when increasing the RES target from 0% to 100% in 2020, whereas it only increases by 5% in

Table 6.5: Impact of demand response on the results for years 2020 to 2050.

Impacts of Demand Response for 2020										
$\beta^{sh,max}$	CHP	Wind	PV	Battery	RM profit [mEUR]				Tot. shift	Tot. cost
	[MW]	[MW]	[MW]	[MWh]	CHP	Battery	DR	Tot.	[GWh]	[mEUR]
0%	16.6	23.5	81.9	0	1.62	0	0	1.62	0	20.70
10%	16.4	24.5	80.3	0	1.44	0	0.63	2.07	20.31	20.00
20%	16.4	25.8	77.9	0	1.31	0	1.25	2.55	39.92	19.30

Impacts of Demand Response for 2050										
$\beta^{sh,max}$	CHP	Wind	PV	Battery	RM profit [mEUR]				Tot. shift	Tot. cost
	[MW]	[MW]	[MW]	[MWh]	CHP	Battery	DR	Tot.	[GWh]	[mEUR]
0%	4.1	38.8	132.0	44.1	0.13	2.79	0	2.92	0	13.14
10%	0	42.4	131.3	44.8	0	2.94	0.55	3.29	20.68	11.99
20%	0	44.4	127.1	52.8	0	3.37	0.87	4.24	40.78	11.18

2050, which is due to the drastic projected cost reductions of renewables in future years. Note that the results might change when different assumptions about the unit cost and the generation profiles are made.

Impacts of demand response

To investigate the impacts of the assumptions regarding the demand response, we run the simulations for investment years 2020, 2030, 2040 and 2050, assuming that the maximum hourly load shifting (i.e. $L^{sh,max}$) to be: 0%, 10%, 20%. The results for 2020 and 2050 under different maximum load shifting assumptions are shown in Table 6.5. It can be seen that as the level of shiftable load increases:

- The profits from the reserve market are increased and the total aggregator costs are reduced. Considering the cost decrease and total demand to be shifted, the profits for each MWh of demand shifting can be calculated as the cost reduction divided by the additional demand to be shifted. In this way, the profits brought by each unit of demand shifting are 34.5 EUR/MWh and 35.7 EUR/MWh when increasing the shifting potential from 0% to 10% and from 10% to 20% in 2020, and the corresponding values for 2050 are 55.61 EUR/MWh and 40.30 EUR/MWh. The higher values of demand response in 2050 could be related to the higher wind and PV installed capacities. Note that this calculation is a simplification of the real-world complexity, but it could provide an insight about how much should be paid for utilizing the DR.

- Investments in CHP units are in general decreased as more flexibilities are provided from the demand side.
- Both increase and decrease are observed in wind and PV investments. This is likely due to the combination of a multitude of effects. Clearly, as DR shifting potential increases, the energy shifting potential of the aggregator increases. This on one hand can be used to reduce the wind and PV curtailment rate, i.e. using more of the available generation, which leads to a lower need in PV and wind investments for the same amount of electricity supply. On the other hand, the flexibility can be also used to increase the market value of PV and wind generations by shifting their generations from the low price period to the high price period, thereby encouraging an increase in PV and wind investments.
- Investments in batteries are increased (without considering the case without battery investments), although this result seems to be against the fact that DRPs and battery units are in general substitutes, it can be explained by two effects: 1) the higher DR shifting potential can allow a higher range of energy and reserve bids that the load can submit to the market, which accordingly increases the flexibility of the reserve capacity that batteries bid into the market, since the reserve market requirement[19] is fulfilled by the coordinated bidding of all energy resources. The possibly higher profits obtained by batteries from the reserve market therefore increases the economic viability of battery investments. This can be verified by the fact that under the same load shifting potential, the RM profit obtained by DR is lower in the case with battery installations than that without battery investments. 2) the higher DR shifting potential can shift more productions from a high variable generation period to a low variable generation period, which leads to a lower need for investment in dispatchable generation units. This, however, in turn could require the installation of more batteries to fill the flexibility gap as batteries serve as flexibility providers.

Effects of forecast error

The forecast error δ_v of variable generation unit v is assumed to belong to an uncertainty set $\{-\overline{\delta}_v \leq \delta_v \leq \overline{\delta}_v\}$ and decision variables are optimized us-

[19] In the Baseline scenario, the reserve bidding is required to be symmetric and the minimum reserve provisioning time is one week.

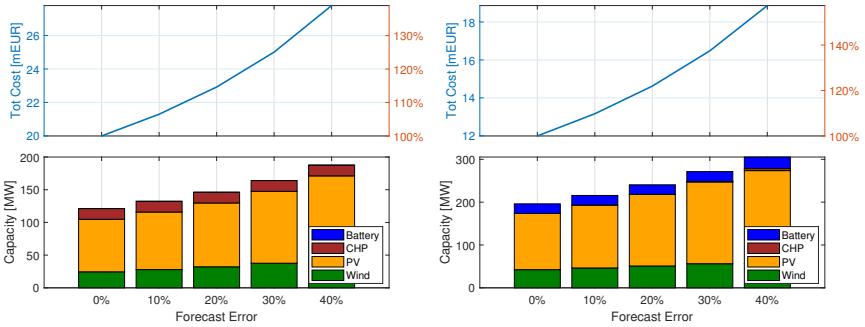

(a) 2020 **(b)** 2050

Figure 6.9: Comparison of the investment and cost results for 2020 and 2050 under different forecast error assumption.

ing robust optimization, i.e. they are feasible for all realizations within the uncertainty set and optimal for the worst-case objective function. It is obvious that the worst-case scenario occurs when the forecast error hits the lower bound of the interval, which means the real-time variable generation is $\max\{x_v^{\text{inv}}(p_{v,t}^{\text{f}} - \overline{\delta}_v), 0\}$. Thus, equation (6.33) is replaced by

$$0 \leq p_{v,t} \leq \max\{x_v^{\text{inv}}(p_{v,t}^{\text{f}} - \overline{\delta}_v), 0\} \tag{6.51}$$

Figure 6.9 shows the results for 2020 and 2050 considering that the worst-case nominal forecast error ranges from 0% to 40%. In general, the investments increase with the increasing forecast errors so as to cover the shortage caused by the worst-case variable generation outputs, which results in the growth in investment costs and thereby the total costs. Furthermore, the rate of the cost increase accelerates with the increasing forecast error as more variable generation units are installed in the system and then the same increase in the forecast error will have bigger impact on variable generations and total costs. The CHP investment is stable in 2020 and it is invested in 2050 when the worst-case forecast error increases to 40%, as increasing the uncertainty in wind and PV outputs is equivalent to decrease the profitability of their investments. In addition, the total aggregator cost could increase by up to more than 30% and

50% in 2020 and 2050 when the nominal worst-case forecast error increases to 40%, which strengthens the importance of the forecasting accuracy and the modeling forecast errors in a proper way.

6.5 Limitations and Future Work

This work has several limitations and a few of which are highlighted in this section. First, policy regulations such as the subsidies for renewables are not considered in this work. However, they are expected to have significant influence on the economic viability of different candidate units (especially wind and PV). As pointed out in [145], the current DER business models are driven more by regulatory and policy factors than by technological factors. The future version should therefore account for influences of the policy regulations and their uncertainties in future years.

Second, electricity market prices are modeled using historical market data and the prices are assumed to be constant over the years. In this way, the influence of the fuel and emission cost increase and the price suppression effect due to the increasing penetration of renewables especially during high wind and PV generation hours cannot be captured. The future work should include a proper modeling of future market prices. In addition, how the investment decisions and the economic viability of different units are influenced by the generation mix of the electricity market should be investigated.

Third, although a comprehensive sensitivity analysis is conducted to analyze the uncertainties that the planners face, most of the uncertainties considered are short-term ones, which are related to the day-to-day variability [146]. The long-term uncertainties, which correspond to the yearly changes, such as demand growth, electricity price developments, technology improvements and cost developments for the candidate units (especially the renewable and battery units) are not incorporated.

Fourth, it is assumed that the DER investment decisions are made by a central planner (i.e., an aggregator) in this work, which however might not always be the case in reality. Although the results provide the insights for the optimal generation mix in terms of the total aggregator cost while respecting the demand and the policy targets, the considered objective function might not be

able to fully reflect the intentions of individual investors to invest in distributed energy resources.

Lastly, the investment decisions are optimized mainly considering the revenue streams from the reserve and the energy markets, while additional revenue streams from providing firm capacities or increasing self-consumptions and so on are not considered.

Some of the limitations described above are addressed in Chapter 8, which focuses on analyzing the economic viability of PV-battery systems in Switzerland.

6.6 Summary and Conclusions

A multi-stage stochastic optimization model to derive optimal generation mix in a market environment is presented. Comprehensive sensitivity analyses are conducted to investigate the impacts of the market participation, coordinated bidding, reserve bidding requirement, policy targets, the demand response shifting potential and the forecast errors on the investment decisions and the aggregator's total costs.

While the renewable target is binding in 2020, as a result of the decreasing costs, the renewable investments gradually replace the CHP investments in the optimal generation mix, resulting in more renewable generations than the renewable target requires from 2030 onwards. Nevertheless, the self-sufficiency target is binding for all examined investment years as it is more favorable to purchase the electricity from the wholesale market under the simulation assumptions.

Coordinated bidding enables the time-varying reserve bidding of the individual unit while satisfying the market requirements with the aggregated bidding quantity, thus realizes higher profits for the aggregator. Numerical results presented also suggest that having access to the reserve market encourages the investments in flexibility providers in the system (e.g. storage units and CHP units). However, for each MW of reserve capacity bidding into the market, the benefits of having more flexible reserve products for the battery and the CHP units might be limited. This is due to the fact that storage units in general bid upward and downward reserves closer to half of the energy capacity and CHP

units mostly bid downward reserves closer to their generation outputs. Furthermore, the aggregator cost decreases with the increasing DR shifting potential, and the value of each MWh of demand shifting increases with the increasing investments in wind and PV units. Sensitivity analysis regarding the policy targets shows that both increasing the renewable and the self-sufficiency target result in higher costs for the aggregator. Moreover, compared to 2020, the impact of increasing the renewable target is less pronounced in 2050 due to the decreasing cost for PV and wind units. Finally, simulation results with varying forecast errors suggest the importance of have an accurate forecast and also modeling the forecast uncertainties in a proper way.

Chapter 7

Investment Optimization Focusing on the Forecast Uncertainty Modeling

In this chapter, we extend the work in the previous chapter by modeling the uncertainties in wind and Photovoltaic (PV) generation forecasts using distributionally robust optimization. Following the principle of distributionally robust optimization, the uncertainties are characterized by an ambiguity set that defines a family of distributions. A multi-stage stochastic programming model is formulated to minimize the worst-case expectation of the total long-term and short-term costs. A case study demonstrates the effectiveness of the proposed distributionally robust optimization model. Out-of-sample tests are conducted to compare its performance with two benchmark models, i.e., a robust optimization model and a stochastic optimization model. Furthermore, the impacts of considering different statistical constraints in the ambiguity set and the imbalance prices are investigated. This chapter is based on [147, 148].

7.1 Introduction

7.1.1 Motivation and Related Work

The electric power system has been experiencing a trend of decentralization, as a result of decreasing costs of distributed generation units, governmental subsidies, increasing electricity tariffs and emission costs, environmental considerations and the concerns of reliance on third-party electricity supply. With the continuous growth in distributed generations, generation companies and system operators face both challenges and opportunities. On one hand, Distributed Energy Resources (DERs) that mainly consist of solar and wind generations are subject to uncertainties in outputs, which may cause high imbalance costs for owners and high system operating costs for system operators; on the other hand, DERs, especially distributed storage units and Demand Response Programs (DRPs), could contribute to system flexibility and generate profits by participating in electricity markets. Therefore, questions regarding the optimal generation mix and how DERs can be better valued considering their output uncertainties need to be answered.

While a significant amount of work has been done in terms of generation investment in the past, most investment models mainly focus on deterministic problems [149], or consider uncertainties using traditional stochastic optimization [121,126,128] or robust optimization [129,130]. Nevertheless, as mentioned in previous chapters, the random parameters' distribution for Stochastic Optimization (SO) is rarely known and SO often suffers from high computational complexity resulting from a large number of scenarios. The Robust Optimization (RO) model on the other hand is often computationally tractable as the uncertainty considered is distribution free and described only by an uncertainty set, which results in much lower computational cost but more conservative results. Ditributionally Robust Optimization (DRO), which is applied in this work, acts as an intermediate between SO and RO. Following the principle of DRO, the decisions are optimized against the worst-case distribution over an ambiguity set, i.e. a family of distributions described by certain statistical characteristics (e.g. expectation and standard deviation) of the unknown data-generating distribution [90, 150].

The focus of this chapter is on optimizing investment decisions of a DER aggregator considering the operational decisions over four representative weeks of the examined year, while uncertainties of wind and PV forecast errors are modeled using DRO.

The contributions of this chapter are:

1. To propose a multi-stage distributionally robust optimization model that jointly optimizes the investment and operational decisions of a DER aggregator that participates in the Reserve Market (RM), the Day-ahead Market (DAM) and the Balancing Market (BM). The considered aggregator includes the DRP, storage units, variable and dispatchable generation units.
2. To model uncertainties of forecast errors of wind and PV generation outputs using distributionally robust optimization.
3. To verify the effectiveness of the proposed distributionally robust optimization model by comparing its results to the results of two benchmark models, i.e. the robust optimization model and the traditional stochastic optimization model.
4. To analyze the effects of including different statistical information into the ambiguity set.

7.1.2 Chapter Organization

The remainder of the chapter is organized as follows: mathematical formulations and the proposed optimization model are given in Section 7.2. Section 7.3 presents the results of a case study. Limitations and future work are discussed in Section 7.4. Finally, conclusions are drawn in Section 7.5. To avoid repetitions, please refer to Section 6.2 of Chapter 6 for the problem description and the main modeling assumptions. Note that instead of robust optimization, we use distributionally robust optimization to model the uncertainties in variable generation outputs.

7.2 Mathematical Formulation

This section presents the derivation of the DRO, SO and RO formulations of the optimization problem detailed in Section 6.3 of Chapter 6. To avoid duplications, we only focus on the changes required for the extension.

7.2.1 General Stochastic Formulations

To be able to adjust the day-ahead bidding based on the expectation of the variable generation forecast errors at real-time, constraint (6.5) is adapted to

$$0 \leq p_{v,t}^{\text{da}} \leq x_v^{\text{inv}} \tag{7.1}$$

Correspondingly, the self-sufficiency and the renewable target constraints (6.21) and (6.22) are adapted to the following equations:

$$\sum_{t=1}^{T} \sum_{v \in V} x_v^{\text{inv}} p_{v,t}^{\text{f}} + \sum_{t=1}^{T} \sum_{i \in I \setminus V} p_{i,t}^{\text{da}} \geq \beta^{\text{ss}} \sum_{t=1}^{T} l_t^{\text{est}} \tag{7.2}$$

$$\sum_{t=1}^{T} \sum_{v \in I^{\text{res}} \cap V} x_v^{\text{inv}} p_{v,t}^{\text{f}} + \sum_{t=1}^{T} \sum_{i \in I^{\text{res}} \setminus V} p_{i,t}^{\text{da}} \geq \beta^{\text{res}} \sum_{t=1}^{T} l_t^{\text{est}} \tag{7.3}$$

To enable the dispatchable generation unit and the battery storage unit to reduce the imbalances caused by the variable generation forecast errors through re-dispatch, constraints (6.31) and (6.37) are relaxed. In addition, the real-time generation of the dispatchable unit is forced not to be greater than the generation capacity, i.e.

$$0 \leq p_{g,t} \leq x_g^{\text{inv}} \tag{7.4}$$

Finally, the optimization problem can be written as:

$$\begin{aligned} \min \ & C^{\text{inv}} + C^{\text{foc}} + \alpha^{\text{d}} \sum_{t=1}^{T} (C_t^{\text{voc}} + C_t^{\text{DAM}} + C_t^{\text{RM}} + C_t^{\text{BM}}) \\ \text{s.t.} \ & \text{Constraints (6.1)-(6.49), with (6.5), (6.21), (6.22), (6.31)} \\ & \text{and (6.37) replaced by (7.1)-(7.4)} \end{aligned} \tag{7.5}$$

7.2.2 Uncertainty modeling

In this section, based on the principle of DRO, an ambiguity set is constructed to describe a family of possible distributions of the random variables, using statistical information extracted from historical data. Then, a tractable second-

order cone model is derived by approximating the uncertainty-related operational decisions using the Linear Decision Rule (LDR).

We first rewrite the problem (7.5) in the following compact form:

$$\begin{aligned} \min \quad & \Theta(\boldsymbol{x}) + \phi(\boldsymbol{x}, \boldsymbol{\delta}) \\ \text{s.t.} \quad & \boldsymbol{x} \in \boldsymbol{X_f} \end{aligned} \tag{7.6}$$

where $\Theta(\boldsymbol{x}) = C^{\text{inv}} + C^{\text{foc}} + \alpha^{\text{d}} \sum_{t=1}^{T} (C_t^{\text{DAM}} + C_t^{\text{RM}})$ includes the uncertainty-unrelated costs. Only uncertainties regarding Day-ahead (DA) variable generation forecast errors are considered in this work. All first-, second- and third-stage decision variables that are not subject to uncertainty, i.e. variables $\{x^{\text{inv}}, q^{\text{DA}}, p_g^{\text{da}}, p_v^{\text{da}}, p_s^{\text{ch/dis,da}}, E_s^{\text{da}}, q^{\text{RU/RD}}, q_g^{\text{RU/RD}}, q_s^{\text{RU/RD}}, q_l^{\text{RU/RD}}\}$, can therefore be described by a vector $\boldsymbol{x}$. The feasibility region $\mathbf{X_f}$ of $\boldsymbol{x}$ is defined by (6.1)-(6.4), (6.6)-(6.20), (6.23)-(6.30) and (7.1)-(7.3). The second part in the objective function $\phi(\boldsymbol{x}, \boldsymbol{\delta}) = \alpha^{\text{d}} \sum_{t=1}^{T} (C_t^{\text{voc}} + C_t^{\text{BM}})$ represents the uncertainty-related cost. The principle of DRO is to describe a family of potential uncertainty distributions I with an ambiguity set F and to optimize the decisions against the expectation of the worst-case distribution. The term $\phi(\boldsymbol{x}, \boldsymbol{\delta})$ therefore can be formulated as:

$$\phi(\boldsymbol{x}, \boldsymbol{\delta}) = \min_{\boldsymbol{y}} \sup_{I \in F} \mathbb{E}_I \left\{ \alpha^{\text{d}} \sum_{t=1}^{T} C_t^{\text{adpt}} \right\} \tag{7.7a}$$

$$\text{s.t.} \quad \boldsymbol{A}(\boldsymbol{\delta}) + \boldsymbol{B}\boldsymbol{y} \leq \boldsymbol{D}(\boldsymbol{\delta}) \tag{7.7b}$$

where $C^{\text{adpt}} = C^{\text{voc}} + C^{\text{BM}}$ and $\boldsymbol{y} = \{p_g, p_v, p_s^{\text{dis/ch}}, E_s, q^{\text{BM}}\}$ is the uncertainty-related decision vector. Constraint (7.7b) corresponds to (6.32)-(6.36), (6.38)-(6.41), (6.46), (6.49) and (7.4), where $\boldsymbol{A}(\boldsymbol{\delta})$ and $\boldsymbol{D}(\boldsymbol{\delta})$ are the affine functions of $\boldsymbol{\delta}$.

Modelling Ambiguity Set The Probability Distribution Function (PDF) of $\boldsymbol{\delta}$, namely I, is uncertain and it belongs to an ambiguity set F, which represents a family of distributions sharing some common statistical features (e.g. expectation, deviation, variance etc.). In this work, we focus on a standard ambiguity set where the family of distributions are characterized by a group of second-

order cone representable constraints and a linear support set. The ambiguity set modelled in this work is:

$$F = \left\{ I: \begin{array}{l} \mathbb{E}_I[\delta_{v,t}] = 0 \\ \mathbb{E}_I[|\delta_{v,t}|] \leq \gamma^1_{v,t} \\ \mathbb{E}_I[(\delta_{v,t})^2] \leq \gamma^2_{v,t} \\ Pr(\boldsymbol{\delta} \in \mathscr{W}) = 1 \end{array} \right\}$$

where the first line defines that the expectation of uncertainty $\delta_{v,t}$ of variable generation unit v at time t is set to zero. The second and third lines limit the expected absolute deviation and variance to $\gamma^1_{v,t}$ and $\gamma^2_{v,t}$, respectively. The last line guarantees that all uncertainty realizations are within set $\mathscr{W}$, where

$$\mathscr{W} = \{\delta^{\min}_{v,t} \leq \delta_{v,t} \leq \delta^{\max}_{v,t}\}$$

As the expectation terms in the second and third constraints are difficult to compute, according to the lifting theorem introduced in [99], a set of auxiliary random variables $\boldsymbol{u} = \{\boldsymbol{u^1}, \boldsymbol{u^2}\}$ is introduced to ensure the tractability of the problem and to increase the flexibility of the later introduced linear decision rule [88]. Thus, the lifted ambiguity set $\overline{F}$ and the second-order cone representable extended uncertainty set $\overline{\mathscr{W}}$ can be written as:

$$\overline{F} = \left\{ J: \begin{array}{l} \mathbb{E}_J[\delta_{v,t}] = 0 \\ \mathbb{E}_J[u^1_{v,t}] \leq \gamma^1_{v,t} \\ \mathbb{E}_J[u^2_{v,t}] \leq \gamma^2_{v,t} \\ Pr\{(\boldsymbol{\delta}, \boldsymbol{u}) \in \overline{\mathscr{W}}\} = 1 \end{array} \right\}$$

$$\overline{\mathscr{W}} = \left\{ \begin{array}{c} \delta^{\min}_{v,t} \leq \delta_{v,t} \leq \delta^{\max}_{v,t} \\ |\delta_{v,t}| \leq u^1_{v,t} \\ (\delta_{v,t})^2 \leq u^2_{v,t} \\ u^1_{v,t} \leq u^{1,\max}_{v,t} = \max\{\delta^{\max}_{v,t}, -\delta^{\min}_{v,t}\} \\ u^2_{v,t} \leq u^{2,\max}_{v,t} = \max\{(\delta^{\max}_{v,t})^2, (\delta^{\min}_{v,t})^2\} \end{array} \right\}$$

where the second and third lines in $\overline{\mathscr{W}}$ set the upper bounds of $|\delta_{v,t}|$ and $(\delta_{v,t})^2$ as $u^1_{v,t}$ and $u^2_{v,t}$, making $\overline{F}$ equivalent to F. To make the support set less conservative, the fourth and fifth lines in $\overline{\mathscr{W}}$ limit $u^1_{v,t}$ and $u^2_{v,t}$ to the worst-case [93], which are constants that can be calculated based on historical data.

Enhanced LDR Approximation Although distributions of the uncertainty $\boldsymbol{\delta}$ are constrained by the ambiguity set, it is still required to loop over all uncertainty realizations to find the optimal solution, which makes the problem intractable. Thus, LDR is used to limit the adaptive decision $\boldsymbol{y}$ to be affinely dependent on the uncertainties. Finally, a tractable second-order cone model is derived. Details of the reformulation process and the tractable second-order cone model are given in Appendix 9.3.

To allow for comparisons of DRO against RO and traditional SO, formulations applying RO and traditional SO are presented in Appendix 9.3.

7.3 Case Study

The case study is simulated using the 2018 load and price data from Elia [138]. The cost parameters for the considered DER units and the input parameters for modeling are based on the values in Table 6.1 and the baseline values in Table 6.2 in Chapter 6, respectively. To focus on modeling the uncertainty of wind and PV output forecast, the Renewable Energy Source (RES) target is set to 100%, the Self-suffiency (SS) target is thus neglected. Furthermore, the reserve bidding is assumed to be asymmetric.

Considering the computational burden, four weeks corresponding to the four seasons are selected to represent the variations in supply and demand over the year. The nominal[20] wind and PV forecast outputs as well as the demand for the four representative weeks are shown in Fig. 7.1.

In this work, we consider the DA wind and PV generation forecast errors as random variables, while other parameters are assumed to be deterministic. The forecast error is defined as the real-time value minus the forecast value and all historical forecast error data are normalized using the corresponding wind

[20]The wind and PV outputs are normalized based on the corresponding wind and PV capacities, while the demand is normalized using the peak demand.

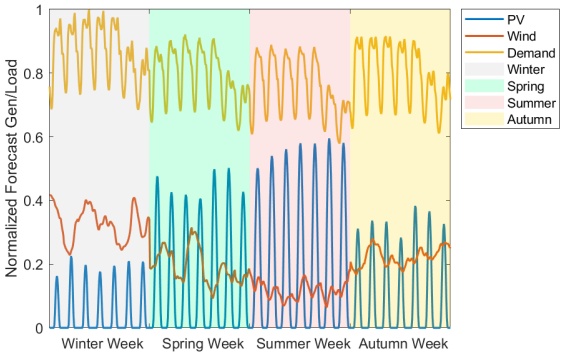

Figure 7.1: Nominal PV and wind power output forecast as well as demand values over four weeks corresponding to four seasons (from left to right: winter, spring, summer, autumn).

or PV capacities. To build the stochastic models, we collect 70'176 historical realizations of day-ahead wind and PV forecast errors that correspond to the difference between the 15-min system wind and PV real-time output data and the DA generation forecast from 2016 to 2017 published by Elia [138].

To analyze how the distributions of wind and PV forecast errors are related to different hours of the day and different seasons of the year, we first categorize the historical data into 4*24 groups, depending on which season[21] of the year and which hour of the day each data point belongs to. Then a whisker plot is drawn in Fig. 7.2 to show the distributions of wind and PV forecast errors over 24 hours of the day and four seasons of the year. A strong seasonal pattern can be observed in the distribution of PV output forecast errors for different hours of the day, which is likely due to the seasonal and diurnal patterns of the PV generation output, while this phenomenon is less obvious for wind output forecast errors. Furthermore, the distributions of wind and PV forecast errors are almost symmetric with mean values close to zero.

In order to make use of the identified seasonal patterns of the forecast errors, we construct the simulation dataset **Data-sim** of the forecast errors by catego-

[21] It is assumed that winter begins on December 1st, spring begins on March 1st, summer begins on June 1st and autumn begins on September 1st.

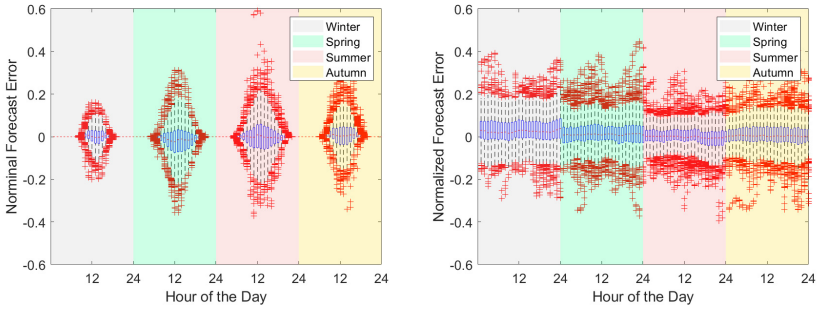

(a) PV **(b)** Wind

Figure 7.2: Whisker plot on nominal PV and wind forecast errors categorized according to the hours of the day and seasons of the year (from left to right: winter, spring, summer, autumn).

rizing the 2016 to 2017 data into 24*4 groups. Then we generate the scenarios required by SO and the uncertainty set parameters used for RO as well as the statistical parameters used to build the ambiguity set for DRO as follows:

- Stochastic Optimization: Under the assumption that the forecast errors follow the Gaussian distribution with zero mean, the function "histfit" in Matlab is used to create Gaussian distribution density functions to fit the data for each one of the 24*4 groups in simulation set Data-sim for both DA wind and PV output forecast errors, respectively. Considering the computational time, for each hour of the four representative weeks, the fitted Gaussian distribution functions created before are then used to generate up to 400 random scenarios of the wind and PV output forecast errors for SO.
- Robust Optimization: For each hour of the four representative weeks, depending on which hour of the day and which season of the year it belongs to, i.e. which one of the 24*4 groups in Data-sim it fits in, the minimum and the maximum values of the corresponding group are drawn to build the corresponding uncertainty set used for RO.
- Distributionally Robust Optimization: Similar to the process to build the uncertainty set for RO, for each hour of the four representative weeks, depending on which hour of the day and which season of the year it belongs

to, i.e. which one of the 24*4 groups in Data-sim it fits in, the minimum, the maximum, the mean absolute deviation and the standard deviations are drawn to build the corresponding uncertainty set and the ambiguity set used for DRO.

Similar to the work in previous chapters, the balancing market prices are modeled following a two-price settlement scheme. It is assumed that the hourly BM prices are dependent on the corresponding day-ahead energy price pr^{DA} and reserve activation prices $pr^{\text{aRD/aRU}}$, which is specified in the following equations. The equations ensure that the aggregator can only sell (purchase) electricity in the BM at a price lower (higher) than the minimum (maximum) of the day-ahead market and the downward (upward) reserve activation prices:

$$pr_t^{\text{BM+}} = a_1 \cdot \min\{pr_t^{\text{DA}}, pr_t^{\text{aRD}}\} \tag{7.8}$$

$$pr_t^{\text{BM-}} = a_2 \cdot \max\{pr_t^{\text{DA}}, pr_t^{\text{aRU}}\} \tag{7.9}$$

where a_1 and a_2 are set to 0.7 and 1.3 in the Baseline scenario. Sensitivity analyses are conducted to investigate the impact of the selected values of a_1 and a_2.

All simulations are conducted on a Windows 10 machine with Intel(R) Xeon(R) Gold 6154 CPU @ 3.00 GHz and 479 GB memory. All optimization models are established by Yalmip [38] in MATLAB and solved with Gurobi.

In the following results sections, we first evaluate the performance of the DRO model by comparing its results to the results obtained by the RO and the SO models. Then we investigate the effects of including different statistical constraints in the ambiguity set for DRO. Finally, the impacts of the imbalance prices are analyzed. Note that while the comparisons between DRO, RO and SO are conducted for all considered investment years (i.e. 2020, 2030, 2040 and 2050), the influences of the statistical constraints and imbalance prices are investigated focusing on the 2020 results so as to eliminate the impacts of transformer capacity limit. Moreover, all quantities, profits and costs shown in this section are the annual values.

7.3.1 Results: Comparison of Different Optimization Models

To compare the performance of distributionally robust optimization, robust optimization and stochastic optimization in a reasonable way, we carry out the following simulations:

1. Run the DRO, SO and RO models described in Section 6.3 and Appendices 9.3-9.3 with the simulation dataset Data-sim. Fix the optimized investment decisions, the week-ahead reserve bidding decisions and the day-ahead decisions.
2. Build the out-of-sample dataset **Data-test** using the historical realizations of the DA wind and PV output forecast errors from 2018. Similar to the process to build the simulation dataset Data-sim based on the 2016-2017 data, we categorize the historical 2018 data into 24*4 groups depending on the hour of the day and the season of the year they belong to. To build one out-of-sample scenario, for each hour of the four representative weeks, the wind and PV forecast errors are simulated by randomly drawing samples correspondingly from one out of the 24*4 groups, depending on the hour and the season the considered hour belongs to. This process is repeated N^{test} times, where N^{test} is the number of the out-of-sample test scenarios.
3. For each one of the out-of-sample test scenarios, solve the deterministic problem with the fixed investment, week-ahead and day-ahead decisions achieved before by the DRO, the SO and the RO model, respectively.

The number of the out-of-sample scenarios N^{test} is set to 1000. In the baseline scenario, we limit the number of scenarios simulated by the SO model to 200, as continuously increasing the number does not affect the result too much but has a significant impact on the computational time of the SO model. The DRO model is simulated with an ambiguity set considering all statistical constraints described in Section 7.2.2, including the expectation, the mean absolute deviation and the variance. Results and the computational complexity of simulating the SO model considering different number of scenarios and the DRO model considering different statistical constraints are analyzed in the following paragraphs.

Comparisons of these three methods, namely the RO, DRO and SO models, are analyzed from the following perspectives: optimal investments, day-ahead

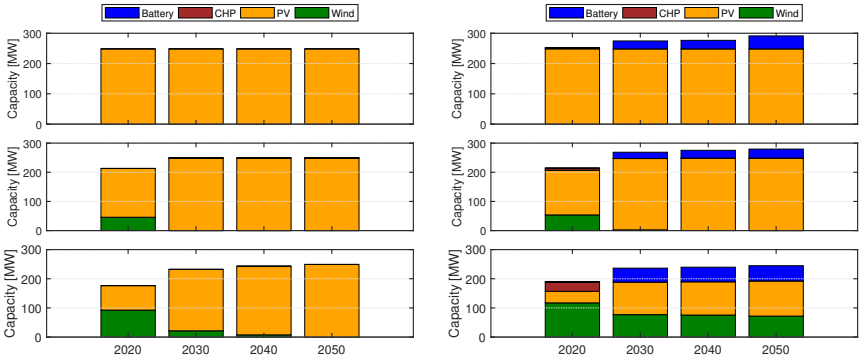

(a) Without Reserve Market **(b)** With Reserve Market

Figure 7.3: Comparison of the resulting investment decisions of the robust optimization (i.e., top figure), the distributionally robust optimization (i.e., middle figure) and the stochastic optimization models (i.e., bottom figure) with and without considering the reserve market participation.

bidding strategies, the expected simulation cost calculated using the simulation set Data-sim, the expected out-of-sample results calculated using test set Data-test and the computational efficiency.

Optimal investments

Figure 7.3 compares the investment decisions of RO, DRO and SO with and without considering the reserve market participation. It is obvious that battery is only invested when the RM participation is considered, since the additional revenue stream from the RM increases the economic viability of battery investments. Moreover, the Combined Heat and Power (CHP) units are only installed in the case with reserve market in 2020, when the costs for wind and PV investments are relatively high and the revenues from the day-ahead and the reserve markets are sufficient enough to cover the total cost of CHP investments.

When focusing on the case without (i.e., Fig. 7.3a) or with the reserve market (i.e., Fig. 7.3b), for each investment year, results show that the share of wind in the investment portfolio in general increases from RO to DRO and then to SO (i.e., from top figure to the bottom figure). The change in wind and PV investments is likely due to the fact that 1) as shown in Fig. 7.2, the volatility of wind

output forecast errors is higher than that of PV. For example, the worst-case wind generation (i.e. 305 MWh/MW-year) is only 16% of the DA generation forecast (i.e. 1880 MWh/MW-year), while the worst-case PV generation (i.e. 265 MWh/MW-year) accounts for 25% of its DA forecasted output (i.e. 1055 MWh/MW-year). Therefore, the profitability of wind investments improves more than that of the PV investments with the decreasing conservativeness of the model solutions. 2) The profitability of PV investment is limited by the fact that the excess PV generation during high solar irradiation hours (e.g. during summer), which exceeds the transformer capacity, needs to be curtailed. This impact is more pronounced when the uncertainty of forecast errors is modeled in a less conservative way, i.e. from RO to SO. However, when comparing the results over the years, it can be seen that the renewable investments in general shift from wind to PV, which can be traced back to the stronger projected cost declines assumed for PV. To be more specific, the investment cost for PV is assumed to decrease from 1481 EUR/kW in 2020 to 677 EUR/kW in 2050 by 54%, while the investment cost for wind only decreases 34% from 2219 EUR/kW in 2020 to 1458 EUR/kW in 2050 (see Appendix 9.3 for more details).

Furthermore, when focusing on the results for one specific optimization method for the case with or without reserve market participation, it can be observed that the difference between the investment decisions over the years (especially between 2030 and 2050) is relatively small. This is because compared to investing in local generations it is in general more favorable to purchase the electricity from the wholesale market and the RES target is binding in all simulated cases. For better illustrations, Table 7.1 shows the results of different optimization methods simulated using Data-sim for 2020 to 2050 in the cases with and without RM participation. Results shown include the annualized investment cost, total simulation cost and the demand cost, which is defined as the cost (including investment cost) incurred to satisfy each MWh of the demand, while respecting the assumptions and constraints. It can be seen that the calculated demand cost is higher than the average DAM price (i.e., 54.45 EUR/MWh) in 2020 and 2030. With the projected cost reductions, the demand costs resulted by DRO and SO are lower than the average DAM price for 2050 in the case without RM and for 2040 to 2050 in the case with RM. However, this seems to be against the observation that the investments ob-

Table 7.1: Annualized investment cost, total annual simulation cost and demand cost of different optimization methods for 2020 to 2050.

Results without considering the Reserve Market												
	2020			2030			2040			2050		
	RO	**DRO**	**SO**	**RO**	**DRO**	**SO**	**RO**	**DRO**	**SO**	**RO**	**DRO**	**SO**
Ann. inv. cost [mEUR]	21.28	20.21	19.06	12.66	12.69	12.72	11.19	11.22	11.28	9.73	9.75	9.75
Ann. tot. cost [mEUR]	34.60	24.77	24.52	24.98	15.58	16.44	23.52	14.11	15.04	21.80	12.40	13.33
Demand cost [EUR/MWh]	131.97	94.48	93.54	95.29	59.44	62.70	89.70	53.83	57.37	83.17	47.29	50.84

Results considering the Reserve Market												
	2020			2030			2040			2050		
	RO	**DRO**	**SO**	**RO**	**DRO**	**SO**	**RO**	**DRO**	**SO**	**RO**	**DRO**	**SO**
Ann. inv. cost [mEUR]	21.64	20.85	22.13	13.62	13.49	14.56	12.10	12.08	13.44	10.91	10.60	12.23
Ann. tot. cost [mEUR]	34.30	24.45	23.34	23.40	14.83	14.21	21.59	13.06	12.48	19.47	10.99	10.50
Demand cost [EUR/MWh]	130.83	94.26	89.01	89.25	56.55	54.19	82.34	49.81	47.59	74.26	41.90	40.05

Demand cost is calculated as the annual total simulation cost divided by the annual demand consumption.

tained by each optimization model from 2030 to 2050 are at a similar level and the RES target is still binding in 2050. This is because the modeled transformer capacity limits the profitability of RES investment (especially PV investment), i.e. the transformer capacity limit and the diurnal pattern of PV generations lead to the curtailment of PV generation during high solar irradiation hours (e.g. during summer).

Additionally, the investment cost decreases over the years, mainly as a result of the projected cost reductions. For each investment year and for each optimization method, the investment costs in the case with RM are higher than the corresponding case without RM, which suggests that the RM participation increases the economic viability of the DER investments.

When focusing on the the total simulation cost, in general it decreases from RO to DRO and then to SO because of the decreasing conservativeness of the model solutions. Nevertheless, exceptions can be observed in the case without RM for years 2030 to 2050, when the total simulation cost for DRO is lower than that of SO. This can be explained by the fact that scenarios used for SO are simulated assuming that the forecast errors are subject to the Gaussian distribution with mean and variance information extracted from Data-sim, without accounting for the mean absolute deviation that is considered by DRO. As the actual distribution of the forecast errors deviates from the Gaussian distribution that is assumed by SO, the variation of the forecast errors could be overestimated by simply using the standard deviation. To visualize this, Fig. 7.4 shows the historical PV and wind forecast errors together with the Gaussian

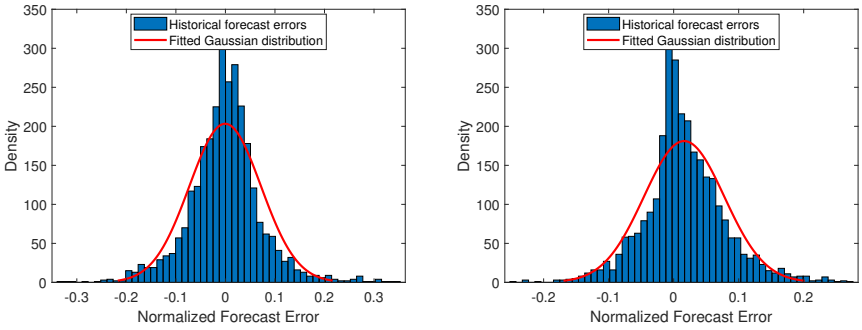

(a) PV **(b)** Wind

Figure 7.4: Historical PV and wind forecast errors and the corresponding Gaussian distribution fitting assumed by stochastic optimization for an example hour.

distribution fitting curves for an example hour. It is obvious that the actual distribution of the forecast errors is leptokurtic (i.e. a shape with high peaks and fatter tails), which significantly deviates from the fitted Gaussian distribution curve. This is consistent with the findings in [76].

Day-ahead bidding strategies

To better understand the results of these three models, we further investigate the difference in their DA bidding strategies. For better illustrations, results shown in this section are for 2020 without considering the reserve market. Figure 7.5 shows the DA biddings of the RO model and the DRO model along with the forecast range, whose upper/lower bound is defined by the sum of the point forecast value and the maximum/minimum forecast errors, over the four representative weeks. It can be observed that the RO model always bids at the lower bound of the forecast range, since the RO solutions are optimized against the worst-case. In contrast, the DRO bidding is less conservative and in general it falls into the purple area that is bounded by the mean absolute deviation[22], since more statistical information of the forecast error uncertainty is incorporated into the ambiguity set for DRO. However, exceptions are observed in the

[22]The upper/lower bound of the purple area is calculated as the DA point forecast plus/minus the mean absolute deviation.

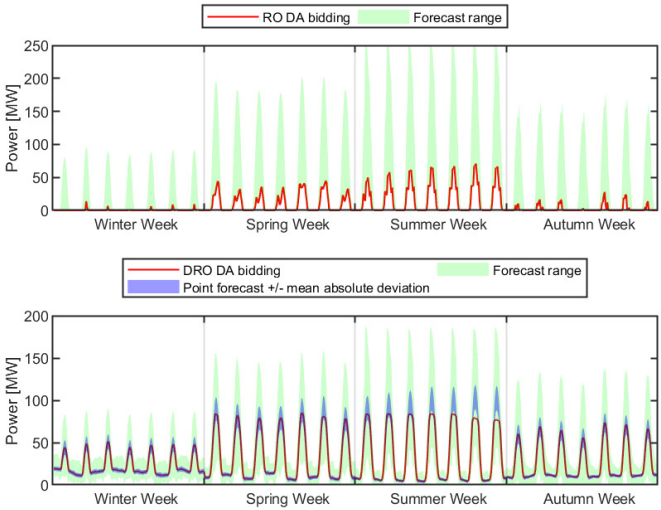

Figure 7.5: Comparison of the day-ahead bidding strategies of the robust optimization and the distributionally robust optimization models for 2020 without considering the reserve market.

summer week when the DRO model bids lower than the lower bound of the purple area. This is because the PV generation during the summer week is so high that the power injection from the aggregator to the transmission system reaches the limit of the assumed transformer capacity, which is defined by a factor of the aggregator's peak demand.

Figure 7.6 shows the DA biddings of the SO model over the four representative weeks in the bottom figure together with the relative difference between the imbalance price and the DAM price using the DAM price as the reference [23] in the top figure. Different from the RO and the DRO models, the SO model represents the uncertainty of the forecast error using a series of scenarios. In the bottom figure of Fig. 7.6, we plot both the DA bidding of the SO model using the red curve and the expected real-time output of the aggregator in blue, which is calculated as the sum of the DA point generation forecast and the av-

[23] The relative difference between the imbalance price and the DAM price is defined as the ratio of the difference between the DAM price and the imbalance price to the DAM price

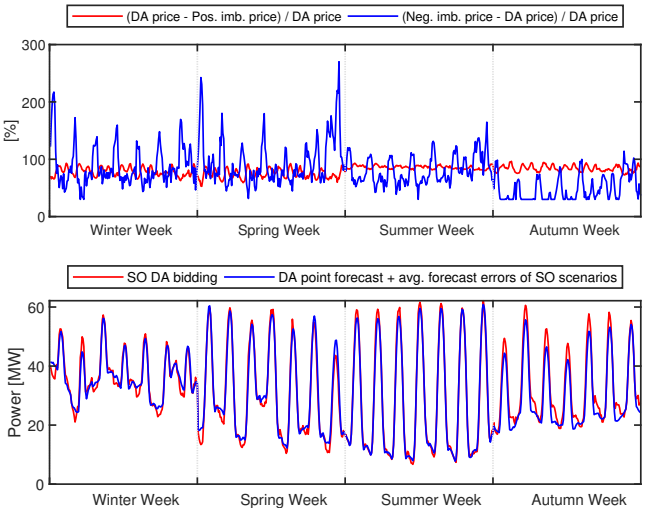

Figure 7.6: The relative difference between the imbalance price and the day-ahead market price over the four representative weeks (top figure); the day-ahead biddings of the stochastic optimization model over the four representative weeks for 2020 without considering the reserve market (bottom figure).

erage forecast errors of all scenarios considered. The SO model is expected to bid exactly the same amount as the expected real-time output so as to minimize the real-time imbalances, however, Fig. 7.6 shows that the DA bidding (i.e. red curve) deviates from the expected real-time output (i.e. blue curve). This can be explained by the relative difference between the positive/negative imbalance price and the DAM price as shown in the top figure of Fig. 7.6. The red curve defines the ratio of the difference between the DA price and the positive imbalance price to the DAM price, whereas the blue curve denotes the ratio of the difference between the negative imbalance price and the DAM price to the DAM price. It can be observed that in general the SO model bids lower/higher than the expected real-time output (i.e. the aggregator tends to be long/short) when the relative difference between the negative imbalance price and the DA price is higher/lower than the relative difference between the DA price and the positive imbalance price so as to minimize the potential imbalance costs. To summarize, while the RO and the DRO models bid into the DAM mainly

Table 7.2: The expected, worst-case and the standard deviation of the out-of-sample imbalance and total costs of different optimization methods for 2020 to 2050 with and without considering the reserve market.

Results without considering the Reserve Market													
	Cost [mEUR]	2020			2030			2040			2050		
		RO	DRO	SO	RO	DRO	SO	RO	DRO	SO	RO	DRO	SO
Expected	Total	32.66	24.74	24.43	23.05	16.45	16.33	21.58	14.98	14.91	19.87	13.26	13.20
	imbalance	-1.94	1.02	2.32	-1.94	0.55	1.40	-1.94	0.55	1.12	-1.94	0.55	0.96
Worst-case	Total	34.60	41.91	43.18	24.98	30.53	32.26	23.52	29.06	29.79	21.80	27.35	27.46
	imbalance	0	18.20	21.07	0	14.63	17.33	0	14.63	16.00	0	14.63	15.22
Standard deviation	Total	0.09	0.32	0.31	0.09	0.30	0.34	0.09	0.30	0.34	0.09	0.30	0.33
	imbalance	0.09	0.32	0.31	0.09	0.30	0.34	0.09	0.30	0.34	0.09	0.30	0.33

Results considering the Reserve Market													
	Cost [mEUR]	2020			2030			2040			2050		
		RO	DRO	SO	RO	DRO	SO	RO	DRO	SO	RO	DRO	SO
Expected	Total	32.22	23.98	23.45	21.39	15.27	14.06	19.56	13.51	12.36	17.40	11.42	10.44
	imbalance	-1.91	0.46	0.16	-2.01	0.15	1.09	-2.01	0.15	1.07	-2.04	0.15	1.22
Worst-case	Total	34.31	40.72	40.39	23.46	29.47	31.97	21.66	27.57	30.00	19.54	25.38	27.89
	imbalance	0	13.91	5.97	0.07	14.35	18.99	0.09	14.20	18.71	0.10	14.11	18.67
Standard deviation	Total	0.09	0.31	0.27	0.09	0.26	0.28	0.09	0.26	0.28	0.09	0.26	0.27
	imbalance	0.09	0.25	0.11	0.09	0.26	0.28	0.09	0.26	0.28	0.09	0.26	0.27

considering the worst-case and the worst distribution of the variable forecast errors, the SO model optimizes the bidding into the DAM considering both the expected real-time forecast errors and the relationship of the DAM price and the imbalance prices at real-time. It is worth noting that the imbalance prices are assumed to be perfectly forecasted in this work and the performance of the SO model might be influenced when the uncertainty of the imbalance prices are considered.

Out-of-sample results

Table 7.2 compares the expected, the worst-case and the standard deviation of the out-of-sample imbalance and total costs obtained by solving the deterministic problem with the fixed investment and day-ahead decisions from the RO, DRO and SO models over 1000 test scenarios from Data-test. As expected, it shows that RO achieves the lowest expected imbalance cost, the lowest worst-case imbalance and total costs, and the lowest standard deviation of the imbalance and total costs in all simulation years and cases. However, this is at the cost of having over-conservative solutions that yield the highest expected total costs among all models. The conservative nature of RO is due to the fact that the uncertainties are captured using an uncertainty set and the decisions are optimized against the worst-case scenario. In contrast to RO, the SO model

in general obtains the lowest expected total costs, the highest worst-case imbalance and total costs, and the highest standard deviation of the imbalance and total costs. This is because the SO model describes the uncertainty using a set of scenarios and computes the optimal expected cost over these scenarios, which could address the over conservatism issue in RO but can hardly protect against extreme cases that rarely happen. As shown in Fig. 7.6, the SO model optimizes the DA bidding considering the relationship of the DAM and the imbalance prices. As the market prices are assumed to be perfectly forecasted, this bidding strategy manages to improve the performance of the SO model in the out-of-sample test. Furthermore, while the difference between the total expected costs achieved by the DRO and the SO models is negligible in the case without considering the RM, the difference becomes greater in the case with RM for years 2030 to 2050. This can be explained by the significant amount of batteries invested by SO from 2030 to 2050 in the case with RM, which helps to reduce the real-time cost through re-dispatch.

The DRO models perform better than the RO model in terms of the expected costs, as they incorporate more of the uncertainty distribution information so as to provide less conservative results. Moreover, while the expected out-of-sample cost that the DRO model achieves are slightly higher than that of the SO model, the worst-case performance of the DRO model is much better than the SO model. To summarize, as an intermediate method between SO and RO, DRO could achieve a good trade-off between the expected performance and the performance in extreme cases.

Computational efficiency

The problem size and the computational time consumed by robust optimization, distributionally robust optimization and stochastic optimization considering different number of scenarios are compared in Table 7.3. The optimality gap is set to 0.05% for all optimization models. While the solver time is the time that Gurobi takes to solve the problem, the total time is the elapsed time from starting to build the model until the model returns the output. It can be seen that the RO model takes the shortest time to solve as it has the lowest number of variables and constraints. Nevertheless, the total time consumed by the RO model is much longer than the solver time, which is likely due to the fact that

Table 7.3: Problem size and the computational time of different optimization methods.

Results without considering the Reserve Market					
	RO	**DRO**		**SO**	
Scenario No.	n/a	n/a	100	200	400
Variable No.	25'570	1'077'932	1'154'530	2'296'930	4'581'730
Constraint No.	11'428	776'165 (26'880 quadratic)	610'180	1'214'980	2'435'332
Solver time [s]	1	221	331	1'951	5'800
Computational time [s]	76	1'312	338	1'969	5'835

Results considering the Reserve Market					
	RO	**DRO**		**SO**	
Scenario No.	n/a	n/a	100	200	400
Variable No.	43'042	1'090'700	1'172'674	2'315'074	4'599'874
Constraint No.	22'180	781'541 (20160 quadratic)	620'932	1'225'732	2'435'332
Solver time [s]	2	222	524	2'243	28'900
Computational time [s]	137	1'808	533	2'264	28'927

Robust optimization was solved using the integrated module in Yalmip.

the it is solved using the integrated RO module in Yalmip. In contrast to the RO model, it takes much longer time to solve and to construct the DRO model since a significant amount of quadratic constraints are incorporated. However, the dimension and the solver time of the DRO model are much smaller and shorter than that of the SO model considering only 200 scenarios. Furthermore, when increasing the scenario number of the SO model from 100 to 400, the corresponding computational time increases more than the problem dimension increase. The results suggest that compared to SO the RO and DRO methods are more applicable for cases with large amounts of historical data available since the dimension of the problem and the computational time of these two models do not increase with the size of the dataset. However, it is worth mentioning that enough memory should be available when applying the DRO model with quadratic constraints.

7.3.2 Results: Effects of Statistical Constraints in the Ambiguity Set

In this section, case studies are conducted to demonstrate how investment decisions and costs, the out-of-sample performance and the computational efficiency are affected by considering different types of statistical constraints

Table 7.4: Impact of considering different statistical data in the ambiguity set.

Results without considering the Reserve Market							
Case	**CHP**	**Wind**	**PV**	**Inv. cost**	**Out-of-sample cost [mEUR]**		**Computational**
	[MW]	**[MW]**	**[MW]**	**[mEUR]**	**Expected**	**Worst-case**	**time [s]**
DRO_simp1	0	0	249.1	21.3	26.1	40.2	232
DRO_simp2	0	45.8	167.3	20.2	24.7	41.9	234
DRO_full	0	45.8	167.3	20.2	24.7	41.9	1'312

Results considering the Reserve Market							
Case	**CHP**	**Wind**	**PV**	**Inv. cost**	**Out-of-sample cost [mEUR]**		**Computational**
	[MW]	**[MW]**	**[MW]**	**[mEUR]**	**Expected**	**Worst-case**	**time [s]**
DRO_simp1	0.3	0	249.1	21.4	25.9	39.9	233
DRO_simp2	7.2	53.6	153.3	20.8	24.0	40.7	241
DRO_full	7.2	53.6	153.3	20.8	24.0	40.7	1'808

Battery storage units are not invested in the above presented cases.

in the ambiguity set. Three cases are defined depending on the statistical constraints included in the ambiguity set:

- **DRO_simp1**: The ambiguity set is constructed only considering the expectation of the forecast errors.
- **DRO_simp2**: The ambiguity set is constructed considering the expectation and the mean absolute deviation of the forecast errors.
- **DRO_full**: The ambiguity set is constructed considering the expectation, the mean absolute deviation and the variance of the forecast errors. This is also the model applied in the baseline scenario.

Table 7.4 shows the investment and the out-of-sample results as well as the computational time for 2020 of the proposed DRO model with different types of statistical data included in the ambiguity set to capture the distribution of forecast errors. It can be seen that in general the expected out-of-sample cost decreases and the worst-case out-of-sample cost increases with more statistical information included into the ambiguity set. This is because the worst-case distribution of wind and PV forecast errors improves with more statistical information and the resulting decisions are therefore less conservative.

Moreover, the results of case DRO_simp2 and case DRO_full shown in Table 7.4 are the same. This seems to be against the expectation that including the additional variance constraints into the ambiguity set could further limit the variability of both the wind and PV output forecast errors and improve the expected worst-case wind and PV forecast error distributions. To investigate

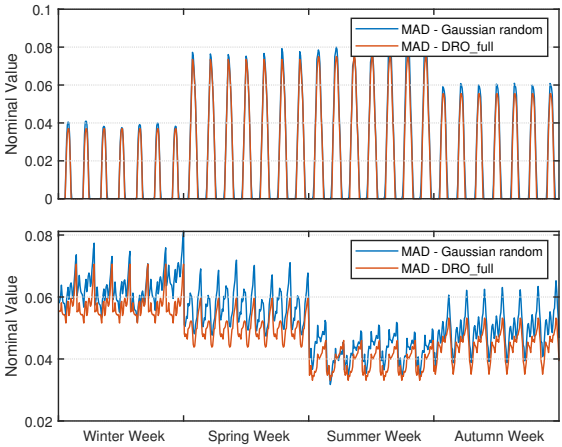

Figure 7.7: Hourly mean absolute deviation of the day-ahead PV output forecast errors (i.e., top plot) and wind output forecast errors (i.e., bottom plot) simulated for distributionally robust optimization and calculated for the Gaussian distributed scenarios with the same mean and absolute deviation.

the reasons behind this observation, we generate 1000 Gaussian distributed random wind and PV forecast error scenarios with the same mean and variance data used by DRO_full. The Mean Absolute Deviation (MAD) of the Gaussian distributed forecast errors together with the nominal MAD of the PV and wind forecast errors used by DRO_full over the considered four representative weeks are shown in Fig. 7.7. Note that the consistent pattern of the days of the same season is due to the fact that for each season the statistical information is only differentiated depending on the hour of the day. It can be noticed that the MAD used by DRO_full is in general lower than the MAD of the Gaussian distributed random scenarios generated with the mean and variance used by DRO_full, i.e. the worst-case distribution is still decided by the mean absolute deviation constraint. As the standard deviation emphasizes the larger deviations by adding more weights to data that are far from the mean value (i.e., extreme values), a dataset with more extreme values could result in a much higher standard deviation. Furthermore, although standard deviation is widely used for statistical analysis, it is argued by researchers that the mean absolute deviation is more efficient as an estimate of a population parameter in the real-life situa-

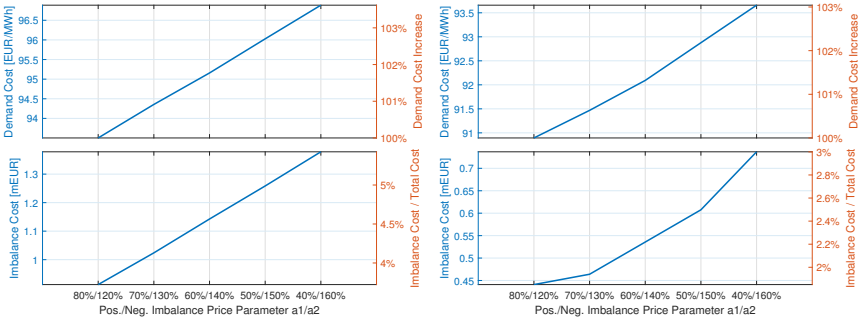

(a) Without RM **(b)** With RM

Figure 7.8: Demand cost and the imbalance cost developments by running the distributionally robust optimization model under different values of positive and negative imbalance price parameters a_1 and a_2.

tion where the data contain tiny errors, or do not form a completely perfect Gaussian distribution [151].

Regarding the computational time, it is obvious that while the computational time consumed by DRO_simp1 and DRO_simp2 is comparable, the computational complexity significantly increases for the DRO_full model since a number of quadratic variance constraints are considered.

To summarize, the investment and total out-of-sample costs in general decrease when more statistical constraints are considered as the worst-case distribution is improved. However, people might need to consider only incorporating the absolute deviation constraints into the ambiguity set especially when the distribution of the uncertainties deviates from the Gaussian distribution, as the model is easier and faster to solve and delivers a result that is comparable to the one that incorporates the additional variance constraints.

7.3.3 Results: Impacts of the Imbalance Price

In this section, we analyze the impacts of imbalance prices by carrying out the simulations with different values of the positive and negative imbalance price parameters a_1 and a_2 in equations (7.8) and (7.9). As a reminder, a lower value of a_1 and a higher value of a_2 mean a lower positive imbalance price and a higher negative imbalance price, which could translate into higher imbalance

penalties for the aggregator. Results of the investment year 2020 for the case with and without considering the RM are shown in Fig. 7.8. It can be seen that the demand cost, i.e. the cost for satisfying each MWh of demand, increases by around 3% when changing the ratio of a_1/a_2 from 80%/120% to 40%/160% for both the cases with and without the RM. Furthermore, the ratio of the imbalance cost to the total aggregator cost increases from 3.5% to 5.5% in the case without RM and from 1.8% to 3% in the case with RM. The lower ratio in the case with RM could be attributed to the investment of battery and CHP units, which help to reduce the real-time imbalances via re-dispatch. However, it is worth noting that the imbalance cost might be underestimated due to the utilization of country-level generation and forecast data from Elia.

7.4 Limitations and Future Work

This work has several limitations and a few of which are highlighted in this section. First, the ambiguity set is constructed considering the mean, the mean absolute deviation and the standard deviation of the wind and PV output forecast errors. Statistical information such as skewness and kurtosis, which are important to characterize the forecast error distributions [76], are not captured. Futhermore, correlations of the forecast errors between hours and the in general inverse correlation of PV and wind forecast errors are not considered [152]. A future version should investigate the impacts of incorporating these statistical characteristics.

Second, the volatility of the wind and PV forecast errors are underestimated using the historical country level data from Elia, which is due to the statistical smoothing effects when aggregating the generation data for a region [44]. The work could be improved by using a more proper dataset.

Third, sensitivity analysis is required to investigate the impacts of the long-term uncertainties of the planning problem, e.g. changes in demand and electricity market prices over the years.

7.5 Summary and Conclusions

A multi-stage distributionally robust optimization model to derive optimal investment decisions for a DER aggregator in a market environment is presented.

Comparison of the proposed distributionally robust optimization model with the robust and traditional stochastic models shows that the distributionally robust optimization model achieves a good balance between the expected performance and the performance in extreme cases with acceptable computational effort. Thus, the distributionally robust optimization model is more appropriate in cases when a large amount of historical data is available and the probability distribution of the random variables is unknown. Analysis regarding the impacts of the statistical constraints included in the ambiguity set suggests that in general the out-of-sample performance improves when more statistical constraints are considered as the worst-case distribution of the forecast errors is improved. However, since the mean absolute deviation provides a good estimation of the variance of the data especially when the data do not form a completely perfect Gaussian distribution [151], adding the variance information to an ambiguity set that already incorporates the expectation and the mean absolute deviation limits does not necessarily improve the performance of the model but greatly increases the computational complexity of the problem.

Part III

Techno-economic Analysis of PV-battery Systems

Chapter 8

Case study: Techno-economic Analysis of PV-battery Systems in Switzerland

This chapter presents a techno-economic optimization model to analyze the economic viability of a Photovoltaic-battery (PVB) system for different customer groups in Switzerland clustered based on their annual electricity consumption values, rooftop sizes, annual irradiation levels, and located regions. The simulations for a static investment model are carried out for the years 2020-2050. A comprehensive sensitivity analysis is conducted to investigate the impacts of individual parameters such as costs, load profiles, electricity prices, and tariffs. Results show that while combining Photovoltaic (PV) with batteries already results in better net present values than PV alone for some customer groups today, the payback periods fluctuate between 2020 and 2035 due to the mixed effects of policy changes, cost and electricity price developments. The optimal PV and battery sizes increase over time, and in 2050 the PV investment is mainly limited by the rooftop size. The economic viability of PVB system investments varies between different customer groups. The investments with the shortest payback period are primarily accessible to customer groups with higher annual irradiation and electricity consumption levels. In addition, investment decisions are highly sensitive to payback periods, future costs, electricity prices and tariff developments. Lastly, the grid impact of the PVB system deployments is investigated

by analyzing the residual Swiss system load profile. The dynamics of residual load profiles caused by the seasonal, daily, and hourly patterns of the solar generation emphasize the need for flexible resources with fast ramping capabilities. This chapter is based on [153].

8.1 Introduction

8.1.1 Motivation

Solar energy is widely recognized as a solution to tackle climate change by lowering worldwide greenhouse gas emissions from the energy sector [154]. After a slowdown in 2018, the global solar energy market experienced a strong recovery in 2019, reaching 627 GW of cumulative PV installations [155]. This capacity accounts for nearly 3% of the global electricity demand and contributes to around a 5% reduction in worldwide electricity related CO_2 emissions [156]. Major drivers for the increasing PV penetration are the provision of subsidies and the overall decreasing costs. But subsidies that aim to compensate the capital-intensive PV investment are changing: feed-in tariffs are decreasing continuously while injection remunerations that are paid by the local Distribution System Operators (DSOs) (which we will refer to as the injection tariff in the following context) are already or will soon be lower than the retail tariff, which encourages self-consumption of PV generation. One of the means to enable the further development of PV installations is the use of battery storage, which is able to increase the PV self-consumption rate and also resolve the real-time imbalances caused by forecast errors [105]. In the past, high costs and limited combinations of use cases were the greatest barriers for battery installations. However, as battery prices have declined dramatically over the last decade[24], mainly driven by developments in the Electric Vehicles (EV) industry, batteries are now considered to be one of the most promising solutions to enable the transition towards renewable energy sources. In addition, with a proper combination of different applications, investments in battery storage units could already be attractive today [118].

8.1.2 Literature review

Techno-economic assessments of PVB systems have been extensively researched in recent years, especially in Germany where favorable renewable policies are implemented. As shown in Table 8.1, the existing techno-economic models can be categorized into optimization and simulation models, depending on whether the capacity of PV and battery units are optimization variables

[24] Battery packs decreased from over 1100 USD/kWh in 2010 to around 150 USD/kWh in 2019.

Table 8.1: Overview of the existing techno-economic studies of the PV-battery system.

Ref.	Year	Region	Model type	Battery type	Main economic indicator	Main sensitivity analysis	Load
[118]	2016	GE	Simulation	Lithium-ion	NPV	Battery application combination	S
[141]	2014	GE	Optimization	Lead-acid	NPV	Wholesale electricity price, retail tariff	R
[157]	2016	GE	Simulation	Lithium-ion	ROI	Battery parameters, electricity price, household size	R
[158]	2016	GE	Simulation	Lithium-ion	Annuity costs	Size and cost of PV and battery	R
[159]	2016	GE	Simulation	n/a	NPV	Load profile, EV profile	R
[160]	2016	SE	Optimization	Lithium-ion	SC, SS	Load profile, battery E-rate	R
[161]	2016	AU	Optimization	Lithium-ion & lead-acid	NPV	Load profile, PVB system cost, electricity tariff	R
[162]	2016	Europe	Simulation	n/a	LCOE	load profile, location	S
[163]	2017	PT	Simulation	Lead-acid	NPV, IRR, PI, DPP, LCOE	Consumption mode	S
[164]	2017	GE	Optimization	Lithium-ion	LCOE	Load profile	R
[165]	2017	GE, IE	Simulation	Lithium-ion	IRR	Load profile	S
[166]	2017	SE	Optimization	Hydrogen & lithium-ion	NPV	Operation strategy, PVB cost	R
[167]	2017	UK	Simulation	Lithium-ion	Net benefit	Battery degradation costs	R
[168]	2017	UK	Optimization	Lithium-ion	Annuity cost	Electricity tariff mode, battery capacity	R
[169]	2017	PT	Simulation	Lithium-ion	Electricity bill, NPV	Battery cost, interest rate	S
[170]	2017	BE	Simulation	Lithium-ion	LCOE	Size of PV and battery, storage price	R
[171]	2017	AU	Simulation	n/a	LCOE, NPV, IRR, DPBP, PBP	Size of PV and battery	R
[172]	2017	CH, UK, IT	Optimization	Lithium-ion & lead-acid	NPV	Location, battery technology	S
[173]	2018	CH	Optimization	Lithium-ion	NPV	PV and battery parameters and cost	R
[174]	2018	US	Simulation	Lithium-ion	LCOE	PVB cost, subsidy, discount rate, battery efficiency	S
[175]	2018	NE	Simulation	Lithium-ion	PI	Battery operation strategy, PVB system size and cost	R
[176]	2019	AU	Simulation	Lithium-ion	DPPB	Discount rate, feed-in-tariff	R
[177]	2019	CN	Simulation	Reused EV battery	NPV	Battery operation strategy	S
[178]	2019	FI	Simulation	Lithium-ion	Annuity cost	Electricity price and tariff mode	S
[179]	2020	IT	Simulation	n/a	NPV, LCOE, IRR, DPBP	Consumption level, investment scheme	S
[180]	2020	TH	Simulation	Lithium-ion	NPV, LCOE	Retail tariff, battery cost and size	R

Note: Definitions of economics indicators can be found in Section 8.3. Load type R and S stand for real-world and synthetic, respectively.

or simulated as exogenous parameters. While most of the existing studies focus on applications of PVB systems in residential sectors, some also investigate commercial and industry sectors [118, 158, 175, 177].

Most of the existing research focuses on lithium-ion or lead-acid batteries, however, recent studies have shown that lithium-ion batteries are more viable, techno-economically, than lead-acid batteries [170, 181] thanks to their recent drastic cost reductions and technology improvements. Some works also investigate hydrogen-based battery units [166] as well as reused electric vehicle batteries [177]. A review of different stationary electricity storage technologies can be found in [182].

Concerning battery operation strategies, most works [141, 167, 170, 173, 174] adopt simple rule-based strategies that aim to maximize the self-consumption rate, i.e. surplus PV generation is primarily used to charge the battery while any demand deficit is first satisfied by the stored energy in the battery. Some consider hybrid operation strategies, e.g. [169] applies batteries to peak shaving while [175] investigates uses in frequency reserve provision. In [118], the benefits of combining different applications of battery storage units are investigated. As mentioned in [166], simple rule-based strategies might underestimate the economic value of the investment and it is indeed important to adopt appropriate operation strategies in the analysis.

Since the input data and parameters such as costs, load profiles, wholesale and retail electricity prices, and local policies vary widely across published studies, different conclusions concerning the economics of PVB systems are drawn. While references [167] and [171], published in 2017, state that the integration of batteries is not attractive at that time in the UK and Australia, [141] and [118], published in 2014 and 2016, indicate that it could be profitable for certain PVB in Germany. However, a comparatively low battery cost, i.e. 171 EUR/kWh + 172 EUR/kW, is assumed in [141]. The work in [174] shows that pairing Battery Energy Storage Systems (BESS) with PV systems can improve the economics and performance of a PVB system in the US and [169] identifies that the electricity bill could be reduced by 87% for the considered residential house in Portugal. Some studies investigate the break-even price of battery units. For example, [158, 159, 168, 173, 180], which were published between 2016 and 2020 and simulated battery costs between 138-400 EUR/kWh, con-

cluded that batteries could be profitable for commercial or residential sectors in Belgium, Germany, the UK, Switzerland and Thailand. In contrast, the study in [164] estimates that the break-even price of BESS in Germany ranges from 900 to 1200 EUR/kWh, whereas the work in [165] finds that battery costs of 500–600 EUR/kWh may make PVB systems generally profitable in Germany even without subsidies.

Based on this literature review, the identified research gaps are as follows:

- Most existing works consider one single representative household for the entire country, i.e one single price and one tariff for the PVB system, thereby neglecting price differences between different PV/battery categories, regional differences within one country, and different trade-offs faced by different household groups. This makes it difficult for policy-makers and regulators to learn from these studies.
- Most existing works assume a simple rule-based battery operation strategy that aims to maximize the self-consumption rate, which underestimates the value of battery investments by ignoring the multi-applications case (e.g. price arbitrage).
- There is limited discussion about battery C-rates (i.e. the rate to quantify the maximum discharging rate of the battery as a reference to its maximum capacity) and most works only make energy-related cost assumptions.
- Specific types of load profiles are utilized for the analyses, e.g. scaled aggregated load profiles as well as synthetic profiles or real measurements taken from individual households. But there is limited analysis of the impact of load profiles, which are expected to affect the PV self-consumption rate and the profitability of battery units.
- There is almost no analysis of the grid impact (e.g., maximum hourly injection and ramping etc.) of PVB system installations.

This work aspires to address these gaps and presents a static investment optimization model to assess the economics of PVB systems by minimizing the total investment and operational costs over a 30-year horizon. The optimization is conducted for a variety of customer groups in Switzerland in the years from 2020 through 2050. The customer group's heterogeneity is modeled using different rooftop sizes, annual irradiation and electricity consumption values, individual load profiles and geographical regions.

8.1.3 Status of PV and Battery in Switzerland

To support the implementation of the Energy Strategy 2050 [183] and a smooth transition towards a nuclear phaseout, Switzerland introduced different policies to encourage the deployment of renewables, especially PV investments, including: a feed-in tariff, investment subsidy, tax rebates and injection remunerations. PV is considered to be the most promising renewable resource in Switzerland due to the high social acceptance and the high deployment potential. The solar installation potential on rooftops and building facades in Switzerland is estimated to be 67 TWh (including 17 TWh from facades) [184]. As a result, the annual PV deployment increased from 26 MW in 2009 to 327 MW in 2019 [155], reaching a cumulative installed capacity of 2.5 GW and accounting for about 3.3% of the annual Swiss electricity demand in 2019 (i.e. 2.11 TWh of PV toward the 63.4 TWh demand). However, to achieve the ambitious net-zero greenhouse gas emissions targets by 2050 and to replace the phasing-out nuclear power, nearly 50 GW of new PV installations are required by 2050 according to Swisssolar [185], which translates into around 1.6 GW of new installations annually.

According to data published by Swisssolar [59], the battery storage market in Switzerland, although still quite small, has experienced an increase in annual installed capacity in the last few years. In 2018, 14.6 MWh were added, while in 2019 new installations increased to 20.4 MWh (including 20.3 MWh lithium-ion and 0.09 MWh lead-acid batteries), leading to a total battery storage capacity of 50.7 MWh. Additionally, the average system size increased from 9.1 kWh in 2018 to 13.5 kWh in 2019, which is consistent with the increase in the average installed PV unit size (from 19.4 kW in 2018 to 22.5 kW in 2019). In addition, around 15% of newly installed PV systems for single-family houses are equipped with battery storage units.

Based on these trends and developments, this work aims to answer questions such as:

- How are the PVB system economics affected by different customer groups that are categorized by rooftop sizes, annual electricity consumption and irradiation values, and geographical location of deployment?
- How does the optimal size of the PVB system change across different customer groups?

- What are the expected cumulative investments of the PVB system at both the regional and the national levels over the coming years?
- How sensitive is the economic viability of the PVB system to uncertainties related to e.g. costs, load profiles, electricity prices, etc. and which are the driving factors?
- What are the potential challenges and opportunities for investors, retailers, electricity system operators and policy-makers?

The rest of the chapter is organized as follows: Section 8.2 describes the data and assumptions in this research. Mathematical formulations of the proposed optimization model are given in Section 8.3. Section 8.4 analyzes the results and a further discussion of the results from different perspectives is given in Section 8.5. Finally, limitations of this work and conclusions are stated in Section 8.6 and Section 8.7, respectively.

8.2 Data

8.2.1 General Assumptions

We run the static investment model for the examined years 2020-2050 with a step of 5 years and the lifetime of the PVB system is assumed to be the same as the lifetime of PV, i.e. 30 years. Weighted Average Cost of Capital (WACC) is set to be 4% [141] and the amortization period is the same as the lifetime of the invested unit. Since the lifetime of battery units are in general shorter than 30 years, a battery replacement is assumed and the potential remaining value of the last reinvested battery by the end of the PVB system lifetime is also calculated.

8.2.2 Rooftop Potential and Data Clustering

We focus on rooftop solar and simulate each potential rooftop based on the Sonnendach dataset [186], which analyzes the solar generation potential for Switzerland by accounting for the roof area, orientation, tilt, utilization type and region. The high level of detail in this dataset thus enables a high level of granularity in our simulation results. According to [186], only buildings with roof areas greater than 10 m^2 and an annual solar irradiation higher than 1000 kWh/m^2 should be considered. The availability factors of the rooftops, which

reduce the effective rooftop area, range between 42% and 80% depending on building types, roof sizes and tilt. This range accounts for the possible unavailability of the roof areas due to factors such as obstructions, windows and shadings (for details see page 7 of [186]). After accounting for these factors, the theoretically available rooftop area is reduced from 630 km^2 to 304 km^2 (i.e. 105 GW to 51 GW assuming 6 m^2/kWp). We further process the data by focusing on detached buildings (i.e. Einzelhaus) with warm water consumption that account for around 94% of the potential solar generations and exclude potentials from bridges, high buildings, buildings under construction, etc. Finally, the total potential rooftop area modeled in this work equals 224 km^2 (i.e. 37 GW), which corresponds to 3'795'145 rooftop data entries.

To lower the computational burden, these nearly 4 million data entries are clustered into different groups depending on their annual irradiation, roof sizes, warm water consumption (which is used to approximate their electricity consumption), and geographical regions:

- **IRR1**-**IRR5**: 5 irradiation categories in kWh/m^2/year with a step of 150 kWh/m^2/year, i.e. 1'000-1'150, 1'150-1'300, 1'300-1'450, 1'450-1'600 and >1'600;
- **A1**-**A40**: 40 roof size categories with a step of 6 m^2 between 12 m^2 and 60 m^2, a step of 12 m^2 between 60 m^2 and 180 m^2, a step of 30 m^2 between 180 m^2 and 600 m^2, a step of 300 m^2 between 300 m^2 and 1'200 m^2, a step of 600 m^2 between 1'200 m^2 and 2'400 m^2 and a step of 1'200 m^2 between 2'400 m^2 and 6'000 m^2;
- **L1**-**L11**: 11 annual electricity consumption categories in kWh/year[25], i.e. 0-1'600, 1'600-2'500, 2'500-3'500, 3'500-4'500, 4'500-5'500, 5'500-7'500, 7'500-13'000, 13'000-25'000, 25'000-30'000, 30'000-150'000 and >150'000;
- **REG1**-**REG26**: 26 regions corresponding to the 26 cantons in Switzerland.

After clustering, all data entries are categorized into 5*40*11*26 = 57'200 groups which we will refer to as customer groups in the following context. We analyze the economic viability of PVB systems across the nearly 4 million rooftops con-

[25]Since the annual electricity consumption data is not available, we approximate the annual electricity load as 125% of the warm water consumption [187, 188, 189]. The corresponding warm water consumption levels in kWh/year are: 0-1'280, 1'280-2'000, 2'000-2'800, 2'800-3'600, 3'600-4'400, 4'400-6'000, 6'000-10'400, 10'400-20'000, 20'000-24'000, 24'000-120'000 and >120'000.

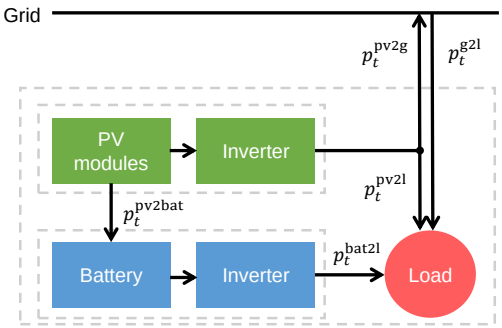

Figure 8.1: Structure and power flows of the modeled PV-battery system.

sidered in Switzerland by evaluating each customer group using the median values from within each group.

8.2.3 Parameters of the PV-battery System

Each one of the 57'200 customer groups faces an investment optimization problem for a PVB system. The fundamental model created for the PVB system consists of five components: the PV module, the battery unit, the inverter, the load and the grid. The structure of the PVB system and the power flows modeled between different components are illustrated in Fig. 8.1. The battery unit is assumed to be AC-coupled since compared to DC-coupling AC-coupling provides higher operational flexibility although it requires an additional battery inverter.

Table 8.2 gives the parameters for the considered PVB system using 2020 as the reference year. Based on historical PV installation data of Switzerland [59], although the average installed capacity of PV is increasing, most of the recent investments are still small-scale. For example, PV categories smaller than 1000 kWp account for almost all PV deployments in 2019, i.e. <30 kWp (40%), 30-100 kWp (16%) and 100-1000 kWp (39%), while >1000 kWp PV investments make up the remaining 5% of the total installed capacity. Therefore, we include five PV categories (i.e., 0-6 kWp, 6-10 kWp, 10-30 kWp, 30-100 kWp, >100 kWp) and limit the minimum and maximum capacity to 2 kWp and 50 MWp, which covers most of the potential investments and also corresponds to the range of PV units that could apply for the one-time investment subsidies in Switzer-

Table 8.2: Parameters of the PV-battery system.

Category	Parameter	Adopted value	Source
PV	Investment cost	754~2'786 EUR/kWp	[3]
	Operational cost	1.7~2.6 cent/kWh	[3]
	Module efficiency	17%	[3]
	Inverter efficiency	98%	[3]
	Performance ratio	80%	[3]
	Lifetime	30 years	[3]
	Area requirement	6 m^2/kWp	[3]
Battery	Investment cost	295~459 EUR/kWh + 249~388 EUR/kW	[190]
	Operational cost	3.7~5.7 EUR/kW/year + 1.1~1.7 EUR/MWh	[190]
	Lifetime	13 years	[190]
	Depth of discharge	100%	[190]
	Charging/discharging efficiency	93%	[190]
	Inverter efficiency	100%	n/a
	Self-discharge	0%	[190]
PVB system	Degradation rate	0.5% per year	[3, 164]

Note: Original values are converted to Euros based on the exchange rate of 0.91 EUR/CHF and 0.85 EUR/USD.

land [191]. The most commonly used batteries combined with a small-scale PV are lithium-ion and lead-acid batteries. Although lead-acid batteries have lower capital costs, lithium-ion batteries are proven to be more cost-efficient as a result of better Depth of Discharge (DOD) and cycle life [172, 192]. In addition, the Swiss battery market is dominated by lithium-ion with only a negligible amount of lead-acid batteries installed in recent years; we therefore only consider lithium-ion batteries in this work. Note that the costs shown in Table 8.2 are for the year 2020 and are given as ranges since they vary according to the invested unit size and the considered scenario. As the assumed battery costs vary greatly between different studies, ranging from 250 EUR/kWh to 1883 USD/kWh, we provide, for comparative reasons, a list of the cost assumptions made by some recent works in Table 8.3 along with the cost data selected in our simulations which are based on [190]. Future investment and operational costs for PV and batteries are estimated using projections from [3] and [193][26], respectively. Details of the costs for future years are provided in Appendix 9.3 and Appendix 9.3.

[26]Data for missing years are estimated using an interpolation or extrapolation method.

Table 8.3: Overview of lithium-ion battery system costs.

Ref.	Year	Country	Battery specifics	Cost			Future development
				Energy-related	Power-related	Others	
[158]	2016	GE	n/a	2015: 1000 EUR/kWh	n/a	n/a	2035: 375 EUR/kWh
[159]	2016	GE	n/a	2018: 500 EUR/kWh	n/a	OM cost: 1% of investment cost	n/a
[165]	2016	GE	0-100 kWh	500 EUR/kWh	n/a	Installation cost: 1330 EUR	n/a
[194]	2015	US	BEV	2014: 300 USD/kWh	n/a	n/a	Learning rate: 6–9%
[195]	2016	US	8-hour battery, utility-scale	2015: 500 USD/kWh	4000 USD/kW	n/a	2015-2050: 34%, 57% and 81% reduction scenarios
[196]	2016	US	3kW/6kWh, DC-coupled	500 USD/kWh for battery	600 USD/kW for inverter	n/a	n/a
[164]	2017	GE	n/a	1000 EUR/kWh	n/a	n/a	n/a
[168]	2017	UK	n/a	990 USD/kWh	n/a	n/a	n/a
[169]	2017	PT	10.2 kWh	550 EUR/kWh (480 EUR/kWh for battery)	n/a	n/a	n/a
[170]	2017	BE	0.5 kW/kWh	600 EUR/kWh	500 EUR/kW for inverter	Installation cost: 200 EUR	n/a
[171]	2017	AU	4-12 kWh	300 AUD/kWh	700 AUD/kW + 400 AUD/kW for inverter	n/a	n/a
[172]	2017	CH,UK,IT	128 Wh/kg	320 EUR/kWh	n/a	Installation cost: 100 EUR +2 EUR/kg Inverter cost: 800 EUR	n/a
[182]	2017	n/a	1 MW, NCA/LTO	923 EUR/kWh	162 EUR/kW	n/a	n/a
[197]	2017	n/a	n/a	2016: 273 USD/kWh for battery	n/a	n/a	Learning rate: 19%
[198]	2017	n/a	n/a	2016: 200–840 USD/kWh	n/a	n/a	2030: 145–480 USD/kWh
[199]	2017	GE	0.33 C-rate	2016: 1883 USD/kWh	n/a	OM cost: 0	2030: 524 USD/kWh; 2040: 397 USD/kWh
[173]	2018	CH	n/a	250–1000 EUR/kWh	n/a	OM cost: 1% of inv. cost Replacement cost: 50% of inv. cost	n/a
[174]	2018	n/a	14 kWh Powerwall	2017: 393 USD/kWh	n/a	BOS cost: 700 USD Installation cost: 1000 USD	In 15 years: battery cost -50%, installation cost -25%, inverter cost 0.12 USD/W
[175]	2018	NE	25-year lifetime	200 EUR/kWh	150 EUR/kW BOS + 150 EUR/kW EPC	OM cost: 1% of inv. cost	n/a
[200]	2018	n/a	n/a	2020: 165–548 USD/kWh for battery	n/a	n/a	2030: 120–250 USD/kWh
[201]	2018	US	10kW/40kWh	639–780 USD/kWh	130–174 USD/kW	OM cost: 1.79–2.2% of inv. cost	n/a
[176]	2019	AU	n/a	900 AUD/kWh	n/a	n/a	-8%/year
[178]	2019	FN	n/a	2020: 100–200 EUR/kWh	80–110 EUR/kW	Installation cost: 200–400 EUR/kWh	n/a
[190]	2019	n/a	n/a	2015: 802 USD/kWh	678 USD/kW	OM cost: 10 USD/kW-year + 3 USD/MWh	Using 2015 cost as reference, costs for 2020-2050 decrease to 55%, 34%, 23%, 18%, 16%, 15%, 14%
[202]	2019	n/a	1kW-100MW	2018: 271 USD/kWh	388 USD/kW for BOP	OM cost: 10 USD/kW-year + 0.3 USD/MWh Installation cost: 101 USD/kWh	2025: 306 USD/kW + 189 USD/kWh capital cost + 96 USD/kWh installation cost OM cost: 8 USD/kW-year + 0.3 USD/MWh
[180]	2020	TH	6.5 kWh/kW, AC-coupled	500–1000 USD/kWh	n/a	n/a	-4%/year to -12%/year

8.2.4 Load and Generation Profiles

We use synthetic load profiles for individual households generated using the "LoadProfileGenerator" [203] with the location set as Munich. Then for each customer group, the load profiles are scaled so that the total consumption matches the annual electricity demand approximated using the warm water consumption. To model the load profile of different consumption categories (i.e. L1-L11), we use different predefined household settings of "LoadProfile-Generator" detailed as follows:

- L1: predefined household CHR07 (i.e. single, employed) with an annual electricity consumption of 1'502 kWh;
- L2: predefined household CHR02 (i.e. couple, 30-64 age, both employed) in energy saving mode with an annual electricity consumption of 1'864 kWh;
- L3: predefined household CHR02 (i.e. couple, 30-64 age, both employed) in energy intensive mode with an annual electricity consumption of 3'346 kWh;
- L4: predefined household CHR04 (i.e. couple, 30-64 age, 1 employed, 1 at home) with an annual electricity consumption of 4'677 kWh;
- L5: predefined household CHR03 (i.e. family, 1 child, both employed) with an annual electricity consumption of 5'460 kWh;
- L6: predefined household CHR05 (i.e. family, 3 children, both employed) with an annual electricity consumption of 6'689 kWh;
- L7-L11: a combination of predefined household CHR02 and CHR03 with an annual electricity consumption of 8'826 kWh. The electricity consumption of buildings with multiple households are assumed to fall into these consumption categories.

Solar irradiation profiles are based on historical hourly data from MeteoSwiss [204], using data of stations located in the capital or the main city to represent the profile of each canton. The irradiation profiles are then scaled according to the annual irradiation category collected from the Sonnendach data. A perfect forecast of PV generation is assumed and the generation profile is calculated as the production resulting from the invested module area, module efficiency, inverter efficiency, performance ratio and the irradiation profile (a summary of the PVB system parameter inputs used in this work is given in Table 8.2).

8.2.5 Policies and Regulations

To account for the impacts of the legislative and regulatory framework on the investment decisions for PV units, we consider available subsidies, DSO injection tariffs and tax rebates:

- Subsidies: Currently, both an output-based feed-in-tariff subsidy scheme and a capacity-based investment subsidy scheme exist in Switzerland. However, the feed-in-tariff scheme is expected to expire in 2022 and due to the long waiting list, only PV units registered before July 2012 could qualify to benefit from it [205]. From 2020 on, units above 100 kWp within the feed-in-tariff scheme are obliged to participate in direct marketing that aims to replace the fixed tariff with a more market-oriented remuneration tariff [206]. Units ranging from 2 kWp to 50 MWp can apply for the one-time investment subsidy that could cover up to 30% of their investment costs based on the installed capacity and the PV category [191]. The current one-time investment subsidy is valid until 2030, but recent reports indicate that the Swiss federal council is planning a possible extension to 2035 [207].
- DSO injection tariffs: To account for income earned from PV generation that is fed back into the local electricity grid, we include the injection tariffs that are set by regional DSOs. Since these injection tariffs vary from DSO to DSO, we use data available from [4] and make an estimation of the average value for each canton as DSO regions and cantons are only partially congruent. The inclusion of this injection tariff is important for quantifying the revenue earned from PV generation that is not self consumed. Even more critically, it is needed to quantify the economic benefits of the PV-batteries that help increase the earnings of the PVB system by reducing the PV generation sold at this injection tariff by storing for later use as self consumption. Sensitivity analysis is conducted to analyze the impact of injection tariffs.
- Tax rebates: The available tax rebate covers 20% of the net investment costs (i.e., investment cost minus the investment subsidy) in all Swiss cantons [208]. We assume these tax rebates to remain constant until 2050.

Policies and regulations modeled in the Baseline scenario including tariffs and the WACC assumption are summarized in Table 8.4. While the investment subsidy and DSO injection tariffs are based on the current year's information (i.e. 2020), we assume the retail and wholesale electricity prices for 2020 using the

Table 8.4: Input parameters for modeled policies and regulations.

Parameter	Value	Source
Investment subsidy	909 EUR + 273~309 EUR/kW	[191]
Investment subsidy change	-2%/year	n/a
Investment subsidy expires	2030	[191]
DSO injection tariff	5.7~11.8 cent/kWh	[4]
DSO injection tariff change	up to -10%/year[27]	[173]
Retail el. tariff	12.3~35.4 cent/kWh	[5]
Retail el. tariff change	+1%/year	[141]
Wholesale el. tariff	0~161.4 EUR/MWh	[209]
Wholesale el. tariff change	+1.5%/year	[141]
Tax rebate	20% of net investment cost	[208]
WACC	4%	[141]

Note: the exchange rate is assumed to be 0.91 EUR/CHF.

historical 2018 data from [5] and [209], respectively. In the Baseline scenario, consumers are assumed to have no access to the hourly wholesale market and the electricity injected back into the grid is reimbursed at the regional injection tariff. The regional injection tariff is assumed to decrease 10% per year. However, if the injection tariff in a given year and in a given region drops below the Swiss average annual wholesale price of that year, the PV injection in that region is instead paid at that average annual wholesale price. This assumption is based on the guidelines provided in the Swiss Energy Ordinance [210] that requires the remuneration to be based on the costs incurred by the grid operator for the purchase of equivalent electricity from third parties or its own production facilities. Details of the regional injection tariff can be found in Appendix 9.3.

8.2.6 Scenarios

The profitability of PVB system investments is subject to uncertainties as the future development of PV and battery costs, injection tariffs, retail and wholesale market prices, subsidy policies etc. are unknown. Additionally, in our model, financial parameters such as WACC and amortization periods are simplified as a constant value for all modeled PV categories, which is likely not the case in reality[28]. To investigate how the profitability of PVB systems, and consequently

[28]In fact, different potential investors, from individual homeowners to larger industrial operators, might have different needs regarding their desired payback periods as well as different considerations about financing an investment in PV including the amount of debt they take on and

the investment decisions, are affected by our assumptions, we conduct a set of one-at-a-time sensitivity analyses on some main parameters, such as the projections of PV and battery costs, load profiles, retail and wholesale electricity price developments, PV injection tariffs, and the WACC. Note that the sensitivity scenarios described below are only simulated for the example of the canton of Zurich in 2050, while the Baseline scenario is simulated for 2020-2050 for all cantons.

PV and battery cost scenarios

In addition to the Baseline scenario (as introduced in Table 8.2), two additional cost sensitivity scenarios, namely a high cost scenario SC1, and a low cost scenario SC2 are simulated. On average, the high (low) cost scenario corresponds to 15% higher (lower) costs for the PV and 54% higher (lower) costs for the battery than the Baseline scenario. The differences among the three scenarios vary across the years. The different size categories and details of the cost projections for these three scenarios based on [3] and [190] can be found in Appendices 9.3 and 9.3.

Load profile scenarios

In the Baseline scenario, we model the load profile of consumption categories L1-L11 using different load profiles generated by "LoadProfileGenerator". The work in [164] indicates that using aggregated load profiles leads to higher shares of self-consumption compared to the use of an individual profile. Figure 8.2 shows the average weekly normalized aggregated load profile for the canton of Zurich in 2018 together with eleven normalized synthetic load profiles adopted for consumption categories L1-L11. It can be seen that the individual load profiles are quite different than the aggregated profile. The individual profiles tend to peak once in the morning and once during the evening while the aggregated profile peaks just once during the day. Furthermore, the aggregated load profile follows a pattern with lower consumption during the weekend whereas the individual customers consume more during the weekend. Such differences could result in different estimates of PV self-consumption and evaluations of the battery installations if aggregated load profiles are used instead

the interest rate set by their lenders. Additionally, the constant assumptions ignore that some investors have non-economic desires, such as early adopters and innovators who might be driven by environmental issues versus laggards and late majority who might have a higher risk aversion.

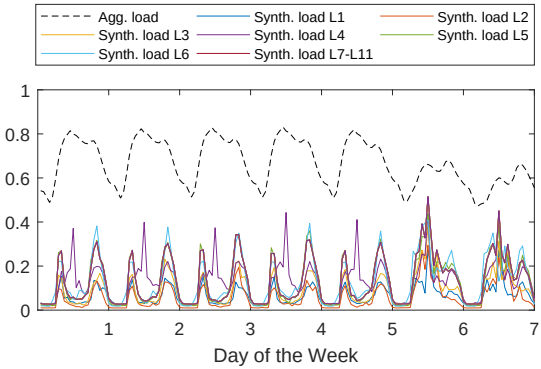

Figure 8.2: Normalized aggregated load profile for canton Zurich and synthetic individual load profiles for consumption categories L1-L11.

of individual profiles. Therefore, we simulate a sensitivity scenario SL, where the synthetic load profiles of all consumption categories are replaced by the corresponding aggregated cantonal load profile, to analyze the impact of using the aggregated load profile.

Electricity price scenarios

In the Baseline scenario, we assume that the retail electricity price increases by 1% per year and the prosumers have no access to the hourly wholesale market. All excess generation injected back into the grid is reimbursed by the regional injection tariff. The regional injection tariff is assumed to decrease 10% per year until it reaches the corresponding yearly average Swiss wholesale electricity price, which is assumed to increase by 1.5% per year. In all years afterwards, the regional injection tariff is instead set equal to the yearly average Swiss wholesale price (see Appendix 9.3 for details of the regional injection tariff).

However, it is highly uncertain how the injection tariffs as well as the retail and wholesale electricity prices evolve in future years and it is also unclear to what extent small prosumers will have access to the wholesale market. To analyze the impact of replacing the injection tariff with the wholesale market price (i.e., simulate the case when end consumers have access to the wholesale market), nine electricity price sensitivity scenarios SP1-SP9 detailed in Table 8.5

Table 8.5: Parameters of price scenarios SP1-SP9.

Scenario name	Retail price change	Wholesale price change
SP1		- 1%/year
SP2	+ 0%/year	+ 1.5%/year*
SP3		+ 3%/year
SP4		- 1%/year
SP5	+ 1%/year*	+ 1.5%/year*
SP6		+ 3%/year
SP7		- 1%/year
SP8	+ 2%/year	+ 1.5%/year*
SP9		+ 3%/year

Note: values that are the same as the Baseline scenario are noted with an asterisk (*).

are simulated similar to the electricity price scenarios modeled in [141]. One other sensitivity scenario (i.e. SP10) is simulated to analyze the extreme case of having an injection tariff equal to zero and no access to the hourly wholesale market while the retail prices increase by 1% per year (same as the Baseline scenario).

Battery scenario

In the Baseline scenario, we set the battery costs based on [190], which projects the development of the battery costs using a number of international reports.

Since the battery costs (especially the labor cost) in Switzerland are generally higher than the global average, we create a sensitivity scenario (i.e., SB1) in which we adjust the battery investment cost assumption for 2020 using the current Tesla Powerwall 2 price in Switzerland (i.e. 14'700 CHF equivalent to 13'364 EUR accounting for the total costs incurred for installing a 13.5 kWh Tesla Powerwall 2), while the cost reduction rate over the years remains the same as the Baseline scenario. Furthermore, we also simulate a sensitivity scenario without any batteries (i.e., SB2) to analyze the financial benefit of installing batteries.

WACC scenarios

Cost of capital is defined as the expected rate of return that market participants require in order to attract funds for a particular investment [211]. In the Baseline scenario, we assume a 4% WACC for all PVB system investments.

The value of WACC varies over time and between different technologies, e.g. smaller PVB systems are mainly invested by households, who face lower WACC

Table 8.6: Summary of the sensitivity scenarios.

Scenario name	Changed parameters	Remarks
SC1-2	PV and battery costs	A high cost (SC1) and a low cost scenario (SC2)
SL	Load profile	Individual load profiles replaced by the aggregate profile
SP1-9	Retail and wholesale el. price development	Access to wholesale market; injection tariff replaced by hourly wholesale price
SP10	Retail el. price development; injection tariff	No access to wholesale market; injection tariff is zero
SB1-2	Battery price; battery investment	Battery price adjusted using current Tesla price in Switzerland (SB1); battery forced not to be installed (SB2)
SW1-2	WACC	A 2% WACC (SW1) and a 8% WACC scenario (SW2)

than investors of larger-sized PVB systems. Therefore, we simulate two sensitivity scenarios assuming a 2% (i.e. SW1) and a 8% (i.e. SW2) WACC to compare against the Baseline assumption.

Table 8.6 summarizes the main parameter changes of the different sensitivity scenarios compared to the Baseline scenario.

8.3 Method

In this section, the mathematical formulation of the optimization problem is first described, followed by the definitions of the technical and economic indicators used for evaluating the investment decisions.

In this work, the investment decisions are optimized using a static model. More specifically, for each region and each examined year we run the optimization considering a 30-year lifetime of the PVB system. The simulation optimizes the investment decisions over the full 30-year lifetime by optimizing the operational decisions for all 8760 hours of the examined year and assuming identical operations along with projections for other parameters (e.g., wholesale price and injection tariff) over the remaining lifetime of the PVB system, i.e. 29 years. The model formulation, described below, is applied to each region, hence the region index is omitted in the following equations for simplification. To optimize the investment and operational decisions, three groups of constraints are considered: 1) investment constraints, 2) operational constraints

and 3) system power balance constraints. The objective is to minimize the total investment and operating costs of the PVB system, which consists of the PV unit, the battery unit and the load, over the 30-year simulation horizon. Details of the objective function are given after the constraints are described.

8.3.1 Investment Constraints

Each rooftop in each region $reg \in REG$ is categorized by which customer group c it fits into, defined by the combination of irradiation category $i \in I$, electricity consumption category $j \in J$, and roof size category $k \in K$ (i.e, for each region this is 1 out of 2200 possible customer groups). In other words, the customer group set C with $c \in C$ includes all combinations of irradiation, electricity consumption and roof size categories, i.e. $C = \{(i,j,k) : i \in I, j \in J, k \in K\}$. Each combination (i,j,k) is represented by a specific customer group c.

As mentioned, five PV candidate units corresponding to five size categories (i.e., 0-6 kWp, 6-10 kWp, 10-30 kWp, 30-100 kWp, >100 kWp) are considered in this work. Let P denote the set of all these five candidate PV categories. For each customer group c, the sum of the installed capacity $cap^{\text{pv}}_{p,c}$ over all PV categories $p \in P$ is non-negative and limited by the maximum deployment potential $dep^{\text{pv,max}}_{c}$, which is equal to the corresponding available rooftop area of the customer group divided by the rooftop area required for 1 kWp of PV (i.e. 6m^2/kWp, provided in Table 8.2). Consequently,

$$0 \leq \sum_{p \in P} cap^{\text{pv}}_{p,c} \leq dep^{\text{pv,max}}_{c} \tag{8.1}$$

The installed capacity $cap^{\text{pv}}_{p,c}$ of each PV category should be greater or equal to the minimum size requirement of that category $cap^{\text{pv,min}}_{p}$, i.e.,

$$cap^{\text{pv}}_{p,c} = u^{\text{pv}}_{p,c} x^{\text{pv}}_{p,c} \tag{8.2}$$

$$cap^{\text{pv}}_{p,c} \geq u^{\text{pv}}_{p,c} cap^{\text{pv,min}}_{p} \tag{8.3}$$

where u^{pv} is a binary variable that indicates whether the PV unit is invested or not and x^{pv} is the continuous investment capacity variable. All investment

decisions are non-negative:

$$cap^{\text{pv}}_{p,c},\ cap^{\text{bat-e}}_{c},\ cap^{\text{bat-p}}_{c} \geq 0 \tag{8.4}$$

where $cap^{\text{bat-e}}$ and $cap^{\text{bat-p}}$ are the invested energy and power capacity of the PV-battery unit, respectively. Note that the battery C-rate is not fixed and is decided by the invested energy and power capacity of the battery.

8.3.2 Operational Constraints

The PV generation output $gen^{\text{pv}}_{t,p,c}$ of PV unit p and customer group c at time t is limited by the invested module area A^{pv} multiplied by the module efficiency $\eta^{\text{pv-mod}}$, inverter efficiency η^{inv}, performance ratio $\eta^{\text{pv-pf}}$ and the solar irradiation I^{pv} at time t, i.e.,

$$0 \leq gen^{\text{pv}}_{t,p,c} \leq A^{\text{pv}}_{p,c}\eta^{\text{pv-mod}}_{p}\eta^{\text{inv}}_{p}\eta^{\text{pv-pf}}_{p}I^{\text{pv}}_{t,c} \tag{8.5}$$

$$A^{\text{pv}}_{p,c} = cap^{\text{pv}}_{p,c}a^{\text{pv}}_{p} \tag{8.6}$$

where a^{pv}_{p} is the rooftop area required by each kWp of the installed PV. The inequality in constraint (8.5) allows the possibility of PV curtailment.

The PV-battery has no direct connection to the grid and, in general, it charges (discharges) when the demand of the customer is lower (higher) than the PV generation. The stored energy of the PV-battery unit E^{bat} is limited by its maximum DOD indicated by DOD^{max} and the installed energy capacity $cap^{\text{bat-e}}$:

$$(1 - DOD^{\text{max}})cap^{\text{bat-e}}_{c} \leq E^{\text{bat}}_{t,c} \leq cap^{\text{bat-e}}_{c} \tag{8.7}$$

The PV-battery inflow p^{ch} and outflow p^{dis} are non-negative and limited by the installed power capacity of the battery $cap^{\text{bat-p}}$. Mathematically,

$$0 \leq p^{\text{ch}}_{t,c} \leq cap^{\text{bat-p}}_{c} \tag{8.8}$$

$$0 \leq p^{\text{dis}}_{t,c} \leq cap^{\text{bat-p}}_{c} \tag{8.9}$$

Finally, the relationship of the storage level E^{bat} at the end of each time step across two consecutive time steps is defined by:

$$E^{\text{bat}}_{t,c} = E^{\text{bat}}_{t-1,c} + \eta^{\text{bat,c}} p^{\text{ch}}_{t,c} \Delta t - p^{\text{dis}}_{t,c} \Delta t / (\eta^{\text{bat,d}} \eta^{\text{bat,inv}}) \tag{8.10}$$

where $\eta^{\text{bat,c}}$ and $\eta^{\text{bat,d}}$ are the charging and discharging efficiencies of the battery, The battery inverter efficiency is denoted as $\eta^{\text{bat,inv}}$ and Δt is the length of one time step.

8.3.3 Power Balance Constraints

As shown in Fig.8.1, the power from the PV units could be used to 1) charge the battery with p^{pv2bat}, 2) supply (at least part of) the demand with p^{pv2l} or 3) be injected into the grid with p^{pv2g}. Note that each customer group c has the choice to invest in any category and any number of PV panels as long as the corresponding rooftop size allows. At each time step, the sum of the power outflows of all PV units installed by customer group c should not be greater than the total PV generation:

$$p^{\text{pv2bat}}_{t,c} + p^{\text{pv2l}}_{t,c} + p^{\text{pv2g}}_{t,c} \leq \sum_{p \in P} gen^{\text{pv}}_{t,p,c} \tag{8.11}$$

$$p^{\text{pv2g}}_{t,c},\ p^{\text{pv2l}}_{t,c} \geq 0 \tag{8.12}$$

$$p^{\text{pv2bat}}_{t,c} = p^{\text{ch}}_{t,c} \tag{8.13}$$

Similarly, at each time step, the demand l can be satisfied by: 1) power from PV to the load p^{pv2l}, 2) power from the battery to the load p^{bat2l} or 3) power from the grid to the load p^{g2l}. Mathematically,

$$p^{\text{pv2l}}_{t,c} + p^{\text{bat2l}}_{t,c} + p^{\text{g2l}}_{t,c} \geq l_{t,c} \tag{8.14}$$

$$p^{\text{bat2l}}_{t,c},\ p^{\text{g2l}}_{t,c} \geq 0 \tag{8.15}$$

$$p^{\text{bat2l}}_{t,c} = p^{\text{dis}}_{t,c} \tag{8.16}$$

The self-consumed portion of the PV generation p^{sc} is defined as the total PV electricity output that is directly or indirectly consumed by the customer [212], which corresponds to the power from PV to load and from battery to

load, respectively, i.e.

$$p_{t,c}^{\text{sc}} = p_{t,c}^{\text{pv2l}} + p_{t,c}^{\text{bat2l}} \tag{8.17}$$

8.3.4 Formulation of the Optimization Problem

The objective is to optimize the investment and operational decisions of the PVB system while minimizing the cost. The cost can be assessed using the discounted cash flow method, which calculates the Net Present Value (NPV) of the investment as the sum of investment costs and all discounted future cash flows.

The total investment cost comprises the net PV investment cost $C^{\text{inv,pv}}$ and the battery investment cost $C^{\text{inv,bat}}$. The PV portion accounts for the investment subsidy $r^{\text{sub,pv}}$ and the tax rebate $r^{\text{tax,pv}}$ per kWp. The investment costs across the five PV categories is then given by

$$C_c^{\text{inv,pv}} = \sum_{p \in P} (1 - r^{\text{tax,pv}})(c_p^{\text{inv,pv}} - r_p^{\text{sub,pv}}) cap_{p,c}^{\text{pv}} \tag{8.18}$$

where $c^{\text{inv,pv}}$ is the cost of PV per kWp for category p. The battery portion considers both the energy-related $c^{\text{inv,bat-e}}$ and the power-related $c^{\text{inv,bat-p}}$ investment costs, namely

$$C_c^{\text{inv,bat}} = c^{\text{inv,bat-e}} cap_c^{\text{bat-e}} + c^{\text{inv,bat-p}} cap_c^{\text{bat-p}} \tag{8.19}$$

Future annual costs $C_{y,c}^{\text{out}}$ in year y include both variable and fixed operational and maintenance costs of the PVB system, i.e.,

$$\begin{aligned} C_{y,c}^{\text{out}} = \sum_{t=1}^{T} \Big(\sum_{p \in P} c_p^{\text{voc,pv}} gen_{t,p,c}^{\text{pv}} + c^{\text{voc,bat-e}} p_{t,c}^{\text{dis}} \Big) \\ + c^{\text{foc,bat-p}} cap_c^{\text{bat-p}} \end{aligned} \tag{8.20}$$

where $c^{\text{voc,pv}}$, $c^{\text{voc,bat-e}}$ and $c^{\text{foc,bat-p}}$ are the variable cost parameter of PV, along with the energy-related and the power-related cost parameters of the PV-battery. The simulation horizon of the examined investment year is denoted by T.

The annual revenues R^{in} include incomes from reimbursement of injecting electricity to the grid and savings from self consumption. To account for the degradation of the system, the annual revenues are multiplied by the annual system degradation rate δ^{deg} to the power of $y - y_0$, which is the difference between the considered year y and the investment year of the PVB system y_0. This results in the following equation:

$$R^{\text{in}}_{y,c} = \sum_{t=1}^{T} (p^{\text{p2g}}_{t,c} pr^{\text{inj}}_{y,t,c} + p^{\text{sc}}_{t,c} pr^{\text{retail}}_{y,t,c})(1-\delta^{\text{deg}})^{y-y_0} \tag{8.21}$$

where pr^{inj} and pr^{retail} are the injection tariff and the retail electricity tariff. The savings from the self-consumed portion of the PV generation in the model is calculated as the product of the self-consumed electricity and the retail electricity tariff, which better reflects the consumers' savings and economic trade-offs. The retail electricity tariff is modeled using a dual tariff system with varying high and low tariffs depending on the corresponding annual electricity consumption category. Details of the retail electricity tariffs for the considered consumption categories L1-L11 are provided in Appendix 9.3.

Furthermore, since the lifetime of the battery unit (i.e., 13 years) is shorter than that of the PVB system (i.e., 30 years), a replacement of the battery unit and the possible residual value of the new battery unit at the end of the PVB system needs to be accounted for. The replacement cost $C^{\text{rpl,bat}}_{y',c}$ in the year of replacement y' is calculated using the investment cost in that year (i.e., $c^{\text{inv,bat-e}}_{y'}$ and $c^{\text{inv,bat-p}}_{y'}$), while the reinvested power and energy capacity of the battery is assumed to be the same as for the initial battery, i.e.

$$C^{\text{rpl,bat}}_{y',c} = c^{\text{inv,bat-e}}_{y'} cap^{\text{bat-e}}_{c} + c^{\text{inv,bat-p}}_{y'} cap^{\text{bat-p}}_{c} \tag{8.22}$$

$$\begin{aligned} y' &= l^{\text{bat}} n' + 1, \\ n' &\in \{n' : n' \in \mathbb{Z}, 1 \leq n' \leq \lfloor (l^{\text{sys}} - 1)/l^{\text{bat}} \rfloor\} \end{aligned} \tag{8.23}$$

where l^{sys} and l^{bat} are the lifetimes of the PVB system and the battery. The number of needed battery replacements is calculated as $\lfloor (l^{\text{sys}} - 1)/l^{\text{bat}} \rfloor$.

The residual value of the last reinvested battery C^{res} is calculated as the multiplication of the annuity factor γ^{ann}, with the corresponding replacement cost

and the residual battery lifetime by the end of the PVB system calculated as $l^{\text{bat-res}}$:

$$R_c^{\text{res,bat}} = \gamma^{\text{ann}} l^{\text{bat-res}} C^{\text{rpl,bat}}_{y'=l^{\text{bat}}\lfloor (l^{\text{sys}}-1)/l^{\text{bat}}\rfloor+1,c} \tag{8.24}$$

$$\gamma^{\text{ann}} = \frac{wacc}{1-1/(1+wacc)^{l^{\text{bat}}}} \tag{8.25}$$

$$l^{\text{bat-res}} = [l^{\text{bat}}(\lfloor (l^{\text{sys}}-1)/l^{\text{bat}}\rfloor + 1) - l^{\text{sys}}] \tag{8.26}$$

where the year when the last required battery replacement takes place is $l^{\text{bat}}\lfloor (l^{\text{sys}}-1)/l^{\text{bat}}\rfloor + 1$. For example, if battery lifetime (i.e., l^{bat}) is 13 years and the PVB system lifetime (i.e., l^{sys}) is 30 years, then the number of needed battery replacements is calculated as two (i.e., $\lfloor (l^{\text{sys}}-1)/l^{\text{bat}}\rfloor$) and the year of the last required battery replacement is the 27th year (i.e., $l^{\text{bat}}\lfloor (l^{\text{sys}}-1)/l^{\text{bat}}\rfloor + 1$) starting from the investment year.

Finally, the optimization problem for the entire lifetime of the PVB system can be formulated as

$$\begin{aligned}\min \quad & \sum_{c\in C}[C_c^{\text{inv,pv}} + C_c^{\text{inv,bat}} + \sum_{y=y_0}^{l^{\text{sys}}} \frac{C^{\text{out}}_{y,c} - R^{\text{in}}_{y,c}}{(1+wacc)^y} \\ & + \sum_{n'=1}^{\lfloor (l^{\text{sys}}-1)/l^{\text{bat}}\rfloor} C^{\text{rpl,bat}}_{y'=l^{\text{bat}}n'+1,c} - R_c^{\text{res,bat}}]\end{aligned}$$

s.t. Constraints (8.1)-(8.26)

where all future revenues and costs are discounted by WACC to convert to the NPV.

8.3.5 Technical and Economic Indicators

Technical indicators for self-consumption rate and an economic indicator for payback period that will be used in the following analysis are described as follows:

Self-consumption rate

Based on definitions given in [212], the Self-consumption Rate (SCR) is equal to the total PV electricity output that is directly or indirectly consumed by the PVB system owner divided by the total PV generation.

Self-sufficiency rate

The Self-suffiency Rate (SSR) represents the ratio of the electricity demand that can be satisfied by the PVB system over the total electricity consumption of the PVB system owner [212].

Payback period

The Payback Period (PBP) is defined as the investment cost divided by the yearly cash flow. The shorter the PBP is, the more attractive the investment is.

8.4 Case Study Results

In the Baseline scenario, we run the model for each region and each customer group considering possible investments between 2020-2050 using a 5-year time step. More specifically, we run the static investment model for each investment year without considering any investments in previous years (i.e., a greenfield investment is simulated and the potentials for deployment are the same for each investment year). Investment decisions are optimized by minimizing all investment and operating costs over a 30-year lifetime assumed for the PVB system, where the operational decisions over all 8760 hours of the examined year are simulated and are assumed to be the same for the years of the remaining lifetime of the PVB system. Different from the dynamic multi-period investment model that also optimizes investment timing and provides investment pathways, this work mainly aims to answer the question of how the economic viability of the PVB system changes over time, i.e. for different investment years and its relation to the characteristics of different customer groups. Each sensitivity scenario is only simulated for one example region (i.e., canton of Zurich) for the investment year 2050.

To better explain the results, in this section, we first show the results of an example customer group in Section 8.4.1, then we illustrate the results for the example of the canton of Zurich in Section 8.4.2. Finally, the results at the national level (i.e., Switzerland) are analyzed in Section 8.4.3. For the first two subsections (i.e., Section 8.4.1 and Section 8.4.2), the Baseline results are presented first, followed by the results of the sensitivity analyses.

8.4.1 Results for One Representative Customer Group

The average annual electricity consumption per household in Switzerland is 5000 kWh [213] and the average annual solar irradiance in Switzerland is 1267 kWh/m^2 [60]. To represent an average customer group in Switzerland, we select the group with the following criteria: canton of Zurich (REG1), rooftop size of 108-120 m^2 (A13), annual irradiation of 1150-1300 kWh/m^2/year (IRR2) and electricity consumption of 4500-5500 kWh/year (L5). As mentioned in Section 8.2.2, each customer group is represented using the median values of the rooftop size, the annual irradiation and the electricity consumption from within the group. Since a range of rooftop sizes in a particular customer group are analyzed together using representative characteristics, the investment decision for each group yields a single combination of PV and battery investments for all rooftops within this group. For example, the selected customer group has a median annual electricity consumption of 5025 kWh, a median annual solar irradiation of 1212 kWh/m^2 and a median rooftop size of 113 m^2 (i.e., equivalent to 18.8 kWp potential of PV). The aggregated rooftop area within the considered customer group is equal to 20'751 m^2, which means the optimized decision for the representative customer is reflective of around 184 customers (i.e., total rooftop size divided by the median rooftop size of the customer group). Note that the results shown in this section are only for the single representative rooftop within the single selected customer group.

Baseline Results - Investment

Table 8.7 shows the optimal investment decisions of the example customer group over the simulation horizon (i.e. 2020-2050) for the Baseline scenario. Comparing the results over the years, the optimal PV and battery sizes for the representative rooftop in this customer group continue to increase. The PBP in general follows a decreasing trend from above 13 years in 2025 to below 10 years in 2050 except for an increase from 2030 to 2035, which is mainly due to the subsidy expiration by the end of 2030. Correspondingly, the NPV in general increases over time except a slight decrease from 2030 to 2035. Changes to these optimal investment decisions and the resulting PBP and NPV over the years can be mainly traced back to the decreasing PV and battery costs and the increasing retail electricity tariffs. The PVB C-rate is fairly consistent over the

Table 8.7: Baseline analysis for the representative rooftop of the example customer group.

Year	Investment size [kW or kWh]			NPV [kEUR]	PBP [Year]	SCR	SSR
	PV	BESS-e / BESS-p	BESS C-rate				
2020	0	0 / 0	n/a	n/a	n/a	n/a	n/a
2025	2.0	3.0 / 0.6	0.20	0.5	13.5	74%	29%
2030	2.3	5.7 / 1.0	0.19	1.4	11.8	80%	36%
2035	2.7	7.2 / 1.4	0.20	1.3	13.0	80%	42%
2040	3.3	8.6 / 1.8	0.21	2.3	11.7	77%	48%
2045	6.0	10.0 / 2.3	0.23	3.4	11.4	56%	64%
2050	6.0	10.3 / 2.3	0.22	5.1	9.5	56%	65%

years between 0.19-0.23, which is reasonable considering the popular household consumer solar battery systems available nowadays (e.g. the 13.5 kWh/3.6 kW Tesla Powerwall2 with a C-rate of 0.27 [214] and the 15 kWh/3.3 kW Sonnenbatterie Eco9 with a C-rate of 0.22 [215]). Furthermore, the SSR increases with the increasing size of the PVB system, meaning that the homeowner is able to supply more and more of its own demand. In contrast, the SCR first increases and then decreases, indicating that the larger PVB systems tend to sell a larger portion of their production to the grid. This result also shows that the investment profitability in early years is driven by the high SCR while further into the future it is instead driven by the decreasing costs. In these future years, it is also profitable to install a PVB system that is larger than required for the consumers' demand.

Baseline results - dispatch

Figure 8.3 shows the generation and load dispatch of the PVB system of an example winter and summer week for 2030 and 2050, respectively. Both the selected winter and summer weeks start from a Monday. Low electricity tariff hours (i.e., off-peak hours) are marked by the gray area, while the rest is the high electricity tariff period.

In general, the battery discharges/charges when the load is higher/lower than the PV generation to increase the self-consumption rate and in turn improve the profitability of the PVB system investment. An exception can be observed on the 7th day (i.e., Sunday) of the winter weeks, when the battery charges even though the load is higher than the PV generation. This is due to

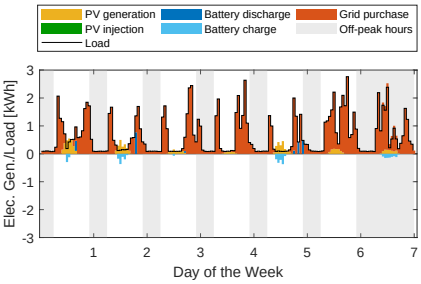

(a) Winter - 2030

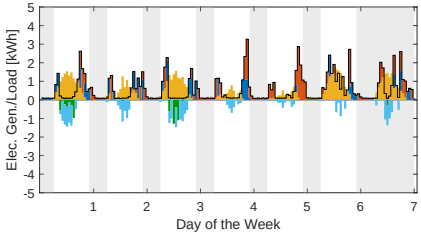

(b) Summer - 2030

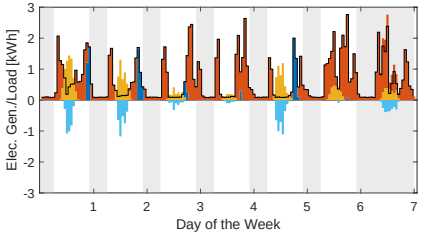

(c) Winter - 2050

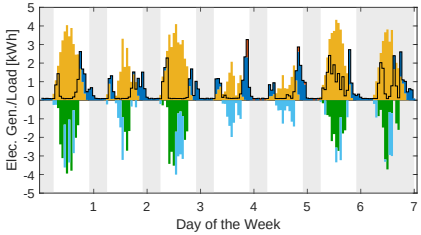

(d) Summer - 2050

Figure 8.3: Dispatch of the PV-battery system for the representative rooftop of the example customer group in 2030 and 2050.

the assumption that all hours on Sunday are low electricity tariff hours (i.e., off-peak). The PVB system therefore takes advantage of the cheap electricity from the grid to supply the demand while the PV-battery absorbs the PV generation for later use during high electricity tariff hours. Furthermore, discharging is ideally done during the peak electricity tariff hours (i.e., 6:00-22:00 from Monday to Saturday) in order to reduce the electricity bill. Note that in the Baseline scenario, the retail electricity tariffs are modeled using a dual system while the injection tariff is assumed to be constant over all hours. Hence, non-unique solutions might occur as the charging/discharging in different hours in the same price tier could result in the same objective value. However, this is irrelevant for our study.

As shown in Table 8.7, the optimal invested battery size increases from 5.7 kWh/1.0 kW in 2030 to 10.3 kWh/2.3 kW in 2050, whereas the optimal PV size increases from 2.3 kW to 6.0 kW between the same years. Comparing the 2050 dispatch results to that of 2030 both shown in Fig. 8.3, the grid purchases decrease while the PV injections increase due to the larger size of the installed PV system. Although the battery size is also expanded, the general pattern of the PVB system behavior does not change significantly. Additionally, the dynamics of the power consumed/sold to the grid are exacerbated since in 2050 the installed battery capacity per kW of PV is lower.

Sensitivity Scenario Results

The results of simulating different sensitivity scenarios in 2050 are provided in Table 8.8. The main observations are:

- Cost sensitivity: The optimal battery size and the NPV decreases/increases, and the PBP increases/decreases in the high/low cost scenario (i.e., SC1/SC2), while the optimal PV size is unchanged. This is due to the fact that the future battery cost is subject to higher uncertainties than that of PV.
- Load sensitivity: When applying the aggregate load profile (i.e. SL) with equal energy consumed, the optimal PV size stays unchanged, but both the optimal battery size and battery C-rate are reduced. This is because the aggregate load profile is flatter and better matches the PV generation profile than the individual load profiles, therefore a smaller battery is required to

Table 8.8: Sensitivity analysis for the representative rooftop of the example customer group in 2050.

Year	Investment size [kW or kWh]			NPV [kEUR]	PBP [Year]	SCR	SSR
	PV	BESS-e / BESS-p	BESS C-rate				
Baseline	6.0	10.3 / 2.3	0.22	5.1	9.5	56%	65%
SC1	6.0	8.6 / 1.9	0.23	3.2	11.8	55%	63%
SC2	6.0	14.4 / 2.7	0.19	7.2	7.0	57%	67%
SL	6.0	7.1 / 1.4	0.20	5.4	8.9	57%	65%
SP1	2.1	5.6 / 1.1	0.19	0.6	14.7	82%	34%
SP2	6.0	8.6 / 2.1	0.24	1.0	14.8	54%	63%
SP3	6.0	7.9 / 2.0	0.25	2.0	12.9	54%	62%
SP4	6.0	10.5 / 2.4	0.22	4.7	9.9	56%	65%
SP5	6.0	10.3 / 2.4	0.23	5.4	9.3	56%	65%
SP6	10.0	10.6 / 2.6	0.24	7.0	9.6	39%	75%
SP7	6.0	11.8 / 2.6	0.22	11.6	6.2	57%	66%
SP8	10.0	12.5 / 2.8	0.22	12.6	7.2	39%	76%
SP9	12.3	12.2 / 3.0	0.24	15.1	7.2	34%	79%
SP10	6.0	10.6 / 2.4	0.22	4.3	10.2	56%	65%
SW1	6.0	10.5 / 2.3	0.22	8.3	9.8	56%	65%
SW2	6.0	10.5 / 2.3	0.22	1.6	8.7	56%	65%
SB1	6.0	7.6 / 1.8	0.23	3.7	11.0	53%	62%
SB2	2.0	n/a	n/a	0.9	11.9	49%	19%

achieve similar SCR and SSR values to those of the Baseline scenario, which results in a higher NPV and a shorter PBP.

- Price sensitivity I: Having access to the hourly wholesale market (i.e. SP1-SP9) has mixed impacts on the investment decisions, the NPV and the PBP, depending on how the retail and wholesale electricity prices evolve.

  Comparing the results under the same retail electricity price (i.e., SP1 vs. SP2 vs. SP3; SP4 vs. SP5 vs. SP6; SP7 vs. SP8 vs. SP9), higher wholesale market prices increase the optimal PV investment size and the NPV, and reduce the SCR since it means greater revenues for the same amount of electricity injection. However, higher wholesale prices in general reduce the optimal battery (energy and power) capacity invested per unit installed PV capacity. This is because the spread between wholesale and retail electricity prices is smaller when higher wholesale electricity is simulated, which lowers the savings earned by using batteries. Interestingly, the battery C-rate increases with the increasing wholesale price development (i.e., from SP1 to SP3, from SP4 to SP6 and from SP7 to SP9) since higher wholesale prices encourage

investments in a larger PV unit, which in turn requires a higher C-rate to cope with the increased dynamics of the net load.

Comparing the results under the same wholesale electricity price (i.e., SP1 vs. SP4 vs. SP7; SP2 vs. SP5 vs. SP8; SP3 vs. SP6 vs. SP9), the higher retail electricity prices (i.e., SP7-SP9) reduce the PBP and increase the NPV and the optimal size of both PV and battery units.

The impact of the wholesale electricity price is limited compared to the influence of the retail electricity tariff as in general the retail electricity price level is higher than the wholesale electricity price.

- Price sensitivity II: When the injection tariff is zero and no wholesale market access is granted (i.e. SP10), the optimal PV size is the same but the battery size is slightly higher. The resulting NPV decreases and the PBP increases slightly compared to the Baseline scenario, which shows the limited impact of injection tariffs in 2050 for the example of the considered customer group.
- WACC sensitivity: Increasing the value of the WACC from 4% (i.e., Baseline) to 8% (i.e., SW1) or reducing it to 2% (i.e., SW2) does not impact the invested PV and battery sizes and only slightly changes the PBP. However, the NPV varies significantly under different assumptions of WACC because of the discounting factor of future cash flows.
- Battery price sensitivity: Adjusting the battery price using the current Tesla Powerwall 2 cost in Switzerland (i.e., SB1) results in even less battery investments than the high cost scenario SC1, which highlights the importance of considering regional differences of the PVB system investment costs.
- Battery integration sensitivity: When no battery installation is considered (i.e., SB2), the NPV is much lower and the PBP is longer than in the Baseline scenario, which shows that the successful combination of battery units with PV does contribute to increasing the profitability of the PVB system for the example customer group in 2050.

The NPV and the PBP are subject to future uncertainties and vary greatly between different sensitivity simulation scenarios. The economic viability of the PVB system is especially sensitive to the future cost of PV and battery and the electricity price development.

Table 8.9: Baseline results analysis for canton Zurich, years 2020-2050.

Year	WAVG investment size [kW or kWh]			WAVG NPV [kEUR]	WAVG PBP [Year]	Cum. PV [GW]	Cum. BESS [GWh / GW]
	PV	BESS-e / BESS-p	BESS C-rate				
2020	4.5	1.1 / 0.3	0.25	2.3	11.5	1.4	0.4 / 0.1
2025	5.8	7.0 / 1.5	0.21	3.3	11.7	2.2	2.7 / 0.6
2030	7.6	14.0 / 2.8	0.20	6.0	11.0	3.0	5.4 / 1.1
2035	7.8	16.7 / 3.4	0.20	6.5	11.6	3.0	6.4 / 1.3
2040	8.3	18.1 / 3.7	0.20	8.9	10.2	3.2	7.0 / 1.4
2045	8.8	18.9 / 3.9	0.20	10.9	9.3	3.4	7.3 / 1.5
2050	9.2	19.8 / 4.0	0.20	13.3	8.3	3.6	7.7 / 1.6

WAVG is the abbreviation for weighted-average.

8.4.2 Results for All Customer Groups within Canton Zurich

To broaden the scope of the results, this subsection discusses the resulting optimal investment decisions for all 2200 customer groups in the canton of Zurich. The combination of these customer groups represents 435'815 individual consumers/households and a combined rooftop space of 28.4 km^2, which is equivalent to a cumulative PV potential of 4.7 GW.

Baseline results

Table 8.9 shows the weighted average size, NPV and PBP as well as the cumulative capacity of the PVB investments across all customer groups in the canton of Zurich. The assigned weights are the number of customers (i.e., rooftops) in each customer group. Different from the results of the example customer group, it is profitable to invest in PV and PV-battery for some customer groups already in the current year (i.e., 2020) in Zurich. Moving from 2020 to 2050, the weighted average size of the invested PV and battery units is increasing, mainly as a result of the decreasing costs. This result is consistent with the observation drawn from the previous results of the example customer group. This growth is prominent for the battery during the period between 2020 and 2035, when the estimated battery price drops significantly (for more details see Appendix 9.3). Although the NPV increases over the years, the weighted average PBP fluctuates between 2020 and 2035 and decreases afterwards, which is due to the mixed impacts of the investment subsidy decrease, the injection tariff variation, the retail tariff increase and the investment cost decrease. In other words, the annual net cash inflow does not increase as much as the in-

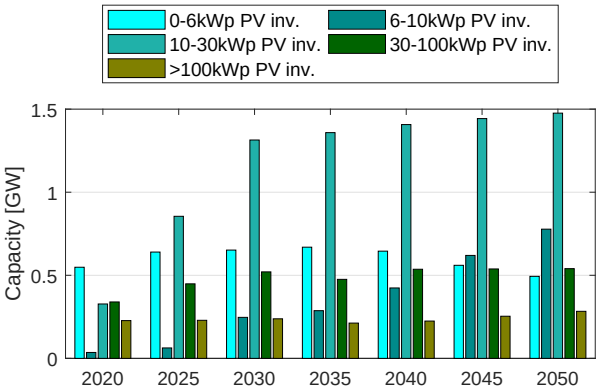

Figure 8.4: Cumulative PV investments in different size categories for the canton of Zurich, years 2020-2050.

vestment cost during this period (i.e., 2020-2035). Individual impacts of some of these important input factors will be further investigated later using sensitivity analysis. Similar to the trend of the weighted average investment capacity, the cumulative PV and battery investment capacities also increase over time from 1.4 GW and 0.4 GWh/0.1 GW in 2020 to 3.6 GW and 7.7 GWh/1.6 GW in 2050, while the total PV deployment potential modeled for the canton of Zurich is 4.7 GW. It is worth noting that the resulting investment capacities account for all investments that could achieve positive NPV, even if small, over the 30-year lifetime of the PVB system, while in reality investors might have higher expectations for the NPV and the PBP.

Figure 8.4 shows the cumulative PV investments in different size categories from 2020 to 2050 for the canton of Zurich. Please note by cumulative, we refer to the summation over all customer groups in any particular year and not over time as we start with a greenfield in every considered year. While the cumulative investments in 6-10 kW and 10-30 kW PV units increase significantly from 2020 to 2050, investments in other PV size categories fluctuate over the years: a) investments in PV sizes below 6 kW first increase then decrease, which is likely due to the fact that investments are driven by high SCR in early years and most customer groups install smaller PV units that do not fully exploit the po-

tential of their rooftop sizes[29]. Since the optimal PV size increases mainly as a result of the decreasing investment cost, the cumulative PV investment capacity gradually shifts from smaller to greater PV size categories; b) investments in PV above 30 kW in general increase over time except for a small decrease between 2030 and 2035, which shows that compared to that of smaller PV units the economic viability of larger PV units relies more on the investment subsidy.

Figure 8.5 depicts the relationship between the total optimal PV and battery investment capacities and the PBP over all 2200 customer groups. In all three plots, each line represents the accumulated capacity of the 2200 customer groups, which have been ordered by increasing PBPs. In general, the total capacities of the invested PV and battery units increase over the years, along with yielding more capacities that have shorter PBP. However, the curves of 2030 and 2035 (especially for the PV investment capacity) intersect/overlap, which is, as elaborated already also earlier, mainly because of the mixed effects of cost reductions and the investment subsidy expiration by the end of 2030.

Sensitivity Scenario Results

Figure 8.6 illustrates the changes compared to the Baseline of the total investment capacities of PV and batteries in the canton of Zurich for each sensitivity scenario in 2050. Focusing on the PV investment results, several different scenarios result in a similar cumulative PV capacity to the Baseline, (i.e. costs SC1-SC2, load profiles SL and WACC values SW1-SW2). In contrast, the optimal PV investment capacity is highly sensitive to the electricity price developments (i.e., SP1-SP10), with the lowest/highest price scenario (i.e., SP1/SP9) yielding the lowest/highest level of PV integration. Alternatively, the cumulative battery energy and power capacities vary significantly among scenarios, with the lowest battery capacity invested in the aggregated load scenario SL and the highest battery capacity invested in the low cost scenario SC2. Considering price scenarios SP1-SP10, the highest total battery investment capacity is obtained under the price scenario SP7 (i.e., highest retail price increase of 2%/year and lowest wholesale price increase of -1%/year), while the lowest

[29] Assuming the considered available rooftop potential in the canton of Zurich is fully exploited (i.e., PV units sizes are maximized for every single house based solely on the corresponding rooftop size), then the maximum investments in 0-6 kW, 6-10 kW, 10-30 kW, 30-100 kW and >100 kW PV units are 0.53 GW, 0.77 GW, 2.29 GW, 0.82 GW and 0.33 GW, respectively.

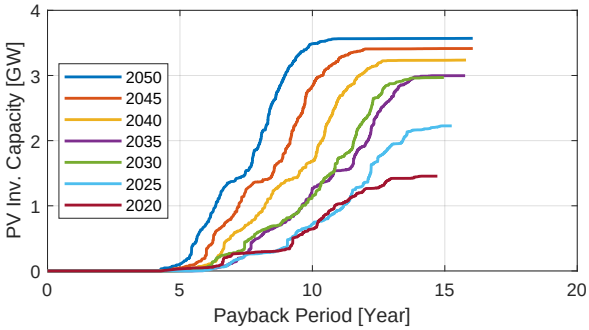

(a) PV investment capacity

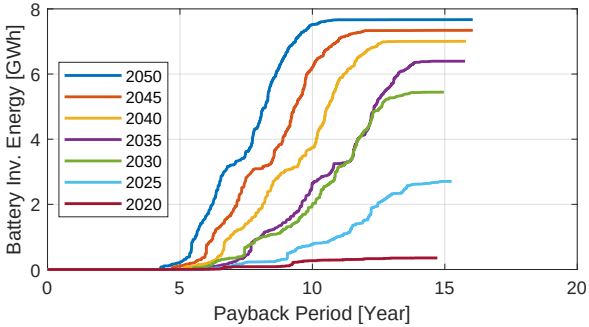

(b) Battery investment energy capacity

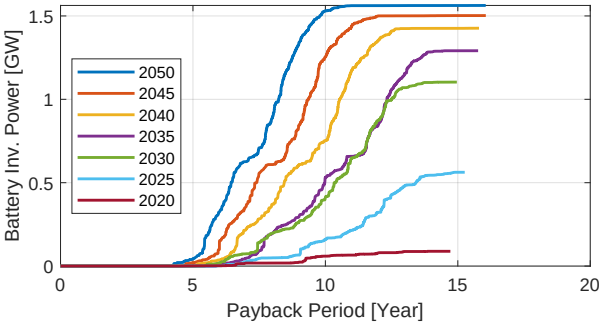

(c) Battery investment power capacity

Figure 8.5: Optimal investments against payback periods of the Baseline scenario of 2020-2050 for the canton of Zurich.

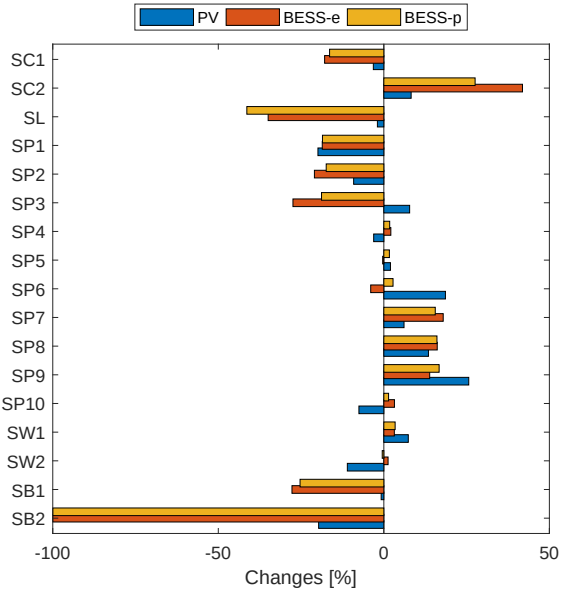

Figure 8.6: Investment changes in the example of the canton of Zurich under different scenarios.

battery investment is obtained under the price scenario SP3 (i.e., lowest retail price increase of 0%/year and highest wholesale price increase of 3%/year). This is likely due to the fact that a smaller spread between wholesale and retail electricity prices in turn decreases the profitability of battery investments in 2050, when in general more PV is invested than required for the consumers' demand and the battery investment is driven more by shifting the PV injection from low to high wholesale electricity price hours than to increase the SCR.

8.4.3 Results for Switzerland

In this section, we only show results for the Baseline scenario and for years 2020, 2030, 2040 and 2050. The results consider all 26 regions (i.e., cantons) in Switzerland with 2200 customer groups within each region. The combination of all these customer groups represents 3'795'145 individual con-

sumers/households and a rooftop area of 224 km^2, which is equivalent to a cumulative PV potential of 37 GW.

Since the investment decisions are optimized by maximizing the NPV of the investment, the resulting PBP could be up to the lifetime of the PVB system (i.e., 30 years). However, most investors would expect a PBP that is much shorter than the lifetime of the PVB system. The PBP of the currently installed PVB systems varies across countries, locations and customer groups. A recent study [216] conducted in Australia shows a PBP of 5 to 12 years, whereas some research [217] suggests that the PBP could be as long as 16 years.

Investments that result in long PBPs are likely not of high interest to customers. We therefore focus on two cases and define them as follows:

- **Fast recoverable** investment: PBP is less than 10 years;
- **Moderately fast recoverable** investment: PBP is less than 15 years.

Baseline Results - Investment

Figure 8.7 shows the optimal investments in Switzerland between 2020-2050. Each year is represented by a whisker plot where each value within this plot represents the cumulative capacity that is built in Switzerland with a PBP from zero to 30 years. The investment decision is highly sensitive to the acceptable PBP, especially between 2030 and 2040, when the cost reduction is not high enough to achieve a short PBP for all customer groups. It can be observed that for each year, the resulting 15-year PBP investment results are almost always on the top edge of the box. This can be explained by the fact that most of the investments have a PBP shorter than 15 years[30], which can also be seen in Fig. 8.5. In 2050, almost all investments achieve a PBP of less than 10 years.

Figure 8.8 shows the regional investment capacities of fast recoverable and moderately fast recoverable investments in both 2020 and 2050, and PV investments are broken down into different PV size categories. In 2020, the fast recoverable investments are mainly large PV units. In cantons with high DSO injection tariffs (e.g. BS and GE), a significant share of deployment potentials

[30]The investment decisions are optimized by maximizing the net present value over the 30-year lifetime of the PVB system, which is not equivalent to allow all investments that have a PVB below 30 years. This is because the NPV is calculated considering the time value of the money, which is not the case when calculating the PBP.

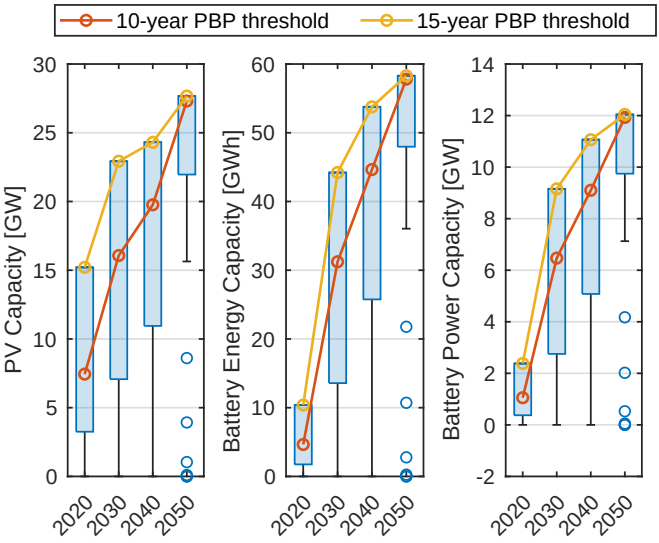

Figure 8.7: Optimal yearly investment under different payback periods.

is already qualified as fast recoverable in 2020. While in 2050, the fast recoverable investments are more evenly distributed between different regions and different PV categories. Moreover, profitable PV investment capacities increase while the corresponding PBPs decrease from 2020 to 2050.

Figure 8.9 presents distributions of the fast recoverable investments in 2050 over different irradiation, rooftop size and annual electricity consumption categories. It can be noticed in Fig. 8.9a and Fig. 8.9b that the most attractive investments mainly belong to the customer groups that are in the higher annual irradiation and higher electricity consumption categories. Furthermore, the optimal PV investment size is generally limited by the rooftop size, as illustrated in Fig. 8.9c with the separated ordering of the colored PV categories from light to dark green, which shows the importance of considering rooftop size limits in the techno-economic model.

Baseline Results - Load

Figure 8.10 shows the average hourly Swiss load per month and the average hourly residual load between 2020-2050 assuming a fast or a moderately fast

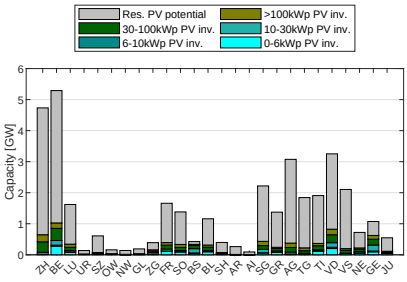

(a) Fast recoverable investment - 2020

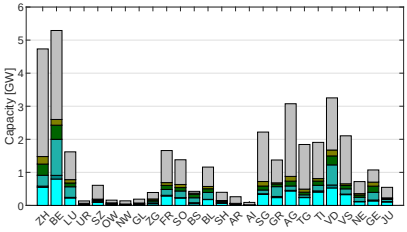

(b) Mod. fast recoverable investment - 2020

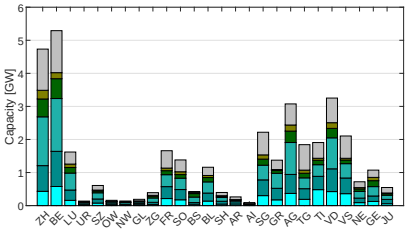

(c) Fast recoverable investment - 2050

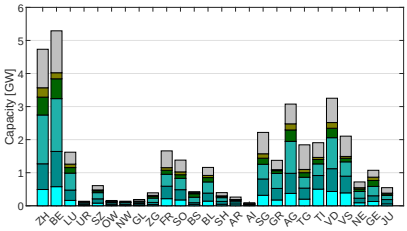

(d) Mod. fast recoverable investment - 2050

Figure 8.8: Optimal regional investment of a fast and a moderately fast recoverable investment cases under the Baseline scenario in 2020 and 2050.

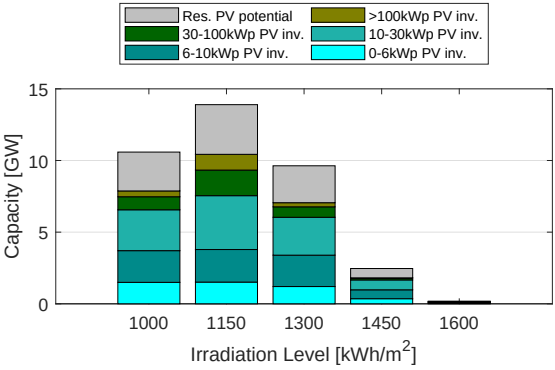

(a) Annual irradiation - PV investment

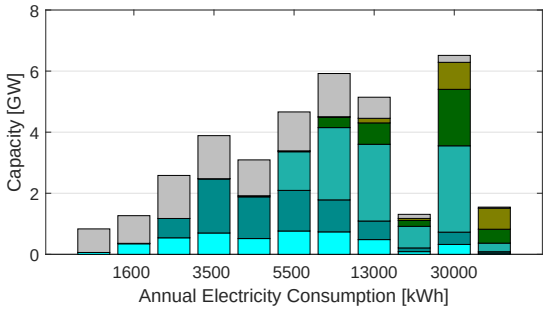

(b) Electricity consumption - PV investment

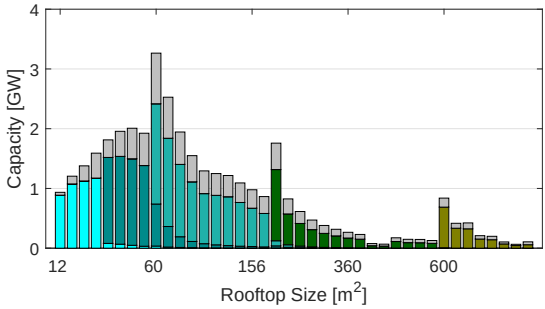

(c) Rooftop area - PV investment

Figure 8.9: Distribution of the fast recoverable investment of the Baseline scenario in 2050.

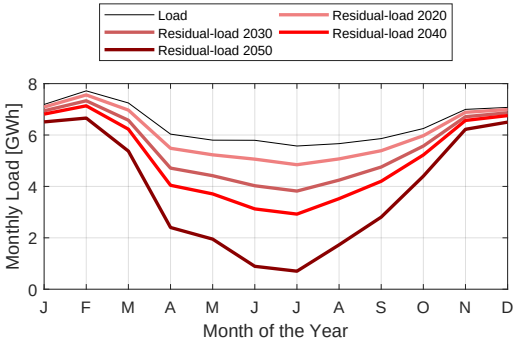

(a) Fast recoverable investment

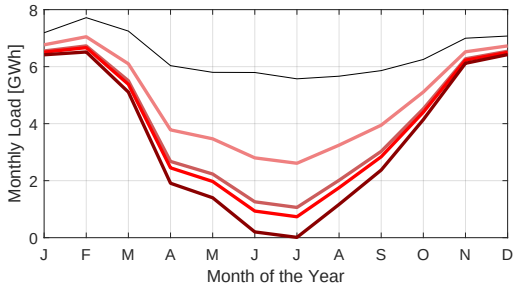

(b) Moderately fast recoverable investment

Figure 8.10: Monthly load and residual-load of different years under a fast and a moderately fast recoverable investment case.

recoverable investment case, i.e. investments are only made if the PBP is less than 10 years or less than 15 years, respectively. This residual load represents the Swiss demand that is not supplied by the invested PVB units, which is equal to the Swiss load minus the consumers' load that is self-supplied by the invested PVB units and minus the excess PV generation that is injected into the grid. The original Swiss load profile is shown to be higher in winter months, with a peak in January, and lower in summer months. This seasonal pattern is impacted by higher electricity demand during the cold winter months along with very limited existing cooling in summer. We see that while the residual load remains high in winter of all years, it is increasingly reduced over time during summer, which is directly attributable to the cumulative PV installations

over all customer groups and regions that fulfill the respective PBP limit in the considered year. This seasonality is more pronounced when moving from fast recoverable to moderately fast recoverable investments since the less stringent PBP threshold enables more PV to be viable. It is worth noting that the original Swiss load is assumed to be constant over the years, but expectations for future demand changes as well as electrification are not expected to make significant differences to the seasonal pattern of the Swiss demand.

Figure 8.11 shows the original hourly load of Switzerland and the residual load for the years 2020 through 2050 for one winter week in January and one summer week in July for both the fast recoverable and the moderate fast recoverable investment cases. In all weeks, the original Swiss load follows a similar pattern with higher consumption during the day and less at night. Over the years, in general the residual load profiles deviate more and more from the original Swiss load profile during the afternoon hours when the PV generation peaks. One exception can be observed on the 7th day (i.e., Sunday) in Fig. 8.11a and Fig. 8.11c when the residual load profile in 2020 is lower than or similar to that of 2030-2050. This is due to the fact that although PV generation is higher in 2030-2050, more batteries are also installed in 2030-2050 and absorb the PV generation during these hours, which is relatively lower due to the winter season, while the load is instead supplied by the grid at the low retail electricity tariff available during these Sunday hours. By 2050, every sunny day in both the winter and summer weeks exhibits a highly dynamic plunge and recovery pattern. It can be seen that the residual load can vary drastically from one day to the next and also from one hour to the next. Both phenomena become more pronounced as the PV penetration level increases from 2020 to 2050 and the analyzed investments extend from fast recoverable to the moderately fast recoverable ones. The increasingly dynamic pattern of the residual load on an hourly and daily basis emphasizes the need for flexible resources with fast ramping capabilities.

Baseline results - self-consumption

Table 8.10 shows the Baseline self-consumption results analysis for the fast and moderately fast recoverable investments from 2020 to 2050. It can be seen that in both cases while the PV generation increases over time, the SCR peaks in

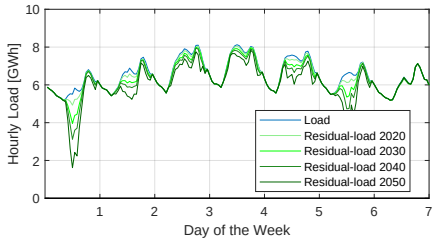

(a) Winter - Fast

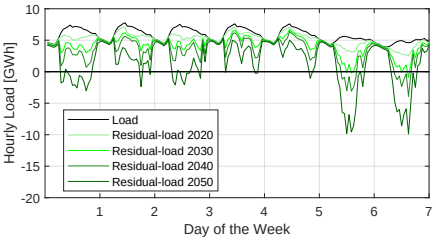

(b) Summer - Fast

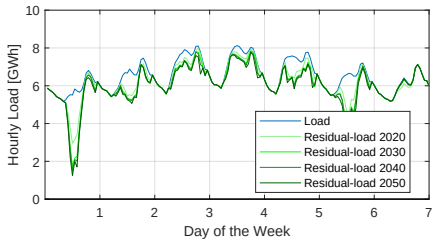

(c) Winter - Mod. fast

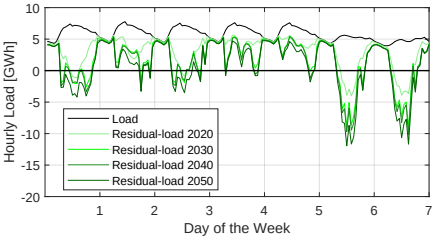

(d) Summer - Mod. fast

Figure 8.11: Hourly original Swiss load and residual-load of a winter and a summer week under a fast and a moderately fast recoverable investment case.

Table 8.10: Baseline self-consumption results analysis for the fast / moderately fast recoverable investments, years 2020-2050.

Year	PV generation [TWh]	SCR	Savings [billion EUR]	Required retail tariff increase [cent/kWh]
2020	3.5 / 14.3	54% / 64%	0.4 / 1.8	0.7 / 4.3
2030	8.7 / 22.2	74% / 72%	1.4 / 3.4	3.0 / 9.7
2040	13.1 / 23.9	76% / 73%	2.4 / 4.0	5.6 / 12.0
2050	24.0 / 27.3	68% / 67%	4.2 / 4.7	12.6 / 15.4

2040 since later investments are more driven by the low cost of the PVB system than by trying to increase the SCR. We can now also analyze the inherent losses for the retailers and DSOs caused by the reduced electricity purchase and compute by how much they would have to increase the retail price in order to recover these losses. The extra retail electricity tariff charge is calculated as the revenue loss of the DSOs divided by the sum of the residual load. The revenue loss is assumed to be equal to the savings earned by end-consumers on their electricity bills as a result of self-consumed PV generation instead of purchasing from the grid. From Table 8.10 we can see that this extra required retail electricity tariff calculated rises significantly over the years, especially from 2040 to 2050, which is due to the strong increase in self-consumption savings and the reduction in residual loads. Using the Swiss average household tariff in 2020 (i.e., 18.8 cent/kWh [218]) as a reference, the 12.6 cent/kWh and the 15.4 cent/kWh required tariff increase in 2050 in the fast and moderately fast recoverable investment cases translate into a total increase of 67% and 82%, which is equivalent to a yearly increase of 1.7% and 2.0% between 2020-2050. This of course is a simplified analysis as it does not take into account the rebound effect on PV and battery investments that would be driven by the increase in these retail prices but it points to an important issue that retailers and DSOs will likely face in the future.

8.5 Discussions

8.5.1 From Investors' Perspective

Results show that combining a battery with a PV unit is in some cases already economically viable today and especially for investors that have high annual

electricity consumption. However, the average payback period might fluctuate between 2020 and 2035 mainly due to the mixed impacts of subsidy policy changes, cost reductions, injection tariff and electricity price developments. A significant decrease of the PBP is expected after 2040.

In addition, profitability and optimal size of the PVB system vary among consumer groups due to their diverse annual electricity consumption, locations, solar irradiation and rooftop sizes. It is therefore important to consider the heterogeneity of different investors when assessing the economic viability of the investment.

Furthermore, the economics of the PVB system are especially sensitive to PV and battery cost developments, injection tariff changes and wholesale and retail electricity price changes. Having access to the wholesale market can either increase or decrease the economic viability of the PVB system, depending on how the retail and wholesale electricity prices develop in the future and their relationship to each other.

Please note that the assumptions made in this work heavily affect our results obtained from the scenario simulations and we do not account for idealistic motivations, i.e., non-economical reasons, to install PV and battery units. Therefore, we do not claim that the optimized investment decisions will be realized, given the modeled regulatory and legislative framework. However, the results indicate how the development of costs and electricity prices over the years affect the PVB system investment and operation decisions. Also, we conducted sensitivity analyses to better understand how our assumptions on different parameters (e.g., payback period and unit costs) affect the potential investments in PVB systems.

8.5.2 From Retailers' Perspective

According to our results with respect to the fast and moderately fast recoverable investments, by the end of 2050, 24.0 TWh and 27.3 TWh of the PV generation, which account for 37.9% and 43.1% of the total Swiss demand in 2019 (i.e. 63.4 TWh), could be self-consumed by the end-consumers. The resulting revenue losses from the decrease in electricity purchases of the prosumers could be recovered by increasing the retail electricity tariff. However, a higher retail

electricity tariff will in turn further encourage investments in PV and battery units.

The current retail electricity tariff (including the grid tariff) scheme is mainly energy-based (i.e. electricity charged based on the kWh of electricity consumed). Although the PVB system investments tend to decrease the annual net electricity consumption, the possibly higher dynamics of their residual load profile and the absolute value of their peak net-load will increase the burden on the grid. Therefore, an additional capacity-based grid tariff could enable a more reasonable pricing scheme and incentivize the prosumers to optimize their dispatch more in favor of the grid.

However, it is also worth mentioning that the future load profile is also subject to uncertainties brought by the electrification of heating and the transportation sector, which could compensate the loss of the self-consumption or further exacerbate the problem by increasing the self-consumption.

8.5.3 From System Operators' Perspective

The seasonality of the residual load increases in all future years and is more pronounced in 2050 as the PV penetration level is higher. This trend indicates a need for greater seasonal flexibility that could impact the operation of centralized power plants as well as the pattern of imports and exports. Similarly, the increasingly dynamic pattern of the residual load on an hourly and daily basis emphasizes the need for flexible resources with fast ramping capabilities such as hydro dams with storage reservoirs and load shifting units like pumped hydro, battery storage, or Demand-side Management (DSM). Furthermore, in future years, more frequent curtailments of non-dispatchable units, while in general not being popular, will likely make economic sense. With the integration of high levels of non-dispatchable PV, a shortage of flexibility in the power system will have a negative effect on grid security and, thus, will contribute to the risk of systemic failures. All these issues will potentially impact the actions of and services provided by the system operator.

8.5.4 From Policy-makers' Perspective

The optimization results in the Baseline scenario show that most PVB systems could result in positive NPV even without policy support after 2030. However,

the payback periods of the invested projects fluctuate between 2020 and 2040 in the Baseline scenario, which indicates that there are competing influences that could reduce the economic attractiveness for customers. The increasing dynamics of residual load profiles require increased levels of flexibility provisions in the distribution and transmission networks while at the same time lower DSO revenues are expected as a result of lower electricity purchases of prosumers. Policy-makers therefore may have to rethink the market design and rules to not only promote investments in renewable generations but also in resources that are capable of providing the required flexibility. We believe that the sensitivity analyses in this work that assess the impacts of different input parameters enable policy-makers to identify the main driving factors for investments in PV and battery units.

8.6 Limitations and Future Work

This work has several limitations and a few of which are highlighted in this section. First, we estimate the load profiles of different customer groups using a number of synthetic load profiles that undoubtedly deviate from real-world data. Thus, we do not capture the variety of different consumption behaviors between various regions and sectors. Furthermore, due to the lack of input data, we approximate the annual electricity consumption of individual customers using the warm water consumption data; additionally, the annual electricity consumption value is assumed to be constant over the years, which does not capture the possibility of an increase in EV penetrations or other electrification. Future work should include a bottom-up representation of buildings' electricity demand by utilizing realistic load patterns that evolve from year to year and differ from region to region.

Second, we group the rooftop data using a limited number of clusters and represent each group using the median data. The groups with highly varied data and the groups with few data therefore cannot be well represented; this is especially important since these two cases mostly correspond to the groups with high electricity consumption or large roofs. However, increasing the number of clusters causes higher computational complexity and longer simulation time. In future work, a proper clustering method is possibly required and a

comprehensive analysis is needed to investigate the impact of the clustering on the results.

Third, we model the investment behavior using a NPV-maximization objective without considering non-economic factors. A future version should account for a heterogeneous investor population, including, for example, varying risk profiles and cost-unrelated objectives such as peer-effects. These enhancements toward a diverse consumer perspective would enable a more realistic assessment of the investment decisions and their impacts on the grid. However, completing such improvements requires additional input data and increases the implementation overhead.

Fourth, we adopt historical wholesale market prices and apply different multiplication factors to simulate the different wholesale electricity price scenarios in the future. However, in this way the price suppression effect of PVB system injections especially during high PV generation hours cannot be captured. In addition, because of the central hub position of Switzerland, the Swiss wholesale electricity prices are also impacted by generation mix changes in surrounding countries.

And finally, a higher time resolution could be employed for both the hourly operational decisions and the 5-year investment optimization to enable a more granular assessment of operations and the economics for investing in PVB systems.

8.7 Conclusions

This chapter presents a techno-economic optimization model to analyze the economic viability of PVB systems for different customer groups in Switzerland clustered based on their annual electricity consumption, rooftop size, annual irradiation, and region. There are in total 2200 customer groups considered for each of the 26 regions in Switzerland. Each of the customer groups is represented using median values for each of the dimensions that define the group. The optimization of a static investment model is carried out considering a greenfield investment for each of the investment years from 2020 through 2050 (i.e., each year run independently without taking investments from previous years into account). The resulting optimal decisions are then applied to all

customers within the corresponding customer group. A comprehensive sensitivity analysis is conducted for an example of a particular canton (i.e., Zurich) in 2050 to investigate the impacts of input parameters such as costs, load profiles, electricity prices and tariffs on the optimal investment decisions.

Results show that the combined PV plus battery system investments for some customer groups already yield a better NPV than PV alone today. The payback period of PVB system investments fluctuates between 2020 and 2035 due to the mixed effects of policy changes, costs, and electricity price developments, but decreases significantly afterwards. The optimal PV and battery sizes increase over time. In 2050, the PVB system investment is profitable for most customer groups and the PV investment with the shortest PBP is mostly limited by the rooftop size. Optimal investment decisions vary between different customer groups and fast recoverable investment (i.e., with the shortest PBP) is mostly accessible to customer groups that have high annual irradiation and electricity demand, which suggests that it is important to consider the heterogeneity of different customer groups when assessing the economic viability of PVB system investments. With regard to the grid impact, dynamics of new system load profiles caused by the seasonal, daily and hourly patterns of the solar generation emphasize the need for system flexibility. Furthermore, the electricity purchases of the end-consumers decrease dramatically over the years since more consumers turn into prosumers. Such a change could require rethinking the current electricity tariff and subsidy policy design. In addition, investment decisions are highly sensitive to the expected payback periods, future costs, injection tariff developments, and wholesale and retail electricity price changes. It is therefore important to identify the driving factors of the PVB system investments and understand the future uncertainties of different input parameters when discussing the economic viability of PVB systems in the future.

Chapter 9

Conclusions and Outlook

9.1 Summary

In this thesis, stochastic optimization models are proposed to solve the investment or/and dispatch scheduling problems of aggregated distributed energy resources (especially variable generation energies) in a market environment.

The first part of the thesis focuses on stochastic dispatch optimization in a market environment. Chapter 2 investigates the benefits of participating in sequential markets and the impacts of including different numbers of intraday auctions for an aggregator that consists of storage devices, loads, dispatchable, and variable generation units. Chapter 3 investigates the impact of considering market power on the optimal dispatch and trading strategies of a hybrid wind-solar aggregator. Chapter 4 improves the uncertainty modeling in the previously introduced models by applying distributionally robust optimization. Then, Chapter 5 extends the works in Chapter 3 and Chapter 4 by integrating storage units into the aggregator and quantifying the additional values brought by the storage units.

The second part focuses on joint investment and dispatch optimization in a market environment. Chapter 6 presents an optimization model to optimize the generation mix and the operations for an aggregator of distributed energy resources' mix jointly to satisfy the demand and policy targets while minimizing the total costs. The aggregator is assumed to have access to both the energy and the reserve markets. Chapter 7 extends the work in Chapter 6 and

proposes a distributionally robust optimization model to incorporate the wind and Photovoltaic (PV) output uncertainties properly.

The third part focuses on the techno-economic analysis of the investments in Photovoltaic-battery (PVB) systems. In Chapter 8, a case study is conducted to analyze the economic viability of PVB systems for different customer groups in Switzerland for the years 2020 through 2050. The customer groups are constructed based on the electricity consumption values, rooftop sizes, annual solar irradiation levels, and geographical regions. Comprehensive sensitivity analyses are conducted to investigate the impacts of individual parameters such as costs, load profiles, electricity prices and tariffs.

9.2 Conclusions

Some of the main conclusions and observations of the thesis are summarized as follows:

- The coordination of different units within the aggregator realizes higher flexibility provisions and increased total profits for the aggregator, although this might reduce the profit of some individual units.
- Including more intraday auctions enables the aggregator to modify the dispatch schedules and market biddings based on the updated information, thus increasing the aggregator's total profits by reducing the imbalance quantities.
- The profits of the aggregator could be increased by implementing the strategic bidding strategies, which enables the aggregator to bid more efficiently into the markets by considering the potential influence of the biddings on the market prices. The market power of the strategic aggregator is influenced by multiple factors, such as the market share of the aggregator, the market price cap, and the price elasticity of the demand bidding curve. Both introducing the market price cap and increasing the price elasticity of the demand curve could reduce the incentives of exerting the market power.
- The strategic aggregator is more risk-seeking with the increasing market share and it offers less to the day-ahead market when the standard deviation of the output forecast error increases.
- Comparison of the proposed distributionally robust optimization model with the robust and traditional stochastic models shows that the distribu-

tionally robust optimization model achieves a good balance between the expected performance and the performance in extreme cases with acceptable computational effort. Thus, the distributionally robust optimization model is more appropriate when a large amount of historical data is available and the probability distribution of the random variables is unknown. The results can be further improved by applying the Auto-regressive Moving Average (ARMA) model to learn the cross-correlations of uncertainties using the historical data and then to simulate the future path of the uncertainties while retaining the same probabilistic properties.

- Sensitivity analysis of including different statistical constraints into the moment-based ambiguity set suggests that, in general, including more statistical information improves the worst-case distribution of the uncertainty and thus improves the model performance. However, exceptions might occur when adding the variance constraints into an ambiguity set that already contains the expectation and the mean absolute deviation information, which results in almost the same out-of-sample performance but requires much more computational effort.
- The introduction of the output-based subsidies could reduce the aggregator's motivation to exert market power and then increase the resulting social welfare. However, the increase in social welfare is not comparable to the subsidies that are paid to the power plants.
- Coordinated bidding of diverse energy resources within the aggregator enables the time-varying reserve bidding of each unit while satisfying the market requirements, thus realizing higher profits for the aggregator.
- The market participation in general increases the profitability of Distributed Energy Resource (DER) investments. Notably, the reserve market participation encourages investments in flexibility providers such as storage units and dispatchable generation units.
- The combined PV plus battery system investments for some customer groups already yield a better Net Present Value (NPV) than PV alone today. However, the payback period of the investments fluctuates between 2020 and 2035 due to the mixed impacts of policy changes, costs, and electricity price developments.

- The optimal PV and battery sizes increase over time mainly due to the projected cost reductions. In 2050, the PVB system investment is profitable for most customer groups in Switzerland, and the PV investment is limited chiefly by the rooftop size.
- Optimal PVB system investment decisions vary between different customer groups, and the fast recoverable investment is mainly accessible to customer groups with higher annual irradiation and electricity demand values.
- Concerning the grid impact, dynamics of new system load profiles caused by the seasonal and diurnal patterns of the solar generation emphasize the need for system flexibility provisions.
- With the expected increasing investments in PVB systems, the electricity purchases of the end-consumers decrease dramatically over time since more consumers turn into prosumers. Such a change could reduce the profits of electricity retailers and therefore requires rethinking the current electricity tariff and subsidy policy design.
- Sensitivity analysis shows that the PVB system investment decisions are susceptible to the expected payback periods, future costs, injection tariff developments, wholesale and retail electricity price changes.

9.3 Outlook

Based on the summary and conclusions drawn above, some of the directions of the future work are summarized as follows:

- The electricity market prices are modeled mainly based on historical data. The future work should apply a proper method to predict the electricity prices in sequential spot markets while accounting for the correlations between the prices of different markets and the generation mix, especially the share of renewables. When the market share of the aggregator is sufficiently high to influence the energy market prices, the mutual influence between the aggregator's balancing position and the balancing market price should also be considered.
- The network constraints, including the transmission limits of the considered region and the cross-border transmission capacity between regions, are not considered when modeling the market clearing problem. Although this is consistent with the current pricing scheme of the European electric-

ity markets, the network constraints are expected to influence the market results and thus the incentive to exert the market power. Moreover, a single-node approach is applied when optimizing the investment decisions of distributed energy resources, i.e., the distribution network constraints and the placement of the units are ignored. Although results in [219] show that the economic benefit of incorporating the network constraints into the DER investment optimization problem is limited compared to modeling an unconstrained network and accounting for the potential network reinforcement costs, the (positive and negative) influences of the DER installations on the system reliability should be analyzed [220].

- In Chapters 3-5, the aggregator is assumed to be the only one that could bid strategically in the market. In this way, the market power and the associated profits of the aggregator might be overestimated as the competitions among multiple strategic producers are not considered. A more realistic market environment should be considered by modeling multiple strategic market participants using an Equilibrium Problem with Equilibrium Constraints (EPEC) model.
- The moment-based ambiguity set considered for Ditributionally Robust Optimization (DRO) in this work includes the mean, the mean absolute deviation, and the standard deviation of the uncertain variables. In order to reduce the conservativeness of the solutions and then improve the performance of the model, additional information on the uncertainty distribution such as the symmetry, the degree of peakedness, and the unimodality should be included. Furthermore, the influence of incorporating the correlation of uncertainties between different time steps and between different uncertainty levels should be investigated. This extension will, however, increase the computational complexity of the method.
- This thesis focuses on the implementation of a moment-based ambiguity set. However, it is interesting to investigate the application of other types of ambiguity sets. A popular alternative is the metric-based ambiguity set, which describes the potential distributions using a reference distribution and a probability distance quantified using metrics such as the Wasserstein metric and the Kullback–Leibler divergence [221].

- In the investment optimization models, long-term uncertainties related to the changes from year to year, e.g., the uncertainties in electricity demand and electricity market price developments, are either not considered or modeled by applying different multiplication factors to the historical values. In this way, the influences of the emission cost increase, the price suppression effect due to the increasing penetration of renewables, especially during high wind and PV generation hours, and the electrification of demand cannot be well captured.
- The investment behaviors are modeled mainly using a cost-minimization or an NPV-maximization objective without considering non-economic factors. The future work should account for the investor heterogeneity by modeling a multi-objective function to include the cost-unrelated influencing factors such as environmental concerns, peer effects and risk appetite.

Bibliography

[1] P. Pinson, H. Madsen, H. A. Nielsen, G. Papaefthymiou, and B. Klöckl, "From probabilistic forecasts to statistical scenarios of short-term wind power production," *Wind Energy: An International Journal for Progress and Applications in Wind Power Conversion Technology*, vol. 12, no. 1, pp. 51–62, 2009.

[2] S. Akar, P. Beiter, W. Cole, D. Feldman, P. Kurup, E. Lantz, R. Margolis, D. Oladosu, T. Stehly, G. Rhodes *et al.*, "2020 annual technology baseline (ATB) cost and performance data for electricity generation technologies," National Renewable Energy Laboratory-Data (NREL-DATA), Golden, CO (United States), Tech. Rep., 2020.

[3] B. Christian, H. Stefan *et al.*, "Potentials, costs and environmental assessment of electricity generation technologies," PSI, WSL, ETHZ, EPFL. Paul Scherrer Institut, Switzerland, Tech. Rep., 2017.

[4] D. Fischer, "pvtarif.ch Jahresbericht 2018 [Online]," Available at: https://www.vese.ch/wp-content/uploads/pvtarif-ch-Weiterführung-2017-2020-Jahresbericht-2019-1.pdf, 2018, accessed on 2020-06-23.

[5] Swiss Federal Authorities, "Die kantonalen Strompreise im Vergleich [Online]," Available at: https://www.strompreis.elcom.admin.ch/Map/ShowSwissMap.aspx, accessed on 2020-02-01.

[6] Navigant Research, "Global DER deployment forecast database [Online]," Available at: https://guidehouseinsights.com/reports/global-der-deployment-database-1q21, 2020.

[7] IRENA and CPI, "Global landscape of renewable energy finance," *International Renewable Energy Agency, Abu Dhabi*, 2020.

[8] IRENA, "Renewable capacity highlights," *International Renewable Energy Agency, Abu Dhabi*, 2020.

[9] X. Han, E. G. Kardakos, and G. Hug, "Trading strategy for decentralized energy resources in sequential electricity markets: A swiss case study," in *2017 IEEE Innovative Smart Grid Technologies-Asia (ISGT-Asia)*. IEEE, 2017, pp. 1–7.

[10] J. Zapata, J. Vandewalle, and W. D'haeseleer, "A comparative study of imbalance reduction strategies for virtual power plant operation," *Applied Thermal Engineering*, vol. 71, no. 2, pp. 847–857, 2014.

[11] W. Gorman, A. Mills, M. Bolinger, R. Wiser, N. G. Singhal, E. Ela, and E. O'Shaughnessy, "Motivations and options for deploying hybrid generator-plus-battery projects within the bulk power system," *The Electricity Journal*, vol. 33, no. 5, p. 106739, 2020.

[12] A. Fabbri, T. G. Roman, J. R. Abbad, and V. M. Quezada, "Assessment of the cost associated with wind generation prediction errors in a liberalized electricity market," *IEEE Transactions on Power Systems*, vol. 20, no. 3, pp. 1440–1446, 2005.

[13] R. Scharff and M. Amelin, "Trading behaviour on the continuous intraday market elbas," *Energy Policy*, vol. 88, pp. 544–557, 2016.

[14] J. Usaola and M. A. Moreno, "Optimal bidding of wind energy in intraday markets," in *2009 6th International Conference on the European Energy Market*. IEEE, 2009, pp. 1–7.

[15] J. M. Morales, A. J. Conejo, and J. Pérez-Ruiz, "Short-term trading for a wind power producer," *IEEE Transactions on Power Systems*, vol. 25, no. 1, pp. 554–564, 2010.

[16] A. Skajaa, K. Edlund, and J. M. Morales, "Intraday trading of wind energy," *IEEE Transactions on power systems*, vol. 30, no. 6, pp. 3181–3189, 2015.

[17] S. Delikaraoglou, A. Papakonstantinou, C. Ordoudis, and P. Pinson, "Price-maker wind power producer participating in a joint day-ahead and real-time market," in *Proc. 12th Conf. Eur. Energy Market (EEM)*. IEEE, 2015, pp. 1–5.

[18] J. Garcia-Gonzalez, R. M. R. de la Muela, L. M. Santos, and A. M. Gonzalez, "Stochastic joint optimization of wind generation and pumped-storage units in an electricity market," *IEEE Transactions on Power Systems*, vol. 23, no. 2, pp. 460–468, 2008.

[19] J. L. Angarita, J. Usaola, and J. Martínez-Crespo, "Combined hydro-wind generation bids in a pool-based electricity market," *Electric Power Systems Research*, vol. 79, no. 7, pp. 1038–1046, 2009.

[20] E. G. Kardakos, C. K. Simoglou, and A. G. Bakirtzis, "Optimal bidding strategies of a mixed RES portfolio by stochastic programming," in *Proc. IEEE PES Innovative Smart Grid Technologies, Europe*, vol. 109. Elsevier, 2014, pp. 141–149.

[21] A. J. Conejo, J. M. Morales, and J. A. Martinez, "Tools for the analysis and design of distributed resources part III: Market studies," *IEEE Transactions on Power Delivery*, vol. 26, no. 3, pp. 1663–1670, 2011.

[22] E. Faria and S.-E. Fleten, "Day-ahead market bidding for a Nordic hydropower producer: taking the Elbas market into account," *Computational Management Science*, vol. 8, no. 1-2, pp. 75–101, 2011.

[23] M. Peik-Herfeh, H. Seifi, and M. Sheikh-El-Eslami, "Decision making of a virtual power plant under uncertainties for bidding in a day-ahead market using point estimate method," *International Journal of Electrical Power & Energy Systems*, vol. 44, no. 1, pp. 88–98, 2013.

[24] I. Kuzle, M. Zdrilić, and H. Pandžić, "Virtual power plant dispatch optimization using linear programming," in *Proc. 10th Int. Conf. Environ. Elect. Eng. (EEEIC)*, 2011.

[25] H. Pandžić, J. M. Morales, A. J. Conejo, and I. Kuzle, "Offering model for a virtual power plant based on stochastic programming," *Applied Energy*, vol. 105, pp. 282–292, 2013.

[26] P. Meibom, R. Barth, B. Hasche, H. Brand, C. Weber, and M. O'Malley, "Stochastic optimization model to study the operational impacts of high wind penetrations in ireland," *IEEE Transactions on Power Systems*, vol. 26, no. 3, pp. 1367–1379, 2010.

[27] K. Neuhoff, N. Ritter, A. Salah-Abou-El-Enien, and P. Vassilopoulos, "Intraday markets for power: Discretizing the continuous trading?" in *DIW Berlin Discussion Paper No. 1544*, 2016.

[28] S. Hagemann and C. Weber, "Trading volumes in intraday markets: Theoretical reference model and empirical observations in selected european markets," EWL working paper, Tech. Rep., 2015.

[29] J. Abrell, "The swiss wholesale electricity market," *tech. rep., Swiss Competence Center for Energy Research*, 2016.

[30] A. J. Conejo, M. Carrión, and J. M. Morales, *Decision making under uncertainty in electricity markets*. New York: Springer, 2010.

[31] J. M. Arroyo and A. J. Conejo, "Optimal response of a thermal unit to an electricity spot market," *IEEE Transactions on power systems*, vol. 15, no. 3, pp. 1098–1104, 2000.

[32] N. Mazzi, J. Kazempour, and P. Pinson, "Price-taker offering strategy in electricity pay-as-bid markets," *IEEE Transactions on Power Systems*, vol. 33, no. 2, pp. 2175–2183, 2017.

[33] E. G. Kardakos, C. K. Simoglou, and A. G. Bakirtzis, "Optimal offering strategy of a virtual power plant: A stochastic bi-level approach," *IEEE Transactions on Smart Grid*, vol. 7, no. 2, pp. 794–806, 2016.

[34] EPEX SPOT, "Annual report 2019 [Online]," Available at: https://www.epexspot.com/en/downloads, 2020, accessed on 2020-03-31.

[35] R. T. Rockafellar and S. Uryasev, "Optimization of conditional value-at-risk," *Journal of risk*, vol. 2, pp. 21–42, 2000.

[36] P. Pinson and R. Girard, "Evaluating the quality of scenarios of short-term wind power generation," *Applied Energy*, vol. 96, pp. 12–20, 2012.

[37] Nord Pool. Historical market data [Online]. Available at: https://www.nordpoolgroup.com/historical-market-data/. [Accessed on 2017-02-01].

[38] J. Lofberg, "Yalmip: A toolbox for modeling and optimization in matlab," in *2004 IEEE international conference on robotics and automation (IEEE Cat. No. 04CH37508)*. IEEE, 2004, pp. 284–289.

[39] European Power Exchange. EPEX market data [Online]. Available at: https://www.epexspot.com/en/market-data. Accessed on 2017-01-30.

[40] J. E. Contreras-Ocana, M. A. Ortega-Vazquez, and B. Zhang, "Participation of an energy storage aggregator in electricity markets," *IEEE Transactions on Smart Grid*, vol. 10, no. 2, pp. 1171–1183, 2017.

[41] J. Contreras, R. Espinola, F. J. Nogales, and A. J. Conejo, "Arima models to predict next-day electricity prices," *IEEE transactions on power systems*, vol. 18, no. 3, pp. 1014–1020, 2003.

[42] R. C. Garcia, J. Contreras, M. Van Akkeren, and J. B. C. Garcia, "A garch forecasting model to predict day-ahead electricity prices," *IEEE transactions on power systems*, vol. 20, no. 2, pp. 867–874, 2005.

[43] I. P. Panapakidis and A. S. Dagoumas, "Day-ahead electricity price forecasting via the application of artificial neural network based models," *Applied Energy*, vol. 172, pp. 132–151, 2016.

[44] U. Focken, M. Lange, K. Mönnich, H.-P. Waldl, H. G. Beyer, and A. Luig, "Short-term prediction of the aggregated power output of wind farms—a statistical analysis of the reduction of the prediction error by spatial smoothing effects," *Journal of Wind Engineering and Industrial Aerodynamics*, vol. 90, no. 3, pp. 231–246, 2002.

[45] X. Han, E. G. Kardakos, and G. Hug, "Offering strategy of a price-maker PV power plant: Multi-stage stochastic programming with probabilistic constraints," in *2018 Power Systems Computation Conference (PSCC)*. IEEE, 2018, pp. 1–7.

[46] A. Mas-Colell, M. D. Whinston, J. R. Green *et al.*, *Microeconomic theory*. Oxford university press New York, 1995, vol. 1.

[47] M. Rahimiyan, J. M. Morales, and A. J. Conejo, "Evaluating alternative offering strategies for wind producers in a pool," *Applied energy*, vol. 88, no. 12, pp. 4918–4926, 2011.

[48] M. Zugno, J. M. Morales, P. Pinson, and H. Madsen, "Pool strategy of a price-maker wind power producer," *IEEE Transactions on Power Systems*, vol. 28, no. 3, pp. 3440–3450, 2013.

[49] L. Baringo and A. J. Conejo, "Offering strategy of wind-power producer: A multi-stage risk-constrained approach," *IEEE Transactions on Power Systems*, vol. 31, no. 2, pp. 1420–1429, 2015.

[50] M. Shafie-khah, E. Heydarian-Forushani, M. E. H. Golshan, M. P. Moghaddam, M. K. Sheikh-El-Eslami, and J. P. Catalão, "Strategic offering for a price-maker wind power producer in oligopoly markets considering demand response exchange," *IEEE Transactions on Industrial Informatics*, vol. 11, no. 6, pp. 1542–1553, 2015.

[51] R. Dominguez, L. Baringo, and A. Conejo, "Optimal offering strategy for a concentrating solar power plant," *Applied Energy*, vol. 98, pp. 316–325, 2012.

[52] E. Nasrolahpour, J. Kazempour, H. Zareipour, and W. D. Rosehart, "A bilevel model for participation of a storage system in energy and reserve markets," *IEEE Transactions on Sustainable Energy*, vol. 9, no. 2, pp. 582–598, 2017.

[53] C. Ruiz and A. J. Conejo, "Pool strategy of a producer with endogenous formation of locational marginal prices," *IEEE Transactions on Power Systems*, vol. 24, no. 4, pp. 1855–1866, 2009.

[54] J. Fortuny-Amat and B. McCarl, "A representation and economic interpretation of a two-level programming problem," *Journal of the operational Research Society*, 1981.

[55] L. Roald, F. Oldewurtel, T. Krause, and G. Andersson, "Analytical reformulation of security constrained optimal power flow with probabilistic constraints," *IEEE*, pp. 1–6, 2013.

[56] Bundesamts für Energie, "Statistik der Wasserkraftanlagen der Schweiz [Online]," Available at: https://www.bfe.admin.ch/bfe/de/home/versorgung/statistik-und-geodaten/geoinformation/geodaten/wasser/statistik-der-wasserkraftanlagen.html, accessed on 2018-02-01.

[57] Bundesamt für Energie, "Kernkraftwerke Dokumentation minimales Geodatenmodell [Online]," Available at: https://www.bfe.admin.ch/bfe/de/home/versorgung/statistik-und-geodaten/geoinformation/geodaten/kernenergie/kernkraftwerke.html, accessed on 2019-04-01.

[58] IEA, NEA and Action, Nuclear Energy, "Projected costs of generating electricity - 2010 edition," *International Energy Agency and Nuclear Energy Agency, France*, 2010.

[59] T. Hostettler, "Markterhebung Sonnenenergie [Online]," Available at: https://www.swissolar.ch/ueber-solarenergie/fakten-und-zahlen/markterhebungen, accessed on 2020-02-01.

[60] C. Bauer, B. Cox, T. Heck *et al.*, "Potential, costs and environmental assessment of electricity generation technologies: An update of potentials and electricity generation costs," PSI, Tech. Rep., 2019.

[61] Bundesamts für Energie, "Windenergieanlagen Geodatenmodell Dokumentation [Online]," Available at: https://www.bfe.admin.ch/bfe/de/home/versorgung/statistik-und-geodaten/geoinformation/geodaten/wind/windenergieanlagen.html, accessed on 2019-04-01.

[62] R. Kannan and H. Turton, "Documentation on the development of the Swiss TIMES Electricity Model (STEM-E)," Paul Scherrer Institute (PSI), Tech. Rep., 2011.

[63] International Energy Agency, "Projected costs of generating electricity," International Energy Agency, Nuclear Energy Agency, Organization for Economic Co-operation and Development, Tech. Rep., 2015.

[64] U.S. Energy Information Adiministration, "Levelized cost and levelized avoided cost of new generation resources in the annual energy outlook 2017," 2017.

[65] International Energy Agency, "IEA Data and Statistics [Online]," Available at: https://www.iea.org/data-and-statistics.

[66] T. V. Jensen and P. Pinson, "RE-Europe, a large-scale dataset for modeling a highly renewable European electricity system," *Scientific data*, vol. 4, no. 1, pp. 1–18, 2017.

[67] R. Tarjanne, A. Kivistö *et al.*, "Comparison of electricity generation costs," *Research report/Faculty of Technology. Department of Energy and Environmental Technology*, 2008.

[68] International Energy Agency, "Energy Policies of IEA Countries: Switzerland 2018 Review [Online]," Available at: https://www.gebaeudetechnik-news.ch/wp-content/uploads/2018/10/energy_policies_of_iea_2018.pdf.

[69] Swissgrid, "Energy statistic switzerland [Online]," Available at: https://www.swissgrid.ch/swissgrid/en/home/experts/topics/energy_data_ch.html, 2017, accessed on 2017-09-01.

[70] Swissgrid, "Einführung Bilanzgruppen-Modell (BGM) [Online]," Available at: https://www.strom.ch/de/media/8134/download, accessed on 2021-01-11.

[71] I. Staffell and S. Pfenninger, "Using bias-corrected reanalysis to simulate current and future wind power output," *Energy*, vol. 114, pp. 1224–1239, 2016.

[72] D. R. Biggar and M. R. Hesamzadeh, *The economics of electricity markets*. John Wiley & Sons, 2014.

[73] M. G. Lijesen, "The real-time price elasticity of electricity," *Energy economics*, vol. 29, no. 2, pp. 249–258, 2007.

[74] E. Bompard, Y. Ma, R. Napoli, and G. Abrate, "The demand elasticity impacts on the strategic bidding behavior of the electricity producers," *IEEE Transactions on Power Systems*, vol. 22, no. 1, pp. 188–197, 2007.

[75] B.-M. Hodge and M. Milligan, "Wind power forecasting error distributions over multiple timescales," in *2011 IEEE Power and Energy Society General Meeting*. IEEE, 2011, pp. 1–8.

[76] B.-M. Hodge, D. Lew, M. Milligan, H. Holttinen, S. Sillanpaa, E. Gómez-Lázaro, R. Scharff, L. Soder, X. G. Larsén, G. Giebel *et al.*, "Wind power forecasting error distributions: An international comparison," National Renewable Energy Lab (NREL), Golden, CO (United States), Tech. Rep., 2012.

[77] X. Han, E. G. Kardakos, and G. Hug, "A distributionally robust bidding strategy for a wind power plant," *Electric Power Systems Research*, vol. 177, p. 105986, 2019.

[78] E. G. Kardakos, C. K. Simoglou, and A. G. Bakirtzis, "Optimal offering strategy of a virtual power plant: A stochastic bi-level approach," *IEEE Transactions on Smart Grid*, vol. 7, no. 2, pp. 794–806, 2015.

[79] M. A. Ortega-Vazquez and D. S. Kirschen, "Estimating the spinning reserve requirements in systems with significant wind power generation penetration," *IEEE Transactions on Power Systems*, vol. 24, no. 1, pp. 114–124, 2008.

[80] E. Lorenz, J. Hurka, D. Heinemann, and H. G. Beyer, "Irradiance forecasting for the power prediction of grid-connected photovoltaic systems," *IEEE Journal of Selected Topics in Applied Earth Observations and Remote Sensing*, vol. 2, no. 1, pp. 2–10, 2009.

[81] R. Marquez and C. F. Coimbra, "Forecasting of global and direct solar irradiance using stochastic learning methods, ground experiments and the nws database," *Solar Energy*, vol. 85, no. 5, pp. 746–756, 2011.

[82] A. L. Soyster, "Convex programming with set-inclusive constraints and applications to inexact linear programming," *Operations research*, vol. 21, no. 5, pp. 1154–1157, 1973.

[83] J. Dupačová, N. Gröwe-Kuska, and W. Römisch, "Scenario reduction in stochastic programming," *Mathematical programming*, vol. 95, no. 3, pp. 493–511, 2003.

[84] J. M. Morales, S. Pineda, A. J. Conejo, and M. Carrion, "Scenario reduction for futures market trading in electricity markets," *IEEE Transactions on Power Systems*, vol. 24, no. 2, pp. 878–888, 2009.

[85] Z. Liang and Y. Guo, "Robust optimization based bidding strategy for virtual power plants in electricity markets," in *Power and Energy Society General Meeting (PESGM)*. IEEE, 2016, pp. 1–5.

[86] M. Rahimiyan and L. Baringo, "Strategic bidding for a virtual power plant in the day-ahead and real-time markets: A price-taker robust optimization approach," in *IEEE Transactions on Power Systems*, vol. 31, no. 4, 2016, pp. 2676–2687.

[87] A. Baringo and L. Baringo, "A stochastic adaptive robust optimization approach for the offering strategy of a virtual power plant," *IEEE Transactions on Power Systems*, vol. 32, no. 5, pp. 3492–3504, 2016.

[88] D. Bertsimas, M. Sim, and M. Zhang, "Adaptive distributionally robust optimization," *Management Science, 2018*, 2018.

[89] P. M. Esfahani and D. Kuhn, "Data-driven distributionally robust optimization using the wasserstein metric: Performance guarantees and tractable reformulations," *Mathematical Programming*, pp. 1–52, 2017.

[90] J. Goh and M. Sim, "Distributionally robust optimization and its tractable approximations," *Operations research*, vol. 58, no. 4, pp. 902–917, 2010.

[91] E. Delage and Y. Ye, "Distributionally robust optimization under moment uncertainty with application to data-driven problems," *Operations research*, vol. 58, no. 3, pp. 595–612, 2010.

[92] D. Bertsimas, D. B. Brown, and C. Caramanis, "Theory and applications of robust optimization," *SIAM review*, vol. 53, no. 3, pp. 464–501, 2011.

[93] P. Xiong, P. Jirutitijaroen, and C. Singh, "A distributionally robust optimization model for unit commitment considering uncertain wind power generation," *IEEE Transactions on Power Systems*, vol. 32, no. 1, pp. 39–49, 2017.

[94] P. Xiong and C. Singh, "Distributionally robust optimization for energy and reserve toward a low-carbon electricity market," *Electric Power Systems Research*, vol. 149, pp. 137–145, 2017.

[95] Y. Zhang, S. Shen, B. Li, and J. L. Mathieu, "Two-stage distributionally robust optimal power flow with flexible loads," in *PowerTech, 2017 IEEE Manchester*. IEEE, 2017, pp. 1–6.

[96] W. Wei, F. Liu, and S. Mei, "Distributionally robust co-optimization of energy and reserve dispatch," *IEEE Transactions on Sustainable Energy*, vol. 7, no. 1, pp. 289–300, 2016.

[97] Y. Cao, W. Wei, J. Wang, S. Mei, M. Shafie-khah, and J. P. Catalao, "Capacity planning of energy hub in multi-carrier energy networks: A data-driven robust stochastic programming approach," *IEEE Transactions on Sustainable Energy*, 2018.

[98] E. G. Kardakos, C. K. Simoglou, and A. G. Bakirtzis, "Optimal bidding strategy in transmission-constrained electricity markets," *Electric Power Systems Research*, vol. 109, pp. 141–149, 2014.

[99] W. Wiesemann, D. Kuhn, and M. Sim, "Distributionally robust convex optimization," *Operations Research*, vol. 62, no. 6, pp. 1358–1376, 2014.

[100] A. Shapiro, *On duality theory of conic linear problems. Semi-Infinite Programming*. Springer US, 2001.

[101] E. J. Anderson and P. Nash, "Linear programming in infinite-dimensional spaces," *John Wiley & Sons Ltd Chichester*, 1970.

[102] A. Ben-Tal, A. Goryashko, E. Guslitzer, and A. Nemirovski, "Adjustable robust solutions of uncertain linear programs," *Mathematical Programming*, vol. 99, no. 2, pp. 351–376, 2004.

[103] S. Boyd and L. Vandenberghe, *Convex Optimization*. Cambridge university press, 2004.

[104] X. Chen, M. Sim, P. Sun, and J. Zhang, "A linear decision-based approximation approach to stochastic programming," *Operations Research*, vol. 56, no. 2, pp. 344–357, 2008.

[105] X. Han and G. Hug, "A distributionally robust bidding strategy for a wind-storage aggregator," *Electric Power Systems Research*, vol. 189, p. 106745, 2020.

[106] H. Ding, P. Pinson, Z. Hu, and Y. Song, "Optimal offering and operating strategies for wind-storage systems with linear decision rules," *IEEE Transactions on Power Systems*, vol. 31, no. 6, pp. 4755–4764, 2016.

[107] J. M. Morales, A. J. Conejo, H. Madsen, P. Pinson, and M. Zugno, *Integrating renewables in electricity markets: Operational problems*. Springer Science & Business Media, 2013, vol. 205.

[108] H. Ding, P. Pinson, Z. Hu, J. Wang, and Y. Song, "Optimal offering and operating strategy for a large wind-storage system as a price maker," *IEEE Transactions on Power Systems*, vol. 32, no. 6, pp. 4904–4913, 2017.

[109] A. Shahmohammadi, R. Sioshansi, A. J. Conejo, and S. Afsharnia, "Market equilibria and interactions between strategic generation, wind, and storage," *Applied energy*, vol. 220, pp. 876–892, 2018.

[110] Danish Energy Agency, "Memo on the Danish support scheme for electricity generation based on renewables and other environmentally benign electricity production," 2017.

[111] International Renewable Energy Agency, "IRENA data and statistics [Online]," Available at: https://www.irena.org/statistics, 2020, accessed on 2020-06-23.

[112] Statkraft [Online], Available at: https://www.statkraft.com/, 2020, accessed on 2021-01-30.

[113] C. Archer, H. Simão, W. Kempton, W. B. Powell, and M. Dvorak, "The challenge of integrating offshore wind power in the us electric grid. part i: Wind forecast error," *Renewable energy*, vol. 103, pp. 346–360, 2017.

[114] L. Soder, "Simulation of wind speed forecast errors for operation planning of multiarea power systems," in *2004 International Conference on Probabilistic Methods Applied to Power Systems.* IEEE, 2004, pp. 723–728.

[115] B. C. Ummels, M. Gibescu, E. Pelgrum, W. L. Kling, and A. J. Brand, "Impacts of wind power on thermal generation unit commitment and dispatch," *IEEE Transactions on Energy Conversion*, vol. 22, no. 1, pp. 44–51, 2007.

[116] A. Boone, "Simulation of short-term wind speed forecast errors using a multi-variate arma (1, 1) time-series model," Master's thesis, KTH Royal Institute of Technology in Stockholm, 2005.

[117] R. Fu, T. W. Remo, and R. M. Margolis, "2018 us utility-scale photovoltaics-plus-energy storage system costs benchmark," National Renewable Energy Lab (NREL), Golden, CO (United States), Tech. Rep., 2018.

[118] A. Stephan, B. Battke, M. Beuse, J. H. Clausdeinken, and T. S. Schmidt, "Limiting the public cost of stationary battery deployment by combining applications," *Nature Energy*, vol. 1, no. 7, p. 16079, 2016.

[119] X. Han and G. Hug, "Joint investment and operation optimization of a distribution system in a market environment," in *2019 IEEE Milan PowerTech.* IEEE, 2019, pp. 1–6.

[120] P. M. de Quevedo, G. Muñoz-Delgado, and J. Contreras, "Impact of electric vehicles on the expansion planning of distribution systems considering renewable energy, storage and charging stations," *IEEE Transactions on Smart Grid*, 2017.

[121] W. Yao, C. Chung, F. Wen, M. Qin, and Y. Xue, "Scenario-based comprehensive expansion planning for distribution systems considering inte-

gration of plug-in electric vehicles," *IEEE Transactions on Power Systems*, vol. 31, no. 1, pp. 317–328, 2016.

[122] M. Asensio, G. Muñoz-Delgado, and J. Contreras, "Bi-level approach to distribution network and renewable energy expansion planning considering demand response," *IEEE Transactions on Power Systems*, vol. 32, no. 6, pp. 4298–4309, 2017.

[123] S. Jin, A. Botterud, and S. M. Ryan, "Impact of demand response on thermal generation investment with high wind penetration." *IEEE Transactions on Smart Grid*, vol. 4, no. 4, pp. 2374–2383, 2013.

[124] M. Asensio, P. M. de Quevedo, G. Munoz-Delgado, and J. Contreras, "Joint distribution network and renewable energy expansion planning considering demand response and energy storage-Part I: Stochastic programming model," *IEEE Transactions on Smart Grid*, 2016.

[125] M. Asensio, P. M. de Quevedo, G. Muñoz-Delgado, and J. Contreras, "Joint distribution network and renewable energy expansion planning considering demand response and energy storage—part ii: numerical results," *IEEE Transactions on Smart Grid*, vol. 9, no. 2, pp. 667–675, 2016.

[126] X. Shen, M. Shahidehpour, Y. Han, S. Zhu, and J. Zheng, "Expansion planning of active distribution networks with centralized and distributed energy storage systems," *IEEE Transactions on Sustainable Energy*, vol. 8, no. 1, pp. 126–134, 2017.

[127] M. Dicorato, G. Forte, M. Pisani, and M. Trovato, "Planning and operating combined wind-storage system in electricity market," *IEEE Transactions on Sustainable Energy*, vol. 3, no. 2, pp. 209–217, 2012.

[128] P. Yang and A. Nehorai, "Joint optimization of hybrid energy storage and generation capacity with renewable energy," *IEEE Transactions on Smart Grid*, vol. 5, no. 4, pp. 1566–1574, 2014.

[129] Z. Wang, B. Chen, J. Wang, J. Kim, and M. M. Begovic, "Robust optimization based optimal DG placement in microgrids," *IEEE Transactions on Smart Grid*, vol. 5, no. 5, pp. 2173–2182, 2014.

[130] H. Wang and J. Huang, "Joint investment and operation of microgrid," *IEEE Transactions on Smart Grid*, vol. 8, no. 2, pp. 833–845, 2017.

[131] S. J. Kazempour, A. J. Conejo, and C. Ruiz, "Strategic generation investment considering futures and spot markets," *IEEE Transactions on Power Systems*, vol. 27, no. 3, pp. 1467–1476, 2012.

[132] C. I. Nweke, F. Leanez, G. R. Drayton, and M. Kolhe, "Benefits of chronological optimization in capacity planning for electricity markets," in *2012 IEEE International Conference on Power System Technology (POWERCON)*. IEEE, 2012, pp. 1–6.

[133] K. Poncelet, E. Delarue, D. Six, J. Duerinck, and W. D'haeseleer, "Impact of the level of temporal and operational detail in energy-system planning models," *Applied Energy*, vol. 162, pp. 631–643, 2016.

[134] A. Belderbos and E. Delarue, "Accounting for flexibility in power system planning with renewables," *International Journal of Electrical Power & Energy Systems*, vol. 71, pp. 33–41, 2015.

[135] C. Yuan, C. Gu, F. Li, B. Kuri, and R. W. Dunn, "New problem formulation of emission constrained generation mix," *IEEE Transactions on Power Systems*, vol. 28, no. 4, pp. 4064–4071, 2013.

[136] A. J. Conejo, L. Baringo, S. J. Kazempour, and A. S. Siddiqui, "Investment in electricity generation and transmission," *Cham Zug, Switzerland: Springer International Publishing*, vol. 106, 2016.

[137] R. Hollinger *et al.*, "Distributed solar battery systems providing primary control reserve," *IET Renewable Power Generation*, vol. 10, no. 1, pp. 63–70, 2016.

[138] Elia System Operator. [Online]. Available at: https://www.elia.be.

[139] A. Papadimitriou, V. Vassiliou, K. Tataraki, E. Giannini, and Z. Maroulis, "Economic assessment of cogeneration systems in operation," *Energies*, vol. 13, no. 9, p. 2206, 2020.

[140] H. C. Gils, "Assessment of the theoretical demand response potential in europe," *Energy*, vol. 67, pp. 1–18, 2014.

[141] J. Hoppmann, J. Volland, T. S. Schmidt, and V. H. Hoffmann, "The economic viability of battery storage for residential solar photovoltaic systems–a review and a simulation model," *Renewable and Sustainable Energy Reviews*, vol. 39, pp. 1101–1118, 2014.

[142] Swissgrid, "Balancing Roadmap Schweiz [Online]," Available at: https://www.swissgrid.ch/dam/swissgrid/about-us/newsroom/publications/balancing-roadmap-ch-de.pdf, April 2018, accessed on 2019-02-01.

[143] S. R. Dabbagh and M. K. Sheikh-El-Eslami, "Risk-based profit allocation to ders integrated with a virtual power plant using cooperative game theory," *Electric Power Systems Research*, vol. 121, pp. 368–378, 2015.

[144] S. Rahmani-Dabbagh and M. K. Sheikh-El-Eslami, "A profit sharing scheme for distributed energy resources integrated into a virtual power plant," *Applied energy*, vol. 184, pp. 313–328, 2016.

[145] S. P. Burger and M. Luke, "Business models for distributed energy resources: A review and empirical analysis," *Energy Policy*, vol. 109, pp. 230–248, 2017.

[146] X. Zhang and A. J. Conejo, "Robust transmission expansion planning representing long-and short-term uncertainty," *IEEE Transactions on Power Systems*, vol. 33, no. 2, pp. 1329–1338, 2017.

[147] X. Han and G. Hug, "Distributionally robust distributed generation expansion planning in a market environment," in *2019 16th International Conference on the European Energy Market (EEM)*. IEEE, 2019, pp. 1–6.

[148] X. Han and G. Hug, "Distributionally Robust Generation Expansion Planning Model Considering RES Integrations," in *2019 IEEE Innovative Smart Grid Technologies-Asia (ISGT Asia)*. IEEE, 2019, pp. 1716–1721.

[149] S. Pereira, P. Ferreira, and A. I. F. Vaz, "Generation expansion planning with high share of renewables of variable output," *Applied energy*, vol. 190, pp. 1275–1288, 2017.

[150] D. Bertsimas, M. Sim, and M. Zhang, "A practicable framework for distributionally robust linear optimization," in *Working paper; available as preprint at Optimization-online*, 2014.

[151] S. Gorard, "Revisiting a 90-year-old debate: the advantages of the mean deviation," *British Journal of Educational Studies*, vol. 53, no. 4, pp. 417–430, 2005.

[152] J. Zhang, B.-M. Hodge, and A. Florita, "Investigating the correlation between wind and solar power forecast errors in the western interconnection," in *ASME 2013 7th International Conference on Energy Sustainability collocated with the ASME 2013 Heat Transfer Summer Conference and the ASME 2013 11th International Conference on Fuel Cell Science, Engineering and Technology*. American Society of Mechanical Engineers Digital Collection, 2013.

[153] X. Han, J. Garrison, and G. Hug, "Techno-economic analysis of pv-battery systems in switzerland," *arXiv preprint arXiv:2103.16298*, 2021.

[154] L. Hoesung and B. Fatih, "Energy is at the heart of the solution to the climate challenge [Online]," Available at: https://www.ipcc.ch/2020/07/31/energy-climatechallenge, 2020, accessed on 2020-10-11.

[155] International Energy Agency, "Photovoltaic power systems programme annual report," International Energy Agency, Tech. Rep., 2019.

[156] PVPS, IEA, "Snapshot of global photovoltaic markets," *Report IEA PVPS T1-37*, 2020.

[157] C. N. Truong, M. Naumann, R. C. Karl, M. Müller, A. Jossen, and H. C. Hesse, "Economics of residential photovoltaic battery systems in germany: The case of tesla's powerwall," *Batteries*, vol. 2, no. 2, p. 14, 2016.

[158] G. Merei, J. Moshövel, D. Magnor, and D. U. Sauer, "Optimization of self-consumption and techno-economic analysis of PV-battery systems in commercial applications," *Applied Energy*, vol. 168, pp. 171–178, 2016.

[159] T. Kaschub, P. Jochem, and W. Fichtner, "Solar energy storage in german households: profitability, load changes and flexibility," *Energy Policy*, vol. 98, pp. 520–532, 2016.

[160] E. Nyholm, J. Goop, M. Odenberger, and F. Johnsson, "Solar photovoltaic-battery systems in swedish households–self-consumption and self-sufficiency," *Applied energy*, vol. 183, pp. 148–159, 2016.

[161] K. R. Khalilpour and A. Vassallo, "Technoeconomic parametric analysis of PV-battery systems," *Renewable Energy*, vol. 97, pp. 757–768, 2016.

[162] S. Quoilin, K. Kavvadias, A. Mercier, I. Pappone, and A. Zucker, "Quantifying self-consumption linked to solar home battery systems: Statistical analysis and economic assessment," *Applied Energy*, vol. 182, pp. 58–67, 2016.

[163] F. M. Camilo, R. Castro, M. Almeida, and V. F. Pires, "Economic assessment of residential pv systems with self-consumption and storage in portugal," *Solar Energy*, vol. 150, pp. 353–362, 2017.

[164] J. Linssen, P. Stenzel, and J. Fleer, "Techno-economic analysis of photovoltaic battery systems and the influence of different consumer load profiles," *Applied Energy*, vol. 185, pp. 2019–2025, 2017.

[165] V. Bertsch, J. Geldermann, and T. Lühn, "What drives the profitability of household pv investments, self-consumption and self-sufficiency?" *Applied Energy*, vol. 204, pp. 1–15, 2017.

[166] Y. Zhang, P. E. Campana, A. Lundblad, and J. Yan, "Comparative study of hydrogen storage and battery storage in grid connected photovoltaic system: Storage sizing and rule-based operation," *Applied energy*, vol. 201, pp. 397–411, 2017.

[167] K. Uddin, R. Gough, J. Radcliffe, J. Marco, and P. Jennings, "Techno-economic analysis of the viability of residential photovoltaic systems

using lithium-ion batteries for energy storage in the united kingdom," *Applied Energy*, vol. 206, pp. 12–21, 2017.

[168] A. S. Hassan, L. Cipcigan, and N. Jenkins, "Optimal battery storage operation for pv systems with tariff incentives," *Applied Energy*, vol. 203, pp. 422–441, 2017.

[169] F. M. Vieira, P. S. Moura, and A. T. de Almeida, "Energy storage system for self-consumption of photovoltaic energy in residential zero energy buildings," *Renewable energy*, vol. 103, pp. 308–320, 2017.

[170] G. d. O. e Silva and P. Hendrick, "Photovoltaic self-sufficiency of belgian households using lithium-ion batteries, and its impact on the grid," *Applied energy*, vol. 195, pp. 786–799, 2017.

[171] M. Akter, M. Mahmud, and A. M. Oo, "Comprehensive economic evaluations of a residential building with solar photovoltaic and battery energy storage systems: An australian case study," *Energy and Buildings*, vol. 138, pp. 332–346, 2017.

[172] S. Barcellona, L. Piegari, V. Musolino, and C. Ballif, "Economic viability for residential battery storage systems in grid-connected pv plants," *IET Renewable Power Generation*, vol. 12, no. 2, pp. 135–142, 2017.

[173] S. Schopfer, V. Tiefenbeck, and T. Staake, "Economic assessment of photovoltaic battery systems based on household load profiles," *Applied energy*, vol. 223, pp. 229–248, 2018.

[174] E. Tervo, K. Agbim, F. DeAngelis, J. Hernandez, H. K. Kim, and A. Odukomaiya, "An economic analysis of residential photovoltaic systems with lithium ion battery storage in the united states," *Renewable and Sustainable Energy Reviews*, vol. 94, pp. 1057–1066, 2018.

[175] G. Litjens, E. Worrell, and W. Van Sark, "Economic benefits of combining self-consumption enhancement with frequency restoration reserves provision by photovoltaic-battery systems," *Applied energy*, vol. 223, pp. 172–187, 2018.

[176] K. Say, M. John, and R. Dargaville, "Power to the people: Evolutionary market pressures from residential pv battery investments in australia," *Energy Policy*, vol. 134, p. 110977, 2019.

[177] B. Bai, S. Xiong, B. Song, and M. Xiaoming, "Economic analysis of distributed solar photovoltaics with reused electric vehicle batteries as energy storage systems in china," *Renewable and Sustainable Energy Reviews*, vol. 109, pp. 213–229, 2019.

[178] J. Koskela, A. Rautiainen, and P. Järventausta, "Using electrical energy storage in residential buildings–sizing of battery and photovoltaic panels based on electricity cost optimization," *Applied Energy*, vol. 239, pp. 1175–1189, 2019.

[179] P. Lazzeroni, F. Moretti, and F. Stirano, "Economic potential of pv for italian residential end-users," *Energy*, p. 117508, 2020.

[180] A. Chaianong, A. Bangviwat, C. Menke, B. Breitschopf, and W. Eichhammer, "Customer economics of residential PV-battery systems in thailand," *Renewable Energy*, vol. 146, pp. 297–308, 2020.

[181] S. Dhundhara, Y. P. Verma, and A. Williams, "Techno-economic analysis of the lithium-ion and lead-acid battery in microgrid systems," *Energy Conversion and Management*, vol. 177, pp. 122–142, 2018.

[182] A. Abdon, X. Zhang, D. Parra, M. K. Patel, C. Bauer, and J. Worlitschek, "Techno-economic and environmental assessment of stationary electricity storage technologies for different time scales," *Energy*, vol. 139, pp. 1173–1187, 2017.

[183] Bundesamt für Energie, "Energiestrategie 2050 [Online]," Available at: https://www.bfe.admin.ch/bfe/de/home/politik/energiestrategie-2050.html, accessed on 2020-12-25.

[184] Bundesamt für Energie, "Schweizer Hausdächer und Hausfassaden könnten jährlich 67 TWh Solarstrom produzieren [Online]," Available at: https://www.bfe.admin.ch/bfe/de/home/news-und-medien/

medienmitteilungen/mm-test.msg-id-74641.html, accessed on 2020-08-31.

[185] Swisssolar, "2.5 Gigawatt installierte Solarleistung: wir brauchen 20-mal mehr [Online]," Available at: https://www.swissolar.ch/services/medien/news/detail/n-n/25-gigawatt-installierte-solarleistung-wir-brauchen-20-mal-mehr/, accessed on 2020-08-31.

[186] Bundesamt für Energie, "Berechnung von Potenzialen in Gemeinden [Online]," Available at: https://www.bfe.admin.ch/bfe/de/home/versorgung/statistik-und-geodaten/geoinformation/geodaten/solar/solarenergie-eignung-hausdach.html, accessed on 2020-06-23.

[187] R. Paschotta, "Warmwasser [Online]," Available at: https://www.energie-lexikon.info/warmwasser.html, 2020, accessed on 2020-08-31.

[188] Die Wiener Volkshochschulen, "Warmes Wasser: Effizient herstellen und sparsam nutzen [Online]," Available at: https://www.umweltberatung.at/download/?id=warmes-wasser-3073-umweltberatung.pdf, 2017, accessed on 2020-08-31.

[189] Rheinisch-Westfälisches Institut für Wirtschaftsforschung (RWI) and forsa Gesellschaft für Sozialforschung und statistische Analysen, "The German Residential Energy Consumption Survey 2009-2010 [Online]," Available at: http://www.rwi-essen.de/media/content/pages/publikationen/rwi-projektberichte/PB_Energieverbrauch-priv-HH-2009-2010_K_E.pdf, 2010, accessed on 2020-08-31.

[190] O. Schmidt, S. Melchior, A. Hawkes, and I. Staffell, "Projecting the future levelized cost of electricity storage technologies," *Joule*, vol. 3, no. 1, pp. 81–100, 2019.

[191] Schweizerische Bundesrat, "Verordnung über die Förderung der Produktion von Elektrizität aus erneuerbaren Energien [Online]," Available at: https://www.admin.ch/opc/de/classified-compilation/20162947/index.html#a7, 2017, accessed on 2020-06-23.

[192] R. Gupta, M. C. Soini, M. K. Patel, and D. Parra, "Levelized cost of solar photovoltaics and wind supported by storage technologies to supply firm electricity," *Journal of Energy Storage*, vol. 27, p. 101027, 2020.

[193] N. Lebedeva, "Li-ion batteries for mobility and stationary storage applications," *Publications Office of the European Union*, 2018.

[194] B. Nykvist and M. Nilsson, "Rapidly falling costs of battery packs for electric vehicles," *Nature climate change*, vol. 5, no. 4, pp. 329–332, 2015.

[195] W. J. Cole, C. Marcy, V. K. Krishnan, and R. Margolis, "Utility-scale lithium-ion storage cost projections for use in capacity expansion models," in *2016 North American Power Symposium (NAPS)*. IEEE, 2016, pp. 1–6.

[196] K. Ardani, E. O'Shaughnessy, R. Fu, C. McClurg, J. Huneycutt, and R. Margolis, "Installed cost benchmarks and deployment barriers for residential solar photovoltaics with energy storage: Q1 2016," National Renewable Energy Lab (NREL), Golden, CO, United States, Tech. Rep., 2016.

[197] C. Curry, "Lithium-ion battery costs and market," *Bloomberg New Energy Finance*, vol. 5, pp. 4–6, 2017.

[198] P. Ralon, M. Taylor, A. Ilas, H. Diaz-Bone, and K. Kairies, "Electricity storage and renewables: Costs and markets to 2030," *International Renewable Energy Agency: Abu Dhabi, UAE*, 2017.

[199] O. Schmidt, A. Hawkes, A. Gambhir, and I. Staffell, "The future cost of electrical energy storage based on experience rates," *Nature Energy*, vol. 2, p. 17110, 2017.

[200] S. Few, O. Schmidt, G. J. Offer, N. Brandon, J. Nelson, and A. Gambhir, "Prospective improvements in cost and cycle life of off-grid lithium-ion battery packs: An analysis informed by expert elicitations," *Energy Policy*, vol. 114, pp. 578–590, 2018.

[201] Lazard, "Lazard's levelized cost of storage analysis [Online]," Available at: https://www.lazard.com/media/450774/lazards-levelized-cost-of-storage-version-40-vfinal.pdf, 2018, accessed on 2020-09-11.

[202] K. Mongird, V. V. Viswanathan, P. J. Balducci, M. J. E. Alam, V. Fotedar, V. S. Koritarov, and B. Hadjerioua, "Energy storage technology and cost characterization report," Pacific Northwest National Lab (PNNL), Richland, WA, United States, Tech. Rep., 2019.

[203] N. Pflugradt, "Load profile generator," *available at: https://www.loadprofilegenerator.de/*, 2017.

[204] Federal Swiss of Meteorology and Climatology MeteoSwiss, "IDAWEB [Online]," Available at: https://gate.meteoswiss.ch/idaweb.

[205] Pronovo AG, "Datensatz PV Installationen in der Schweiz," 2020.

[206] Swisssolar, "Direktvermarktung [Online]," Available at: https://pronovo.ch/de/foerderung/evs/direktvermarktung/, accessed on 2020-08-31.

[207] J. Spaes, "Switzerland renews support for renewables [Online]," Available at: https://www.pv-magazine.com/2020/04/08/switzerland-renews-support-for-renewables, 2020, accessed on 2020-08-31.

[208] energieschweiz, "Fördergelder und Vergütungen [Online]," Available at: https://www.energieschweiz.ch/page/de-ch/Foerdergelder-und-Verguetungen, accessed on 2020-06-23.

[209] European Power Exchange, "EPEX market data [Online]," Available at: https://www.epexspot.com/en/market-data, 2019.

[210] Eidgenossenschaft, Schweizer, "Energieverordnung per 1. November 2017 [Online]," Available at: https://www.admin.ch/opc/de/classified-compilation/20162945/index.html, 2017, accessed on 2020-03-31.

[211] R. J. Grabowski and S. P. Pratt, *Cost of capital: applications and examples*. John Wiley & Sons, 2014.

[212] R. Luthander, J. Widén, D. Nilsson, and J. Palm, "Photovoltaic self-consumption in buildings: A review," *Applied energy*, vol. 142, pp. 80–94, 2015.

[213] Bundesamt für Energie, "Schweizerische elektrizitäts statistik 2019 [online]," Available at: https://www.bundespublikationen.admin.ch/cshop_mimes_bbl/14/1402EC7524F81EEAADACAC6DECD626F5.pdf, accessed on 2020-01-31.

[214] Tesla, "Powerwall [Online]," Available at: https://www.tesla.com/de_CH/powerwall, accessed on 2020-02-01.

[215] Sonnen, "Sonnenbatterie [Online]," Available at: https://sonnen.de/stromspeicher/, accessed on 2020-10-28.

[216] S. Choice, "Solar Batteries – Are They Worth It? [Online]," Available at: https://www.solarchoice.net.au/is-home-battery-storage-worth-it/, 2020, accessed on 2020-10-28.

[217] S. Meredith, "Do I Need a Battery System and What's the Payback Period? [Online]," Available at: https://www.renewableenergyhub.co.uk/blog/do-i-need-a-battery-system-and-whats-the-payback-period/, 2017, accessed on 2020-10-28.

[218] N. Valev, "Switzerland electricity prices [Online]," Available at: https://de.globalpetrolprices.com/Switzerland/electricity_prices/, 2020, accessed on 2020-10-11.

[219] C. Calvillo, A. Sánchez-Miralles, and J. Villar, "Assessing low voltage network constraints in distributed energy resources planning," *Energy*, vol. 84, pp. 783–793, 2015.

[220] I. A. Quadri, S. Bhowmick, and D. Joshi, "A comprehensive technique for optimal allocation of distributed energy resources in radial distribution systems," *Applied Energy*, vol. 211, pp. 1245–1260, 2018.

[221] P. M. Esfahani and D. Kuhn, "Data-driven distributionally robust optimization using the wasserstein metric: Performance guarantees and tractable reformulations," *Mathematical Programming*, vol. 171, no. 1, pp. 115–166, 2018.

Curriculum Vitae

2016 - 2021	Research Assistant at Power Systems Laboratory, ETH Zurich, Switzerland
2015	Internship at MGV PULS GmbH, Germany
2015	Internship at Stadtwerk München, Germany
2013 - 2016	Master of Science in Electrical Engineering, Technical University of Munich (TUM), Germany
2012	Internship at State Grid Corporation of China, China
2011	Exchange Semester at Department of Electrical Engineering, National Cheng Kung University, Taiwan, China
2009 - 2013	Bachelor of Engineering in Electrical Engineering, Southeast University, China
2009	High School Diploma, Beijing Foreign Language School at Yangzhou, China

Appendices

Appendix: Total and Flexible Load Estimation

Table 9.1 describes the hourly total and flexible load estimation used in Chapter 2 based on data from [33].

Table 9.1: Estimation of the total load and the flexible load.

Hour	Total Load	Flexible Load
1	6	0
2	6	0
3	6	0
4	6	0
5	6	0
6	12	0
7	24	12
8	36	24
9	36	24
10	60	0
11	108	0
12	108	0
13	108	0
14	84	0
15	72	0
16	72	0
17	84	0
18	96	36
19	144	36
20	144	36
21	108	36
22	84	0
23	24	0
24	6	0

Appendix: Future Costs of Candidate Units

Tables 9.2-9.5 describe the cost data used in Chapter 6.

Table 9.2: Battery (2-hour) cost for 2020-2050 [2].

	2020	**2030**	**2040**	**2050**
Investment cost [EUR/MWh]	364'000	205'000	179'000	154'000
Fixed operational cost [EUR/MW-year]	31'000	17'000	15'000	13'000

Table 9.3: PV cost for 2020-2050 [2].

	2020	**2030**	**2040**	**2050**
Investment cost [EUR/MW]	1'481'000	881'000	779'000	677'000
Fixed operational cost [EUR/MW-year]	10'000	6'000	6'000	5'000

Table 9.4: Wind cost for 2020-2050 [2].

	2020	**2030**	**2040**	**2050**
Investment cost [EUR/MW]	2'219'000	1'597'000	1'531'000	1'458'000
Fixed operating cost [EUR/MW-year]	36'000	33'000	31'000	28'000

Table 9.5: CHP cost for 2020-2050 [3].

	2020	**2030**	**2040**	**2050**
Investment cost [EUR/kW]	1564	1491	1418	1346
Variable operating cost [EUR/MWh]	16.2	16.2	15.9	15.5
Fuel cost [EUR/MWh]	55.6	77.8	94.2	109.7
Electrical efficiency [%]	37	38	39	40
Thermal efficiency [%]	50	49	48	47
Gas price efficiency [EUR/MWh]	86.9	97.9	107.5	117.1

Appendix: Additional Results

This section provides the additional results for Chapter 6.

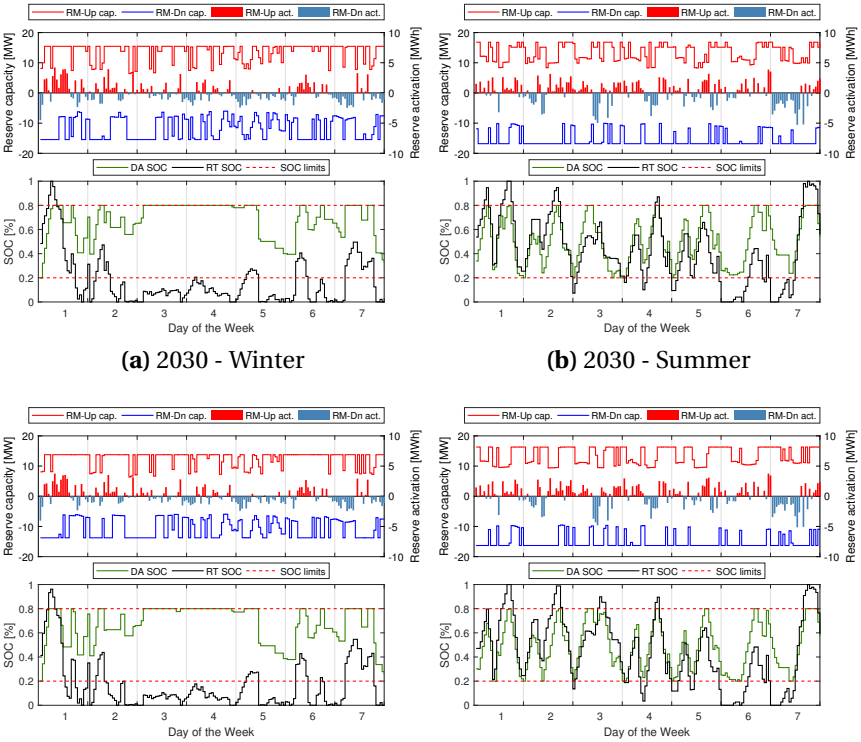

(a) 2030 - Winter

(b) 2030 - Summer

(c) 2040 - Winter

(d) 2040 - Summer

Figure 9.1: Battery operations over an example winter and summer week for years 2030 to 2050 under the Baseline scenario.

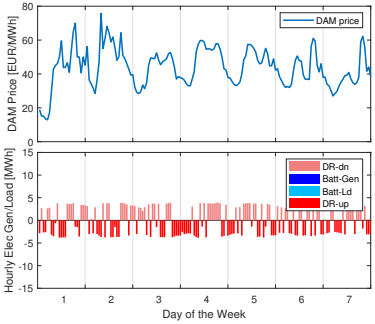

(a) 2020 - Winter

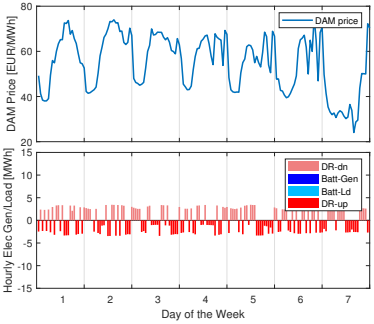

(b) 2020 - Summer

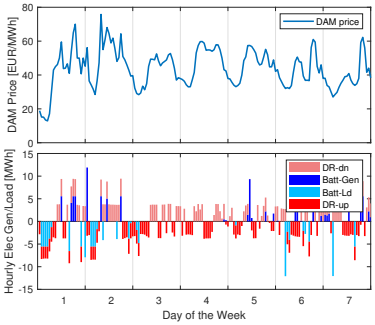

(c) 2030 - Winter

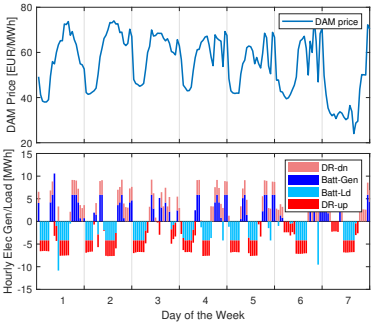

(d) 2030 - Summer

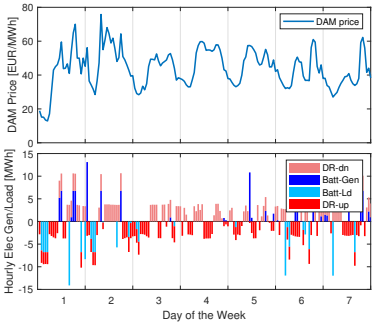

(e) 2040 - Winter

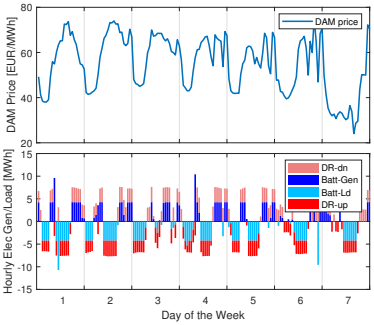

(f) 2040 - Summer

Figure 9.2: Day-ahead dispatch of battery and demand response programs over an example winter and summer week for 2020 to 2040.

Appendix: Reformulation of the Distributionally Robust Optimization Model

Following the principle of Linear Decision Rule (LDR), the adaptive decision $\boldsymbol{y}$ is approximated by an affine function of $\boldsymbol{\delta}$ and $\boldsymbol{u}$, i.e.,

$$\boldsymbol{y_t}(\boldsymbol{\delta}, \boldsymbol{u}) = \boldsymbol{k_t^0} + \boldsymbol{k_t^1}\boldsymbol{\delta_t} + \boldsymbol{k_t^2}\boldsymbol{u_t^1} + \boldsymbol{k_t^3}\boldsymbol{u_t^2} \tag{9.1}$$

where $k_t^0 \in \mathbb{R}^{I_2}$, $k_t^1 \in \mathbb{R}^{I_1 \times I_2}$, $k_t^2 \in \mathbb{R}^{I_1 \times I_2}$ and $k_t^3 \in \mathbb{R}^{I_1 \times I_2}$, with I_1 and I_2 being the number of uncertainty levels and the dimension of $\boldsymbol{y}$. Therefore, $\phi(\boldsymbol{x}, \boldsymbol{\delta})$ can be rewritten as:

$$\phi(\boldsymbol{x}, \boldsymbol{\delta}) = \min_{\boldsymbol{k_t^{0\sim 3}}} \sup_{J \in \overline{F}} \mathbb{E}_J \left\{ \alpha^{\mathrm{d}} \sum_{t=1}^{T} C_t^{\mathrm{adpt}}(\boldsymbol{\delta}, \boldsymbol{u}) \right\} \tag{9.2a}$$

$$\text{s.t.} \quad \boldsymbol{A}(\boldsymbol{\delta}) + \boldsymbol{B}\boldsymbol{y}(\boldsymbol{\delta}, \boldsymbol{u}) \leq \boldsymbol{D}(\boldsymbol{\delta}) \tag{9.2b}$$

which can be solved by optimizing parameters $\boldsymbol{k_t^{0\sim 3}}$.

Based on the constraints in the lifted ambiguity set $\overline{F}$, the inner maximization problem of (9.2) can be written as:

$$\sup_{J \in \overline{F}} \mathbb{E}_J \left\{ \alpha^{\mathrm{d}} \sum_{t=1}^{T} C_t^{\mathrm{adpt}}(\boldsymbol{\delta}, \boldsymbol{u}) \right\}$$

$$= \sup \int_{\overline{\mathscr{W}}} \alpha^{\mathrm{d}} \sum_{t=1}^{T} C_t^{\mathrm{adpt}}(\boldsymbol{\delta}, \boldsymbol{u}) df(\boldsymbol{\delta}, \boldsymbol{u}) \tag{9.3a}$$

$$\text{s.t.} \quad \int_{\overline{\mathscr{W}}} \boldsymbol{\delta} df(\boldsymbol{\delta}, \boldsymbol{u}) = 0 \qquad : \boldsymbol{\rho} \tag{9.3b}$$

$$\int_{\overline{\mathscr{W}}} \boldsymbol{u} df(\boldsymbol{\delta}, \boldsymbol{u}) \leq \boldsymbol{\gamma} \qquad : \boldsymbol{\beta} \tag{9.3c}$$

$$\int_{\overline{\mathscr{W}}} df(\boldsymbol{\delta}, \boldsymbol{u}) \quad = \mathbf{1} \qquad : \eta \tag{9.3d}$$

$$f(\boldsymbol{\delta}, \boldsymbol{u}) \geq 0, \qquad \forall (\boldsymbol{\delta}, \boldsymbol{u}) \in \overline{\mathscr{W}} \tag{9.3e}$$

$$\boldsymbol{A}(\boldsymbol{\delta}) + \boldsymbol{B}\boldsymbol{y}(\boldsymbol{\delta}, \boldsymbol{u}) \leq \boldsymbol{D}(\boldsymbol{\delta}) \tag{9.3f}$$

where $f(\boldsymbol{\delta}, \boldsymbol{u})$ is the density function. Constraints (9.3b)-(9.3d) correspond to the four lines in $\overline{F}$, and $\boldsymbol{\rho}$, $\boldsymbol{\beta}$ and η are the corresponding dual variables. According to the derivations in [100] using Lagrange duality, the dual form of (9.3) is:

$$\begin{aligned} \min \quad & \eta + \boldsymbol{\gamma}\boldsymbol{\beta} \\ \text{s.t.} \quad & \boldsymbol{\beta} \geq 0 \\ & \eta + \boldsymbol{\rho}\boldsymbol{\delta} + \boldsymbol{\beta}\boldsymbol{u} \geq \alpha^{\mathrm{d}} \sum_{t=1}^{T} C_t^{\mathrm{adpt}}(\boldsymbol{\delta}, \boldsymbol{u}) \\ & \boldsymbol{A}(\boldsymbol{\delta}) + \boldsymbol{B}\boldsymbol{y}(\boldsymbol{\delta}, \boldsymbol{u}) \leq \boldsymbol{D}(\boldsymbol{\delta}) \end{aligned} \tag{9.4}$$

Therefore, the combined problem of all stages is:

$$\min \ \Theta(\boldsymbol{x}) + \eta + \boldsymbol{\gamma}\boldsymbol{\beta} \tag{9.5a}$$

$$\text{s.t.} \quad \boldsymbol{\beta} \geq 0 \tag{9.5b}$$

$$\eta + \boldsymbol{\rho}\boldsymbol{\delta} + \boldsymbol{\beta}\boldsymbol{u} \geq \alpha^{\mathrm{d}} \sum_{t=1}^{T} C_t^{\mathrm{adpt}}(\boldsymbol{\delta}, \boldsymbol{u}) \tag{9.5c}$$

$$\boldsymbol{A}(\boldsymbol{\delta}) + \boldsymbol{B}\boldsymbol{y}(\boldsymbol{\delta}, \boldsymbol{u}) \leq \boldsymbol{D}(\boldsymbol{\delta}) \tag{9.5d}$$

$$\boldsymbol{x} \in \boldsymbol{X_f} \tag{9.5e}$$

As $\boldsymbol{\delta}$ and $\boldsymbol{u}$ are also subject to constraints in the uncertainty set $\overline{W}$, $\boldsymbol{\delta}$- and $\boldsymbol{u}$-related constraints (9.5c) and (9.5d) need to be rewritten incorporating these

limits. For example, (9.5c) is satisfied only if the worst-case is satisfied, i.e.

$$\min_{J\in\overline{F}} \{\eta + \boldsymbol{\rho\delta} + \boldsymbol{\beta u} - \alpha^{\mathrm{d}} \sum_{t=1}^{T} C_t^{\mathrm{adpt}}(\boldsymbol{\delta}, \boldsymbol{u})\} \geq 0 \tag{9.6a}$$

$$\text{s.t.} \quad \left\| -\boldsymbol{\delta} + \boldsymbol{\delta}^{\min} + 1 \right\| \leq \boldsymbol{\delta} - \boldsymbol{\delta}^{\min} + 1 \quad : \boldsymbol{\pi^1}, \boldsymbol{\zeta^1} \tag{9.6b}$$

$$\|\boldsymbol{\delta} - \boldsymbol{\delta}^{\max} + 1\| \leq -\boldsymbol{\delta} + \boldsymbol{\delta}^{\max} + 1 \quad : \boldsymbol{\pi^2}, \boldsymbol{\zeta^2} \tag{9.6c}$$

$$\left\| \boldsymbol{\delta} - \boldsymbol{u^1} + 1 \right\| \leq -\boldsymbol{\delta} + \boldsymbol{u^1} + 1 \quad : \boldsymbol{\pi^3}, \boldsymbol{\zeta^3} \tag{9.6d}$$

$$\|0\| \leq \boldsymbol{u^1} \quad : \boldsymbol{\pi^4}, \boldsymbol{\zeta^4} \tag{9.6e}$$

$$\|\boldsymbol{u^1}\| \leq \boldsymbol{u}^{1,\max} \quad : \boldsymbol{\pi^5}, \boldsymbol{\zeta^5} \tag{9.6f}$$

$$\left\| \begin{pmatrix} \frac{1-\boldsymbol{u^2}}{2} \\ \boldsymbol{\delta} \end{pmatrix} \right\| \leq \frac{\boldsymbol{u^2}+1}{2} \quad : \boldsymbol{\pi^6}, \boldsymbol{\zeta^6} \tag{9.6g}$$

$$\|\boldsymbol{u^2}\| \leq \mathbf{u}^{2,\max} \quad : \boldsymbol{\pi^7}, \boldsymbol{\zeta^7} \tag{9.6h}$$

where $\boldsymbol{\pi^{1\sim7}}$ and $\boldsymbol{\zeta^{1\sim7}}$ are the corresponding dual variables and the equivalent dual problem is:

$$\begin{aligned}\eta + \alpha^{\mathrm{d}} \sum_{t=1}^{T} \Big[& -(c_g^{\mathrm{voc}} + c_g^{\mathrm{fuel}}) k_t^{g,0} - pr_t^{\text{BM-}} k_t^{\text{BM-},0} + pr_t^{\text{BM+}} k_t^{\text{BM+},0} \\ & - \big(\delta_{v,t}^{\min 1} \pi_{v,t}^1 + \delta_{v,t}^{\min 2} \zeta_{v,t}^1 + \delta_{v,t}^{\max 1} \pi_{v,t}^2 + \delta_{v,t}^{\max 2} \zeta_{v,t}^2 \\ & + \pi_{v,t}^3 + \zeta_{v,t}^3 + u_{v,t}^{2,\max} \zeta_{v,t}^5 + [1/2, 0] \pi_{v,t}^6 + \frac{\zeta_{v,t}^6}{2} + u_{v,t}^{1,\max} \zeta_{v,t}^7 \big) \Big] \geq 0 \end{aligned} \tag{9.7a}$$

$$\sum_{t=1}^{T}(-\pi_{v,t}^{1}+\zeta_{v,t}^{1}+\pi_{v,t}^{2}-\zeta_{v,t}^{2}+\pi_{v,t}^{3}-\zeta_{v,t}^{3}+[0,1]\pi_{v,t}^{6})$$

$$= \sum_{t=1}^{T}\Big[\rho_{v,t}+\alpha^{\mathrm{d}}(-(c_{g}^{\mathrm{voc}}+c_{g}^{\mathrm{fuel}})k_{v,t}^{g,1}-pr_{t}^{\text{BM-}}k_{v,t}^{\text{BM-},1}+pr_{t}^{\text{BM+}}k_{v,t}^{\text{BM+},1})\Big] \quad (9.7b)$$

$$\sum_{t=1}^{T}(-\pi_{v,t}^{3}+\zeta_{v,t}^{3}+\zeta_{v,t}^{4}+\pi_{v,t}^{5})$$

$$= \sum_{t=1}^{T}\Big[\beta_{v,t}^{1}+\alpha^{\mathrm{d}}(-(c_{g}^{\mathrm{voc}}+c_{g}^{\mathrm{fuel}})k_{v,t}^{g,2}-pr_{t}^{\text{BM-}}k_{v,t}^{\text{BM-},2}+pr_{t}^{\text{BM+}}k_{v,t}^{\text{BM+},2})\Big] \quad (9.7c)$$

$$\sum_{t=1}^{T}([-1/2,0]\pi_{v,t}^{6}+\frac{\zeta_{v,t}^{6}}{2}+\pi_{v,t}^{7})$$

$$= \sum_{t=1}^{T}\Big[\beta_{v,t}^{2}+\alpha^{\mathrm{d}}(-(c_{g}^{\mathrm{voc}}+c_{g}^{\mathrm{fuel}})k_{v,t}^{g,3}-pr_{t}^{\text{BM-}}k_{v,t}^{\text{BM-},3}+pr_{t}^{\text{BM+}}k_{v,t}^{\text{BM+},3})\Big] \quad (9.7d)$$

$$\|\pi_{v,t}^{m}\| \leq \zeta_{v,t}^{m}, \quad 0 \leq \zeta_{v,t}^{m}, \quad m=1,2,...,7; \; v=1,...,I_{1} \quad (9.7e)$$

where $\delta_{v,t}^{\text{min1}}$, $\delta_{v,t}^{\text{min2}}$, $\delta_{v,t}^{\text{max1}}$ and $\delta_{v,t}^{\text{max2}}$ in equations above are assigned to $\delta_{v,t}^{\text{min}}+1$, $-\delta_{v,t}^{\text{min}}+1$, $-\delta_{v,t}^{\text{max}}+1$ and $\delta_{v,t}^{\text{max}}+1$, respectively.

Following a similar process, constraints in (9.5d) are reformulated as a set of equivalent linear constraints. Finally, the overall problem can be written as:

$$\min \; \Theta(\boldsymbol{x})+\eta+\boldsymbol{\gamma\beta}$$

s.t. $\boldsymbol{\beta} \geq 0$

Constraints (9.7a)-(9.7e)

Reformulated constraints equivalent to (6.32)-(6.36), (6.38)-(6.41), (6.46), (6.49) and (7.4) in (9.5d)

$\boldsymbol{x} \in \boldsymbol{X_f}$

Appendix: Formulations of Alternative Methods

This section describes the formulations for two additional optimization methods, i.e. stochastic optimization and robust optimization, used in Chapter 7.

Stochastic Optimization Formulation

The objective of Stochastic Optimization (SO) is to optimize the sum of the deterministic cost and the expectation of all uncertainty-related costs over all realization scenarios, while the constraints for each scenario ω need to be satisfied, i.e.

$$\begin{aligned} \min\ & C^{\text{inv}} + C^{\text{foc}} + \alpha^{\text{d}} \sum_{t=1}^{T} [C_t^{\text{DAM}} + C_t^{\text{RM}} + \sum_{\omega=1}^{N^\omega} \xi_\omega (C_{t,\omega}^{\text{voc}} + C_{t,\omega}^{\text{BM}})] \\ \text{s.t.}\ & \text{Constraints (6.1)-(6.49), with (6.5), (6.21), (6.22), (6.31)} \\ & \text{and (6.37) replaced by (7.1), (7.2), (7.3) and (7.4)} \\ & \text{for each scenario } \omega \end{aligned} \tag{9.8}$$

where ξ_ω is the realization probability of scenario ω and N^ω is the total number of scenarios.

Robust Optimization Formulation

The principle of Robust Optimization (RO) is to optimize against the worst-case realization of the uncertainty:

$$\begin{aligned} \min\ & C^{\text{inv}} + C^{\text{foc}} + \sup_{\delta \in U} \left\{ \alpha^{\text{d}} \sum_{t=1}^{T} (C_t^{\text{voc}} + C_t^{\text{DAM}} + C_t^{\text{RM}} + C_t^{\text{BM}}) \right\} \\ \text{s.t.}\ & \text{Constraints (6.1)-(6.49), with (6.5), (6.21), (6.22), (6.31)} \\ & \text{and (6.37) replaced by (7.1), (7.2), (7.3) and (7.4)} \end{aligned} \tag{9.9}$$

where U is the uncertainty set of $\boldsymbol{\delta}$.

Appendix: Input Data of Cost Scenarios for PV Units

Table 9.6 describes the three Photovoltaic (PV) cost scenarios used in Chapter 8 based on data from [3] and [60].

Table 9.6: A Baseline, a high and a low PV cost scenario for 2020-2050.

Baseline PV Cost Scenario					
		2020	**2030**	**2040**	**2050**
PV investment cost (EUR/kWp)	**0-6 kWp**	2'496	2'060	1'770	1'654
	6-10 kWp	2'393	1'964	1'578	1'204
	10-30 kWp	1'916	1'572	1'308	1'102
	30-100 kWp	1'272	1'036	895	816
	>100 kWp	814	664	573	523
PV operational cost (cent/kWh)	**0-6 kWp**	2.6	2.1	1.9	1.7
	6-10 kWp	2.6	2.1	1.8	1.7
	10-30 kWp	2.6	2.1	1.8	1.7
	30-100 kWp	2.6	2.1	1.8	1.7
	>100 kWp	1.7	1.4	1.2	1.2

High PV Cost Scenario					
		2020	**2030**	**2040**	**2050**
PV investment cost (EUR/kWp)	**0-6 kWp**	2'786	2'322	2'060	1'857
	6-10 kWp	2'546	2'241	1'854	1'411
	10-30 kWp	2'066	1'813	1'561	1'308
	30-100 kWp	1'382	1'225	1'083	989
	>100 kWp	885	784	694	633
PV operational cost (cent/kWh)	**0-6 kWp**	2.6	2.2	1.9	1.7
	6-10 kWp	2.6	2.2	1.9	1.7
	10-30 kWp	2.6	2.2	1.9	1.7
	30-100 kWp	2.6	2.2	1.9	1.7
	>100 kWp	1.7	1.5	1.3	1.2

Low PV Cost Scenario					
		2020	**2030**	**2040**	**2050**
PV investment cost (EUR/kWp)	**0-6 kWp**	2'351	1'799	1'480	1'422
	6-10 kWp	2'241	1'715	1'300	996
	10-30 kWp	1'790	1'354	1'056	996
	30-100 kWp	1'178	864	691	644
	>100 kWp	754	553	442	412
PV operational cost (cent/kWh)	**0-6 kWp**	2.6	2.1	1.9	1.7
	6-10 kWp	2.6	2.1	1.8	1.7
	10-30 kWp	2.6	2.1	1.8	1.7
	30-100 kWp	2.6	2.1	1.8	1.7
	>100 kWp	1.7	1.4	1.2	1.1

Appendix: Input Data of Cost Scenarios for Battery Units

Table 9.7 describes the three battery cost scenarios used in Chapter 8 based on data from [190].

Table 9.7: A Baseline, a high and a low battery cost scenario for 2020-2050.

Baseline Battery Cost Scenario							
	2020	**2025**	**2030**	**2035**	**2040**	**2045**	**2050**
Investment cost (energy-related) EUR/kWh	377	233	158	123	110	103	96
Investment cost (power-related) EUR/kW	319	197	133	104	93	87	81
Operation cost (energy-related) EUR/MWh	1.41	0.87	0.59	0.46	0.41	0.38	0.36
Operation cost (power-related) EUR/kW-year	4.70	2.91	1.97	1.54	1.37	1.28	1.20

High Battery Cost Scenario							
	2020	**2025**	**2030**	**2035**	**2040**	**2045**	**2050**
Investment cost (energy-related) EUR/kWh	459	329	247	206	178	171	158
Investment cost (power-related) EUR/kW	388	278	209	174	151	145	133
Operation cost (energy-related) EUR/MWh	1.72	1.23	0.92	0.77	0.67	0.64	0.59
Operation cost (power-related) EUR/kW-year	5.73	4.10	3.08	2.56	2.22	2.14	1.97

Low Battery Cost Scenario							
	2020	**2025**	**2030**	**2035**	**2040**	**2045**	**2050**
Investment cost (energy-related) EUR/kWh	295	137	69	41	41	34	34
Investment cost (power-related) EUR/kW	249	116	58	35	35	29	29
Operation cost (energy-related) EUR/MWh	1.10	0.51	0.26	0.15	0.15	0.13	0.13
Operation cost (power-related) EUR/kW-year	3.68	1.71	0.85	0.51	0.51	0.43	0.43

Appendix: Assumed DSO Injection Tariff by Canton

Table 9.8 describes the PV injection tariff data used in Chapter 8.

Table 9.8: The DSO injection tariff in cent/kWh for PV estimated for each Swiss Canton for years 2020 to 2050 [4].

Canton	2020	2025	2030	2035	2040	2045	2050
ZH	6.6	5.6	6.1	6.5	7.0	7.6	8.2
BE	6.9	5.6	6.1	6.5	7.0	7.6	8.2
LU	7.3	5.6	6.1	6.5	7.0	7.6	8.2
UR	9.0	5.6	6.1	6.5	7.0	7.6	8.2
SZ	7.0	5.6	6.1	6.5	7.0	7.6	8.2
OW	10.0	5.9	6.1	6.5	7.0	7.6	8.2
NW	5.9	5.6	6.1	6.5	7.0	7.6	8.2
GL	6.8	5.6	6.1	6.5	7.0	7.6	8.2
ZG	11.2	6.6	6.1	6.5	7.0	7.6	8.2
FR	8.5	5.6	6.1	6.5	7.0	7.6	8.2
SO	8.7	5.6	6.1	6.5	7.0	7.6	8.2
BS	11.8	7.0	6.1	6.5	7.0	7.6	8.2
BL	9.1	5.6	6.1	6.5	7.0	7.6	8.2
SH	7.3	5.6	6.1	6.5	7.0	7.6	8.2
AR	5.7	5.6	6.1	6.5	7.0	7.6	8.2
AI	9.1	5.6	6.1	6.5	7.0	7.6	8.2
SG	8.2	5.6	6.1	6.5	7.0	7.6	8.2
GR	9.1	5.6	6.1	6.5	7.0	7.6	8.2
AG	6.2	5.6	6.1	6.5	7.0	7.6	8.2
TG	7.3	5.6	6.1	6.5	7.0	7.6	8.2
TI	8.2	5.6	6.1	6.5	7.0	7.6	8.2
VD	7.4	5.6	6.1	6.5	7.0	7.6	8.2
VS	7.0	5.6	6.1	6.5	7.0	7.6	8.2
NE	8.5	5.6	6.1	6.5	7.0	7.6	8.2
GE	11.1	6.6	6.1	6.5	7.0	7.6	8.2
JU	6.9	5.6	6.1	6.5	7.0	7.6	8.2

Appendix: Assumed Retail Electricity Tariff by Canton

Table 9.9 describes the retail electricity tariff data for 2020 used in Chapter 8.

Table 9.9: The base retail electricity tariff in cent/kWh estimated for consumption categories L1-L11 of each Swiss Canton in 2020 [5].

Canton	L1	L2	L3	L4	L5	L6	L7	L8	L9	L10	L11
ZH	20.5	18.3	16.7	16.7	15.8	15.8	15.5	14.3	12.3	16.3	14.3
BE	27.7	25.1	23.1	23.1	22.1	22.1	22.2	19.7	17.6	22.3	19.9
LU	23.0	22.7	21.0	21.0	20.7	20.7	22.1	17.8	14.9	21.0	17.0
UR	28.4	25.5	23.3	23.3	22.2	22.2	22.2	19.2	15.8	20.9	16.7
SZ	23.9	21.7	20.1	20.1	19.2	19.2	18.7	16.9	15.0	19.2	16.7
OW	26.9	24.0	22.1	22.1	21.0	21.0	20.8	19.1	16.6	19.9	17.7
NW	24.2	21.4	19.9	19.9	18.8	18.8	18.1	17.0	15.6	17.5	16.1
GL	27.7	25.1	22.3	22.3	20.1	20.1	18.5	17.1	15.1	20.9	19.5
ZG	21.0	20.1	18.2	18.2	17.4	17.4	17.7	14.9	12.8	18.1	15.3
FR	24.5	22.2	20.1	20.1	19.3	19.3	19.8	17.3	14.0	19.9	19.1
SO	26.1	23.2	21.6	21.6	20.7	20.7	20.6	18.6	16.2	21.0	18.8
BS	27.4	27.2	25.8	25.8	25.9	25.9	27.3	23.1	21.0	29.6	25.6
BL	25.4	23.0	21.5	21.5	20.7	20.7	20.4	17.1	17.2	20.7	18.8
SH	24.8	22.1	20.6	20.6	19.6	19.6	19.1	16.4	15.3	19.3	16.7
AR	21.0	19.3	17.8	17.8	16.6	16.6	16.0	14.2	13.1	16.3	13.5
AI	22.2	19.2	17.6	17.6	16.5	16.5	15.9	14.3	13.0	16.2	14.1
SG	23.2	20.5	18.8	18.8	17.7	17.7	17.0	15.5	14.1	17.8	15.2
GR	24.9	22.2	21.1	21.1	20.4	20.4	20.4	18.8	16.6	19.9	19.6
AG	26.8	20.4	18.7	18.7	17.6	17.6	17.0	15.5	13.3	17.1	16.2
TG	23.2	20.6	19.0	19.0	17.9	17.9	17.3	159	14.3	18.6	16.5
TI	21.4	20.2	18.9	18.9	18.6	18.6	18.6	17.0	15.6	18.8	19.2
VD	24.1	22.6	20.9	20.9	20.2	20.2	20.5	183	15.7	20.3	17.7
VS	20.3	18.3	17.3	17.3	18.6	18.6	15.4	16.0	13.3	16.8	15.2
NE	25.4	23.8	214	21.4	20.1	20.1	20.2	18.0	14.9	21.1	18.8
GE	20.5	20.2	19.1	19.1	19.0	19.0	20.0	18.1	16.2	20.7	19.5
JU	32.2	28.6	26.3	26.3	25.3	25.3	25.6	21.1	17.6	25.5	21.8

Note: the low retail electricity tariff for off-peak hours and the high retail electricity tariff for peak hours are assumed to be 71% and 107% of the base tariff.

Table 9.10 describes the information of electricity consumption categories used in Chapter 8.

Table 9.10: Information of electricity consumption categories [5].

Category	Annual electricity consumption	Electricity tariff category
L1	0-1'600 kWh	H1
L2	1'600-2'500 kWh	H2
L3	2'500-3'500 kWh	H2, H3
L4	3'500-4'500 kWh	H2, H3
L5	4'500-5'500 kWh	H3, H4
L6	5'500-7'500 kWh	H3, H4
L7	7'500-13'000 kWh	H8
L8	13'000-25'000 kWh	H7
L9	25'000-30'000 kWh	H6
L10	30'000-150'000 kWh	C2
L11	>150'000 kWh	C3